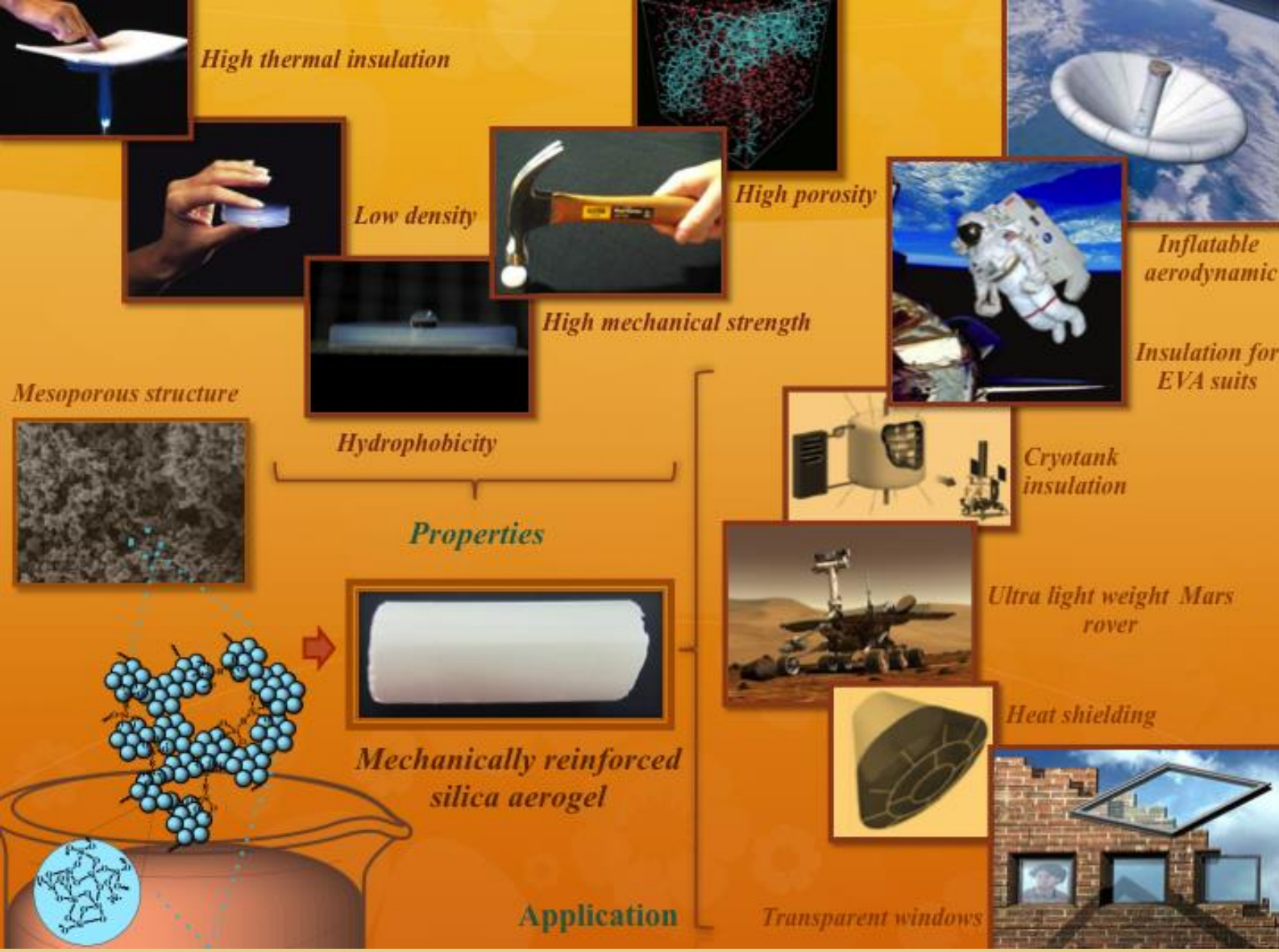

Hajar Maleki

DEVELOPMENT OF MECHANICALLY REINFORCED POLYMER-SILICA AEROGELS FOR THERMAL INSULATION IN SPACE APPLICATIONS

Tese de Doutoramento em Engenharia Química, orientada por Professor Doutor Antonio Alberto T. G. Portugal e co-orientada por Professora Doutora Luisa Maria Rocha Durães e apresentada ao Departamento de Engenharia Química da Faculdade de Ciências e Tecnologia da Universidade de Coimbra

September 2014

· U C ·

UNIVERSIDADE DE COIMBRA

The cover photo is describing the excellent material properties of silica aerogels with their aerospace and earthly domain applications, which are reprinted from:

High thermal insulation:

http://webberenergyblog.wordpress.com/2013/03/31/aerogel-the-future-of-insulation/

Low density:

http://spinoff.nasa.gov/Spinoff2010/cg_2.html

High mechanical strength:

https://www.youtube.com/watch?v=k8OhJKR3AA4

Hydrophobicity

http://www.aerogeltechnologies.com/aerogel-materials

High porosity:

http://www.mse.engin.umich.edu/people/kieffer/projects/a-computational-study-of-the-molecular-structure/147

Inflatable aerodynamic:

http://www.prlog.org/10316724-ilc-dover-celebrates-successful-irve-inflatable-aeroshell-flight-test.html

Insulation for EVA suits:

http://www.asc-csa.gc.ca/eng/educators/resources/training.asp

Cryotank insulation, Ultra light weigh Mars rover, Heat shielding:

http://nextbigfuture.com/2012/08/flexible-aerogels-that-are-500-times.html

Transparent windows:

http://tpe-aerogel.mem-eau.net/?page_id=1019

Hajar Maleki

Development of mechanically reinforced polymer-silica aerogels for thermal insulation in Space applications

Supervisors:

Professor Doutor António Alberto T.G. Portugal
Professora Doutora Luísa Maria Rocha Durães

Thesis submitted for the degree of Doctor of Philosophy in Chemical Engineering
Department of Chemical Engineering, Faculty of Sciences and Technology, University of Coimbra

Coimbra 2014

UNIVERSIDADE DE COIMBRA

Financial support by:

MANANO (Manufactured and Application of Nanostructured Materials)

FP7-PEOPLE-2010-ITN Marie-Curie Action: "Initial Training Networks"

Grant Agreement 264710

Dedication

To my parents, for their love, encouragements and endless support.

To my greatest blessing, my husband, the most decent and loving person I've ever known.

To my little angel, who is going to bring so much love, happiness & joy to my life.

To all my teachers from the beginning, who have been inspiring me throughout these years.

Acknowledgments

Generous financial support made my doctoral studies possible. I would like to express my gratitude to Manufacturing and Applications of Nanostructured Materials project (MANANO) (FP7-PEOPLE-2010-ITN, Marie-Curie Action), for the excellent financial supporting during my PhD thesis.

I am deeply indebted to my supervisor Prof. Dr. António Portugal from the University of Coimbra for his help, support and encouragement to do my Ph.D. program. I was fortunate to have found an advisor with drive and determination for research as he displayed.

I would like to thank my co-supervisor Prof. Dr. Luísa Durães from the University of Coimbra for investing significant amount of her time for advancing the project and for her valuable scientific hints, interest and support.

I must thank all the members of sol-gel research group, especially Telma Matias, who have actively spent her time generously and patiently for better leading the instrumental tasks of this project. Although we are a young group, I believe that we have built a foundation that will allow for future generation of students to grow from.

I would like to thank Active Space Technologies company for their valuable support, hint during my secondment activities.

I would not be the person I am today without my parents and my family. It was them who raised me in the right way and showed me what a work ethic was and how to implement that work ethic in achieving my goals. I thank you both for all sacrifices which you made to see my successes.

Finally, I must thank my husband, Mohsen, whose patient love and compassion and motivation was priceless to start this incredible journey.

ABSTRACT

Silica aerogels have extremely high surface area, high porosity and very low density, showing suitable characteristic for several potential applications such as thermal and acoustic insulators, radiation detectors and cometary dust trappers. However, due to their high fragility, the processing and handling of native silica aerogels is not possible without making severe damage on them. This has led to the development of silica aerogel composites with high strength and improved mechanical properties by adding surface modifiers and compounding with appropriate polymers. To date, attempts to strengthen the mechanical properties of aerogels have been accompanied by significant increase in the bulk density along with long processing time as well as risky and expensive supercritical drying conditions. In this work, I will describe our research to overcome these problems by one pot and streamline synthesis of tri-methacrylate crosslinked silica aerogels containing different underlying silica structures. This approach led to the development of strong aerogels within hours with different silica nanostructures and having different material properties. The strongest aerogels achieved more than one order of magnitude improvement in the compression strength with only doubling the density and negligible increase in their thermal conductivity. We also developed strong ambient pressure dried (APD) silica aerogel-like monoliths with controlled shrinkage, and avoiding high risk and costly supercritical drying by replacing it by low cost subcritical drying conditions. In this approach, we were also able to optimize and model the aerogels' main properties by using a statistical experimental design methodology and develop APD aerogels with similar properties as their supercritically dried counterparts. In terms of material properties, our developed aerogel and aerogel-like monoliths were perfectly suitable for their intended space applications.

We also developed a first approach to control the molecular weight of the polymer that reinforce the silica aerogels by surface initiated reversible addition-fragmentation chain

transfer (SI-RAFT) polymerization. With this method, a correlation between the molecular weight of the polymer and different aerogel properties was established. Therefore, with such versatile approach we prepared strong silica aerogel composites that to some extent retain their other main physical properties.

Resumo

Os aerogéis de sílica exibem área de superfície extremamente elevada, alta porosidade e muita baixa massa volúmica *bulk*, potenciando o seu uso em várias aplicações, tais como em isoladores térmicos e acústicos, detetores de radiação e captadores de poeiras cósmicas. Contudo, devido à sua baixa densidade e elevada fragilidade, o processamento e manuseamento dos aerogéis de sílica nativos não é possível sem os danificar significativamente. Isto impulsionou o desenvolvimento de aerogéis de sílica compósitos, com elevada resistência e propriedades mecânicas melhoradas, por adição de modificadores de superfície e/ou polímeros apropriados. Até à data, as tentativas que foram feitas para melhorar as propriedades mecânicas dos aerogéis de sílica foram acompanhadas por um aumento significativo da massa volúmica bulk e do tempo de processamento, assim como da utilização de condições supercríticas para secagem, as quais são arriscadas e de implementação dispendiosa.

Nesta dissertação, é descrito o trabalho de investigação por nós realizado para ultrapassar estes problemas. Para isso, usou-se um processo de síntese simples, em um passo, de aerogéis de sílica contendo diferentes estruturas de sílica subjacentes e reticulados com trimetacrilato. Esta estratégia conduziu à preparação de aerogéis resistentes em apenas algumas horas, com nanoestruturas de sílica e propriedades diferenciadas. Os aerogéis mais fortes exibiram mais de uma ordem de grandeza de melhoria na resistência à compressão, com apenas a duplicação da densidade e aumento desprezável da sua condutividade térmica.

Também foram desenvolvidos aerogéis monolíticos e resistentes recorrendo secagem à pressão ambiente (APD), e evitando assim o passo de secagem supercrítica, mais perigoso e caro do que a secagem subcrítica. Nesta abordagem, foi possível otimizar e modelar as principais propriedades dos aerogéis usando uma metodologia estatística de planeamento de experiências e desenvolver aerogéis secos por APD com propriedades semelhantes às dos

seus homólogos secos em condições supercríticas. Em termos de propriedades, os aerogéis preparados por ambas os processos de secagem mostraram-se adequados para as aplicações espaciais em vista.

Desenvolvemos ainda uma primeira aproximação para controlar o peso molecular do polímero que reforça a rede dos aerogéis de sílica, recorrendo a polimerização por *surface initiated reversible addition-fragmentation chain transfer* (SI-RAFT). Com este método, estabeleceu-se a correlação entre o peso molecular do polímero e diferentes propriedades do aerogel. Assim, com esta estratégia versátil preparámos aerogéis de sílica compósitos resistentes mecanicamente e retendo, em certa extensão, as suas propriedades físicas relevantes.

List of Contents

Acknowledgments ..... **v**

ABSTRACT ..... **vi**

Resumo ..... **viii**

List of Figures ..... **xiv**

List of Tables ..... **xxi**

Chapter I. Introduction **2**

I. 1 Introduction **2**

I. 2 Objective of the present dissertation **5**

I. 3 Chapter classification and outline of thesis **8**

I.4 List of publications **9**

Chapter II. Historical background and chemistry of the sol-gel process, drying techniques and state of the art for mechanical reinforcement of silica aerogels. **11**

II. 1 Historical background of sol-gel process **11**

II. 2 Sol-gel chemistry **14**

II. 3 Aging **17**

II. 4 Drying techniques **18**

II. 4.1 Advances in drying approaches of silica aerogels 21

II. 5 Silica Aerogel Drawbacks **24**

II. 6 Development of strong silica aerogels **25**

II. 6.1 Structural reinforcement of silica aerogels 27

II. 6.2 Polymer reinforced silica aerogels 35

II. 6.2.1 Class I hybrid composite aerogels 35

II. 6.2.2 Class II hybrid composite aerogels 37

II. 6.2.2.1 Liquid and vapour phase polymer cross-linking 38
II. 6.2.3 Advanced methods for polymer reinforcing of silica aerogels 43
II. 6.2.4 Cost estimation of polymer silica aerogels 48
II. 6.3 Additional approaches to strengthen silica aerogels 50
II. 7 Summary and conclusions from literature 50
Chapter III. Synthesis of lightweight polymer-reinforced silica aerogels with improved mechanical and thermal insulation properties for space applications. 54
III. 1 Introduction 54
III. 2 Experimental 57
III. 2.1 Materials 57
III. 2.2. Methods 58
III. 2.2.1 General 58
III. 2.2.2 Preparation of polymer-reinforced silica wet gels 59
III. 2.2.3 Preparation of nonreinforced silica aerogels 60
III. 2.2.4 Diagram of the supercritical drying (SCD) system 60
III. 2.2.5 SCD Procedure for Silica Aerogel Preparation 63
III. 2.3 Characterization techniques 65
III. 3 Results and discussion 66
III. 3.1 Chemical characterization 67
III. 3.2 Physical and microstructural characterization 74
III. 3.2.1 Density, porosity and dimensional changes 74
III. 3.2.2 Micro and mesoporous structures of the developed aerogels 77
III. 3.3 Thermal stability 83
III. 3.4 Mechanical and thermal conductivity properties 86
III. 4 Conclusions 92

Chapter IV. Development of mechanically strong ambient pressure dried silica aerogels with optimized properties. 95

IV. 1 Introduction 95

IV. 2 Experimental 99

IV. 2.1 Materials 99

IV. 2.2 Methods 99

IV. 2.2.1 General 99

IV. 2.2.2 Preparation of polymer-reinforced ambient pressure dried (APD) silica aerogel-like monoliths 100

IV. 2.3 Physicochemical analysis 101

IV. 2.4 Vacuum outgassing and thermal cycling screening tests 102

IV. 2.5 Response Surface Methodology 104

IV. 2.5.1 Central Composite Rotatable Design (CCRD) 105

IV. 3 Results and discussion 109

IV. 3.1 Chemical characterization 110

IV. 3.2 Modeling the responses for BTMSH and BTESB derived aerogel-like materials 114

IV. 3.3 Optimization of the properties of ambient pressure dried BTMSH and BTESB derived aerogel-like samples 121

IV. 3.4 Evaluation of sample properties for Space applications 126

IV. 4 Conclusion 130

Chapter V. Develoment of mechanically reinforced silica aerogels *via* Surface-Initiated Reversible Addition-Fragmentation Chain Transfer (RAFT) Polymerization. 133

V. 1 Introduction 133

V. 2 Background of controlled radical polymerization 134

V. 2.1 Reversible Addition-Fragmentation Chain Transfer (RAFT) polymerization technique 135
V. 2.2 RAFT polymerization on solid supports 137
V. 3 Materials 138
V. 4 Method 138
V. 4.1 Preparation of *S*-Benzyl *S′*-trimethoxysilylpropyltrithiocarbonate (BTPT) and *S*-benzyl *S′*-propyltrithiocarbonate (BPTT) 138
V. 4.2 Synthesis of RAFT modified silica (RAFT-Silica) aerogels 140
V. 4.3 RAFT Polymerizations 141
V. 4.4 General procedure to cleave grafted chains from the silica surface by aminolysis 142
V. 5 Characterization techniques 143
V. 5.1 Size exclusion chromatography - determination of molecular weight and molecular weight distributions of grafted polymers 143
V. 5.2 Bulk and skeleton density and nitrogen gas adsorption 143
V. 5.3 Thermo gravimetric analysis (TGA) 144
V. 5.4 Scanning electron microscopy (SEM) 144
V. 5.5 Thermal conductivity and mechanical properties 144
V. 6 Results and discussion 145
V. 7 Conclusion 155
Chapter VI. Conclusions and brief perspective on future directions 158
Chapter VII. References 163
VII. 1 References 163

List of Figures

Figure II. 1 A significant increase in the number of publications occurred from early 1980's. Number of publications counted using ″sol-gel″ as a keyword (Scopus record). 13

Figure II. 2 Application of Sol-Gel method according to a S. Sakka [72]. 13

Figure II. 3 Overview of the sol-gel process. Initial step is hydrolysis of alkoxy silanes followed by the condensation of the newly formed silanols. Once the polymerization is initiated, they occur simultaneously. 16

Figure II. 4 Typical SEM image of Si aerogels with schematic representation of primary and secondary silica particles (left); (i) neck growth mechanism of secondary silica particles and (ii) relative aging rate as a function of time for two mechanisms (a, b) (right, Adapted from [98] and [95]). 17

Figure II. 5 Schematic representation of typical sol-gel synthesis procedure. 24

Figure II. 6 Reinforcing the weak necks between the silica particles. 26

Figure II. 7 Three dimensional network of MTMS-derived aerogels with its detailed molecular structure. 28

Figure II. 8 Maximum possible bending of the MTES-derived aerogels prepared with a) *S*=6.45, b) *S*=12.96, and c) *S*=19.35. Reprinted from ref. [20], Copyright (2009), with permission from Elsevier. 29

Figure II. 9 Organo(alkoxy) and bridged silanes used as precursors for sol-gel-derived (hybrid) materials. 31

Figure II. 10 a) Stress strain curves of a monolithic sample of aerogel made from TMOS and a high portion of BTSPD b) recovery after compression *vs.* time. The inset is showing the

aerogel sample compressed by finger pressure and demonstrating full recovery. Reprinted from ref. [21], with permission from the Royal Society of Chemistry (RSC). 32

Figure II. 11 Three dimensional network of MTMS/BTMSH-derived silica aerogels with its detailed molecular structures. 33

Figure II. 12 Reaction strategy for preparation of non-modified polysilsesquioxane aerogels with incorporation of four types of flexible linking groups in the silica backbone. The chemical structures of the alkyl linked bis-silane precursors are indicated in Figure 8 with their related numbers. 34

Figure II. 13 a) Concept of polymer reinforcement using reactive groups on the silica surface; b) Epoxy cross-linking of silica aerogels. Inspired in [49]. 40

Figure II. 14 a) Traditional method to prepare cross-linked aerogels. Each wash step takes 24 hrs, and heating to cross-link can take as long as 72 hrs (This process require approximately 1 liter of solvent to prepare one ~20 ml cylindrical monolith), b) One-pot synthesis of cross-linked aerogels; the gray counterparts are prepolymers in the sol that are inert to gelation. Once the gel is formed, it can react to initiate cross-linking. After one wash, which removes any unreacted components, the monolith is supercritically dried. 42

Figure II. 15 APTES-End-Capped Pre-polymer [180]..... 42

Figure II. 16 Chemical structure of silica wet gels obtained from a bis-triethoxysilane derivative of AIBN. Inspired in [177]. 46

Figure II. 17 Formation of an initiator-modified gel, ATRP growth of PMMA on surface and supercritical drying to afford a silica-PMMA composite aerogel. Adapted from ref. [24]. 47

Figure II. 18 Illustration showing reactions leading to silica network formation. Path 1 shows formation of unmodified silica networks, and path 2 shows modification of silica networks by

POSS molecules. Illustration shows how a tri-POSS molecule can covalently bond to the silica network [187], with permission. 48

Figure III. 1 Three proposed molecular structures of methacrylate-modified silica aerogels: a) methacrylate-modified aerogel without bridging groups ([Bis-silane]=0%), b) methacrylate-modified aerogel with a part of the total silicon derived from BTMSH, c) methacrylate-modified aerogel with a part of the total silicon derived from BTESB.....……...…...56

Figure III. 2 Practical approach for the synthesis of polymer-reinforced and nonreinforced silica aerogels. 61

Figure III. 3 Diagram of SCD system. 62

Figure III. 4 Sample vessel/cell. 63

Figure III. 5 Proposed cross-linking reaction for silica aerogels with different underlying silica structures. 69

Figure III. 6 Solid ^{29} Si NMR spectra of aerogel samples formulated from a) TMOS alone, b) Non-X-TMOS 80 mol% + TMSPMA 20 mol% (Nb), c) Non-X-TMOS 40 mol%+ BTMSH 40 mol% + TMSPMA 20 mol% (B_40), d) Non-X-TMOS 70 mol% +BTESB 10 mol% + TMSPMA 20 mol% (Bz_10), (X=cross-linked). 71

Figure III. 7 Solid ^{13} C NMR spectra of aerogel samples a) B_40, b) B_40_R_0.3, c) B_40_R_2 and d) Bz_10_R_2. 72

Figure III. 8 a) Bulk density changes and b) dimensional shrinkage of aerogel samples with different mol % of Si from BTMSH and BTESB as a function of [Tri-meth]/[TMSPM] molar ratio..... 75

Figure III. 9 Photographs of some of selected tri-methacrylate reinforced silica aerogel monoliths, (X=cross-linked)..... 77

Figure III. 10 a) Comparative N_2 sorption isotherms of selected (cross-linked) X-aerogels Nb_R_2, B_40_R_2 and Bz_10_R_2; the inset is the magnified isotherm of B_40_R_2; b) BJH pore size distributions from the desorption branches of the isotherms for cross-linked aerogels Nb_R_2, B_40_R_2 and Bz_10_R_2. 79

Figure III. 11 Scanning electron microscopy images of selected nonreinforced and reinforced aerogels. 81

Figure III. 12 TEM micrographs of selected (cross-linked) X-aerogels: a) B_40_R_2, b) Bz_10_R_2, and, c) Nb_R_2. 82

Figure III. 13 a) TGA of native TMOS-derived aerogel along with simultaneous TG/DSC curves for methacrylate modified non-X-aerogels with different bridges within the silica structure, b) TG/DSC curves of tri-methacrylate cross-linked silica aerogels B_40_R_2, Bz_10_R_2 and neat polymer. TGA curves of tri-methacrylate cross-linked silica aerogels containing c) 40 mol% of Si from BTMSH and d) 10 mol% of Si from BTESB with different *R* values, (heating rate: 10°C/min) (X=cross-linked). 84

Figure III. 14 a) Stress-strain curves for BTMSH contained tri-methacrylate reinforced aerogels, b) Stress-strain curves for BTESB contained tri-methacrylate reinforced aerogels, c) Elastic modulus versus [Tri-meth]/[TMSPM] molar ratio at different mol% of Si from BTMSH and BTESB, d) Maximum stress at break versus [Tri-meth]/[TMSPM] molar ratio at different mol% of Si from BTMSH and BTESB. 87

Figure III. 15 a) Power law dependency between elastic modulus and bulk density, b) Power law dependency between maximum strength at break and bulk density. 89

Figure III. 16 Thermal conductivity of reinforced and nonreinforced aerogels with different underlying silica structures. 91

Figure IV. 1 Proposed molecular structures of silica gels having a) BTMSH and b) BTESB in the underlying structure……....97

Figure IV. 2 Central composite rotatable design (CCRD) for two experimental factors, X_1 and X_2 variables, respectively Si mol% derived from BTMSH and BTESB, and *R* ratio. 107

Figure IV. 3 Standard error of design plot for BTMSH derived aerogels. 108

Figure IV. 4 Proposed cross-linking scheme with TMSPM and tri-methacrylate. 109

Figure IV. 5 Solid-state ^{29}Si NMR spectra of aerogel-like samples formulated by a) TMOS 40 mol% + BTMSH 40 mol% + TMSPMA 20 mol%, b) TMOS 70 mol% + BTESB 10 mol% + TMSPMA 20 mol%. 111

Figure IV. 6 ATR FT-IR spectra of a) Non-X-BTMSH 40 mol%, b) X-BTMSH 40 mol%, *R*=2, c) Non-X-BTESB 10 mol%, d) X-BTESB 10 mol%, *R*=2, (X: cross-linked). 112

Figure IV. 7 Water contact angle measurements for the cross-linked aerogels with and without BTMSH and BTESB precursors. 114

Figure IV. 8 Response surface models of a) density, b) mechanical strength and c) thermal conductivity of BTMSH derived APD-aerogel-like monoliths versus the mol% of silicon from BTMSH and *R;* response surface models of d) density, e) mechanical strength and f) thermal conductivity of BTESB derived APD-aerogel-like monoliths versus the mol% of silicon from BTESB and *R*. 118

Figure IV. 9 Stress-strain curves of a) BTMSH and b) BTESB derived APD-aerogel-like monoliths. 119

Figure IV. 10 a) Comparative N_2 sorption isotherms of selected cross-linked APD-aerogel-like monoliths. 120

Figure IV. 11 a) Desirability versus Si mol% of BTMSH and *R* for BTMSH derived APD-aerogel-like monoliths, b) Desirability versus Si mol% of BTESB and *R* for BTESB derived APD-aerogel-like monoliths. 122

Figure IV. 12 a) Optimized APD-BTMSH derived aerogel-like samples and their $scCO_2$ dried counterparts and, b) optimized APD-BTESB derived aerogel-like samples versus their $scCO_2$ dried counterparts, c) stress-strain curves for monoliths in a) and b). 125

Figure IV. 13 SEM images of optimized APD and $scCO_2$ dried aerogels. 126

Figure IV. 14 ATR FT-IR spectra of a) BTMSH and b) BTESB derived APD-aerogel-likes and $scCO_2$ dried aerogels after vacuum outgassing test. 128

Figure IV. 15 Thermogravimetric analysis (TGA) data of BTMSH and BTESB derived APD-aerogel-like monoliths. 129

Figure V. 1 Mechanism of RAFT polymerization ……137

Figure V. 2 Preparation of *S*-Benzyl *S′*-trimethoxysilylpropyltrithiocarbonate (BTPT) to be used as a surface bond RAFT initiator. 139

Figure V. 3 ^{1}HNMR spectra of a) *S*-Benzyl *S′*-trimethoxysilylpropyltrithiocarbonate (BTPT), and b) *S*-benzyl *S′*-propyltrithiocarbonate (BPTT). 140

Figure V. 4 Copolymerization of TMOS and silica-BTPT for preparation of a wet gel with surface bound RAFT initiator 141

Figure V. 5 RAFT growth of PSt and PBA on silica surface..... 142

Figure V. 6 a) SEM image of surface functionalized silica aerogel with RAFT-silica, b) PBA-silica aerogel composite and c) PSt-silica aerogel composite after 30h polymerization. 147

Figure V. 7 FT-IR spectra of RAFT-silica (a), PBA-silica (b) and PSt-silica aerogels. 148

Figure V. 8 Size exclusion chromatography traces for a) PSt, and b) PBA polymers isolated from silica composites. 149

Figure V. 9 TGA curves of a) PBA-silica aerogels and b) PSt-silica aerogel composites. ... 150

Figure V. 10 TGA analysis of samples from interior and exterior of silica aerogels RAFT modified with PBA for 20 and 30 hours. 152

Figure V. 11 Nitrogen adsorption and desorption isotherms (a, b) and Barrett–Joyner–Halenda (BJH) pore-size distribution (c, d) of aerogels calculated from the desorption branch of the isotherm. Relative pressure=P/P_0. 152

Figure V. 12 Thermal conductivity versus polymerization time. 153

Figure V. 13 a) stress strain curves of different developed reinforced and nonreinforced aerogels b) photograph of plain TMOS-derived aerogel and initiator-modified aerogel (RAFT-silica) along with reiforced PBA-silica and PSt-silica aerogels with 30 hours polymerization time……...…….154

Figure VI. 1 Mechanical strength of silica aerogel composites plotted against their density. Different polymer crosslinked silica aerogels are listed at Table II. 2 in Chapter II....……..159

Figure VI. 2 Strength of silica aerogel composites plotted against the processing time required to prepare them. 160

List of Tables

Table II. 1 Brief list of liquids and their supercritical values used in supercritical drying of silica aerogels. 21

Table II. 2 Examples of polymeric systems, with the method of cross-linking to silica aerogels and selected properties of cross-linked aerogels. 45

Table II. 3 Comparison of the required resources for preparation of reinforced silica aerogels/aerogel-like monoliths using different synthesis methodologies (for and aerogel with 12 cm length, 1 cm diameter and bulk density ≈ 0.3 g cm^{-3}) 49

Table III. 1 Synthesis parameters of reinforced silica aerogels……...59

Table III. 2 Measured properties of polymer reinforced aerogels..... 68

Table III. 3 Measured properties of nonreinforced aerogels. 69

Table III. 4 Water contact angles of selected nonreinforced and reinforced aerogels. 73

Table III. 5 Surface area, porosity, skeletal density (ρ_s), pore volume and average pore size values for representative nonreinforced and reinforced samples. 78

Table IV. 1 Coded and actual levels of variables considered for design for APD BTMSH and BTESB derived aerogel-like monoliths……..106

Table IV. 2 Monomer contribution in the different aerogel-like composites. 113

Table IV. 3 Coded operating variables with measured properties of BTMSH and BTESB derived aerogel-like monoliths. 115

Table IV. 4 Significant terms and statistics summary for response surface models for BTMSH derived aerogel-like material and BTESB derived aerogel-like material. 116

Table IV. 5 Specific surface areas (BET), pore volumes, pore average sizes and porosity values of selected APD-aerogel-like monoliths. 120

Table IV. 6 Optimal design points for BTMSH and BTESB derived aerogel-like monoliths with their predicted response values. 123

Table IV. 7 Comparison of important physical and mechanical properties of optimized APD-aerogel-like monoliths and $scCO_2$ dried aerogels under the same synthesis conditions. 124

Table IV. 8 Vacuum outgassing data for optimized APD-aerogel-like samples and $scCO_2$ dried aerogel samples. 129

Table IV. 9 Thermal cycling data for optimized APD and $scCO_2$ dried aerogels. 130

Table V. 1 Properties of silica, PBA and PSt-silica aerogel composites..... 146

Table V. 2 Results of TGA and SEC analysis for RAFT graft Polymerization. 151

Chapter I. Introduction

General introduction, objectives, goals and thesis structure/chapter classification

I. 1 Introduction

Silica aerogels are materials with unique properties such as high specific surface area (500–1200 m^2/g), high porosity (80–99.8%), low density (~0.003-0.5 g/cm^3), low thermal conductivity (0.005-0.1 W/mK), ultra-low dielectric constant (k = 1.0–2.0) and low index of refraction (~1.05) [1, 2]. Due to their unusual characteristics, much attention has been given to silica aerogels in recent years for their use in several technological applications including Cherenkov radiators in particle physics experiments [3] and thermal insulation materials for skylights and windows [4]. Silica aerogels have also been used for making heat storage devices used in windows defrosting and as acoustic barrier materials [5]. Other aerogels have been demonstrated good performance for battery electrodes [6], catalyst supports [7], oxygen and humidity sensors [8] and adsorbents for environmental clean-up [9] due to their large internal surface areas and facile changing of their surface chemistry. The low values of thermal conductivity and the very low density make silica aerogels attractive materials for a number of aerospace applications. One example involves insulation around the battery packs in the Mars Sojourner Rover for protection of electronic units [10]. More robust and flexible aerogels are being considered to insulate extra-vehicular activity (EVA) suits for future manned missions to Mars [11]. Aerogel composites are the only materials that come close to meet the requirements for EVA suit insulation [12]. Robust aerogel composites are also considered as insulation materials of inflatable decelerators for entry, descent, and landing (EDL) applications for future space missions on Mars [13].

It should be noted that aerogel applications in space are not all limited to thermal insulation. Indeed, silica aerogels can also be applied to collect aerosol particles [14], to protect space mirrors or to design tank baffles [15, 16]. However, these applications of silica aerogels have been restricted because of their extreme fragility and poor mechanical properties and hygroscopic nature [17]. Therefore, with the purpose of expanding the application range of aerogels, while fully retaining their outstanding properties, mechanically robust aerogels are needed.

Different methods have been explored to improve the mechanical properties of silica aerogels such as structural reinforcement using flexible silica precursors in silica gel backbone [18-21], conformal coating of silica backbone via surface cross-linking with a polymer [22-26], dispersing carbon nanofibers in the initial sol of silica aerogel [27]. In principle, to improve flexibility or elastic recovery in silica aerogels, it is required either to include organic linking groups in the underlying silica structure or to promote cross-linking of the skeletal gel network through surface silanol groups by reacting them with monomers/polymers.

Since the silica aerogels consist of silica particles that are connected to each other via only Si-O-Si stiff bonds, the compounding of the silica aerogel with polymer leads to an increase of the connection points between the silica particles, with the formation of strong extra –(C-C-) covalent bonds between these particles [28]. Therefore, such methodology leads to an increase of the strength of the reinforced silica aerogels over native silica aerogels [29]. Thus, the objective of such compounding with organic polymers is to provide an aerogel with good compressive strength to be able to adapt to the design of components and to absorb the energy involved in shock compressions [14, 15, 30, 31]. However, manufactured aerogels are not strong enough to be reshaped and must be casted to the final forms during synthesis and processing [32]. But, it has been proven that elasticity/flexibility can be significantly

enhanced in non-cross-linked aerogels by altering the chemical nature of the silica backbone. For example, for TMOS/BTMSH-derived aerogels of densities bellow 0.06 g cm^{-3}, it was possible to bend by 50° the material without breaking it [33]. Additionally, Kramer *et al.* [34] demonstrated that an addition of up to 20% (w/w) poly(dimethylsiloxane) in (TEOS)-derived aerogels resulted in rubbery behaviour with up to 30% recoverable compressive strain. Shea and Loy [35] have developed hybrid aerogels from bridged polysilsesquioxanes, using building blocks comprised of organic bridging groups attached to two or more trialkoxysilyl groups via nonhydrolyzable carbon–silicon bonds. All of these methods proved to be different ways of tuning mechanical properties to the application requirements.

As it is indicated by Fricke *et al.* [36] and Pekala *et al.* [37], due to the trade off between mechanical properties (*e.g.* Young's modulus or maximum strength) of silica aerogels with their density, the most straightforward methods of mechanical reinforcing of silica aerogels result in an increase of the density and therefore an increase in thermal conductivity [38-40]. This is caused by the increase of the total amount of material used for the production of the gel matrix, due to the need of increasing the total number of connection points within the silica aerogel. The most recent achievements involve the preparation of aerogels with significant improvement in their maximum compression strength at break with only doubling the density and thermal conductivity [29].

General physical and chemical issues involved in the synthesis of silica gels were explained in books [41, 42]. Additionally, many reviews on aerogels, with particular focus on silica aerogels, have already been published [1, 43-47], which give a more specific and complete description about the aerogels processing, properties and applications. For the purpose of strengthening the mechanical properties of silica aerogels, different possible strategies of surface chemistry modification of aerogels, followed by compounding their surfaces with appropriate organic polymers, namely epoxide [48, 49], polyurea [50], polyurethane [33, 51],

polyacrylonitrile [22], polystyrene [52, 53], are reviewed by Leventis *et al.* [26, 54], and more recently by Meador *et al.* [29, 32].

Despite of the reasonable mechanical strength achieved the majority of the developed polymer reinforced silica aerogels displayed high densities normally ranged over 0.5 g cm^{-3} and thermal conductivities values above 0.04 W m^{-1} K^{-1}.

I. 2 Objective of the present dissertation

The global objective of this research was the synthesis of mechanically strong silica aerogels with expanded aerospace application and retaining their outstanding properties as much as possible. Having in mind this goal, the initial attempt for mechanical reinforcement of native silica aerogels was to create extra connectivity through addition of strong covalent bonds in the connection points of silica nanoparticles inside the aerogel network. Relying on the extensive literature survey [55], the compounding of silica aerogel networks with appropriate organic polymers or cross-linker was a first and common approach to strengthen the silica aerogels. Motivated by this idea, we also selected this approach, and developed organic-inorganic hybrid silica aerogels. Initially, in this context, the surface chemistry of silica nanoparticles in the aerogels body has been modified by appropriate functional groups. In the next step, a multifunctional methacrylate cross-linker reacted with silica surface functionality by free radical polymerization approach. Upon cross-linking, extensive branching within the silica network and, therefore, an increased compressive strength of the aerogel monoliths with an approximately constant overall intrinsic flexibility of the silica backbone were anticipated. In order to compensate for the increase in the backbone thermal conductivity due to the cross-linking, we changed the microstructure pattern of the silica aerogels by co-gelation of the silica backbone with the alkyl-linked bis-silane 1,6-bis(trimethoxysilyl)hexane, BTMSH, and the aryl-linked bis-silane 1,4-bis(triethoxysilyl benzene, BTESB.

Previous studies [29] have been focused in the development of aerogels with several varied length of alkyl-bridged bis-silane in the silica backbone to correlate the elastic recovery response of developed aerogels with the length and type of the alkyl moieties. However, alkyl moieties on the underlying silica can affect other aerogels properties namely the thermal conductivity of the resulting aerogels, which has not been extensively investigated. As a complementary study, in the present work, we attempted to address the aforementioned properties of alkyl-bridged based aerogel and compared them, for the first time, with aerogels containing aryl-bridges in their backbone structures. The introduction of aryl-linked bis-silane to underlying silica structures can cause a great control on the size of porosity and indirectly on the thermal insulation performance of the aerogels. In this procedure, by varying the synthesis parameters, reasonable results in terms of mechanical strength (more than one order of magnitude improvement) with density of < 0.4 g cm^{-1} and thermal conductivities of < 0.04 W m^{-1} K^{-1} (for BTESB based aerogel) have been achieved. In this phase of the project, a further goal was to establish a streamline and simple synthesis procedure, thus avoiding lengthy and tedious traditional aerogel preparation methods. Therefore, we developed a one-pot synthesis strategy in which sol-gel reaction and diffusion of the monomer to the silica gels have been carried out at one single step without actually interfering with silica precursors' function during hydrolysis and condensation steps.

After having a global idea of the development of strong aerogels with improved mechanical strength and enhanced thermal insulation performance, the next phase of the project was to improve drying conditions for safe and facile silica aerogel's development. This phase is decisive for future large-scale production and commercialization of the developed product with different geometries or sizes. Our objective was to avoid the need of fitting the samples in cell/chamber of the supercritical autoclave. For this, we have explored a safe and cost effective drying procedure by applying ambient pressure drying conditions that avoid the need

for the risky and costly supercritical drying step. The ambient pressure drying of wet gels was possible by removing the capillary pressure/stresses at the menisci of the solid-liquid-vapor interfaces inside the gel structure upon evaporation of solvent. By performing several post gelation washing and solvent exchange of silica aerogels with a low-surface tension solvent, crack free aerogels without any serious dimensional shrinkage were anticipated. Therefore, a simple and streamline procedure and easy drying conditions by removing supercritical drying was an advantage of this procedure.

In this step of the project, in order to be able to predict and control the main properties of ambient pressure dried silica aerogels toward developing material properties similar to the supercritical counterparts, optimization studies were conducted. Therefore, the physical and mechanical properties of ambient pressure dried cross-linked silica aerogels having different aryl-linked and alkyl-linked silanes were examined and modeled by applying Central Composite Rotatable Design (CCRD) methodology. Finally, we built predictive models to optimize the test parameters as well as levels of each variable using the response surface methodology (RSM).

After optimization of the main properties of ambient pressure dried silica aerogels (APD), the evaluation of the material specification for intended space application followed, in the next stage. Several pre-defined standard thermal tests for Space application of materials have been made on APD samples and the results have been compared with the results of their supercritical dried counterparts under the same preparation conditions.

The further attempt of the project was to develop, for the first time, silica-polymer composite aerogels by conducting a surface initiated controlled polymerization approach. For this, we proceeded with the synthesis of polymer reinforced silica nanocomposites using a surface-initiated reversible addition-fragmentation chain transfer (SI-RAFT) technique. This approach was used to grow well-defined polystyrene (PSt) and poly butyl acrylate (PBA) with low

polydispersities and establish the structure-property relationship between the grafted polymer molecular weight and physical properties of hybrid aerogels.

I. 3 Chapter classification and outline of thesis

The results of research on the above objectives are presented in this document in several chapters. The general introduction to silica aerogels is summarized in Chapter I. In Chapter II, firstly, a general history of sol-gel process with chemistry beyond their methods of synthesis and the principles of the drying techniques is given. This was followed by an extensive study of very recent published works about the development of silica aerogels with improved mechanical properties with particular emphasis on recent advanced methods for preparing class II hybrid polymer-silica aerogels. Chapter III presents details on the effect of the incorporation of alkyl-linked 1,6-bis(trimethoxysilyl)hexane (BTMSH), and aryl-linked 1,4-bis(triethoxysilyl)-benzene (BTESB) into the underlying silica structure of tri-methacrylate cross-linked aerogels. In this chapter, the improvement in the mechanical strength for the whole aerogels along with improvement in the mesoporous nature and thermal insulation performance of BTESB derived aerogels as a result of the inclusion of aryl chain linkages within the silica aerogel backbone are discussed.

Ambient pressure dried (APD) silica aerogel-like monoliths with different underlying silica developed through simple wet chemical approaches are studied in the Chapter IV. Also, a statistical experimental design approach is extensively explained for better understanding the influence of several factors, including the type, concentration of bridged bis-silane and concentration of cross-linker on aerogels' final properties. The present chapter also addresses the method of optimization of APD aerogels by means of fitted empirical models for each silica aerogels' property and desirability function. Finally, a comparison of the key properties of optimized APD aerogel-like monoliths with their supercritical dried ($scCO_2$) aerogels in the

same preparation condition was accomplished. Additionally, the suitability of these monoliths for intended space applications was discussed.

In chapter V, we report the synthesis of mechanically reinforced polymer silica nanocomposites by surface-initiated reversible addition-fragmentation chain transfer (*SI-RAFT).* In this chapter, *SI-RAFT* approach is used to grow polystyrene (PSt) and poly butyl acrylate (PBA) with low polydispersities and establish the structure-property relationship between the grafted polymer molecular weight and physical properties of hybrid aerogels.

Chapter VI summarizes the conclusion and brief perspective on future direction of silica aerogels. Additionally, the open challenging areas for future development of silica aerogels are discussed.

At the end, a list of references in this manuscript is presented in Chapter VII.

I.4 List of publications

1. Hajar Maleki, Luisa Durães, António Portugal, An overview on silica aerogels synthesis and different mechanical reinforcing strategies**, J. Non-Cryst. Solids, 2014; 385:55–74.**

2**. Hajar Maleki**, Luisa Durães, António Portugal, Synthesis of lightweight polymer-reinforced silica aerogels with improved mechanical and thermal insulation properties for space applications**, Microporous Mesoporous Mater. 2014; 197:116–129.**

3. **Hajar Maleki,** Luisa Durães, António Portugal, Development of mechanically strong ambient pressure dried silica aerogels with optimized properties, **submitted to J. Phy. Chem. C (2014).**

4. **Hajar Maleki,** Luísa Durães, António Portugal, Develoment of mechanically reinforced silica aerogels *via* Surface-Initiated Reversible Addition-Fragmentation Chain Transfer (RAFT) Polymerization, **J. Mat. Chem. A, (2015), DOI:** 10.1039/C4TA05618C.

.

Chapter II. Historical background and chemistry of the sol-gel process, drying techniques and state of the art for mechanical reinforcement of silica aerogels.

This chapter comprises the work published at Journal of Non-Crystalline Solids (2014); An overview on silica aerogels synthesis and different mechanical reinforcing strategies, 385:55–74, by: Hajar Maleki, Luísa Durães, António Portugal.

II. 1 Historical background of sol-gel process

Silica and silicates are the earth's most abundant minerals since Oxygen and Silicon are found in great abundance in the earth's crust, 46.6% and 27.7%, respectively [56]. These minerals have been used widely over the course of history, starting as simple stone tools [57], to more sophisticated devices today, such as, optical components of lasers [58]. Traditionally, production of glasses and ceramics using these minerals involves melting them at elevated temperatures (<1000^{o}C) to obtain usable shapes and forms. This procedure not only consumes a large amount of energy, but also limits the ability to incorporate organic molecules into the silica matrix, due to their decomposition (~ 500^{o}C) at the temperatures used. An alternative and milder approach in silica materials, was developed in 1820 by Berzelius, who used soluble silanes in the presence of ammonium hydroxide to form silica powder [59]. A later approach by Ebelman in 1847, was the formation of transparent material using tetrachlorosilanes in the presence of an alcohol. In this way, a silica network is formed as a result of prolonged exposure of the alcohol/silane solution to a humid atmosphere [60]. This approach is similar to what is used today for the preparation of silica gels from the tetraalkoxysilane precursors [61]. This was a breakthrough because of the mild processing

conditions at low temperatures (<100^{o}C). However, this research remained unnoticed for the most part until the early 1900's when Schott glass company established the way of preparation of thin oxide films by sol-gel process by using a combination of metal-containing precursors by deep-coating [62]. During the same time period, the use of porous silica as desiccants and absorbent materials started to grow [63]. This led to the discovery of silica aerogels in the early 1930's by Kistler [64] These discoveries initiated a period of research in which sol-gel methods produced a large number of patents, publications, new materials, applications and an extensive body of knowledge.

In the following decades, the sol-gel process was used to prepare materials in applications such as anti-reflective coatings [65], silica filled composites [66], ceramic monoliths [67], ceramic nuclear fuels [68] and fibers [69]. In the 1970's the sol-gel process began to see a number of uses in hybrid coatings [70], and optical applications [71]. In the few decades, a drastic increase in the number of publications emerged in the field of sol-gel science, with over 6000 new journal articles and patent being published (Figure II. 1) in 2013. The significant expansion of the sol-gel field led to several sub fields of research utilizing the sol-gel processes leading to the development of many new advanced technologies (Figure II. 2).

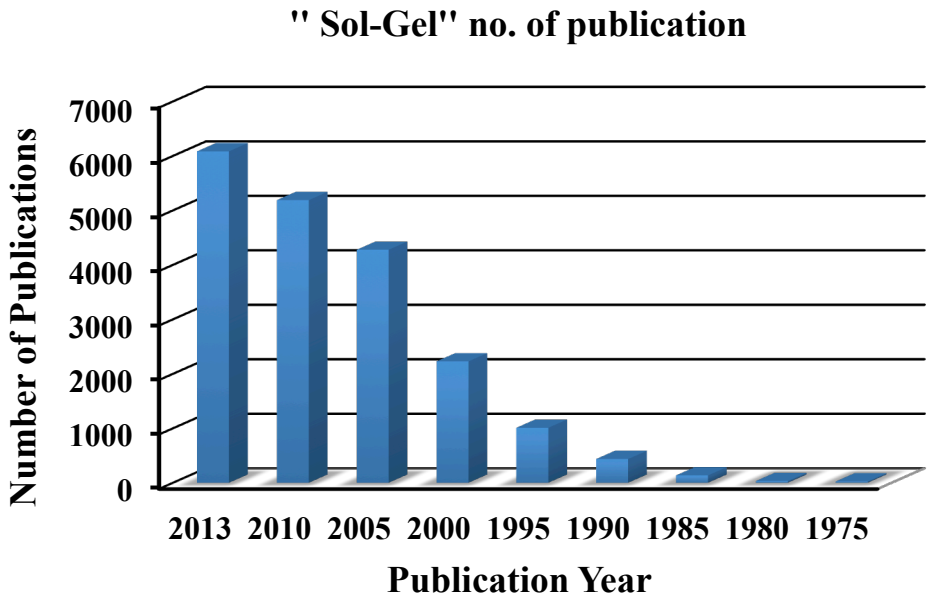

Figure II. 1 A significant increase in the number of publications occurred from early 1980's. Number of publications counted using ″sol-gel″ as a keyword (Scopus record).

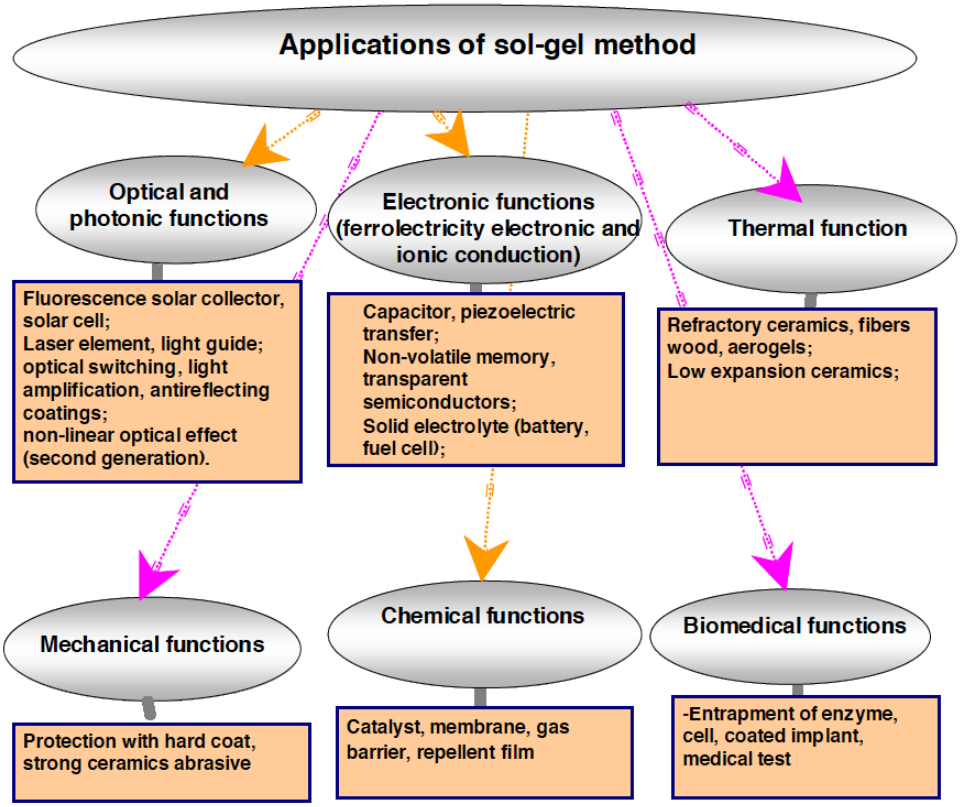

Figure II. 2 Application of Sol-Gel method according to a S. Sakka [72].

II. 2 Sol-gel chemistry

Generally, a nanostructured solid network of silica is formed as a result of a hydrolysis and condensation process of the silica precursors, in which siloxane bridges (Si–O–Si) are formed. Such reactions are equivalent to a polymerization process in organic chemistry, where bonds between the carbon atoms of organic precursors lead to linear chains or branched (cross-linked) structures [73].

The manufacturing process to form silica aerogels comprises two steps: the formation of a wet gel by sol-gel chemistry, and the drying of the wet gel.

Originally, silica wet gels were made by Kistler in the early 1930s [64, 74] through the condensation of sodium silicate (also termed as waterglass). However, the reaction formed salts within the gel that needed to be removed by many long and laborious repetitive washings steps [75]. In following years, Teichner's group extended this approach to prepare optically transparent monoliths using tetraalkoxysilanes ($Si(OR)_4$) as the silica source [76]. The key of this process was to use an alcohol (*e.g.* methanol or ethanol), thus, the need for the tedious water to alcohol solvent exchange was eliminated [76-80]. This reduced the time required to make a final dried aerogel to approximately one day, which was a drastic reduction relatively to Kistler's original method. Presently, with the further developments of the sol-gel process, different alkoxysilane derivatives are used all together and with different solvents, which are needed for the homogenization of the mixture and control of concentrations. Although, when switching from a protic to an aprotic (hydrocarbon) medium, alcohols are ideal intermediary solvents, as their bifunctional nature (polar/non-polar) promotes miscibility of water and the organic phase. But, surprisingly, the choice of the alcohol has a tremendous effect on pore structure and therefore also on final material properties [81-83]. The indication of different gelation solvents and related methodologies applied by different investigators, along with the

different properties of the resulting aerogels, are reviewed by Soleimani *et al*. and Siouffi [47, 84].

Due to the rapid development of sol-gel chemistry over the last few decades, the majority of silica aerogels are prepared today using silicon alkoxides as precursors [85-91]. The most common of the silicon alkoxides are the tetramethylorthosilicate (TMOS, $Si(OCH_3)_4$) and tetraethylorthosilicate (TEOS, $Si(OCH_2CH_3)_4$) [42], with common chemical formula of $Si(OR)_4$, that lead to the aerogels called ‘’Silica’’. Many other alkoxides [92], containing various organic functional groups linked to silicon, can be used to give different properties to the gel. They have a general formula $R'_XSi(OR)_{4-X}$ ($1 \leq X \leq 3$), being mono, di and trifunctional organo silanes, which lead to the aerogels named as ″orgonosilsesquioxanes″ [89]. Other common organo silica precursors with chemical formula of $(OR)_3SiR'Si(OR)_3$ in which R′ is an alkyl, aryl or alkenyl bridged moieties between two elements of silica, lead to the ″bridged organosilsesquioxane″ products [19, 35, 93, 94]. Alkoxide-based sol-gel synthesis avoids the formation of undesirable salt by-products, and allows a much greater degree of control of the final products. A general overview of the polymerization of the soluble alkoxy silanes is represented below (Figure II. 3)

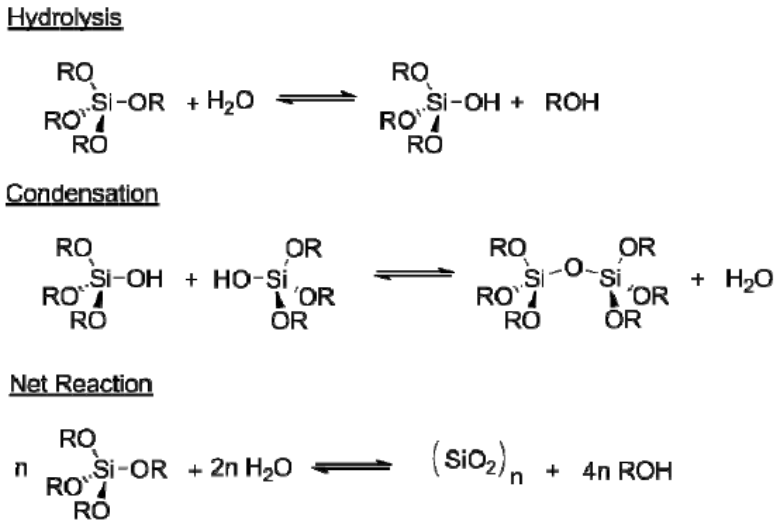

Figure II. 3 Overview of the sol-gel process. Initial step is hydrolysis of alkoxy silanes followed by the condensation of the newly formed silanols. Once the polymerization is initiated, they occur simultaneously.

Sol-gel polymerizations has two primary steps, the first being hydrolysis which converts a halo or an alkoxy to a silanol. The second subsequent step in the polymerization is condensation where two silanols condense forming the siloxane linkage and an equivalent of water. If condensation results from a silanol and an alkoxide, a siloxane bond and an equivalent of alcohol are formed. Once the polymerization is initiated, hydrolysis and condensation occur at the same time. The significant change from the liquid to the solid stage is termed the sol–gel transition. When a sol reaches the gel point, it is often assumed that the hydrolysis and condensation reactions of the silicon alkoxide reactant are complete. During this event, initially, the primary particles are formed, then they aggregate into secondary particles, and finally link together in a pearl necklace morphology [95]. The diagram presented in Figure II. 4 shows the 3D network of porous silica, which is constructed by primary and secondary silica particles.

The kinetics of the sol-gel reactions is slow at room temperature and often requires several days to reach completion. For this reason, acid or base catalysts are added to the system [96, 97]. The amount and type of the used catalysts play key roles in the microstructural, physical and optical properties of the final aerogel product. Acid catalysts can be any protic acid, such as HCl [18]. Basic catalysis usually uses ammonia, or ammonia buffered with ammonium fluoride [42].

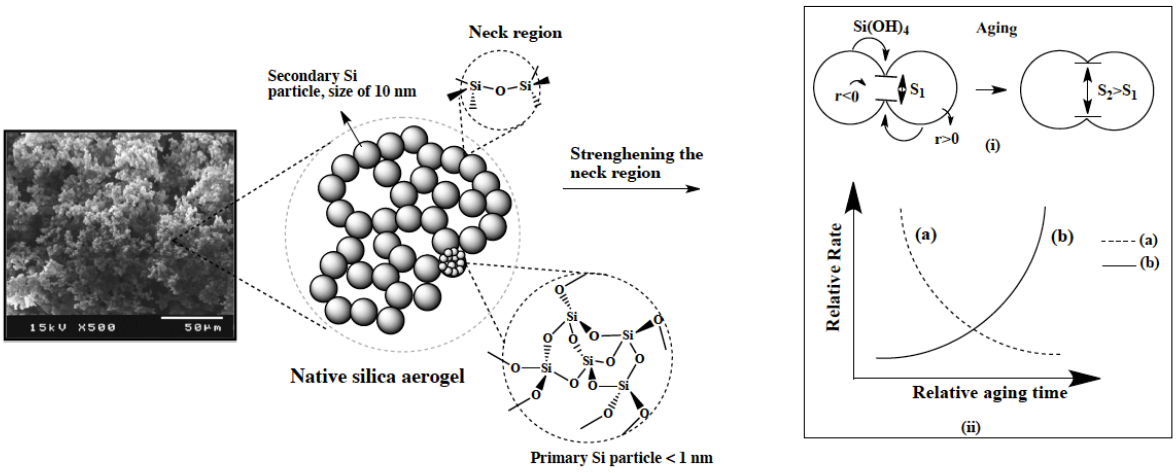

Figure II. 4 Typical SEM image of Si aerogels with schematic representation of primary and secondary silica particles (left); (i) neck growth mechanism of secondary silica particles and (ii) relative aging rate as a function of time for two mechanisms (a, b) (right, Adapted from [98] and [95]).

II. 3 Aging

Silica aerogels comprises highly open structures in which the secondary particles of silica are connected to each other with only few siloxane bonds, therefore, structure of native aerogels is too fragile to be handled. One elegant but time consuming method to strengthen the solid skeleton of a silica gel is to enlarge the connection point between the secondary particles with more siloxane bonds via an ‘’aging process’’ [99-101]. Common aging procedures for base catalyzed gels typically involve soaking the gel in an alcohol/water mixture of equal proportions to the original sol at a pH of 8-9 (ammonia) [102-104]. It has

also been demonstrated that simply performing a thermal aging of the wet gel in water can be a key factor to decrease the gel microporosity before drying [42].

During the aging process shrinkage of the gel is noticed and referred to as syneresis [40]. This shrinkage is the result of further condensation reactions, which form new siloxane bonds near the site at which the two colloids ("the neck") are connected.

Generally, two different mechanisms might operate during aging that affect the structure and properties of a gel: (a) neck growth, from reprecipitation of silica dissolved from particle surface onto necks between secondary particles (Figure II. 4 (i)); and (b) dissolution of smaller particles and precipitation onto larger ones (Ostwald ripening mechanism) [101]. These two mechanisms will operate at different rates, but simultaneously, as illustrated in Figure II. 4 (ii). In addition, the particle clusters are brought in contact by brownian motion and react with each other, increasing the number of siloxane bridges and reinforcing the silica network in neck regions [98]. The most effective and applied methods to overcome the weak mechanical properties of silica aerogels are reviewed in the upcoming section.

II. 4 Drying techniques

The final, and most critical, process in the synthesis of silica aerogels is the drying step. This is when the liquid within the gel is removed leaving only the linked silica network. Three main routes are commonly used for drying: (1) freeze-drying, in which the solvent inside of pores needs to cross the liquid-solid then the solid-gas equilibrium curve; (2) evaporation, which implies the crossing of the liquid–gas equilibrium curve of the solvent; (3) supercritical fluids drying (SFD), in which the supercritical condition is reached without crossing the equilibrium curve of the solvent [73].

Generally, in the freeze drying technique, the solvent in the pores is frozen and then sublimed under vacuum. The material obtained in this way is called a "cryogel". However, due to crystallization of the solvent within the pores, this process leads to cracked or even powder-like silica products with very large pores [42]. But this problem can be attenuated by using solvents with low expansion coefficient and high sublimation pressure, and also by using rapid freezing in liquid nitrogen at cooling rates over 10 Ks^{-1} [105, 106].

The capillary pressure, P_c (Pa), that develops during evaporative drying, causes the shrinkage of the gels. This pressure can be calculated by [42],

$$P_c = \frac{-\gamma_{1v}}{(r_p - \delta)} \qquad (II-1)$$

γ_{1n} is the surface tension of the pore liquid (N/m), r_p is the pore radius (m); δ is the thickness (m) of a surface adsorbed layer.

Evaporation without specific surface treatments [107-110] usually results in "dense" (*e.g.,* > 0.25 g cm^{-3} [109]) and cracked materials, the so-called "xerogels". As explained by Phalippou *et al.* [111], the densification during evaporation comes from condensation of the remaining reactive silica species. When the silica wet gel is subjected to the capillary pressure, the initially far distance surface hydroxyl/alkoxy groups comes close enough to each other to react and generate new siloxane bonds, leading to the irreversible shrinkage due to the inherent flexibility of silica chains. In addition, often the pore structures of xerogels collapse when compared to those of aerogels with the same composition [90, 110, 112-115]. Due to the different existing pore sizes within the gel, a high capillary pressure gradient develops inside the porous structure during the drying, which leads to mechanical damage. The capillary pressure in evaporative drying may reach 100–200 MPa [47], and since the siloxane

bonds within the aerogel monolith are not strong enough to withstand the capillary pressure then it results in shrunk and cracked xerogels [116].

One of the ways to overcome this problem is by strengthening the gel to stand the capillary stresses. This can be achieved by replacing some of siloxane (Si-O-Si) bonds with flexible and non hydrolysable organic bonds (Si-R), through the use of organosilanes as precursors to produce the aerogel network [20, 117, 118]. The organic group will allow the aerogel to spring back to its original wet gel size without resulting in any crack within the gel. Other methods involve changing the capillary force experienced by the network through surface modification of the silica with alkyl groups, and providing a surface with lack of Si-OH groups [119]. Here, the general goal for the surface treatment is to produce a more hydrophobic surface by reacting the surface hydroxyl groups with hydrophobic reagents, such as [$(CH_3)_3$-Si-OR] [120, 121], or hexamethyldisilazane [122, 123]. On the contrary to the surface rich Si-OH gels, during the evaporation of the solvent in the hydrophobically surface treated gels, the alkyl groups repel one another originating the referred spring back of the aerogel [81, 117, 124]. The other methods to overcome the induced capillary pressures involve using low surface tension solvents [125], or adding additives to control the drying process [79]. Evaporation of a low surface tension solvent from the silica wet gel network reduces the capillary pressure when compared to the evaporation of an alcohol, since there is a direct relation between the surface tension and capillary pressure [126] according to equation (II-1).

In the supercritical fluids drying method, the liquid in the pores is removed above its critical temperature (T_{cr}) and pressure (P_{cr}), *i.e.* in supercritical state. Critical pressure is achieved by heating the liquid within a confined space. At its supercritical state, the liquid-vapor meniscus responsible for the gels collapse is eliminated, allowing for crack free monolithic silica aerogels to be produced. From Kistler's initial work using ethanol as a supercritical fluid to

develop silica aerogels, a number of other solvents have been used as seen in Table II. 1 [127].

Table II. 1 Brief list of liquids and their supercritical values used in supercritical drying of silica aerogels.

Liquid	Critical Temperature (°C)	Critical Pressure (MPa)
Methanol	240	8.09
Ethanol	243	6.3
Acetone	235	4.66
Carbon Dioxide	31	7.37
Nitrous Oxide	36	7.24
Water	374	22.04

II. 4.1 Advances in drying approaches of silica aerogels

The supercritical fluid drying method is performed in organic solvents in their supercritical state (generally with the synthesis alcohols and, consequently, near 260°C if ethanol or methanol is used), the process is called HOT process [42]. Perhaps one of the most significant changes to Kistler's original method [74] for the production of aerogels was the switch from alcohol to liquid CO_2 as the solvent of choice for supercritical drying. In 1984, a pilot plant in Sweden for the production of silica aerogel monoliths using the supercritical methanol method was destroyed when a 3000 liter autoclave leaked and eventually exploded [128]. There were no fatalities, but this event prompted the aerogel community to explore alternate routes for drying. To the possible safety issues, these elevated temperatures could also add possible variations in the aging of silica gels. Hunt and coworkers [129] demonstrated that carbon dioxide could be used in place of methanol in the supercritical drying process. By using CO_2, the system only needed to be heated to 32°C instead of 260°C to go supercritical, and the required pressure was reduced slightly as well. The lower temperature in the drying

step and non-flammability of CO_2 made the process safer and cheaper. Therefore, whenever the synthesis solvent is extracted with supercritical CO_2 at a temperature slightly above the critical temperature of CO_2 (~31°C), the process is called COLD process. In this process, the liquid part of the wet gels has to be exchanged with CO_2, either in the liquid state [130], or directly in the supercritical state [131]. Once the supercritical point for carbon dioxide is reached (31°C, 7.37 MPa), the liquid-vapor meniscus disappears and a supercritical fluid is formed. At this point the supercritical carbon dioxide is vented off slowly causing a lowering in the pressure and expelling CO_2 from within the pores of the silica gel. This process continues until all of the carbon dioxide is fully removed from the silica gel. The phase diagram for carbon dioxide can be seen in Figure II. 5 with a probable path that would be followed during the supercritical drying of silica aerogels. This process produces monolithic silica aerogels of rather large dimensions (for the typical cylindrical samples, the diameter is about 1-2 cm and length 5-6 cm), but the dimensions of aerogel are obviously scaled by the sizes of the supercritical drying autoclave [28].

The development of the evaporative drying process to dry the silica wet gels by properly controlling the critical drying parameters (*T*, *P*, evaporation area and times) to achieve a ambient pressure dried (APD) aerogel-like or ‘’xerogel’’ material with final properties comparable with their aerogel counterpart, would be a tremendous potential for scaling-up and cost reduction of such a materials [110, 132, 133]. However, from an economical and large scale production point of view, there are also other items which can be significant in cost reduction of such materials [133]. Especially the cost of the starting silica precursors (normally, sodium silicate is cheaper than silicon alkoxides) and the several processing steps (*e.g.* the washing, the solvent exchange, surface treatment, *etc.*) influence the global cost of the final aerogels or xerogels [75, 107].

Figure II. 5 illustrate the complete aerogel synthesis process with its detailed steps, as explained before. Generally, the silica aerogels are made in two main steps: (1) the sol-gel process (the preparation of an alcogel), (2) supercritical drying. Initially, the alcogel is prepared by promoting the hydrolysis and condensation reactions of silica precursors in the solution with solvent/water/catalysts, based on sol-gel chemistry. During this step, the primary silica particles will be created, and, then, during gelation, the primary particles coalesce and link to each other to form the secondary silica particles (see Figure II. 5), resulting in a rigid three-dimensional network of silica. Then, the prepared silica wet gels can be subjected to different post-gelation treatments before drying, such as solvent exchange, washing and aging. In the drying step, the silica aerogel monolith can be obtained when the solvent inside the pores experience its supercritical condition and is released in this state without introducing any damage to the solid part.

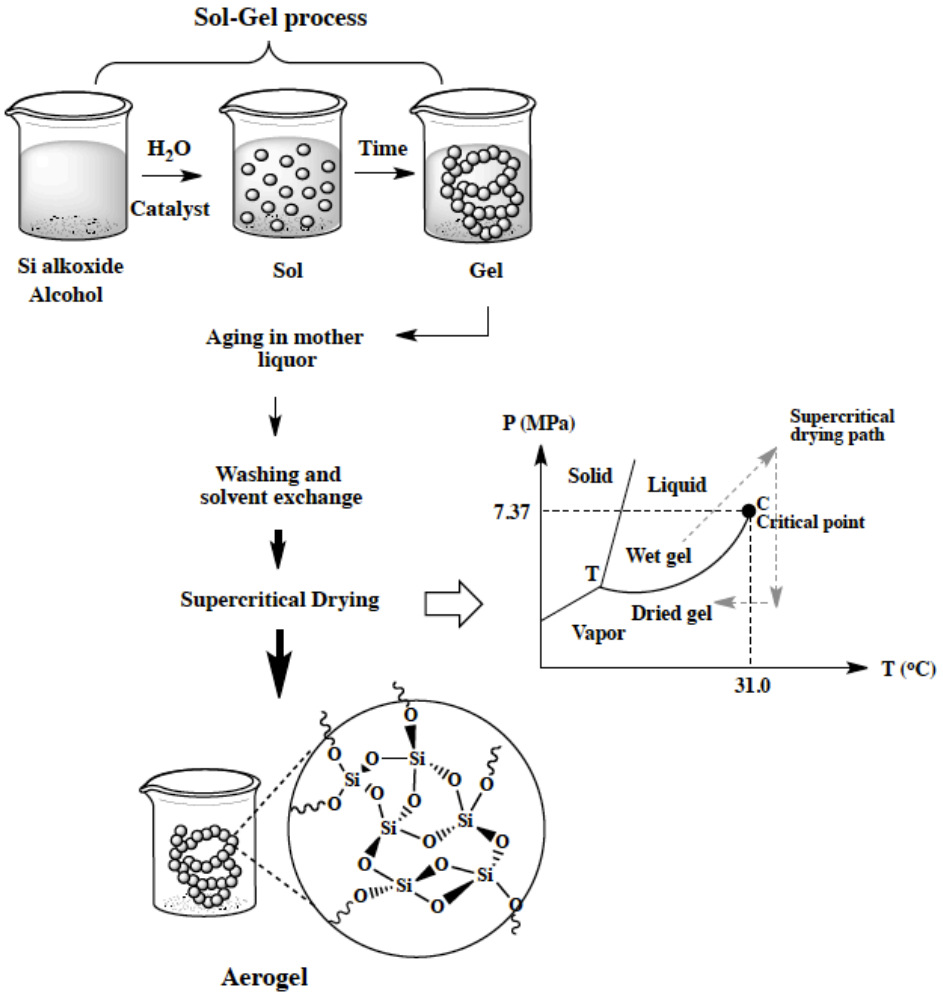

Figure II. 5 Schematic representation of typical sol-gel synthesis procedure.

II. 5 Silica Aerogel Drawbacks

Silica aerogels are fascinating materials, which have been used in several applications as mentioned in the Introduction. In most cases, using silica aerogels in applications is based on their properties rather than their practicality. The two main drawbacks of silica aerogels for their use in potential applications are the cost of production and their extremely weak mechanical properties. Silica aerogels posses a reduced mechanical strength compared to their nonporous analog [134] and the cost for silica aerogel production is expensive and non safe due to the supercritical drying step which is needed in their preparation. The cost of silica

aerogel production while improving the mechanical properties will be addressed in the proceeding Chapter II. However, even if the cost of production for silica aerogels can be substantially reduced, the resulting aerogel is still mechanically weak. By improving the mechanical properties of silica aerogels, they could be used in numerous applications not currently achievable.

II. 6 Development of strong silica aerogels

Silica aerogels are cellular solids with a pearl-necklace-like skeletal network [95]. As indicated in Figure II. 4, the weak points of such structure are the interparticle neck regions [135, 136]. Although the native silica aerogels are sufficiently strong to be handled, their mechanical strength still is not adequate for them to endure and remain monolithic in some practical applications [54]. In fact, their intrinsic fragility that leads to low mechanical strength, imposes severe constrains on different potential load bearing applications of silica aerogels. It was believed that the mechanical properties of silica aerogels could be improved by increasing the amount of connectivity between particles (Figure II. 6). However addition of any material to strengthen the silica aerogel must be minimal to ensure that the physical properties, which made them attractive to so many applications, are retained.

Several techniques have been reported in the literature [28, 29] to reinforce silica aerogel's mechanical properties. The aim of such techniques is to develop aerogels of low density that can be easily deformed and show a capability to absorb shock energy during bending and compression [14, 30]. As stated before, the aging of wet gels leads to mechanically stronger inorganic networks [136, 137], by increasing the strength of the final silica aerogels through dissolution and reprecipitation of silica at the surface of interparticle necks [138]. With this process, an improvement of approximately a factor of two in the modulus of elasticity will be

achieved. But clearly, at the end, the reinforcement agent is still silica and remains a brittle material with low tensile strength.

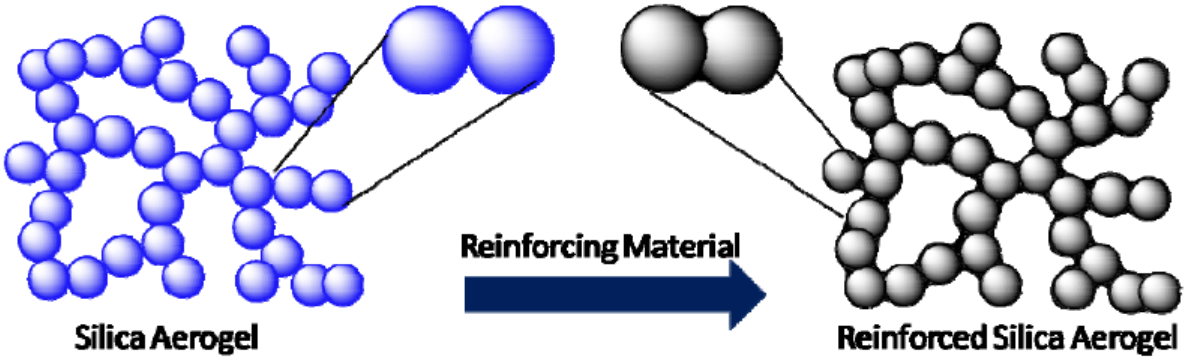

Figure II. 6 Reinforcing the weak necks between the silica particles.

Hybridization of silica aerogels [34, 139, 140] can be an alternative solution for strengthening purposes, by promoting the co-gelation of the silicon alkoxide with hybrid precursors such as poly(dimethylsiloxane) (PDMS). Gels obtained in this way are termed "ORMOSIL" (ORganically MOdified SILica) hybrids. They have a more rubber-like flexibility. With 20 wt% PDMS, they can be elastically compressed to 30% (by volume) with no damage [34].

Compounding of the inorganic network of aerogels with different polymeric systems has been performed by several chemical procedures. This method leads to a dramatic increase of tensile strength and robustness of the aerogels [26]. Moreover, incorporation of various fibrous supporting materials, such as polymeric fibers [141, 142], carbon nanofibers [26], fiberglass [143], *etc*., into the aerogel systems, was also found to be quite effective in improving the mechanical properties of aerogels. Fiber matrix can support the aerogel and decrease the bulk size of aerogel within aerogel–fiber matrix composite [144]. So far,

composites of fiber and silica aerogels have been produced with various methods in order to fortify the structure of silica aerogels.

The proceeding section will address all of above mentioned mechanical reinforcement strategies of the silica aerogels, and are a rather complete and updated literature survey on the subject.

II. 6.1 Structural reinforcement of silica aerogels

Generally, the trifunctional organosilane compounds of the type $RSiX_3$ (where, R = alkyl, aryl or vinyl groups, X = Cl or alkoxy groups) produce flexible aerogels with reduced overall bonding and good hydrophobicity [91, 145], since one of the ends of Si atom contains a non-hydrolysable R group. Due to the presence of this organic group, R, attached to the silica polymer chains, the inter-chain bonding is reduced resulting in an elastic and flexible three-dimensional matrix [19]. Kanamori *et al.* have shown that MTMS-derived gels can have reversible deformation upon compression [146]; Figure II. 7 shows schematically the molecular structure of MTMS-derived silica aerogels. Rao *et al.* [19, 118] studied the elasticity of these aerogels in terms of the Young's modulus (g), using uniaxial compression measurements. Aerogels with high elasticity, flexibility and with Young's modulus as low as 1.094×10^4 Nm^{-2} could be obtained. They attributed the easiness of hydrolysis and condensation reactions to the length of methyl and methoxy groups within the silica precursor, as these are the smallest among all alkyl and alkoxy groups.

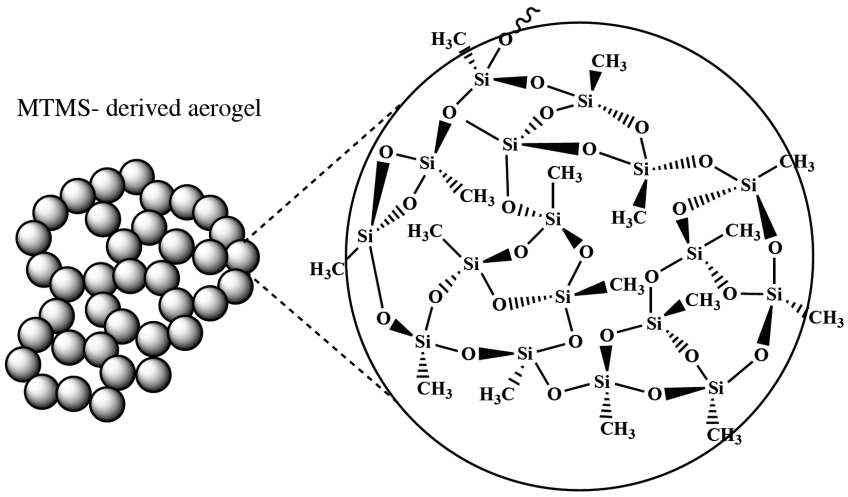

Figure II. 7 Three dimensional network of MTMS-derived aerogels with its detailed molecular structure.

The MTES (H_3C-Si-$(OC_2H_5)_3$) precursor has also been used as a trifunctional organosilane compound to synthesize superhydrophobic and flexible aerogels [20, 147, 148]. In this case, each monomer of the MTES has one non-hydrolysable methyl group (CH_3), as in MTMS, and three hydrolysable ethoxy groups (OC_2H_5). Therefore, only hydrolysable ethoxy groups are responsible for the matrix formation. As the condensation and hence the polymerization progresses, the number of hydrophobic Si-CH_3 groups increases compared to the number of hydrophilic Si-OH groups, leading to an inorganic-organic hybrid silica network which is superhydrophobic and highly flexible and can recover or springs back after compression [20, 118].

Figure II. 8 (a-c) shows the maximum bending possibility for MTES-derived aerogels with different dilutions (*S*=MeOH/MTES) of the silica precursor. Here in, increasing the S molar ratio (MeOH/MTES=19.35), the distance between the reacting silica monomers and oligomers increases. Therefore, higher gelation time and less polymerization degree are observed. In addition, for higher dilution, the silica chains are quite separated from each other

and large empty spaces or pores are formed in the aerogel network, leading to flexible aerogels. On the contrary, at lower dilution of the MTES precursor (MeOH/MTES=6.45), due to the less separation distance between the silica monomers and oligomer chains in the sol, the reacting species can react easily, leading to extensive polymerization in three dimensions, which results in dense and rigid polysilsesquioxane structures [19, 20].

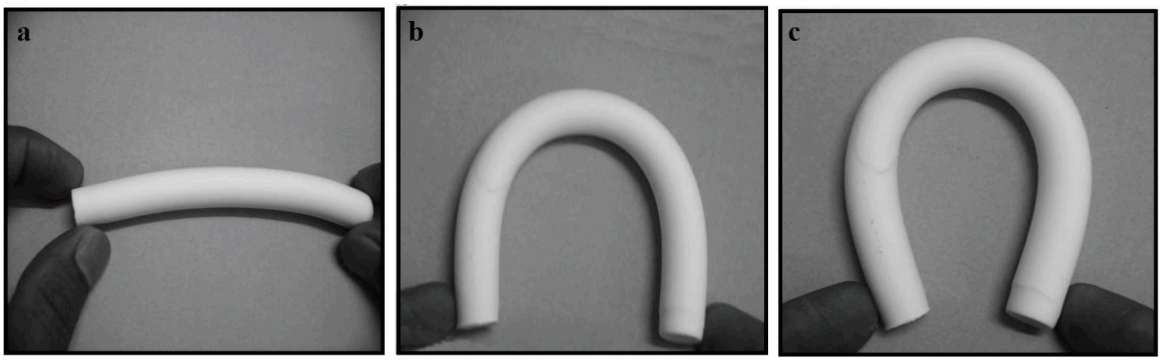

Figure II. 8 Maximum possible bending of the MTES-derived aerogels prepared with a) *S*=6.45, b) *S*=12.96, and c) *S*=19.35. Reprinted from ref. [20], Copyright (2009), with permission from Elsevier.

As it can be seen, the lowest dilution of organosilane leads to less flexibility; on the contrary, the aerogels with the highest S ratio show the highest flexibility. Further bending of these samples resulted in crack formation within the structure. Because of this new property, *i.e.* flexibility, the aerogel can be bent to any shape and acts as a good shock absorber as well [20].

A limited selection of the monofunctional and difunctional organosilane compounds of the type R_1SiX_3, R_2SiX_2 as well as $X_3Si\text{-}R\text{-}SiX_3$ bis silane precursors, in which R is an alkyl or aryl group, are provided in Figure II. 9 [94, 149-152]. In this figure, different organosilica precursors are separated into different categories and, from them; various aerogels with different material properties can be prepared. Some of these silica precursors contain special organic functionalities that carry useful function for surface decoration or surface treatment of

the aerogel for application of one's needs. To a certain extent, the inorganic-organic (hybrid) materials (ORMOSIL) that can be obtained from these precursors, combine the most important properties of their constituents, like high transparency (glasslike), low processing temperatures (polymer-like), sufficient thermal stability (silicone-like), and are easily prepared because of a unique availability of the respective precursors.

Besides the simple metal or silicon alkoxide precursors (for example, TMOS) that, after hydrolysis and condensation, lead to the formation of an inorganic oxidic network with only siloxane (Si-O-Si) bonds, the organo (alkoxy)silanes, depending on what type of functionalities they have, can be used to incorporate polymerizable organic substituents, such as epoxy, vinyl, or methacryloxy groups, into the final aerogel product [29]. The Si-C bonds in such molecules are stable under the mild conditions of sol-gel processing [153].

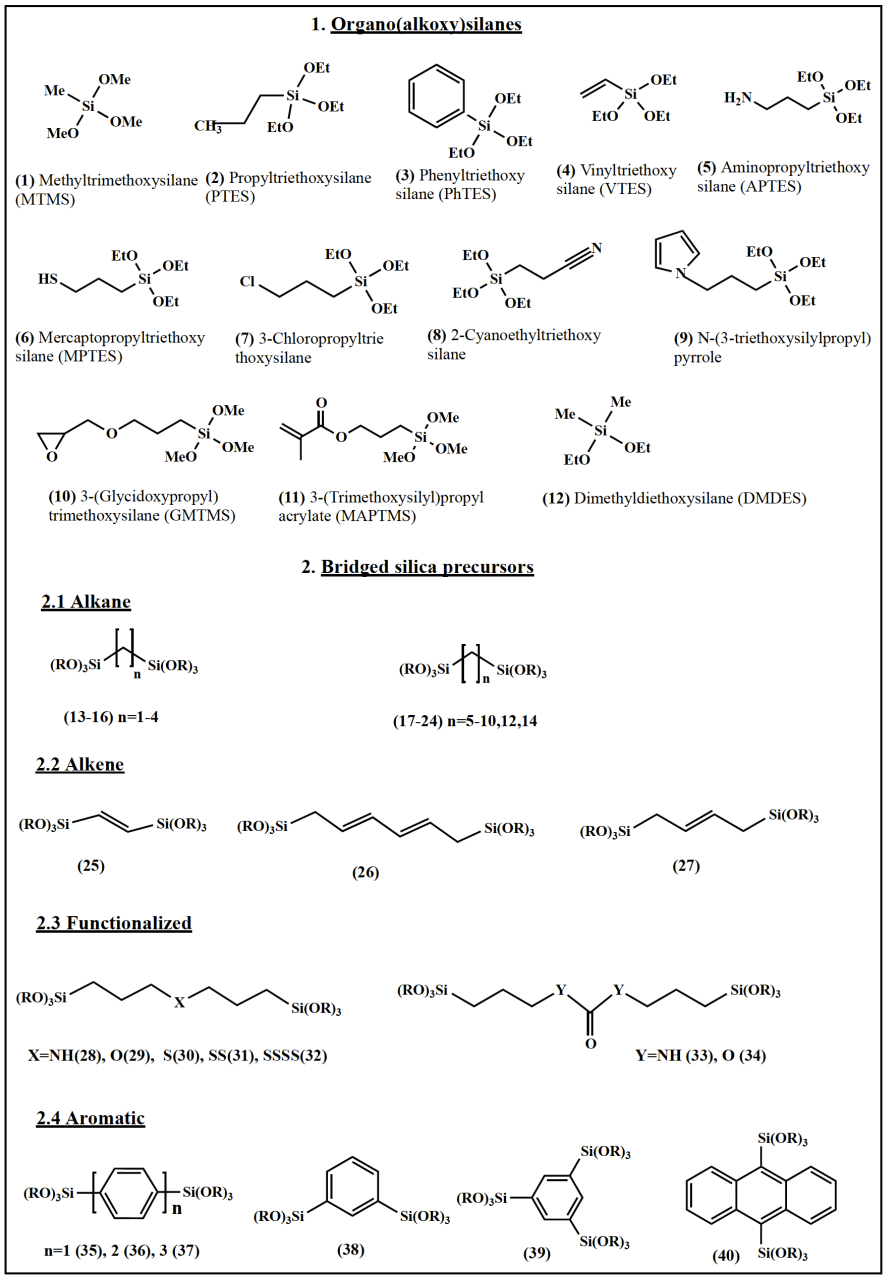

Figure II. 9 Organo(alkoxy) and bridged silanes used as precursors for sol-gel-derived (hybrid) materials.

In addition to hybrid organo (alkoxy) silane precursors, the cross-linking of the silica backbone with more flexible and elastic alkyl bridged bis-silane precursors can improve the strength of the aerogels systematically. For example, as reported by Meador *et al.* [21], a non-cross-linked aerogel made from a combination of TMOS and BTSPD showed complete

recovery after 25% compression, with an approximate modulus of 4 MPa and densities of 0.2 g/cm^3. A high concentration of the disulphide in the formulation yielded lower density monoliths, which recovered completely from as much as 75% compression, as shown in Figure II. 10 a. The inset of Figure II. 10 shows the same sample before, during and after compression with finger pressure. This sample recovered 98% of its original length during the first ten minutes after compression and, after thirty minutes, the recovery was 99.6%.

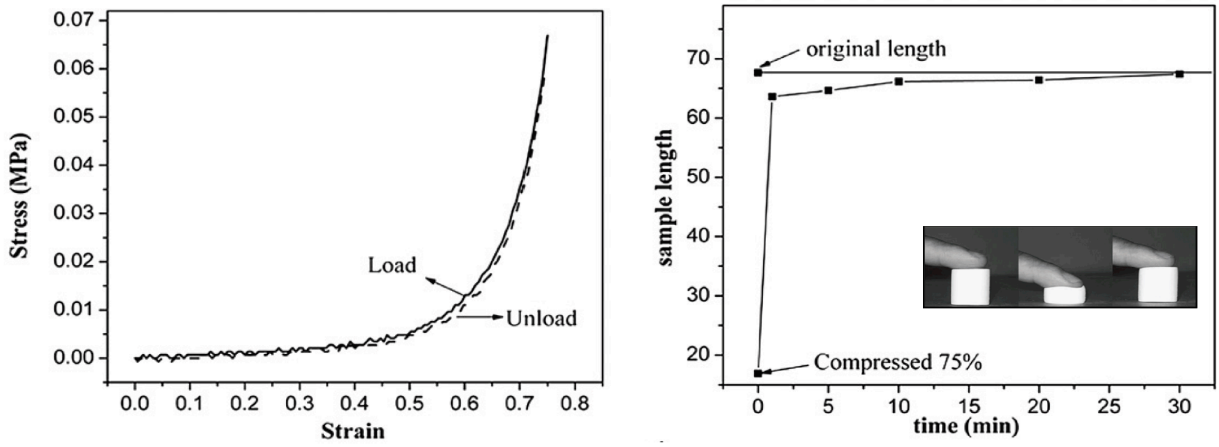

Figure II. 10 a) Stress strain curves of a monolithic sample of aerogel made from TMOS and a high portion of BTSPD b) recovery after compression *vs.* time. The inset is showing the aerogel sample compressed by finger pressure and demonstrating full recovery. Reprinted from ref. [21], with permission from the Royal Society of Chemistry (RSC).

Similar results have been reported by Meador *et al.* [49, 154], for aerogels synthesized by replacing up to 40% of TEOS or TMOS in the silica backbone with the alkyl linked BTMSH. As can be seen from Figure II. 11, the BTMSH reduces stiffness in the silica backbone by replacing some of the more rigid Si-O-Si bonds with flexible hexyl linkages. The resulting aerogels presented a modulus up to 23 MPa and almost complete recovery from a state of 25% compressive strain. The evidence of increasing mechanical performance using hybrid

organic-inorganic bridged alkoxysilanes is consistent with the work of Loy, Shea and co-workers [35, 94, 155], which have examined a wide range of precursors to synthesis bridged silsesquioxanes. Typically, bridged bis-silane precursors allow the pore size control that is directly related to the nature and length of the bridge. Best results for controlling the porosity were obtained using a stiffer structure such as an arylene chain. More flexible bridges such as alkyl chains lead to more compliant aerogels but tended to shrink more, reducing porosity.

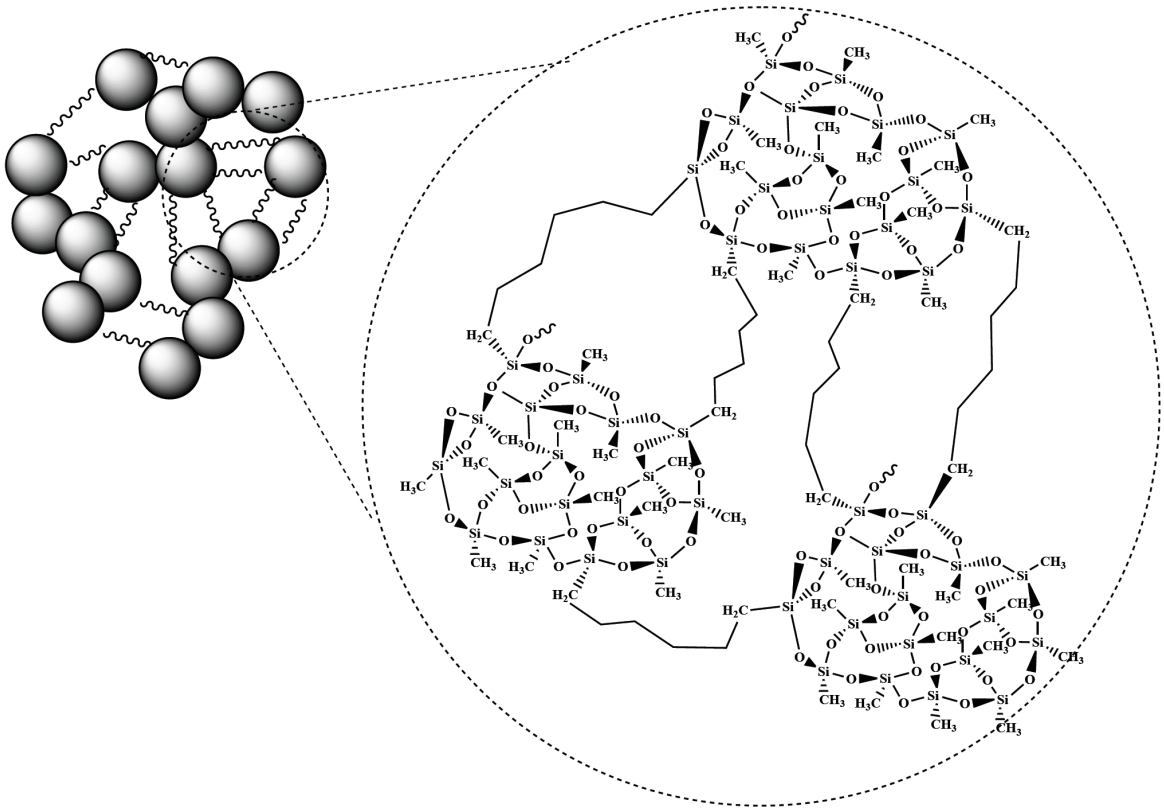

Figure II. 11 Three dimensional network of MTMS/BTMSH-derived silica aerogels with its detailed molecular structures.

More recently, Randall *et al.* [29] examined the relative merit of three types of bis-silane precursors with different lengths of the alkyl groups on epoxy reinforced silica aerogels. As shown in Figure II. 12, this research team applied four types of bridged alkyl linked bis-

silanes and a difunctional silica precursor to which the extended chemical structures are shown in Figure II. 9. In the case of co-gelation of bridged bis-silane precursors with TEOS, the flexible alkyl links/bridges between the secondary silica particles, depending on the size of the bridge, can confer flexibility to the network. All of these precursors improved the elastic recovery of the aerogels with an amount as small as 15% included in silica backbone. Randall *et al.* also reduced the number of Si-O-Si bonds by using a difunctional silane, DMDES, in order to improve the elastic response by reducing the stiffness of the silica network.

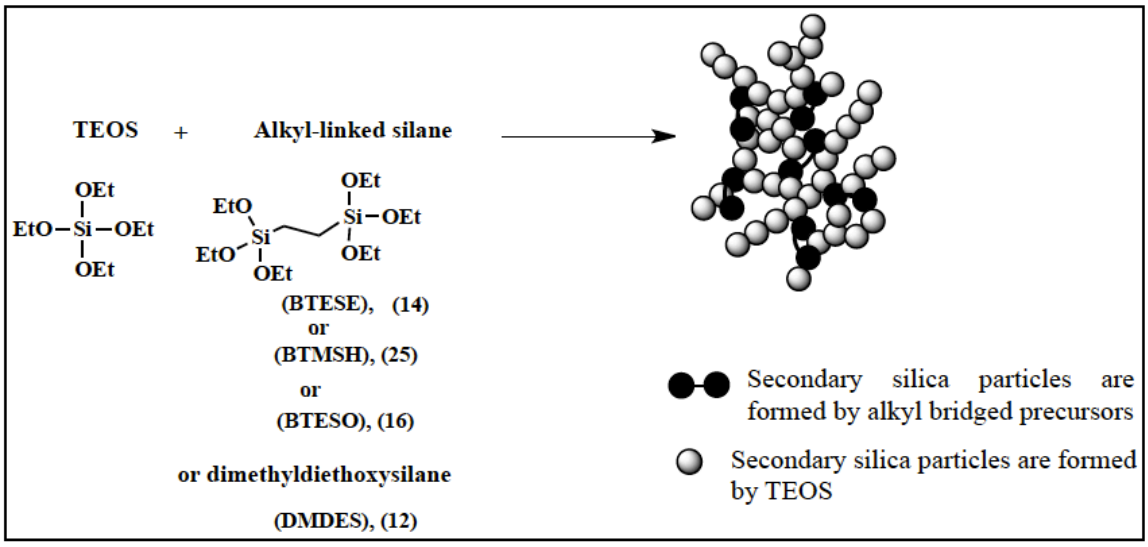

Figure II. 12 Reaction strategy for preparation of non-modified polysilsesquioxane aerogels with incorporation of four types of flexible linking groups in the silica backbone. The chemical structures of the alkyl linked bis-silane precursors are indicated in Figure 8 with their related numbers.

However, additional incorporation of bis-silane precursors (up to 45% of any bis-silane) reduces the compressive modulus. Authors indicated that the hexyl linked bis-silane (BTMSH) is the most effective among the bis-silanes as compared with others in their work. Only BTMSH produced aerogels with high mass yields, indicating complete hydrolysis and

condensation under the reaction conditions they studied. Nearly similar results have been reported by Vivod *et al.* [156], in which the incorporation of the hexane linked precursor (BTMSH) in the silica backbone was found to enhance the flexibility and the strength of the aerogels. The wet gel could be bent easily without any fracturing and this can improve the manufacturability of BTMSH-derived aerogels. This sample also displayed great recovery at higher Si concentrations after compression to 25% strain.

II. 6.2 Polymer reinforced silica aerogels

It has been proved that compounding of silica backbone with polymer is an effective way to increase mechanical strength by as much as three orders of magnitude while only doubling the density over those of native or non-reinforced aerogels [32, 133]. Compounding the silica network with polymer can be achieved by different type of interfacial interaction of secondary silica particles (inorganic parts) with appropriate functionality on the organic polymers. Depending on the chemical relationship between the polymer and the surrounding silica network, polymer/sol–gel composites are placed into two categories: Class I hybrid composite aerogels and Class II hybrid composite aerogels [157-159].

II. 6.2.1 Class I hybrid composite aerogels

The composites that is formed as a result of weak interactions, like van der Waals forces, electrostatic forces, or hydrogen bonding, between the organic and inorganic phases are in the category of this class of hybrid materials [160, 161]. In this type of composite materials, organic molecules, pre polymers or even polymers are embedded in the inorganic matrix being totally independent from each other. These materials are synthesized by carrying out a

number of different routes, *e.g.* the formation of the inorganic network through hydrolysis and condensation of the silica precursors, in the presence of the organic compound or by polymerizing organic monomers in the porous inorganic host. The most prominent examples representing class I are organic dyes or biomolecules incorporated in porous sol-gel matrixes [162, 163]. The guest molecules are physically dissolved together with the precursors of the inorganic host (*e.g.,* TEOS or TMOS) or introduced to the sol state, and become entrapped in the gel that results from condensation and drying of the mixture.

Other examples of this group of hybrids are provided by composites formed upon incorporation of different polymers, such as poly(ethylene oxide) [164, 165], derivatives of nylon 6 [166] and poly(ethyl acrylate) [167], into SiO_2 matrices synthesized by the sol–gel method. Here, in the composites whose organic components have polar groups, the formation of hydrogen bonds between the components of the system [168] is important to understand the nature of the synthesized materials. The hydroxyl groups in the repeating units of the polymer, like ethylene glycol oligomers [165] or poly(vinyl alcohol) [169, 170], are expected to produce strong secondary interactions with the residual silanol groups generated from acid-catalyzed hydrolysis and poly-condensations of the SiO_2 matrix.

Although the resulted hybrid gels possess proper transparency and thermal stability without any phase separation between the two components, there is no particular example from this family of composite with the purpose of mechanical reinforcing of native silica aerogels. Indeed, this class of hybrid materials are traditionally used to improve the very poor mechanical properties of organic polymers such as polysiloxanes polymer (PDMS) with incorporation of an inorganic filler of SiO_2 [171, 172].

Since post-gelation washing is often required in the processing of the silica aerogels, class I hybrid silica composite aerogels are rarely studied. This is due to the existence of weak interfacial bonds between the two phases, and consequent easy leaching of the polymer from

the pores of silica by the extensive solvent exchange, either during the post-gelation washing steps or solvent passing through the gel pores during the supercritical drying [160, 161].

Instead, this class of polymer composite aerogels seems to be straightforward to make mainly xerogel composites through the introduction of the monomer inside the initial sol or by polymerizing of the appropriate monomer in the post-gelation steps. The composites obtained from this method shows a decrease in the elastic modulus with substantial increase (3 times) in their ultimate compressive strength [160].

From a practical point of view, the ambient dried aerogel-like class I composites are advantageous, since they are cost effective and easy to produce. Moreover, the elimination of the post-gelation processing steps is an asset for further mass production of this type of materials [173].

II. 6.2.2 Class II hybrid composite aerogels

Class II hybrid aerogel composites are referred to the composite network in which the interfacial bonding between the organic phase and silica is based on strong covalent bonds. This type of hybrid aerogels were studied by Mackenzie *et al*. [174] that considered the different rearrangement of covalent bonding between the two phases.

Generally, this approach requires molecular precursors that contain a hydrolytically stable chemical bond between the element that will form the inorganic network during the sol-gel processing and the organic moieties. Since, in these materials, the polymer connects points along the skeletal framework of 3D assemblies of nanoparticles, the resulting composites are referred to as polymer cross-linked aerogels. These materials possess the advantages of both organic and inorganic materials and are expected to present unique properties that are different from the individual organic or inorganic materials.

Until now, several polymeric systems such as polyurea, polyurethane, poly (methyl methacrylate), polyacrylonitrile and polystyrene have been used to reinforce silica aerogels [22-24, 26, 175]. In fact, the underlying inorganic framework plays the role of structure-directing agent (template). The mechanical properties improvement is attributed to reinforcement of interparticle necks, which are the weak points of the aerogel skeletal network (Figure II. 6). In turn, the stabilization provided by the cross-linking polymer is attributed to the extra chemical bonds created by interparticle polymeric tethers.

Extending polymer cross-linked aerogel composition to additional polymers, optimization processes for desired material properties and simple manufacturing are currently the focus of attention of several research groups such as Leventis *et al.* [26, 133], and the group led by Meador [29, 32] at the NASA Glenn Research Center.

II. 6.2.2.1 Liquid and vapour phase polymer cross-linking

Native silica aerogels can be reinforced with different organic polymers, starting from the functionalization of secondary silica particle surfaces with appropriate functional groups. The functionalization of the surface of silica particles within the inorganic network can be achieved through co-condensation of the core precursors, namely TMOS or TEOS, with silica precursors containing the special organic functionality in their chemical structures. Then, the polymerization normally can be performed by introducing the organic monomer through the post-gelation solvent exchange and then promoting the reaction of the silica functionality with monomers (Figure II. 13). This multistep liquid-phase based reinforcing approach is quite long due to the solvent exchange process, the slow diffusion rates of monomers in the wet gel and the heating necessary to promote the reaction of the monomers with the silica surface, which is followed by more solvent exchanges and supercritical drying [23, 28, 29, 48, 52, 53,

95, 176-178]. In addition, the monomer is usually introduced into the wet gel by soaking the gel in a monomer solution and, thus, sometimes the monomer does not uniformly diffuse in the gels and, during the replication process, deviations of the aerogel properties are detected [49].

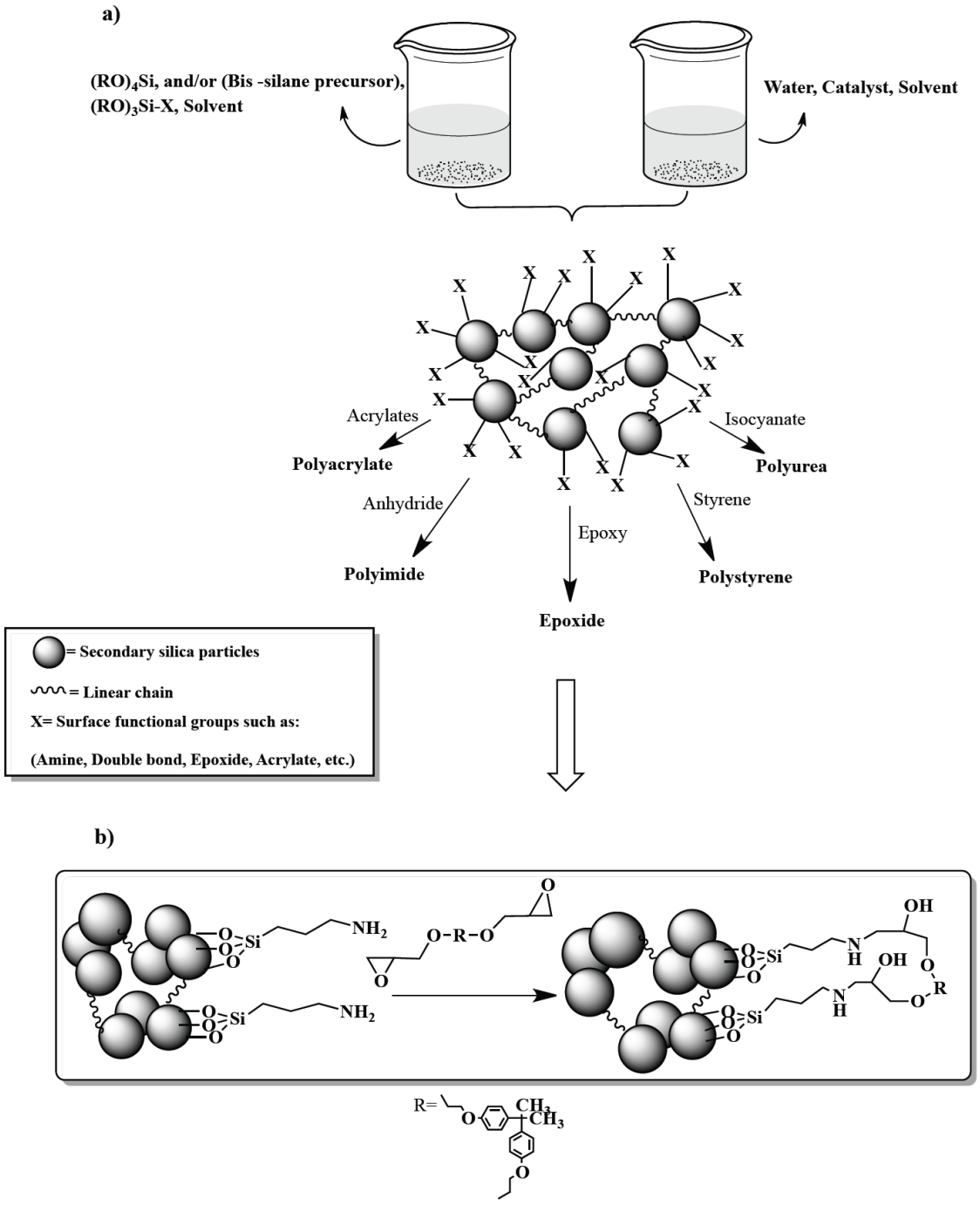

Figure II. 13 a) Concept of polymer reinforcement using reactive groups on the silica surface; b) Epoxy cross-linking of silica aerogels. Inspired in [49].

In order to eliminate these time consuming and tedious post-gelation steps, two effective alternatives to the previous approach can be used. The first alternative is to introduce the organic monomers in the initial sol, which contains the whole silica precursors and gelation

solvent, in order to carry out the procedure in a simple one pot fashion [22, 49, 179]. This method provides the *in situ* formation of inorganic silica network with organic monomer contained in the pores. As in this step the monomers are already present inside the inorganic matrix of the wet gels, the diffusion of the monomer to the gel is not a limiting factor, therefore, the polymerization reaction is more efficient. Moreover, the elimination of time consuming steps of soaking the wet gel inside the monomer solution, in the *in situ* process, makes it more cost effective [54]. Figure II. 14 presents precisely the difference between the two liquid based routes for the development of polymer reinforced silica aerogels.

Very recently, Duan *et al.* [180] established a new one-pot reinforcement strategy with the scope of shorter production time of strong silica aerogels. In this work, firstly APTES end capped polymer chains (Figure II. 15) prepared then integration of polymer to silica gel network was achieved simply via condensation of APTES end groups with TEOS precursors.

In this study a factor of 5-fold increase in compressive modulus with 60% increase in density was achieved with great reduction in time of production of aerogels from 10 days to approximately 4-5 days.

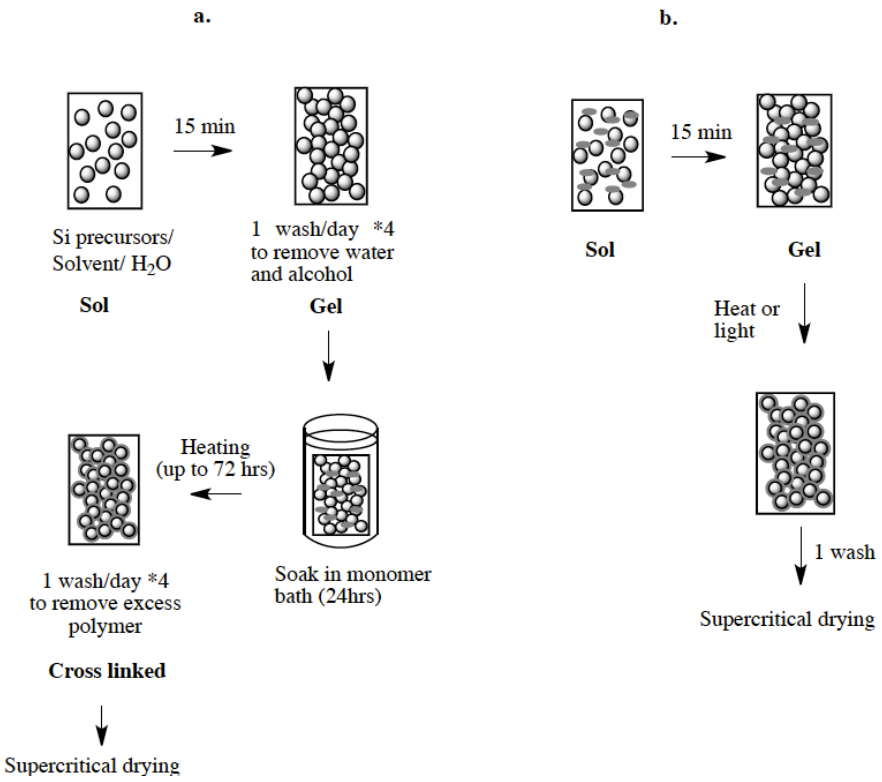

Figure II. 14 a) Traditional method to prepare cross-linked aerogels. Each wash step takes 24 hrs, and heating to cross-link can take as long as 72 hrs (This process require approximately 1 liter of solvent to prepare one ~20 ml cylindrical monolith), b) One-pot synthesis of cross-linked aerogels; the gray counterparts are prepolymers in the sol that are inert to gelation. Once the gel is formed, it can react to initiate cross-linking. After one wash, which removes any unreacted components, the monolith is supercritically dried.

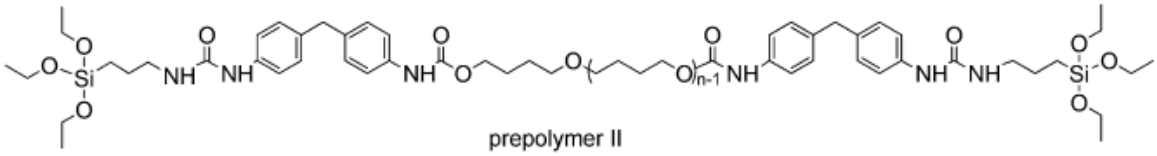

Figure II. 15 APTES-End-Capped Pre-polymer [180].

The other recent approach for eliminating the post-gelation treatment is to cross-link the aerogels through gas phase after being dried supercritically [25, 181]. This can be carried out through the deposition of a desired monomer throughout the pores surface of an aerogel, by means of chemical vapour deposition (CVD) or atomic layer deposition (ALD) [25, 181-183].

Overall, all liquid-phase cross-linking strategies, whether one pot or multi step, cause significant increase in strength (up to 8 MPa) but, on the other hand, they increase the density (≈ 0.5-0.8 g/cm^3) and decrease the surface area (≈ 40-600 m^2/g). The density and then mechanical properties can be well controlled by varying several factors, such as silicon molar concentration in the sol [21, 23, 29, 48, 49, 154, 184], the organic monomer concentration [23, 48, 49, 51, 154, 179], the gelation solvents [154, 184] and so on. The best samples with optimum physical and mechanical properties were selected by some authors through a statistical DoE studies [29, 32].

For the CVD procedures, the density of the silica aerogel composites was in the range 0.095-0.230 g cm^{-3}, and it also could be controlled by variation of the exposure times of the functionalized silica aerogel in the monomer vapour [25]. In this approach, the typical cross-linked aerogels can be 31 times stronger than the original silica aerogels before CVD treatment, with only 2-fold reduction in the surface area.

Different possible polymer reinforcements of silica aerogels, with their detailed chemical approaches, are extensively studied and reviewed within different research groups. Table II. 2 summarize some examples of polymeric systems that have been applied to improve the mechanical properties of silica aerogels by cross-linking. Some of the physical and mechanical properties of the obtained materials are also presented.

II. 6.2.3 Advanced methods for polymer reinforcing of silica aerogels

As outlined in the previous section, the one pot, *in situ*, cross-linking process of silica is efficient for large scale production of these materials and can eliminate the time consuming of post-gelation treatments of the wet gels. But, performing the cross-linking part with hydrolysis and condensation of silica precursors is not always responsive to some kind of

polymerization techniques. In fact, gelation of silica is based on acidic and basic catalyzed ionic processes, and to perform the cross-linking reaction simultaneously it is necessary to have a polymerization system with higher activation barrier than gelation, or performing through non-ionic process like free radical polymerization [133]. The implementation of this procedure for free radical polymerization seems to be effective but still needs further post-gelation thermal or light treatment.

The free radical polymerization can be achieved through modification of silica surface with olefins. From there, the polymerization follows the ‘’grafting to’’ or radical coupling process, in which the coupling of the radicals to the surface of silica aerogels occurs [52]. It can be also performed via surface decoration of silica with radical initiator, followed by polymerization through the ‘’grafting from’’ approach, initiating the polymerization from the surface of silica aerogels [177, 185].

With the modification of the silica surface with Si-AIBN radical initiator (Figure II. 16), Leventis *et al*. [177] applied the ‘’surface initiated grafting from’’ approach for integration of polymethylmethacrylate (PMMA), polydivinylbenzene (PDVB) and polystyrene (PS) in the silica network, with polymerization starting from the surface of the silica aerogel. The radicals were used to initiate the polymerization of vinyl groups grafted to the surface of the silica gel. Although this approach is simple and allows high control on polymer coating around silica and mechanical properties comparable with the ‘’grafting to’’ approach, the polymerization still is uncontrolled, which increases the polydispersity of the polymer.

Table II. 2 Examples of polymeric systems, with the method of cross-linking to silica aerogels and selected properties of cross-linked aerogels.

Silica	Method of crosslinking	Cross linking polymer	Density (g cm^{-3})	Ultimate strength (MPa)	Surface area (m^2 g^{-1})	Reference
Non-modified Silica (Si-OH)	Post gelation washing	Polyurea	0.241-0.564	0.01-4	140-541	[28, 89]
	Gas phase	Poly cyanoacrylate	0.235	- [a]	200	[181]
NH_2-modified	Post gelation washing	Polyurea	0.48	186±22	261	[176]
			0.06-0.523	26.62-261.26	8.3-320	[23]
			0.3-0.954	0.25-1.24	-[d]	[178]
		Poly styrene	0.413-0.768	0.059-0.251	180-393	[53]
		Epoxide	0.21-0.59	0.04-1.9	267-856	[29, 48]
	One pot synthesis	Epoxide	0.198-0.842	1.5-2.7	36-392	[49]
		Polyimide	~0.1	Up to 2.5	240-260	[179]
	Gas phase	Poly (cyanoacrylate)	0.095-0.23	0.021-0.651[b]	522.7-964.2	[24]
VTMS modified	Post gelation washing	Poly styrene	0.122-0.332	0.6[c]	8-750	[52]
AIBN-modified	Post gelation washes & one pot synthesis	Poly styrene	0.2-0.549	0.09-28.86	65.98-668.3	[177]
		Poly methyl methacrylate	0.198-0.807	93.13	46.05-781	
		Poly divinylbenzene	0.27-0.31	0.85	247-731	
	One pot synthesis	polyacrylonitrile	0.177-0.475	-[d]	144-681	[22]

a - The rupture strength increased (32×) to 17.6 N
b - Three-point bend-beam flexural strength
c - Only in 25% strain
d - Not reported

On the other hand, if a significant portion of the initiator remains in the silica matrix, it causes the decomposition of the azo bridged silsesquioxane during the heating of the gels, and this leads to a weakening of the mechanical properties.

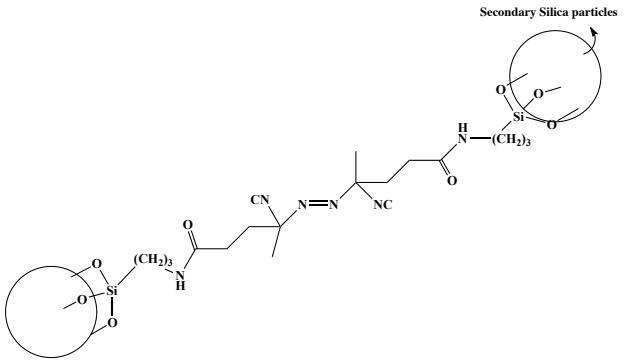

Figure II. 16 Chemical structure of silica wet gels obtained from a bis-triethoxysilane derivative of AIBN. Inspired in [177].

In order to overcome the problem arising from free radical surface initiated reaction, and to allow a greater control on molecular weight of the polymer and, indirectly, on the mechanical properties of the silica aerogels, Boday *et al.* [24] applied a controlled polymerization reaction for cross-linking the surface of silica with PMMA. For this purpose, they implemented the ‘’Atom Transfer Radical Polymerization’’ (ATRP) technique [186], for controlling the molecular weight and polydispersity of the polymer on silica aerogel surfaces. In their approach, initially, the sol-gel processable ATRP initiator was synthesized. Afterwards, as shown in Figure II. 17, the surface of silica was modified with the ATRP precursor through co-gelation with TMOS precursor. Then, in next step, the vinyl polymer grew from colloidal secondary particles of silica via the ATRP process and, after supercritical drying; the polymer covered the surface of the silica network and reinforced it. This approach allows the incorporation of well-defined polymers with a versatile methodology for polymerization with controlled amount of vinyl groups and cross-linkable monomers. The resulted polymer reinforced aerogels comprised polymers with polydispersities from 1.2 to 1.8. The aerogel bulk densities were in the range of 0.177-0.47 g cm^{-3}, and flexural strength ranges from 15.4 to 63.5 KPa, with surface areas in the interval 144-681 m^2 g^{-1}.

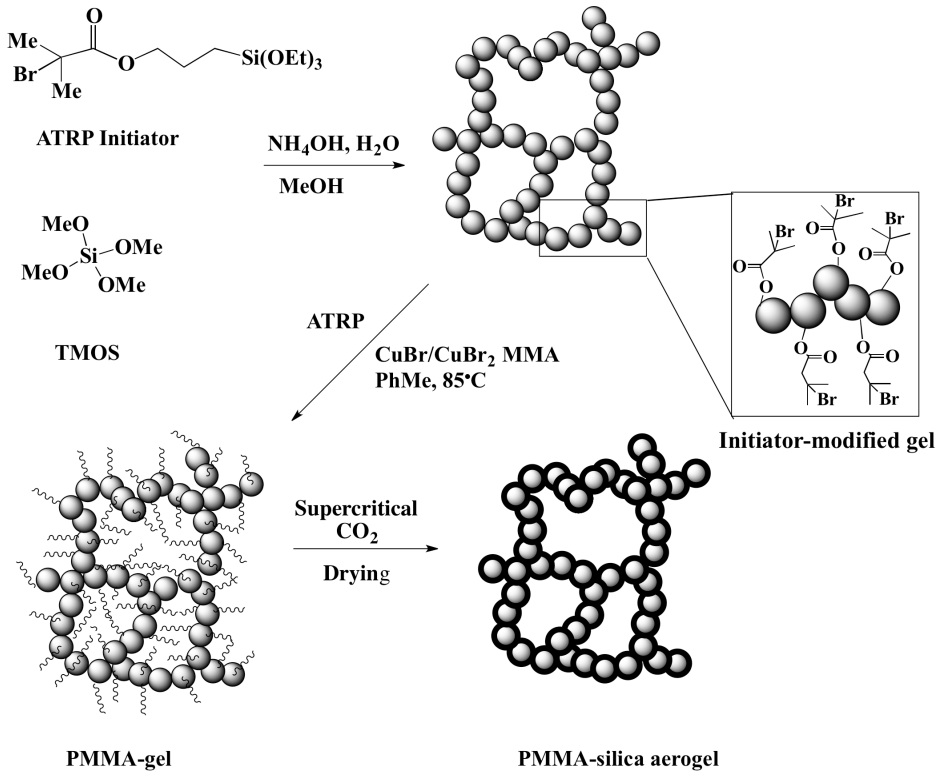

Figure II. 17 Formation of an initiator-modified gel, ATRP growth of PMMA on surface and supercritical drying to afford a silica-PMMA composite aerogel. Adapted from ref. [24].

Recently, Duane et al [187] modified silica network by reacting them with polyhedral oligomeric silsesquioxane (POSS) as a multifunctional reinforcing agents. POSS molecule with phenyl, isobutyl, and cyclohexyl organic side groups and several Si-OH functionalities were incorporated into silica networks via reaction between Si-OH functionalities in POSS molecules and silanes (Figure II. 18). The POSS modified aerogel structures offered significant reduction of polarity and a 3-fold increase in the compressive modulus compared to the native aerogels with negligible changes in the bulk density.

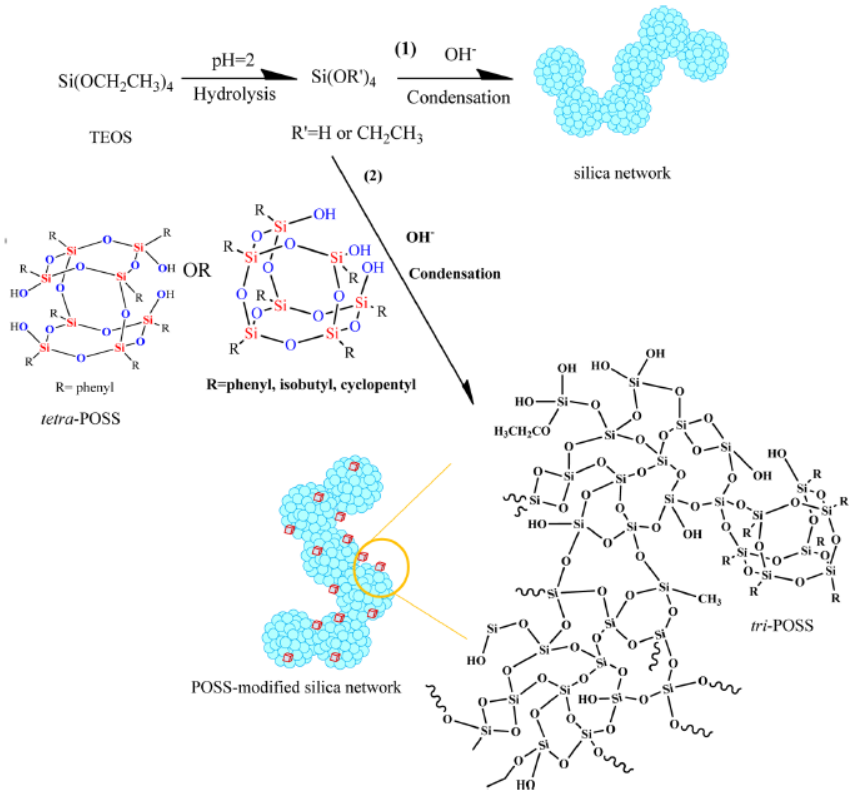

Figure II. 18 Illustration showing reactions leading to silica network formation. Path 1 shows formation of unmodified silica networks, and path 2 shows modification of silica networks by POSS molecules. Illustration shows how a tri-POSS molecule can covalently bond to the silica network [187], with permission.

II. 6.2.4 Cost estimation of polymer silica aerogels

For the production of aerogels with approximately the same physical properties and mechanical strength by different reinforcing strategies, Table II. 3 was built to give a global comparative idea about the cost efficiency to produce a typical cylindrical strong aerogel with 12 cm length, 1 cm of diameter and bulk density of ≈ 0.3 g cm^{-3}. In this table, several issues such as consumption of starting material, amount of solvent, drying conditions and resources (representing mainly the energy needs) and time of preparation (representing the human resources) are compared for different strategies considered in Section II. 6.2. This table may be useful to estimate the cost inherent to each of these methodologies and to choose a certain

route according with the existent resources. It should also be noted that due to the non-consistency between the extracted synthesis/processing/drying information in the literature, the data presented in this table is defined for the production of lab scale aerogels with the conditions that are optimized within the authors' research group.

Table II. 3 Comparison of the required resources for preparation of reinforced silica aerogels/aerogel-like monoliths using different synthesis methodologies (for and aerogel with 12 cm length, 1 cm diameter and bulk density ≈ 0.3 g cm^{-3})

Type of reinforced silica		**Silica precursors/ Other starting materials**	**Total time for preparation (Days)**	**Solvent for post-gelation washing and/or monomer diffusion (Liter)**	**Drying methods**
Polymer reinforced aerogel-like material (xerogel)		Main precursor: 4.47 mL Surface modifier [a]: 1.5 mL Monomer: 5.25 gr	≈5 days	≈1 L	Ambient pressure drying in an oven: a) Electricity – 2-3 days
Class I hybrid aerogels		Main precursor [b]: 4.47 mL Monomer: 5.25 gr	≈5 days	≈0.5 L	SFD: a) Electricity – 4-5 h; b) CO_2 – 51.55 L (STP), 450 mL (40°C, 130 bar) c) Solvent – 120 mL
Class II hybrid aerogels	Multi-step synthesis	Main precursor: 4.47 mL Surface modifier: 1.5 mL Monomer: 5.25 gr	≈5 days	≈1 L	SFD: a) Electricity – 4-5 h; b) CO_2 – 51.55 L (STP), 450 mL (40°C, 130 bar) c) Solvent – 120 mL
	One pot synthesis	Main precursor: 4.47 mL Surface modifier: 1.5 mL Monomer: 5.25 gr	≈3 days	≈0.5 L	SFD: a) Electricity – 4-5 h; b) CO_2 – 51.55 L (STP), 450 mL (40°C, 130 bar) c) Solvent – 120 mL
	Gas phase	Main precursor: 4.47 mL Surface modifier: 1.5 mL Monomer: 5.25 gr	≈4 days	≈0.1 L	SFD: a) Electricity – 4-5 h; b) CO_2 – 51.55 L (STP), 450 mL (40°C, 130 bar) c) Solvent – 120 mL

[a] It is assumed that silica surface modifier contributes 20 ml% of total silicon.
[b] This technique may require less silica precursors, since the surface modification of silica surface is not so crucial, therefore less silica precursors are used.

II. 6.3 Additional approaches to strengthen silica aerogels

Mechanical strengths of silica aerogels have also been improved using polymer nanoparticles (PNP) which are functionalized with reactive alkoxysilanes [188]. However, the strength is only improved at very high loadings of the PNPs. The size of the PNPs are large, on the scale of 100 nm and the cross-linking of the silica only furthered with the limited number of alkoxysilanes on the surface of the PNPs, without significant increase in the particle connectivity. Silica aerogels have also been prepared by templating aerogels during the sol-gel polymerization, where the aerogel is prepared from sol-gel polymerizations with methyl triethoxysilane [146], the addition of reactive silanes to the sol-gel polymerization [189] and even fiber reinforcing [141]. However, none of these approaches have resulted in the strengths achieved by the polymer cross-linked silica aerogel composites.

II. 7 Summary and conclusions from literature

Tailoring the underlying silica backbone structures with more flexible silica precursors, compounding the three-dimensional network of silica structure with different polymeric systems and integrating a low percentage of different fibers in the silica network, not only improves the strength of the aerogels, but also, in most cases, their elasticity [32]. In general, increasing the amount of polymer cross-linker leads to a dense and stiff structure of silica and weakens the thermal insulation properties [177]. Section II. 6.2 and Table II. 2 summarized a few major advancement in the synthesis and reinforcing of silica aerogels.

A few conclusions can be drawn from the published work on aerogels, as presented below:

1. Silica aerogels can be reinforced by cross-linking with organic compounds such as urethanes (isocyanate), epoxies, *etc.* Acrylate and methacrylate derivatives in particular

are a good choice since they are readily polymerized and they have not been investigated extensively to improve mechanical properties of silica aerogels.

2. An alkyl-linked bis-silane, bis(trimethoxysilyl)hexane, has shown to increase elastic recovery in polymer reinforced aerogels. However additional studies on this type of aerogels compared to the aerogels containing aryl bridged bis-silane precursor in their structures is required for a better understanding of the role of the alkyl/aryl moieties on the physical, mechanical, thermal and insulation properties of this type of aerogels.
3. Replacing some of the network siloxane (-Si-O-Si-) by a rigid spacer of aryl-linked bis-silane has been also shown to control the size of porosity and probably cause open structures with large pore volume. Large mesopore volume in turn would be in favor of thermal insulation performance of aerogels, however larger quantity of these groups might cause some rigidity in the silica network. Developing aerogels by insertion of aryl linkage between silica particles at optimal quantity and investigating their final material properties compared to the silica having alkyl linkage is a possible point of interest exploited here.
4. It was felt that gelation and reinforcement if achieved in one-pot synthesis could reduce the total time of the process. Therefore, it is anticipated any nonuniformity of the reinforcement induced by slow poly mer chain diffusion in post-gelation reinforcements step could be avoided. The present work was motivated by the later needs and implement on-pot strategy of synthesis.
5. In recent years, there is a growing number of researchers that focused in the low energy and cost effective development of aerogels in order to make the large scale or mass production and commercialization of this material possible. In this context, the replacement of costly and risky supercritical drying process by sub-critical ambient pressure drying condition can be an effective solution in this context. The combination

of reinforcing of silica gels with polymers and simultaneously extra pos-gelation treatment by submerging silica wet gels in low surface tension solvent prior to drying would be a possible solution to avoid capillary pressure inserted by alcoholic solvents upon drying. Therefore, this strategy is a possible solution for a facile development of crack free aerogel in various sizes and geometries, when the size of wet gels does not fit with supercritical drying chamber/cell.

6. Due to the trade off between aerogels properties, optimization studies using statistical design of experiment (DOE) are a possible way to have materials with balanced and optimized properties without scarifying specific main properties to improve other desired material properties.
7. Based on the literature surveys, the silica-polymer aerogels synthesized by means of controlled polymerization technique has not been investigated yet. It was felt that by controlling the grafting ratio and molecular weight of polydispersed polymer grown on the silica particles' surface, the main properties including bulk density, mechanical properties of silica aerogels can be controlled and, therefore, somehow a structure-property relationship can be established. This work was also motivated by this strategy and is a contribution to the mechanical reinforcement of aerogels by initiating the polymerization from the silica surface by conducting controlled polymerization technique.

Chapter III. Synthesis of lightweight polymer-reinforced silica aerogels with improved mechanical and thermal insulation properties for space applications.

This Chapter comprises the work published in Microporous and Mesoporous Materials 197 (2014) 116-129, by: Hajar Maleki, Luísa Durães, António Portugal.

III. 1 Introduction

From the previous work on improving the mechanical properties of silica aerogels the greatest improvement was achieved by the reinforcement with polymers. It has also been shown that adjusting the nanoskeleton of silica aerogels using different silica precursors can lead to improved mechanical properties, mesoporosity and thermal conductivity.

In the present work, the general goal is also to synthesis strong polymer reinforced aerogels with reasonable mechanical strength, densities and thermal conductivities as low as possible in order to meet the requirement for aerospace applications. In order to compensate for the increase in the backbone thermal conductivity due to the cross-linking with polymer, we changed the microstructure pattern of the silica aerogels by co-gelation of the silica backbone with the alkyl-linked bis-silane 1,6-bis(trimethoxysilyl)hexane, BTMSH, and the aryl-linked bis-silane 1,4-bis(triethoxysilyl)-benzene, BTESB. Recently, Randall *et al.* [29] investigated aerogels made by different alkyl-linked bis-silane precursors with different lengths of the spacer groups (bridges), in order to tailor the elastic properties of the reinforced aerogels. The purpose of this research was to promote flexibility/elasticity in the aerogel as well as to achieve higher compression strength by the polymer reinforcement. They indicated that the hexyl-linked bis-silane BTMSH, was the most effective of the bis-silanes tested due to the results of higher mass yield and elastic recovery. However, no special attention was given to

thermal conductivity of this type of aerogels. On the other hand, until now, there is no report in the literature focusing an the relative merit of a bis-silane type precursor having an aryl spacer, when compared to other types of bridged bis-silane. Loy *et al.* and Shea *et al.* [35, 94, 153] made extensive studies on arylene-bridged polysiloxanes and concluded that, aryl-bridged precursors lead to the aerogels with less shrinkage and more controlled porosity when compared to the aerogels derived from alkyl-linked bis-silanes. However, they did not make any systematic comparative report about their mechanical and thermal insulation properties.

The particular focus of this work is the synthesis and mechanical reinforcement of silica aerogels with alkyl and aryl moieties, in order to study the role of the underlying silica backbone on the resulting properties of aerogels in a single type of polymerization.

The BTESB precursor contains a rigid aryl group that does not favour the elasticity of the aerogel. In the present work, we introduced this precursor in a very low concentration (up to 10 mol% of the total silicon), in order to develop aerogels with open porous structures, which favour higher thermal insulation performance. A significant improvement in compression strength was obtained by polymer cross-linking. In order to react the inorganic silica backbone with an organic component (multi-functional methacrylate), we modified the surface chemistry of the silica aerogels with methacrylate-containing silica precursors, through co-condensation of core silica precursors namely TMOS (Tetramethylorthosilicate) and aryl or alkyl linked bis-silanes with TMSPM (3-(trimethoxysilyl)propyl methacrylate). Figure III. 1 presents the proposed molecular structures of nonreinforced surface modified silica aerogels with the three different underlying silica structures prepared in this work. The selected organic monomer is a multifunctional methacrylate, which can cause extensive branching and reinforcement. Therefore, an increased compressive strength of the aerogel monoliths is expected with an approximately constant overall intrinsic flexibility of the silica

backbone. Since, the tri-methacrylate cross-linker is soluble in methanol (gelation solvent), we added the organic monomer to the gelation solvent in the initial step of the sol preparation.

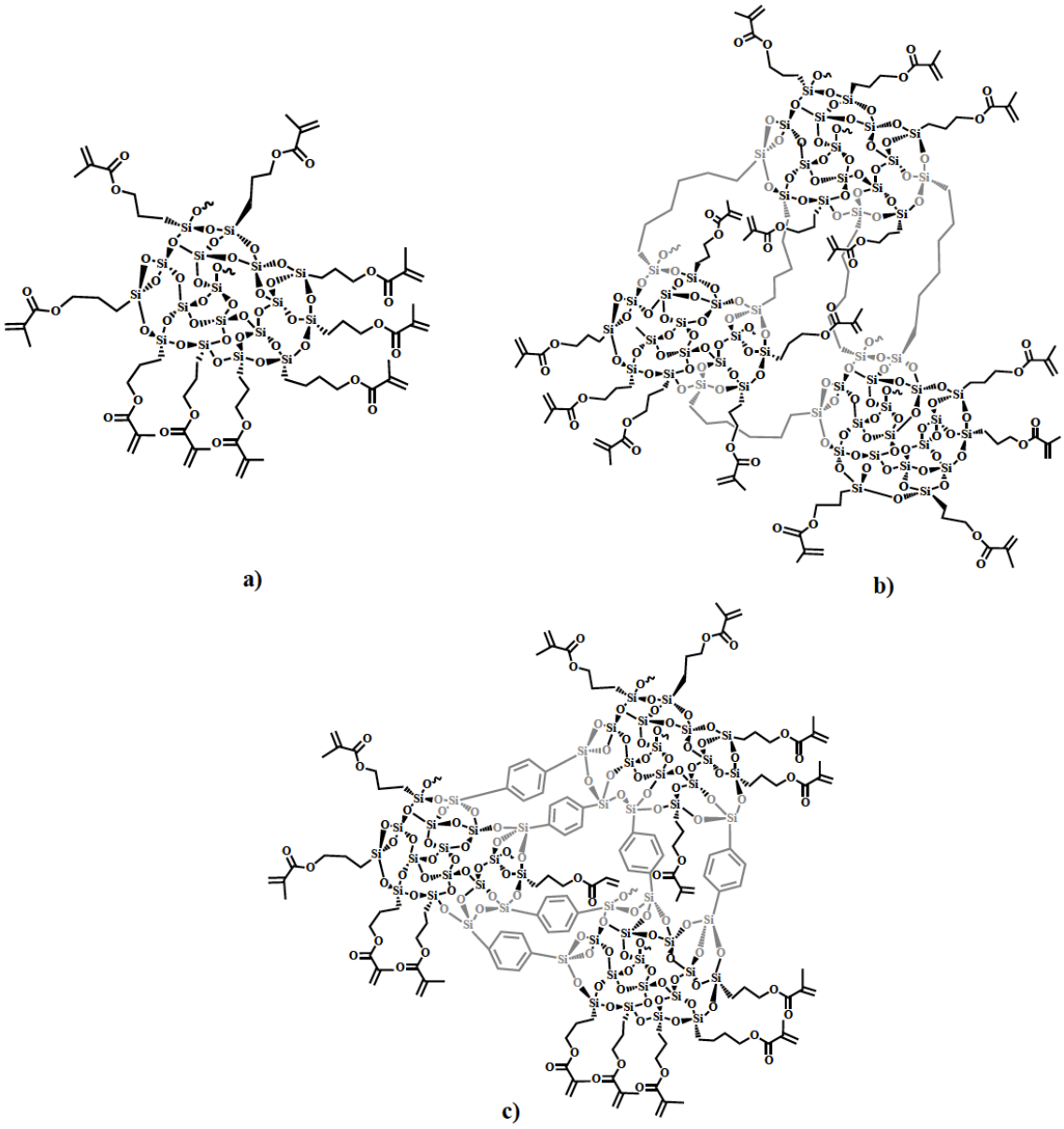

Figure III. 1 Three proposed molecular structures of methacrylate-modified silica aerogels: a) methacrylate-modified aerogel without bridging groups ([Bis-silane]=0%), b) methacrylate-modified aerogel with a part of the total silicon derived from BTMSH, c) methacrylate-modified aerogel with a part of the total silicon derived from BTESB.

Then, polymerization occurs after the sol-gel process by applying a post-gelation thermal treatment. Such a one pot strategy leads to a significant simplification in the synthesis of silica composites and reduced the total preparation time of silica monoliths to approximately two days, which is a drastic reduction when compared to the multistep traditional approaches to prepare isocyanate and styrene cross-linked silica aerogels [49, 52, 177, 190].

Additionally, the presence of the monomer inside of silica gel monolith causes less consumption of the solvent during the post-gelation treatment, therefore to some extent leads to less energy and raw material consumption [55].

In this study, we evaluated the effect of different critical factors on some selected physicochemical properties of the resulting aerogels. Such an experimental design was a starting point to understand the relation between the variations of each factor and the target properties of the silica aerogels for further exploration.

III. 2 Experimental

III. 2.1 Materials

Tetramethylorthosilicate (≥99%; TMOS), 3-(trimethoxysilyl)propyl methacrylate (98%; TMSPM), ammonium hydroxide (NH_4OH; 28-30 wt% solution), methanol (MeOH), ethanol (EtOH), tris[2-(acryloyloxy)ethyl]isocyanurate, 2,2′-azobis(2- methylpropionitrile) (98%; AIBN), 1,4 - Bis(triethoxysilyl)-benzene (96%; BTESB) and acetone were purchased from Aldrich. 1,6 - Bis(trimethoxysilyl)hexane (98%; BTMSH) was purchased from Cymit. All reagents were used without further purification.

III. 2.2. Methods

III. 2.2.1 General

Variables used in this study include the bis-silane type (BTMSH, BTESB), the mole fraction of the total silicon derived from BTMSH and BTESB (note that these precursors contribute with two silicon atoms in every molecule, and the rest of the silicon is derived from TMOS and TMSPM). By keeping the amount of silicon derived from TMSPM as 20 mol% of total silicon for the whole formulation, the amount of silicon derived from BTMSH varied from 0 (named as aerogel without bridging group), to 20 and 40 mol%; in the aerogel derived from BTESB, the amount of silicon from this procedure had values of 0, 5 and 10 mol% of the total silicon.

The amount of Tris[2-(acryloyloxy)ethyl] isocyanurate cross-linker (tri-methacrylate) was another variable, given as mole fraction to TMSPM. It is assumed that each tri-methacrylate cross-linker molecule reacts with the methacrylate groups of three TMSPM molecules via radical polymerization. Hence, a [Tri-meth]/ [TMSPM] molar ratio (R) of 0.3 is stoichiometric, whereas ratios of 0.6 and 2 represent an excess of monomer.

For the water/total silicon mole ratio, r, a value of 2 is normally considered as a stoichiometric value for hydrolysis and condensation of TMOS [42]. However, an excess of water is usually needed to complete the reaction. In this study, r was kept constant at a value of 4 for all formulations. Table III. 1 summarizes the defined parameters of this study, with their levels, and the specific nomenclature used in this paper.

III. 2.2.2 Preparation of polymer-reinforced silica wet gels

To illustrate, a typical procedure is outlined for a formulation with total silicon concentration of 1.3 mol/L in the sol, a TMSPM Si fraction of 20 mol %, a BTMSH Si fraction of 40 mol% and the tri-methacrylate monomer in a 0.3 to 1 ratio to TMSPM (Run: B_40_*R*_0.3)-see Table III. 2.

Table III. 1 Synthesis parameters of reinforced silica aerogels**.**

Parameters	Levels	Nomenclature
Bis-silane types	BTMSH	B
	BTESB	Bz
	-	Nb
R=[Tri-meth]/[TMSPM] Molar ratio	0.3	R_0.3
	0.6	R_0.6
	2	R_2
[BTMSH] Si mol%	0%	Nb
	20%	B_20
	40%	B_40
[BTESB] Si mol%	0%	Nb
	5%	Bz_5
	10%	Bz_10

A solution of 1.52 mL (10.56 mmol) of TMOS, 1.74 mL (10.56 mmol) of BTMSH, and 1.23 mL (5.2 mmol) of TMSPM was cooled to below 0°C in an ethanol mixed dried-ice bath (Solution 1). Solution 2 was prepared by adding 12.9 mL of gelation solvent (methanol), 0.73 g of Tris[2-(acryloyloxy)ethyl] isocyanurate monomer, 1.9 mL of H_2O (r=4), 0.7 mL of NH_4OH and 0.07 g of AIBN (formulated to 10 wt% of the organic monomer). The two solutions were mixed and poured into two propylene cylindrical molds, nominally with 17.2 mm in diameter. The gels were formed within 5 min to 2 hours depending on the formulation. After aging for 24 hours, the wet gel was demolded and placed in a cylindrical reaction flask, containing enough ethanol solvent to cover the gel and the same concentration of initiator

used in the gelation step. The sample was refluxed at 70°C, for 6 hours, to promote free radical polymerization of organic monomers inside the pores of the wet gel with silica surface functionalities. After cross-linking, in order to remove residual water and ethanol, the samples were washed three times with the gelation solvent, giving an 8 hours interval between each washing step, and, then the cylindrical wet gels were introduced to supercritical fluid extraction chamber to dry.

III. 2.2.3 Preparation of nonreinforced silica aerogels

The nonreinforced aerogel for the same proportion of silica precursors was prepared following a procedure similar to that described above. In this case, the addition of the monomer and radical initiator to the Solution 2, as well as the polymerization reaction step were eliminated. After the gelation of the samples and 24 hours aging, they were demolded and washed three times with the methanol. After, the wet gels were dried using supercritical CO_2 fluid extraction under the conditions explained in following section. Figure III. 2 present briefly the whole chemical procedure to develop cross-linked and non-cross-linked aerogels with a representative synthesized wet gel and cross-linked aerogel sample.

III. 2.2.4 Diagram of the supercritical drying (SCD) system

The silica aerogels used in the above experiments were prepared by SCD with carbon dioxide (CO_2) as the supercritical solvent. The diagram below (Figure III. 3) represents the design of the supercritical drying system.

The system contains a pump for the CO_2, a pump for the solvent, a pressure cell to place the sample, several regulating valves and a means for heating and maintaining pressure in the system.

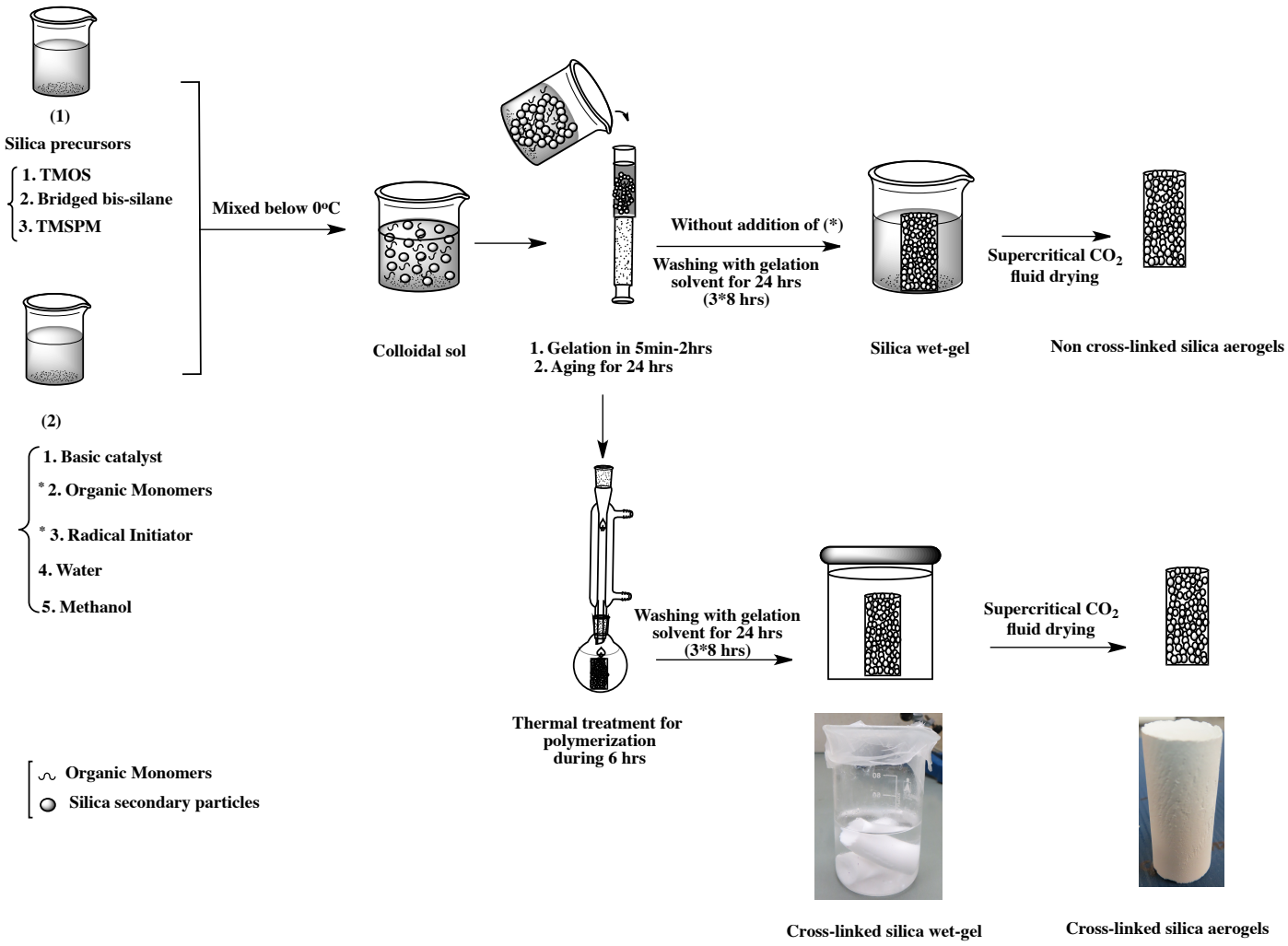

Figure III. 2 Practical approach for the synthesis of polymer-reinforced and nonreinforced silica aerogels.

Drying of the silica gels involves dealing with several important valves, in which, each valve is carrying out the role of the regulation of the flow of the solvent or CO_2 during pressurizing and depressurizing steps.

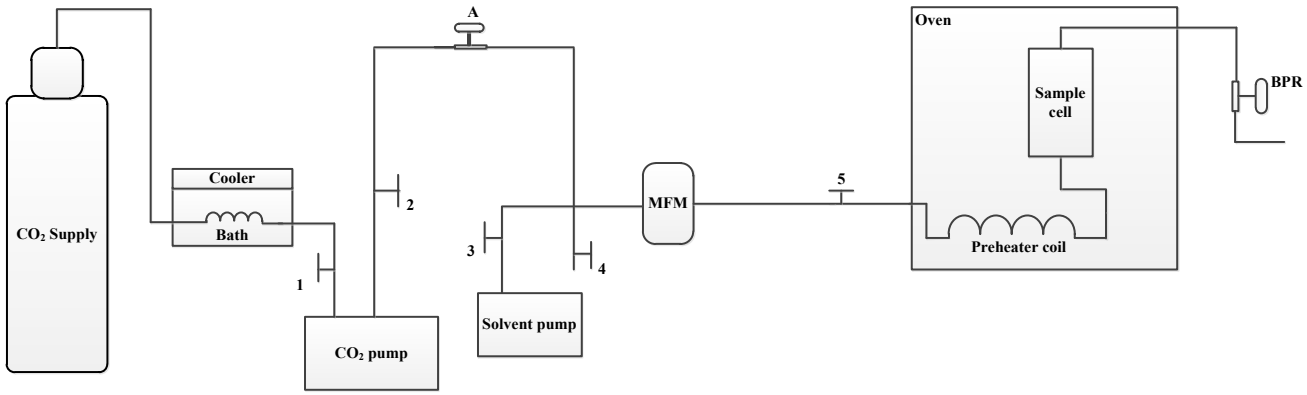

Figure III. 3 Diagram of SCD system.

Basically, during the flux of the solvent through the system and switching to the CO_2 passing, valves 2, A and 3 need to be carefully regulated. Valve 1 and 5 are permanently open. Carbon dioxide (CO_2) is pumped as a liquid, usually below 5°C, therefore a cooling bath (*JULABO*) or circulator is mounted in the system before the pump head of CO_2.

The pump of solvent (*KNAUER*) operates at a maximum flow rate of 15 mL/min and maximum pressure of 150 bar. The pressure and flow rate of the solvent can be adjusted by choosing the desired values by function buttons and display on the pump. The pump for the CO_2 is a pneumatic pump (*k-1900*) operating at a maximum pressure of 1000 bar and equipped with air pressure gauge and regulator for compressed air.

The silica wet gels are placed inside of the cylindrical sample vessel, which has approximately 50 cm^3 of volume. The vessel is made of stainless steel and is manufactured to resist the gas or solvent pressure. The sample vessel must be heated, which is accomplished by placing it inside an oven. In terms of CO_2 flux in the system, CO_2 is cooled before pumping it to maintain liquid conditions, and, then heated after pressurization.

The pressure in the system is maintained from the pump right through the pressure vessel by a back-pressure regulator (BPR). Heating of the BPR must be supplied, as the adiabatic

expansion of the CO_2 results in significant cooling. This is problematic, if the water residue is present in the system, as it may freeze and cause blockage in the system.

III. 2.2.5 SCD Procedure for Silica Aerogel Preparation

To use the above SCD system the following procedure was followed. Before drying the sample with $scCO_2$, the cylindrical silica wet gel samples were carefully placed in the sample cell by initially introducing the sample in another cylindrical open-ended glass tube.

The thick metal back of the cell is screwed tightly into place and is set vertically in the oven, as shown in Figure III. 4. Primarily, all system' s valves related to the flow of CO_2 must be closed and all valves in path of the methanol solvent flow (valves 3 and 5) should be opened to wash the silica wet gels. In this way, we can be certain of the purification of monoliths and improve the flow of CO_2 due to the extensive solubility of CO_2 in the methanol. Normally, the solvent passes through the system at 125 bar and at a mass flow rate of 2 mL min^{-1}. The flow rate of solvent is regulated with function buttons in the solvent pump while the BPR valve regulates the pressure.

Figure III. 4 Sample vessel/cell.

Unreacted silica precursors and organic residues are eliminated by passing the solvent through the monoliths for 1 hour at constant temperature of 50°C. Afterward, the solvent flow is stopped and the system is depressurized by slowly opening the BPR valve. When the cell pressure in the digital counter is fixed at 0.5 bar, the valve 3 completely closed and instead valves 1, 2 and A opened followed by closing the BPR thoroughly to pressurize the system with supercritical CO_2. The CO_2 cylinder should be opened slowly and followed by the opening of the emergency shut off valve. Before adding the liquid CO_2 to the cell, the flushing valve in the pump head should be opened to check the flow of CO_2. The slight pressure of smoky and icy CO_2 can be felt by placing the finger over the valve. By slowly opening the regulator for compressed air in the CO_2 pump, the pressure of the CO_2 in the cell reaches the supercritical values. However, the system is set for a pressure above the critical pressure of CO_2 to increase the diffusivity of CO_2 in the methanol, which is present in the silica wet gel pores. When the pressure and temperature are both above the supercritical point of CO_2 (50ºC, 130 bar), the sample is exposed to the flow of supercritical CO_2 for 90 minutes, having a mass flow rate of 5 mL/min and a CO_2 volume of 51L (STP).

In the final step, the flow of CO_2 in the system is interrupted by closing the regulator for compressed air in the pump followed by the CO_2 shut off valve closed on the cylinder. The evacuation of the CO_2 from the cell is accomplished by opening the BPR valve at a constant rate. Once the CO_2 is completely removed, the processing for the preparation of silica aerogels is complete. At this point the system is cooled back to 20ºC and the cell sample is opened.

III. 2.3 Characterization techniques

Solid ^{29}Si and ^{13}CNMR spectra of the aerogels were obtained by using an *Inova 500 spectrometer* using a 4 mm solids probe with cross-polarization and magic angle spinning at 11 kHz.

The bulk density (ρ_b) was determined by measuring the weight and volume of the sample. Dimensional shrinkage (%) is taken as the difference between the diameters of the aerogel monolith and of the 20 mL syringe mold (nominally 17.2 mm). He picnometry (*Accupyc 1330*, *Micromeritics*) was used to measure the real (skeleton) density of the samples. Combining the information of the skeleton and bulk densities, it is possible to evaluate the porosity of the samples. In addition, we used the Nitrogen gas adsorption (*Accelerated Surface Area and Porosimetry ASAP 2000*, *Micromeritics*) for determination of the specific surface area, pore size distribution, pore surface area and pore volume of the material. Before the analysis, the sample was outgassed at 60^{o}C in vacuum (10^{-5} bar) during 24 h, to remove adsorbed species. In the analysis, volumes of the adsorbed nitrogen at five different relative pressures (0.05 to 0.2) were taken at 77 K, to obtain the specific surface area by the BET theory. The desorption isotherm and the BJH theory were used for the porosimetry measurements.

Scanning electron microscopy (SEM) (*JMS-5310*, *JOEL*) was used to observe the materials microstructure. Due to the low electrical conductivity of the highly porous silica-based samples, an Au film was deposited on their surface, using the PVD (Physical Vapor Deposition) technique during 20 s.

For transmission electron microscopy (TEM), the specimens have been prepared by cleaving a small section with a razor blade, and then attaching this section to a copper-mesh TEM grid.

Grids were visualized with a microscope (*JEOL JEM 1400),* operated at 120 kV. Much of the specimens were too thick for analysis, but the thin edges were electron transparent.

The thermal conductivity of the reinforced aerogels was measured using a transient method (*Thermal constants analyzer TPS 2500 S*, *Hot Disk*). The sensor is clamped between two identical disc shaped pieces of the sample, which have a diameter of 1cm and thickness of 0.5 cm (properly cut from the cylindrical aerogel samples). This analysis was carried out at 20ºC and the equipment presents a reproducibility and accuracy over 1% and 5%, respectively.

Thermal gravimetric analysis (TGA) was performed using a TA model *TGA-Q500* instrument with a heating rate of 10°C min^{-1}, from room temperature to 600°C in a nitrogen atmosphere. This equipment allowed the evaluation of the weight contribution of the cross-linker in the materials. In addition, a simultaneous differential thermal analyzer (SDT), *SDT-Q600*, from *TA*, was used to obtain the complementary DSC curves, in order to better discuss the nature of the thermal phenomena (endothermic or exothermic). The analyses in this equipment had the same operation conditions as the TGA analyses.

For the mechanical test, samples were cut with dimensions ratio of 2:1 (length: diameter), and were polished to make sure that top and bottom side were smooth and parallel. The compression test was conducted following the *ASTM standard D695-02a*. All tests were done at nominal room conditions with a stroke speed of 1.3 mm/min.

III. 3 Results and discussion

Resulting properties of the synthesized polymer-reinforced and nonreinforced aerogels monoliths under different preparation conditions are presented in Table III. 2 and Table III. 3 respectively.

For each formulation in Table III. 2, two independent replicates were performed, and the

density and thermal conductivity of all obtained aerogels were measured. Comparing the results shown in Table III. 2 with those on Table III. 3 it can be seen that the density in the aerogels has been influenced by the type and concentration of the bis-silane as well as by the cross-linker concentration (in the reinforced aerogels).

Mechanical strength of aerogels was improved by introducing bis-silane precursors for the reinforced (Table III. 2) and nonreinforced (Table III. 3) materials. It can also be seen that cross-linked aerogels have improved in terms of structural integrity (or mechanical properties) compared to the nonreinforced counterparts. Basically, in terms of BTMSH based aerogels and aerogels without bridged-bis-silane precursor in their underlying silica structure, the mechanical properties improvement always is accompanied by an increase in the network connectivity and, consequently, an increase in the density and thermal conductivity. While, in terms of BTESB based aerogels with comparable density, it has been found that despite of the macroscopic and microscopic mechanical strength improvement upon cross-linking, the initial thermal insulation performance of native aerogels has been retained or, in most of cases, to some extent has been even improved. Therefore, this observation suggests the profound influence of the type of underlying silica and cross-linker on the aforementioned properties.

A deeper discussion of these results is carried out in the next sections.

III. 3.1 Chemical characterization

The chemical structures of prepared reinforced and nonreinforced silica aerogels have been confirmed by solid ^{29}Si NMR and ^{13}C NMR. Figure III. 5 shows the proposed cross-linking strategies to obtain the silica aerogels of this study as well as the schematic expected chemical structures.

Table III. 2 Measured properties of polymer reinforced aerogels.

Sample	Density (g cm^{-3})	Shrinkage (Diam.%)	Average Elastic Modulus (kPa)	Thermal Conductivity (W m^{-1} K^{-1})	Average Max. Stress at break (kPa)
Nb_*R*_0.3	0.173 0.189	9 10	1.73	0.044 0.046	22.8
Nb_*R*_0.6	0.183 0.187	12 18	0.93	0.0548 0.0512	137.0
Nb_ *R*_2	0.290 0.240	17 20	3.33	0.0938 0.0925	257.0
B_20_*R*_0.3	0.141 0.162	5 8	0.95	0.044 0.047	25.0
B_20_*R*_0.6	0.197 0.188	8 11	0.93	0.052 0.050	32.2
B_20 _*R*_2	0.271 0.314	14 12	6.77	0.053 0.053	400.0
B_40_*R*_0.3	0.220 0.213	14 12	2.74	0.065 0.067	213.0
B_40_*R*_0.6	0.220 0.192	11 14	2.27	0.067 0.068	248.0
B_40_*R*_2	0.390 0.330	15 16	5.96	0.089 0.085	270.0
Bz_5_*R*_0.3	0.129 0.143	6 10	1.11	0.039 0.042	17.7
Bz_5_*R*_0.6	0.144 0.149	11 15	1.17	0.039 0.043	87.8
Bz_5_*R*_2	0.314 0.318	13 13	5.42	0.051 0.053	131.0
Bz_10_R_0.3	0.167 0.163	12 12	1.44	0.039 0.038	10.7
Bz_10_*R_0.6*	0.179 0.175	14 13	0.74	0.049 0.048	78.7
Bz_10_*R*_2	0.250 0.295	10 12	3.61	0.050 0.054	279.0

Table III. 3 Measured properties of nonreinforced aerogels.

Sample	Density (g cm^{-3})	Shrinkage (Diam.%)	Average Elastic Modulus (kPa)	Thermal Conductivity (W m^{-1} K^{-1})	Average Max. Stress at break (kPa)
Nb	≈0.243	28	-[a]	-[b]	-[a]
B_20	0.192	15	1.98	0.050	32.1
B_40	0.185	10	1.68	0.057	10.0
Bz_10	0.145	20	-[a]	0.051	-[a]

a. Samples are too fragile for measurement of this property.
b. Samples lose their monolithic structure, which hinders the measurement of their thermal conductivity.

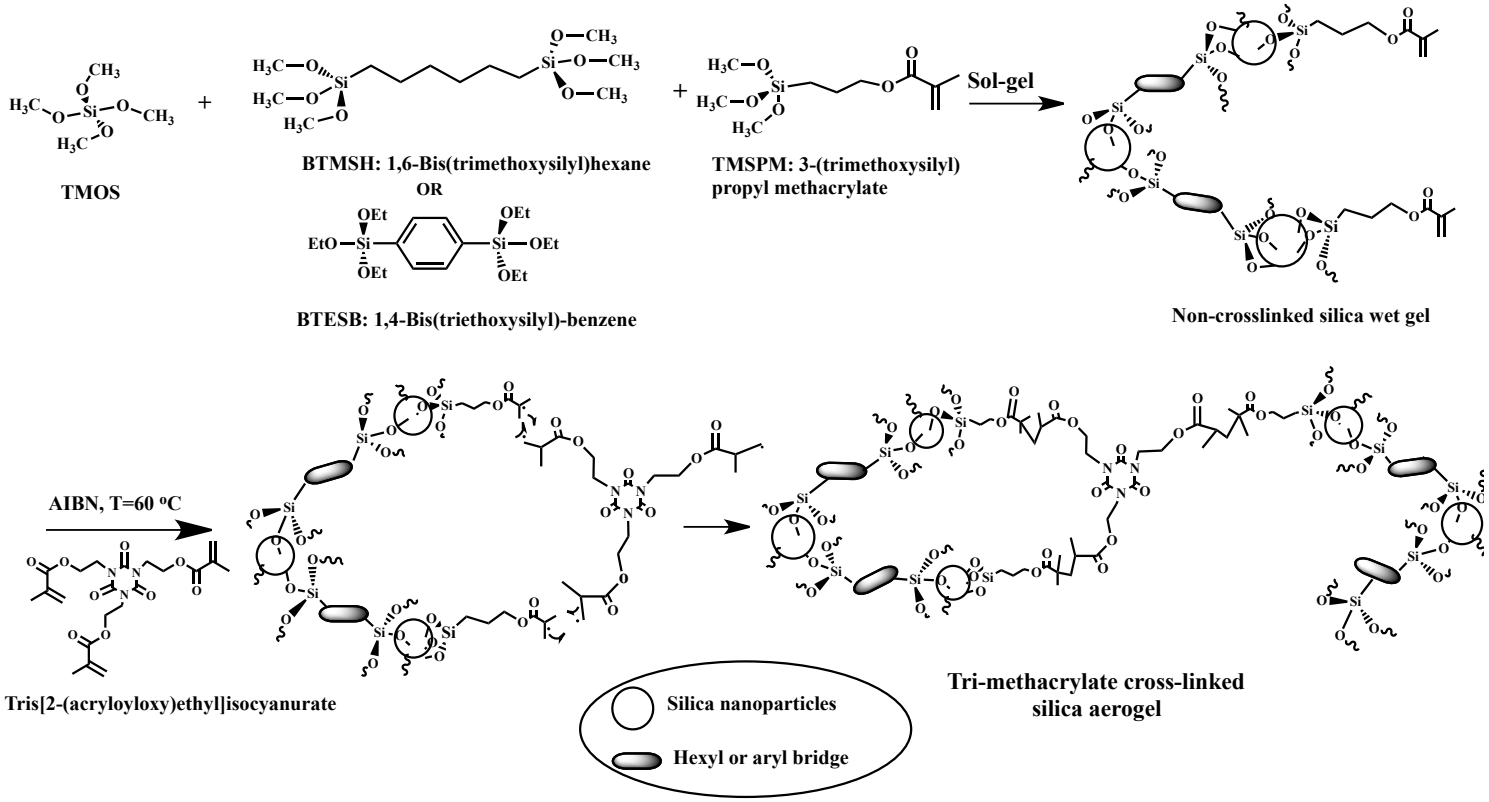

Figure III. 5 Proposed cross-linking reaction for silica aerogels with different underlying silica structures.

Solid ^{29}Si NMR spectra of selected reinforced aerogel samples are shown in Figure III. 6, along with that for the sample prepared from plain TMOS only. As shown in Figure III. 6a, TMOS-derived silicons appear at -110 ppm (Q_4, small peak), -100 ppm (Q_3) and -95 ppm (Q_2), which correspond to the formation of four, three and two Si-O-Si bridges, respectively

Figure III. 6b shows the spectrum for monoliths without BTMSH or BTESB. Two broad peaks are observed for TMSPM-derived silicon, a peak at -69 ppm (T_{3M} peak) and at -61ppm (T_{2M} peak). The peak T_{2M} integrates about half of the area of the peak T_{3M}, indicating that 2/3 of TMSPM silicon atoms had completely reacted. Spectrum of Figure III. 6c belongs to the silica aerogels 40 mol% of silicon derived from BTMSH. In this spectrum, the three broad additional peaks are due to the silicon derived from BTMSH groups. Fully reacted BTMSH derived silicon (T_{3B}) appears at -67 ppm, while the T_{2B} peak appears at -58 ppm and the T_{1B} appears at -49 ppm [52]. Due to the strong overlapping of T_{3B} and T_{2B} peaks with T_{3M} and T_{2M}, it is difficult to figure out the extent of reaction of the silicon atoms for BTMSH. However, assuming the same extent of reaction for TMSPM as spectra b and subtracting the T_{3M}, T_{2M}, it can be deduced that the area of the T_{2B} peak is to some extent larger than T_{3B}. Therefore, it can be concluded that more than half of BTMSH silicon atoms are not fully reacted. Figure III. 6d, shows the spectrum for monoliths with 10 mol% of silicon atoms derived from BTESB. Two broad and low intense peaks are observed for BTESB-derived silicons, a peak at -78 ppm (T_{3Bz}) and other at -71 ppm (T_{2Bz}) [191]. The T_{2Bz} peak is strongly overlapped with the T_{3M} and has slightly larger peak area than T_{3BZ}, which indicates a non-complete reaction of BTESB within the aerogel monoliths. Representative solid ^{13}C NMR spectra of selected prepared aerogels are shown in Figure III. 7a-d. The spectrum of Figure 5a belongs to the nonreinforced silica aerogels prepared with 40 mol % of silicon derived from BTMSH. The broad peaks at 121 ppm, 134 ppm and 174 ppm belong to the aliphatic double bond and carbonyl bonds of silica surface methacrylate group derived from TMSPM. The methylene groups from hexyl link of BTMSH appear at 12, 22, 32 ppm (Figure III. 7b-c), which are masked with other aliphatic carbon due to the polymerization. Figure III. 7b and Figure III. 7c belong to the formulations with the same underlying silica as in the spectrum of

Figure III. 7a, but with cross-linking with tri-methacrylate, using *R*=0.3 and *R*=2, respectively. Clearly, the aliphatic carbon double bonds due to the silica surface methacrylate disappear in both spectra. Instead, a peak at 150 ppm and the intense and overlapped peak at 171 ppm, due the insertion of cyanurate groups and the carbonyl bond of tri-methacrylate monomer, show up.

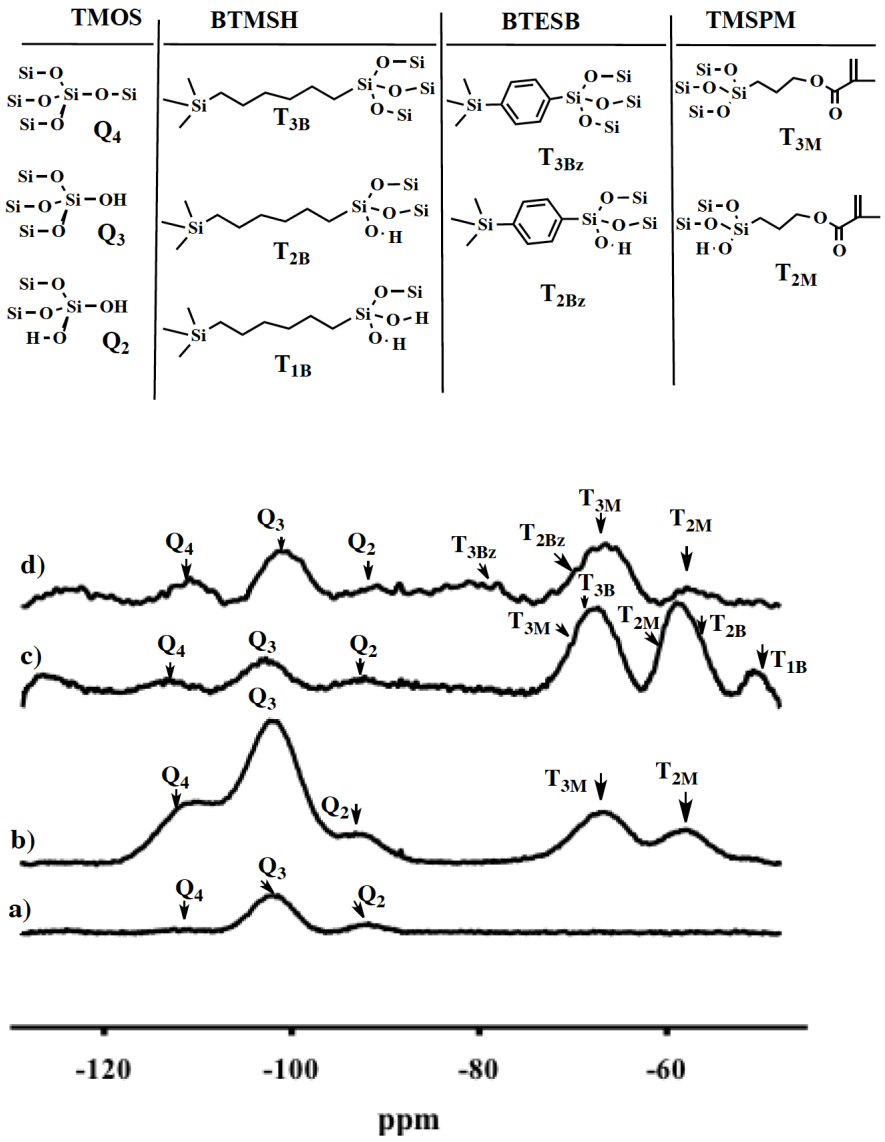

Figure III. 6 Solid ^{29} Si NMR spectra of aerogel samples formulated from a) TMOS alone, b) Non-X-TMOS 80 mol% + TMSPMA 20 mol% (Nb), c) Non-X-TMOS 40 mol%+ BTMSH 40 mol% + TMSPMA 20 mol% (B_40), d) Non-X-TMOS 70 mol% +BTESB 10 mol% + TMSPMA 20 mol% (Bz_10), (X=cross-linked).

The spectrum at Figure III. 7b indicates that the reinforced aerogel with R=0.3 still has some unreacted carbon double bonds, due to the lower addition of cross-linker to the silica surface, and the intensity of the characteristic peak of cyanurate is very low.

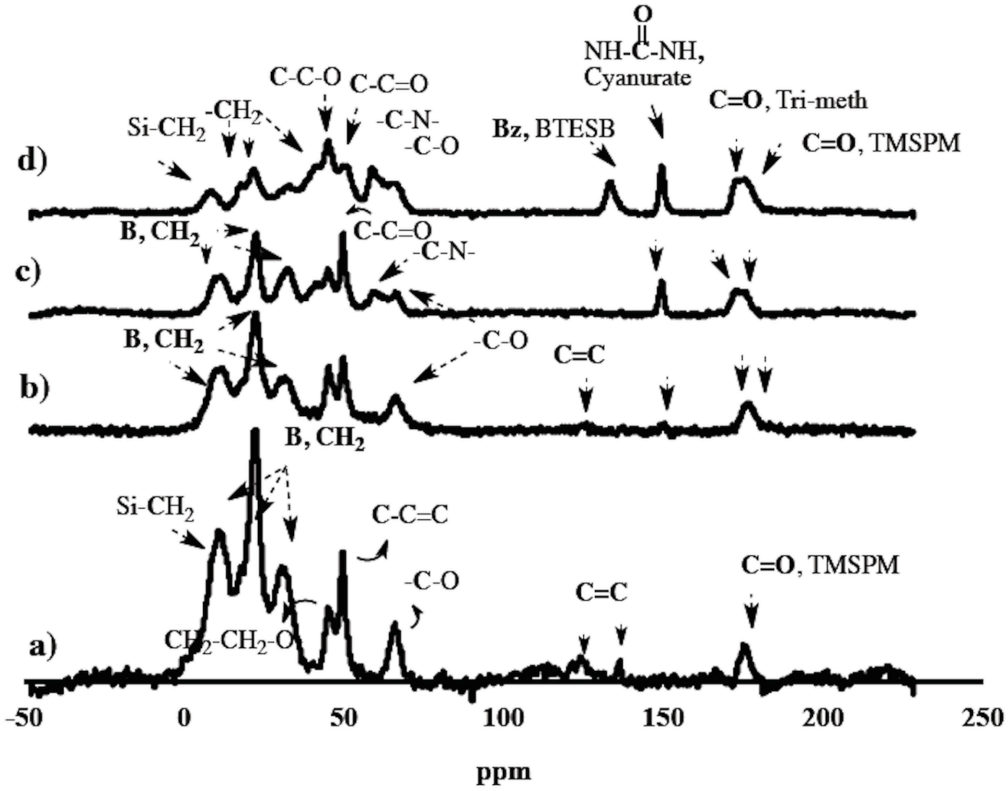

Figure III. 7 Solid ^{13}C NMR spectra of aerogel samples a) B_40, b) B_40_R_0.3, c) B_40_R_2 and d) Bz_10_R_2.

In Figure III. 7c the carbon double bonds were totally reacted and the peak area of cyanurate is four times higher than the corresponding peak area at Figure III. 7b, Figure III. 7d belongs to the cross-linked aerogel with *R*=2 and 10 mol% of silicon derived from BTESB. In this spectrum, with full reaction of aliphatic carbon double bonds, the peak at 135 ppm is the evidence of the insertion of aryl group of BTESB to the aerogels. The peak area of the cyanurate group in this figure is about 1.5 times higher than the peak area of same group in the spectrum of Figure III. 7c. Therefore, it can be proved that, comparing with aerogel

samples with 40% BTMSH in their underlying silica network, the extent of polymerization for the aerogel sample with 10 mol% of silicon from BTESB is relatively high. Due to the lower introduced amount of BTESB (maximum 5-10 mol% of silicon in each formulation) into the aerogel and its rigid nature, less steric hindrance and less possible masking of silica surface functionality exists in such an aerogel. Therefore, high accessibility of surface methacrylate groups leads them to react easily with the cross-linker and, consequently, a higher extent of polymerization occurs. Finally, the peak at 65 ppm for all spectra might be due to the presence of residual methoxy groups during the incomplete hydrolysis of silica precursors.

Hydrophobic/hydrophilic properties of some selected samples were evaluated by studying their water contact angles. Table III. 4 presents the measured values for samples without bis-silane along with samples containing 10% and 40 mole % of silicon derived from BTESB and BTMSH at given *R* values (0.3 and 2), respectively. Basically, the native TMOS-derived aerogels of this study, upon exposure to water, tend to interact promptly with water molecules and decompose thoroughly. However, due to the surface functionalization of this aerogels or/and cross-linking with tri-methacrylate, this effect has been slightly improved; after dispensing the water droplets on the surface, they tend to make holes instead of the total decomposition of the silica aerogel.

Table III. 4 Water contact angles of selected nonreinforced and reinforced aerogels.

Bis-silane	**Water contact angle (°)**		
	*R*_0	*R*_0.3	*R*_2
Nb	0	30±7	0
Bz_10	130±5	90±8	66±6
B_40	139±3	102±2	76±5

As expected, underlying silica has a major contribution on the hydrophobic nature of the prepared aerogels. This can be confirmed by the high contact angle for nonreinforced BTMSH (139^{o}) and BTESB (130^{o}) derived gels, which indicates that the hexyl and aryl groups are present in the surface and contribute to the hydrophobic nature of the aerogels. Apart from the underlying silica effect, the effect of *R* values on the contact angle of the reinforced aerogels also is pronounced, indicating that the cross-linker of this study some how suppresses the surface hydrophobicity upon coating the silica particles surface. However, despite of the cross-linker interaction with water, the contact angle measured here for the reinforced BTMSH derived aerogel (B_40_R_0.3) is in good agreement with the contact angle of styrene reinforced aerogels containing BTMSH precursors [52].

III. 3.2 Physical and microstructural characterization

III. 3.2.1 Density, porosity and dimensional changes

Figure III. 8a shows the bulk density changes for tri-methacrylate cross-linked and non-cross-linked aerogels with 0-40 mol% Si from BTMSH and 5-10 mol% Si from BTESB versus the [tri-methacrylate]/[TMSPM] molar ratio. This figure shows, as expected, that with increasing molar concentration of tri-methacrylate monomers, the density increases, especially at a higher concentration of BTMSH due to the insertion of additional mass of hexyl groups. At the lowest concentration of tri-methacrylate monomer, due to the little incorporation of cross-linker in the aerogels, almost similar densities are obtained for non-cross-linked and cross-linked aerogels. Porosity always follows the opposite trend of density and it is calculated by Equation (III-1) from the measured bulk density (ρ_b) and the skeletal density (ρ_s), being the second measured by helium pycnometry.

$$\text{Porosity (\%)} = \left(\frac{1}{\rho_b} - \frac{1}{\rho_s}\right) \Big/ \left(\frac{1}{\rho_b}\right) \times 100 \qquad (\text{III} - 1)$$

The results of skeletal density (ρ_s) and measured porosity of representative reinforced and nonreinforced aerogel samples are indicated in Table III. 5.

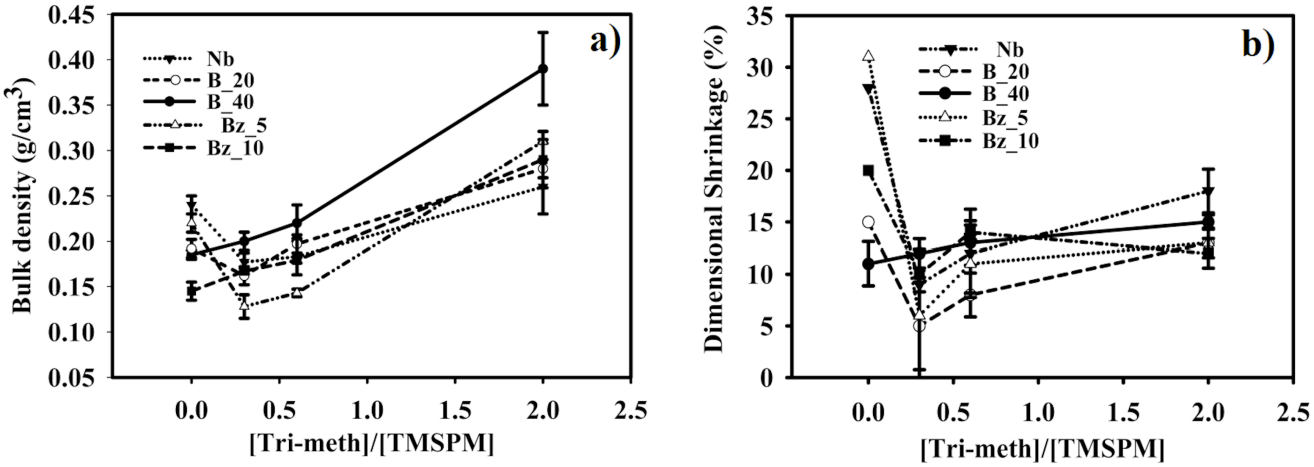

Figure III. 8 a) Bulk density changes and b) dimensional shrinkage of aerogel samples with different mol % of Si from BTMSH and BTESB as a function of [Tri-meth]/[TMSPM] molar ratio.

Considering Equation (III-1), the cross-linked samples of this study have relatively open structure, for instance, the typical reinforced aerogel with average bulk density of ρ_b =0.390 g cm^{-3} has 71% porosity, whereas with same underlying silica, the nonreinforced aerogel with average density of ρ_b=0.185 g cm^{-3} is 85% porous. Examining the porosity of some selected samples, it can be concluded that the porosity decreases with increasing molar concentrations of both BTMSH and tri-methacrylate cross-linker. Both density and porosity of aerogels are a consequence of the dimensional shrinkage of the aerogel during the drying and processing steps. As indicated in Figure III. 8b and Table III. 2, Table III. 3 all the aerogels of this study present a dimensional shrinkage, from 6-18% for reinforced aerogels and 10-31% for nonreinforced aerogels. Although there is no regular trend between the dimensional shrinkage

and the synthesis parameters of the aerogels under study, it has been shown that altering the silica backbone with bridged precursors leads to less shrinkage. Basically, introducing the non-polar alkyl and aryl bridged bis-silane precursors and the surface methacrylate groups into the nonreinforced aerogels leads to a decrease in the shrinkage. In fact, creation of silica surface with lack of Si-OH groups by introducing alkyl/aryl bis-silane precursors and more importantly by surface methacrylate functionality makes these groups repel each other causing less shrinkage during the drying stage. However, for reinforced samples, the shrinkage of the aerogels is influenced by both the introduction of bridged bis-silanes and the concentration of the cross-linker. For instance, the sample with 0% of bridged precursor and a *R* value of 2 exhibits higher shrinkage during the course of drying and processing, which means that alkyl and aryl linked bis-silane to some extent decrease the shrinkage. In the other hand, for samples with the same underlying silica backbone, increasing the cross-linker concentration leads to an increase of the dimensional shrinkage. This is likely due to the type of the multifunctional cross-linker on the silica surface, which due to the high extent of polymerization and consequent steric hindrance, leads to less spring back to the original dimension of the aerogel.

Representative cross-linked aerogels of the whole samples made in this study are shown in Figure III. 9. More transparent aerogels could be prepared with lower concentration of bridged bis-silanes and less extent of polymerization. But, stronger aerogels with high structural integrity, handling and processing capability can be obtained when higher extent of polymerization occurs on the silica surface.

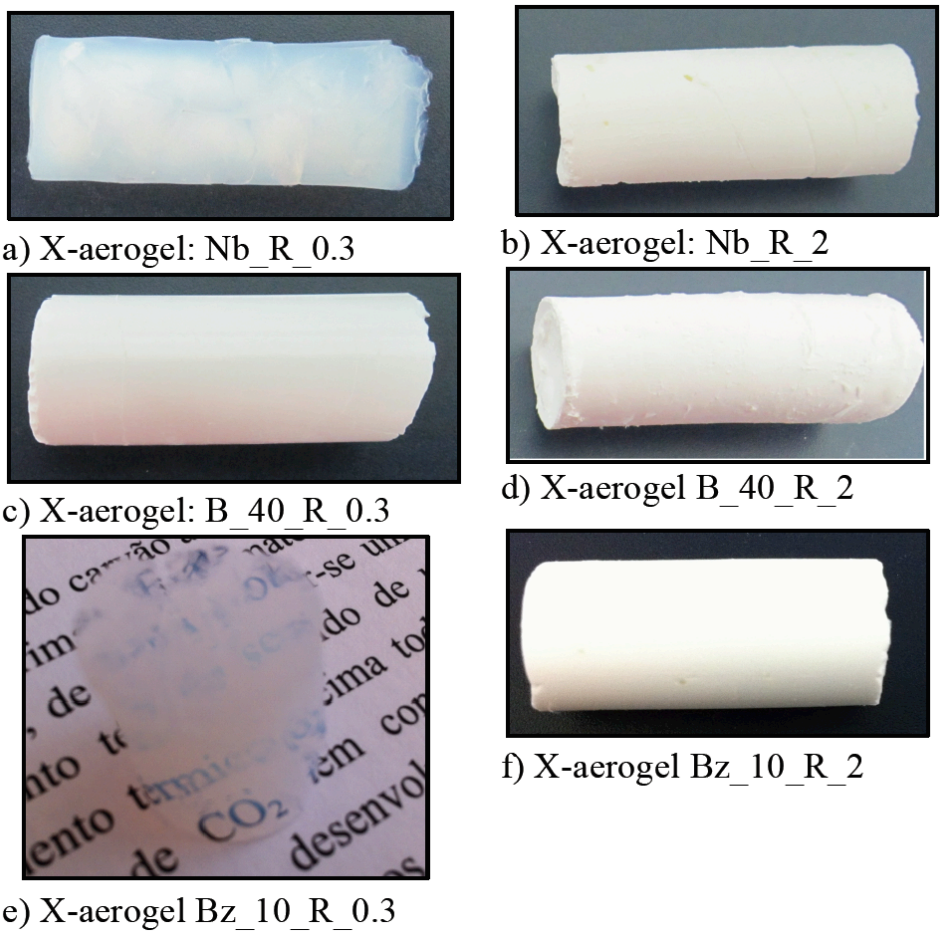

Figure III. 9 Photographs of some of selected tri-methacrylate reinforced silica aerogel monoliths, (X=cross-linked).

III. 3.2.2 Micro and mesoporous structures of the developed aerogels

The porous nature of representative nonreinforced and reinforced aerogels was evaluated by nitrogen physisorption measurements. The details of pore size; pore volume and specific surface area of the aerogels are presented at Table III. 5. Representative isotherms of three types of reinforced aerogels along with their pore size distributions are also shown in Figure III. 10a and Figure III. 10b, respectively.

Table III. 5 Surface area, porosity, skeletal density (ρ_s), pore volume and average pore size values for representative nonreinforced and reinforced samples.

Sample	BET surface area ($m^2\ g^{-1}$)	Average pore diameter (nm)	Pore volume ($cm^3\ g^{-1}$)	Porosity (%)	ρ_s ($g\ cm^{-3}$)
Nb	854.9	4.9	1.44	91	2.78
Nb_R_0.3	481.3	10.1	1.33	86	1.28
Nb_*R*_2	178.8	9.2	0.43	77	1.08
B_40	203.6	7.5	0.51	85	1.23
B_40_*R*_0.3	249.0	9.2	0.50	87	1.69
B_40_*R*_0.6	82.2	7.8	0.27	84	1.25
B_40_*R*_2	7.0	6.4	0.01	71	1.20
Bz_10	719.0	9.1	1.41	93	2.07
Bz_10_R_0.3	710.0	10.7	0.71	89	1.50
Bz_10_*R*_2	208.9	13.1	0.68	86	1.92

The specific surface areas and the pore size distributions were evaluated from the adsorption and desorption branches of the isotherms applying the Brunauer-Emmett-Teller (BET) and Barrett-Joyner-Halenda (BJH) methods, respectively. It was found that the isotherms of the samples were of type IV, according to the IUPAC classification, which is a typical profile for mesoporous materials recognized by their characteristic hysteresis loop. The decrease in adsorption value for whole reinforced aerogels is due to the fact that the pore structure of aerogel is lost/closed by the cross-linking with polymer. The results also show that the micro and mesoporosities are also significantly influenced by the underlying inorganic silica structures. For instance, the reinforced aerogels Bz_10_R_2, despite the higher extent of polymerization on their surfaces (higher than the reinforced aerogel B_40_R_2, confirmed by ^{13}CNMR), show relatively higher adsorption volumes and, consequently, higher specific surface areas. As explained by Loy *et al.,* this is probably due to the rigid nature of the aryl spacer, which allows less dimensional shrinkage of the silica skeleton and, therefore, less collapse of the pores occurs [153].

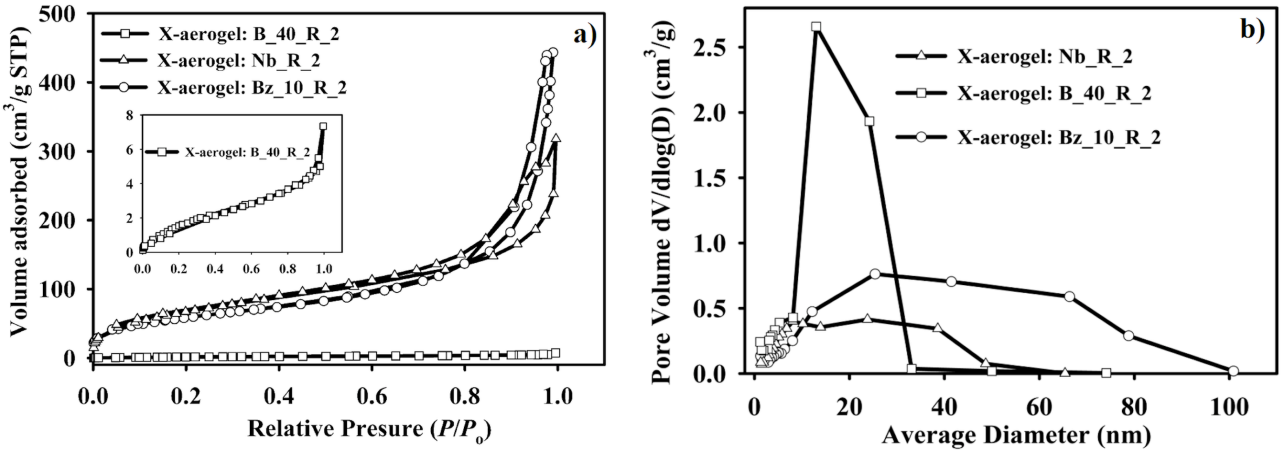

Figure III. 10 a) Comparative N_2 sorption isotherms of selected (cross-linked) X-aerogels Nb_R_2, B_40_R_2 and Bz_10_R_2; the inset is the magnified isotherm of B_40_R_2; b) BJH pore size distributions from the desorption branches of the isotherms for cross-linked aerogels Nb_R_2, B_40_R_2 and Bz_10_R_2.

As indicated in Table III. 5, in the reinforced aerogels, the size of the pores decreases with cross-linking as the pores get gradually filled by polymer. Therefore, the average pore diameter of native aerogel samples generally is larger than pore diameters of their corresponding reinforced aerogels. Figure III. 10b indicates that the majority of the pores of the reinforced samples fall in the mesopores region, with relatively few micropores. Although the most part of microporosity is lost during the reinforcing process for aerogels made with 10 mol% of Si from aryl bridged bis-silane, the diameter of mesopores (peak) increases to 13.1 nm, due to the rigid nature of aryl bridges and, then, probably to less shrinkage of aerogels (specially at *R*=2) during cross-linking and drying.

For further elaboration in terms of microstructure of the prepared aerogels, we also observed the scanning electron micrographs (SEM) of the selected samples. Figure III. 11a-i reveals that all aerogel networks appear as a 3D agglomerate of nanoparticles and the microstructures of the native nonreinforced and polymer-reinforced aerogels are not identical. The native TMOS-derived aerogel network, Figure III. 11a, has a more closed packed arrangement of the

secondary silica particles with few nanometers size and high percentage of porosity. The incorporation of the alkyl-bridged precursor (40 mol% of Si), Figure III. 11b, leads to a network with more open structure and larger pores sizes. The network of the nonreinforced BTESB-derived aerogels also shows a uniform arrangement of the secondary silica particles and a regular distribution of their mesoporosities, which was already confirmed by gas adsorption porosimetry.

In the aerogels that are cross-linked with polymer (R=2), regardless of the type of the underlying silica network, the microstructure patterns change and the network appears more collapsed and dense – Figure III. 11c, f, i. In these types of aerogel, the surface of silica is subjected to a higher extent of polymerization, which resulted in silica aerogels with increased sizes of secondary silica particles as well as the significant lost of fine pore structures. This effect is not so obvious in the reinforced aerogels with less polymer (R=0.3) – Figure III. 11b, e, h. In fact, enhancing the cross-linker concentration from R=0.3 to R=2 leads to large number of silica surface methacrylate groups to react with the cross-linker and, pronounced differences in terms of the network appearance are caused.

For aerogels without alkyl or aryl bridges in their inorganic underlying silica structures (Figure III. 11b, c), increasing the cross-linker leads to a more compact structure with loss of the microporosity of the aerogel.

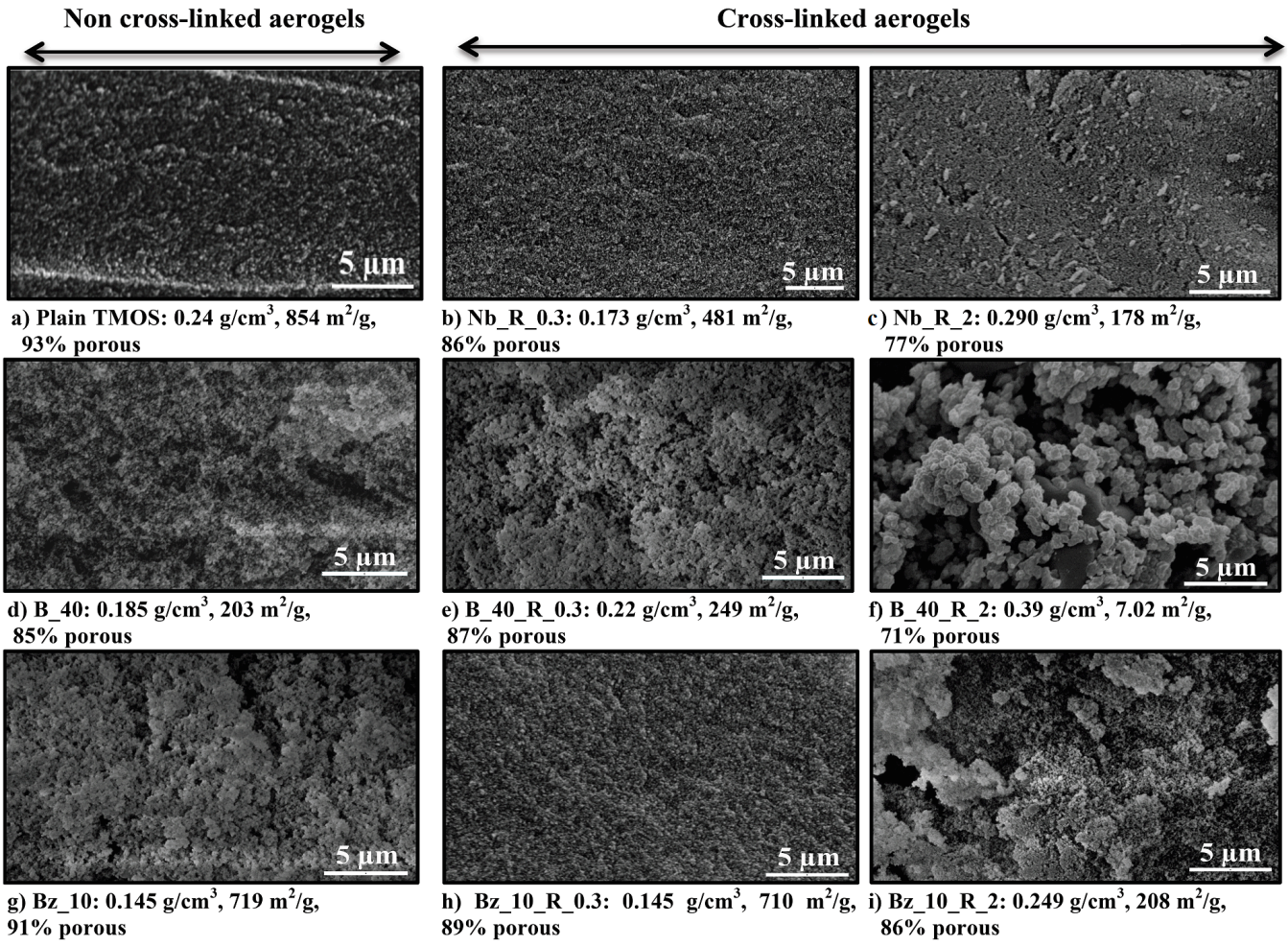

Figure III. 11 Scanning electron microscopy images of selected nonreinforced and reinforced aerogels.

Overall, the concentration of cross-linker does not cause a marked difference in the microstructure appearance of this type of aerogel. Instead, increasing the cross-linker concentration for both type of BTMSH and BTESB-derived aerogels, as shown in Figure III. 11e, f and Figure III. 11h, i, respectively, leads to a pronounced effect in terms of secondary silica particle sizes and porosity arrangements. Indeed, the aerogels containing bridged precursors, in higher cross-linker concentration, possess larger clusters of silica nanoparticles with higher extent of macroporosity in the network and significant loss of their micro and mesoporosity.

The porous texture of some selected samples is also well illustrated in Figure III. 12a-c, which shows the transmission electron microscopy (TEM) micrographs of BTMSH and BTESB based aerogel as well as for an aerogel without bridged bis-silane in its structure. The TEM images for aerogel samples show a porous interconnected dendritic-type network structure, similar in nature to the one commonly observed in conventional silica aerogels [192].

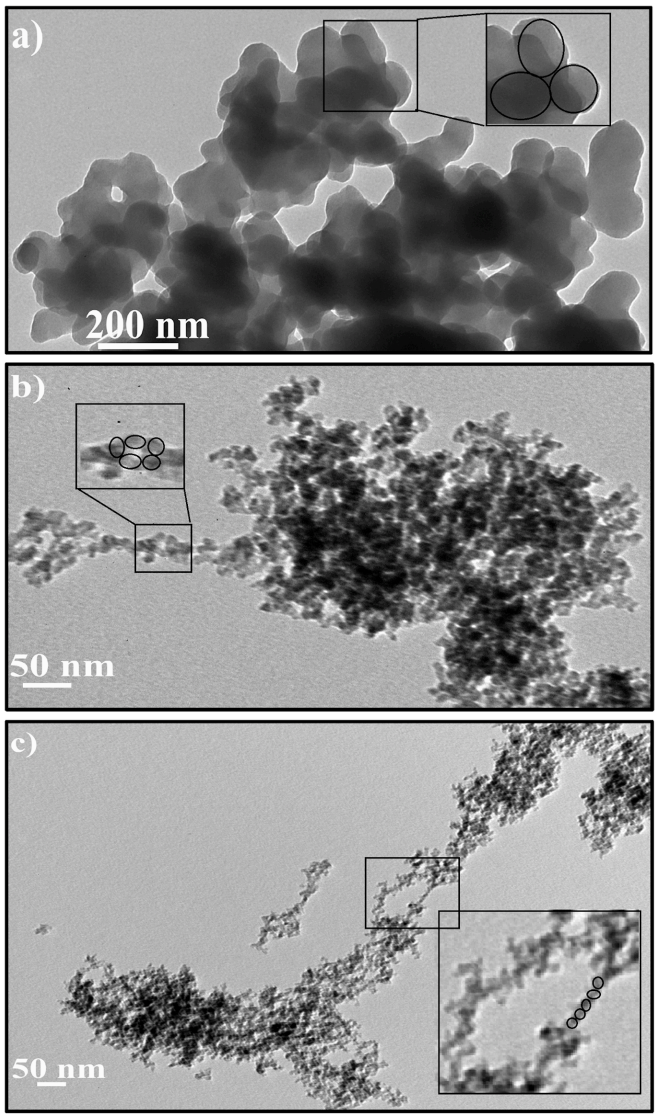

Figure III. 12 TEM micrographs of selected (cross-linked) X-aerogels: a) B_40_R_2, b) Bz_10_R_2, and, c) Nb_R_2.

The average size of individual (secondary) particle appears to be less than 10 nm for the aerogel without bis-silane. The introduction of BTESB and BTMSH bis-silane to the silica structure leads to an increase in the average size of secondary particles of the order of 20 and 50 nm, respectively. The inset of magnified section of each image well illustrates the pearl necklace arranging the semispherical connected silica secondary particles, which are composed by silica primary nanoparticles with an average size in the order of ~1 nm, as suggested also elsewhere [95]. However, the secondary particles aggregated and formed larger size clusters of about 200, 100 and less than 100 nm for reinforced aerogels B_40_R_2, Bz_10_R_2 and B_0_R_2, respectively.

III. 3.3 Thermal stability

Thermogravimetric analysis (TGA) and simultaneous TG/DSC thermal analysis were conducted from ambient temperature to 600°C. The native TMOS-derived aerogel loses up to ~9% of its weight at 73ºC due to the evaporation of physically adsorbed water - Figure III. 13a. This mass loss could also caused by the loss of the OH groups at the network ends. In this figure, the simultaneous TG/DSC curves showed that B_40 looses 4% of weight at 67ºC and Bz_10 looses <1% of weight at 73ºC, due the evaporation of adsorbed water in the network. These weight losses are accompanied by the endothermic peaks in the DSC curves at the same temperature for both samples. The observed adsorbed water mass losses indicate the ability of the TMOS-derived aerogels to retain adsorbed water throughout processing and, more importantly, can elucidate about the increase in the degree of hydrophobicity of the final aerogels when alkyl and aryl bridges are incorporated in their microstructures. Further mass losses take place at 496°C due to the pyrolysis of the hexyl and silica surface methacrylate

groups, for B_40, and at 392°C due to the pyrolysis of aryl groups and silica surface methacrylate groups, for Bz-10. The small endothermic peaks at 518°C for B_40 and at 425°C for Bz_10 confirm the thermal decomposition of the organic content inside of these aerogels.

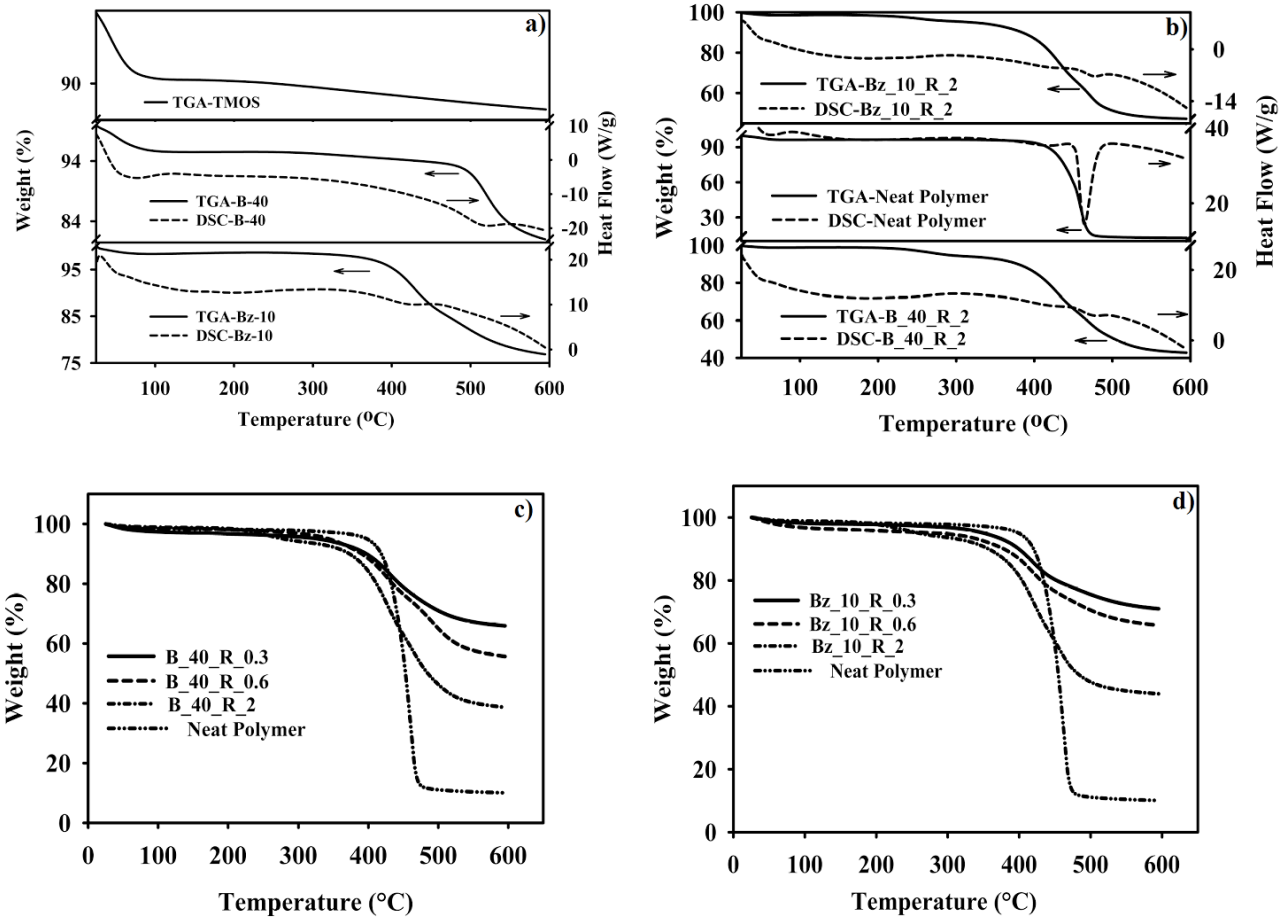

Figure III. 13 a) TGA of native TMOS-derived aerogel along with simultaneous TG/DSC curves for methacrylate modified non-X-aerogels with different bridges within the silica structure, b) TG/DSC curves of tri-methacrylate cross-linked silica aerogels B_40_R_2, Bz_10_R_2 and neat polymer. TGA curves of tri-methacrylate cross-linked silica aerogels containing c) 40 mol% of Si from BTMSH and d) 10 mol% of Si from BTESB with different *R* values, (heating rate: 10°C/min) (X=cross-linked).

The tri-methacrylate cross-linked B_40_R_2 aerogel loses all of their cross-linker and hexyl groups at 392°C, being slightly less stable than the neat polymer that decomposes at ~ 439°C – Figure III. 13b. The DSC curves indicate that these mass losses are accompanied by a small endothermic peak at 477°C, for B_40_R_2, and a sharp and intense peak at 464°C, for the neat polymer. In the tri-methacrylate cross-linked Bz_10_R_2 aerogels, the decomposition of polymer and aryl bridges occurs at 394°C along with a slight endothermic peak at 476°C. In these composites, the incorporation of aryl bridges leads to more stability of the aerogel composite compared to the BTMSH contained aerogels.

In summary, the TG/DSC studies are describing that the aerogel material absorbs heat during the observed mass losses. In other words, basically, the chemical reactions that happen in these aerogel insulating materials during the heating process are endothermic processes [193].

After assigning the weight loss contributions of the underlying silica at non-cross-linked aerogel, from Figure III. 13a, the cross-linker weight loss contribution at Figure III. 13c and d can be obtained by subtracting these values from the overall weight loss of the aerogel composite. Therefore, cross-linker contributions for the cross-linked BTMSH contained aerogels with *R* ratios of 0.3, 0.6 and 2 are 8.65%, 12.38% and 23.42% w/w (Figure III. 13c), respectively. This observation is in good agreement with increase in the bulk density and decrease in the specific surface area of this type of aerogels upon increasing cross-linker concentration.

The aryl groups, also, due to their intrinsic rigidity, and to some extent less steric hindrance of the aerogel structure, favours the accessibility of the monomer to the surface methacrylate groups. Therefore, polymer content in these composites is 20.232%, 23.32% and 31.66% w/w for aerogels with *R* ratios of 0.3, 0.6 and 2 - Figure III. 13d, respectively, which shows higher

introduction of the tri-methacrylate cross-linker in the aerogel than for the case in which BTMSH is used.

In analogy with recent arguments that has been given by Ilhan *et al.* [53] and Meador *et al.* [48], for epoxy and poly styrene reinforced aerogels, the average number of monomer units (N_t) in the tri-methacrylate cross-linked aerogel samples can be calculated by Equation (III-2).

$$N_t = \frac{\rho_{b,cross-linked} - \rho_{b,native}}{MW_{monomer} \times S_{cross-liked} \times \rho_{b,cross-linked}} \times \frac{1}{10^{-6}} \qquad (III-2)$$

Where S is the BET surface area, ρ_b is the bulk density and assuming that the monolayer coverage with a small molecule of monomer requires 10^{-6} mol m^{-2}.

For tri-methacrylate cross-linked aerogel samples, including 0% of bis-silanes, 40 mol% of Si from BTMSH and 10 mol% of Si from BTESB precursors, at R=2, a typical polymer chain contains 3.2, 1.7 and 2.5 monomer units, respectively. These values are consistent with ^{13}CNMR and TGA results, which indicate that the extent of polymerization is relatively low for the cross-linked BTMSH-derived aerogel.

III. 3.4 Mechanical and thermal conductivity properties

The stress-strain curves obtained from compression tests to the reinforced and nonreinforced aerogels are shown on the Figure III. 14a, b. The elastic modulus for each curve is calculated from the slope of data near the origin (slope of initial linear part of stress-strain curves) – Figure III. 14c. The maximum stress at break of each aerogel is indicated in Figure III. 14d. From these figures, and data from Table III. 2, it is clear that the maximum stress at break is improved for cross-linked aerogels but the modulus is slightly higher for the reinforced

samples over their nonreinforced counterparts. The polymer-reinforced aerogels have as much as one order of magnitude higher maximum strength at break than their nonreinforced counterparts, indicating that the cross-linker indeed enhances their mechanical strength.

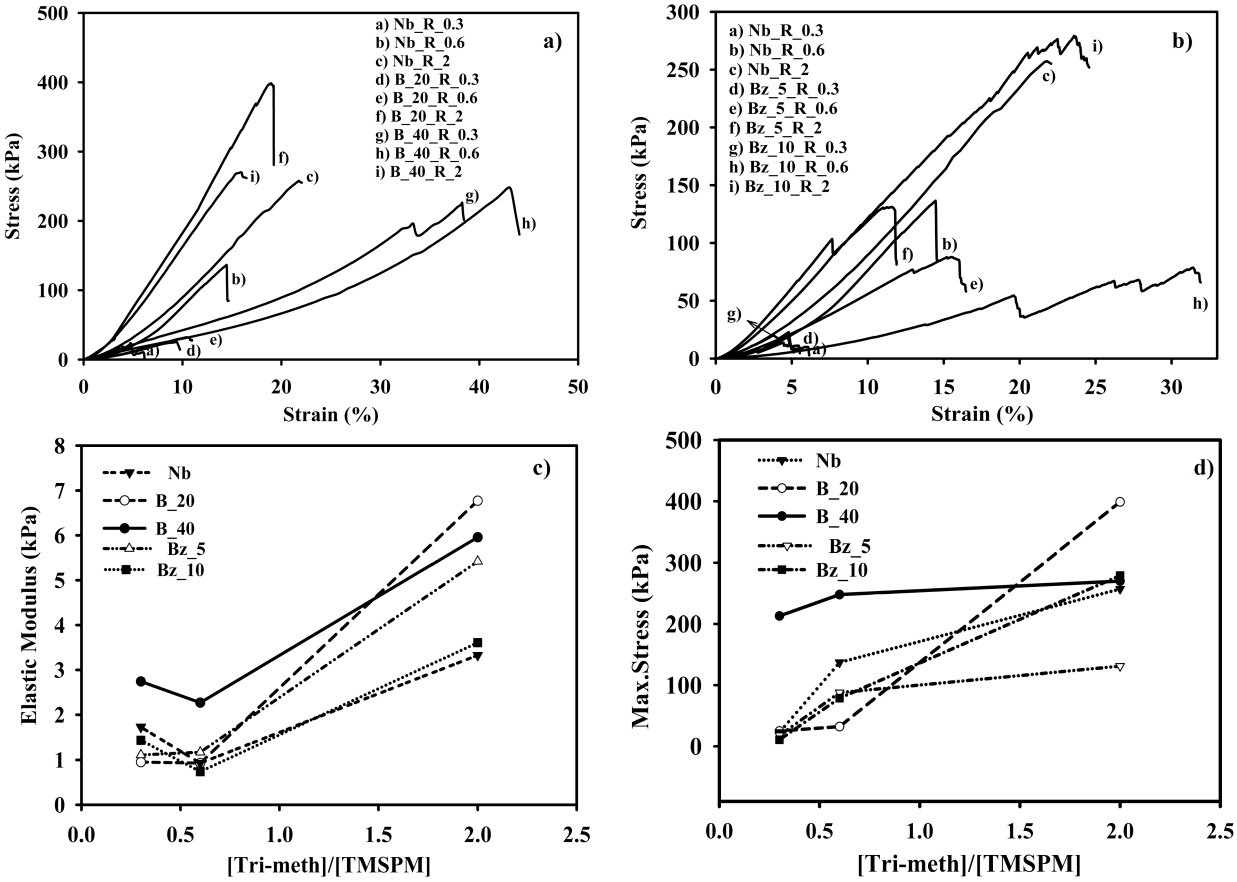

Figure III. 14 a) Stress-strain curves for BTMSH contained tri-methacrylate reinforced aerogels, b) Stress-strain curves for BTESB contained tri-methacrylate reinforced aerogels, c) Elastic modulus versus [Tri-meth]/[TMSPM] molar ratio at different mol% of Si from BTMSH and BTESB, d) Maximum stress at break versus [Tri-meth]/[TMSPM] molar ratio at different mol% of Si from BTMSH and BTESB.

Among the reinforced aerogels made by 0-40 mol% of Si from BTMSH, the aerogel with 20 mol% and *R*=2 has the highest strength and elastic modulus. The higher strength values for this aerogel is probably due to a higher extent of cross-linking on the silica surface than the

aerogel made with 40 mol% of Si from BTMSH. As it was noted before, based on the ^{13}CNMR results, a higher percentage of BTMSH leads to a higher steric hindrance in the aerogel structure, which hinders the accessibility of the cross-linker to the silica surface functionality.

For the aerogels made using the aryl bridged precursor (BTESB), the elastic modulus of the aerogel prepared with 5-10 mol% of Si from BTESB generally decreases with increasing percentage of BTESB. Additionally, the reinforced aerogel made with 10 mol% of Si from BTESB and R=2, due the higher extent of polymerization in its surface, has a maximum strength at break slightly higher than the aerogel containing 40 mol% of Si from BTMSH with the same R value.

Fricke *et al.* [36] and Pekala *et al.* [37] presented the relation between mechanical properties (*e.g.* Young's modulus or maximum strength *etc.,* (E)) of silica aerogels and their bulk density (ρ_b) as power law relationship $E \sim \rho_b^a$. Therefore, according to this scaling law, the most straightforward methods of mechanical reinforcing of silica aerogels result in increasing the density and therefore increasing the thermal conductivity [38-40]. This is caused by the increase of the total amount of material used for the production of the gel matrix, due to the need of increasing the total number of connection points within the silica aerogel.

The graphs of the power law dependency between the elastic modulus and bulk density, and between the maximum stress at break and bulk density for all tri-methacrylate reinforced aerogels are shown in Figure III. 15a, b. The power law exponent between the elastic modulus and bulk density for silica aerogels, without organic part, are reported to be 3 [194]. It is also reported that this exponent strongly depends on the synthesis route and connectivity between the secondary silica particles [40]. The power law exponent for polymer-reinforced silica

aerogels is higher due to the conformal coating of the silica aerogel and reinforcement of the silica backbone by increasing the network connectivity between secondary silica particles.

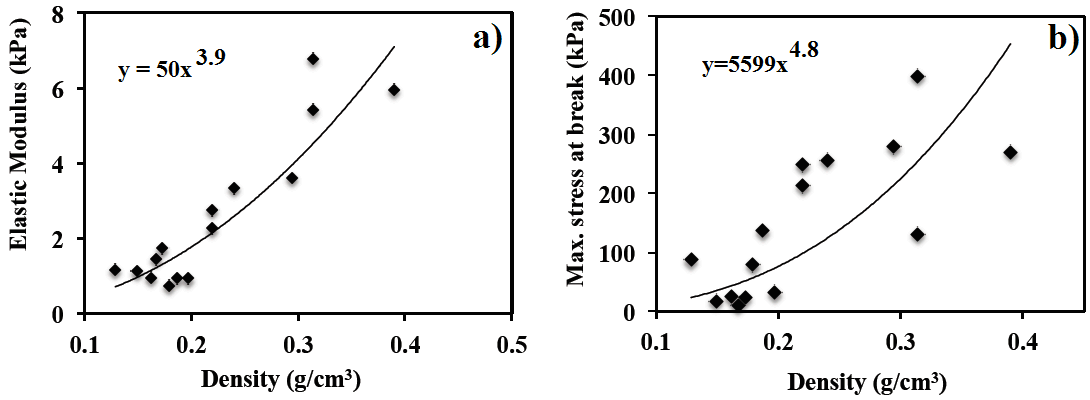

Figure III. 15 a) Power law dependency between elastic modulus and bulk density, b) Power law dependency between maximum strength at break and bulk density.

The method of least-squares was used in this study to approximate the exponent of power law for the obtained reinforced aerogels. As shown in Figure III. 15a, the power law dependency between the elastic modulus and the bulk density of the aerogels has an exponent of approximately 3.9. This value is comparable with those reported for the power law relationship between the modulus and density for tri-isocyanate reinforced silica with dipropyl amine linking groups from bis(trimethoxysilylpropyl)amine (BTSMPA) ([α]=4.5) [184]. Similar to the previous studies [52] [184] in which flexible alkyl bridges of bis-silanes contribute to the network connectivity, in the present work, the hexyl and aryl bridging groups from BTMSH and BTESB provide connections within the network. The obtained exponent for the power law relationship between the modulus and density is in agreement with the reported values by Nguyen *et al.* [184], which applied the tri-isocyanate cross-linker with molecular structure similar to that of the cross-linker used in the present work.

The maximum stress at break (Figure III. 15b) for the reinforced aerogels shows a higher influence of the power law dependency from polymer reinforcement. In this case, the exponent [α] is 4.8, higher than the reported values by Nguyen *et al.,* [α]=4.3, for their reinforced aerogels [184]. The higher value of this exponent for the tri-methacrylate cross-linked aerogels in this study is probably due to the higher structure variation possible in this system, *i.e.* the fact that the amount of the total silicon concentration, fraction of silicon derived from TMSPM and BTMSH/ BTESB, amount of cross-linker and mechanism of cross-linking all contribute to the density, modulus and maximum strength in different ways.

Aerogels, due to their vast internal empty space, generally exhibit low thermal conductivities and, in that regard, an obvious application is in thermal insulation [42, 43].

As shown in Figure III. 16 and Table III. 2, the thermal conductivity of reinforced aerogels is higher than the thermal conductivity of nonreinforced aerogels (Table III. 3) and it increases with the increasing in the cross-linker concentration and, consequently, with the increasing in the bulk density. The thermal conductivity of the aerogel without bridged precursors, at maximum concentration of the cross-linker, is higher than for those containing Si from BTMSH and BTESB within their structure. As it was noted before, this is due to the higher extent of polymerization that occurs in this type of aerogel without bis-silane precursors (0% bis-silane, R=2), which leads to higher thermal conductivity (TC=0.094±0.005) than the aerogel containing 40 mol% of Si from BTMSH and R=2, with a TC value of 0.084±0.002.

The thermal conductivity of the aerogel made with 5-10 mol% of Si from BTESB is far less (TC=0.050±0.002, for 10 mol% BTESB, R=2) than for other aerogels made with BTMSH or without bis-silane precursors with comparable densities and mechanical strength. The lower thermal conductivity can be explained by open structure of aerogel due the high extent of porosity or volume (confirmed by porosimetry) compared to the other type of aerogels.

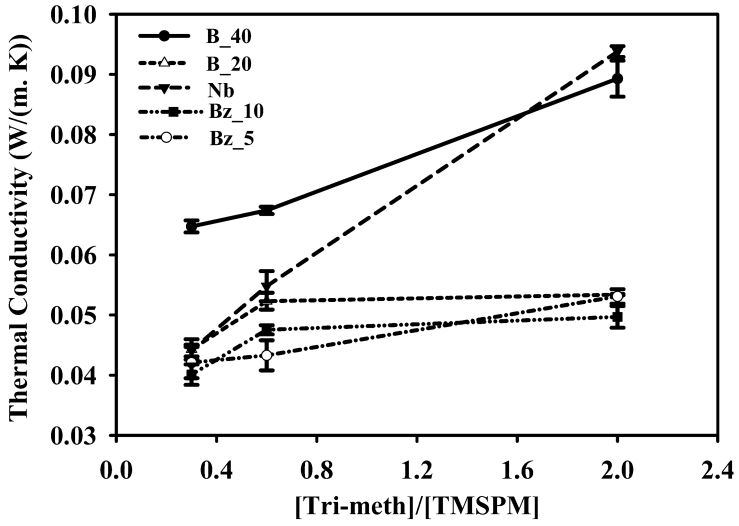

Figure III. 16 Thermal conductivity of reinforced and nonreinforced aerogels with different underlying silica structures.

The thermal transfer in porous media like silica aerogels is conducted by three pathways: i) solid transfer, which is the heat transfer through the chain of primary particles forming the solid silica network; ii) thermal radiation; iii) heat transfer by gaseous molecules present in the porous structure of the aerogel. In the cross-linked aerogels, due to the additional mass inserted by the reinforcement agents and bis-silane precursors, an increase in the density and, consequently, in the solid or backbone thermal conductivity of the aerogel is observed. The increase of Si mol% from BTESB in the range of 5-10 mol% causes an improvement in the thermal conductivity, but further increasing over 10 mol% likely leads to rigid and non-elastic properties which are not favorable in terms of mechanical properties. The pore sizes of BTESB-derived and nonreinforced aerogels were found to be larger than those of aerogels made with and without BTMSH. The large pores sizes often lead to large pore volumes and, thus, lead to large porosity. Large porosity, in turn, favours low thermal conductivity.

III. 4 Conclusions

The incorporation of alkyl and aryl bridges of bis-silane precursors in the underlying silica of aerogels along with cross-linking of the silica surface functionality with tri-methacrylate cross-linker is examined. In this work, the synthesis process was simplified by eliminating the diffusion step of the monomer into the silica network, and aerogels with low densities along with improvement in the mechanical strength and thermal insulation performance have been obtained. Although moderate improvement in terms of the elastic modulus for all aerogels has been achieved, still more than one order of magnitude improvement in the final compression strength (up to 400 kPa) has been attained. The mechanical strength improvement is somewhat limited by the aerogel's bulk density (ρ_b) of ≈ 0.13 to 0.39 g cm^{-3}, which is far below the values of the previously reported reinforced aerogels with $\rho_b > 0.4$ g cm^{-3} [29] [22-24, 26].

Notably, in terms of BTESB derived aerogels, the surface area and extent of porosity even after cross-linking was quite high, confirming a high contribution of the underlying silica on the mesoporous structure of the aerogel. When compared to the other types of aerogel, in the reinforced BTESB based aerogel, despite of higher extent of cross-linking (proved by TGA and ^{13}CNMR), shows quite ordered and larger mesopores, leading to further improvement in terms of thermal insulation performance. In fact, the introduction of the aryl bridges of BTESB precursor in the silica structure of the reinforced aerogels resulted in thermal conductivity values lower than 0.04 W m^{-1} K^{-1}, which is less than the values found for epoxy, styrene and isocyanate reinforced aerogels, reported so far [26].

It is also worthy to note that the aerogel made by 10 mol% of Si derived from BTESB is at the same time stiffer and stronger than those made by incorporation up to 40 mol% of Si from BTMSH, with comparable density values. However, a remarkable improvement in the

mechanical strength of BTMSH based aerogel was also achieved, even at low concentration of cross-linker (R=0.3), with little changes in the density, over the non-cross-linked counterparts.

In summary, the strong silica aerogels with improved mechanical and thermal insulation performance developed here can be robust thermal insulator candidates for different potential aerospace applications.

Chapter IV. Development of mechanically strong ambient pressure dried silica aerogels with optimized properties.

This chapter comprises the work submitted to the Journal of Physical Chemistry C (2014) by: Hajar Maleki, Luísa Durães, António Portugal.

IV. 1 Introduction

The expanded industrial and commercial use of silica aerogels has been difficult to implement because of their poor mechanical properties and fragility. Moreover, the need for drying wet gels by supercritical drying (SCD) during manufacturing makes the preparation process more costly and non-safe, which limits the broadening of the aerogels applications.

The ambient pressure drying is safer and less expensive than the supercritical drying process, and has been more actively investigated in recent years [83, 110, 173, 178, 195, 196]. Evaporation of the liquid in the pores causes serious shrinkage and cracking due to the high capillary pressure at the menisci of the solid-liquid-vapor interfaces inside the gel structure during drying. This is particularly severe when the solvent wets the solid, *i.e.* when the contact angle of the menisci is lower than 90°.

The most common approach to overcome the capillary tension during evaporation of solvent from the porous structure was reviewed at Chapter II of the present dissertation. In general, the surface modification of silica by reacting surface silanol groups with hydrophobic reagents and producing hydrophobic surfaces [81, 117, 119, 122, 123, 197] and replacing some of (Si-O-Si) bonds with flexible and non-hydrolysable organic bonds (Si-R) [20, 117, 118, 195, 198] [120, 121] [81, 117, 119, 122, 123, 197] have been investigated for the developing of ambient pressure dried aerogels. In this context, cross-linking of silica aerogels

with appropriate organic polymers to prepare hybrid materials [173, 195, 196, 199] were counted as an elegant and straightforward method. The silica surface organic groups allow the aerogel to spring back during drying and partially recover its initial wet gel size without resulting in any cracks within the monolith structure [81, 117, 197]. Evaporation of low surface tension hydrocarbons from silica wet gels [125, 173, 178] or the introduction of additives to control the drying process [79, 200] can also be possible ways to overcome the induced capillary pressures. Evaporation of a low surface tension solvent from the silica network reduces the capillary pressure when compared to the evaporation of an alcohol [126].

Recent articles list several mechanical reinforcing strategies of silica aerogels [29, 199]. The polymer reinforced silica aerogels have good mechanical properties, but still are not strong enough to withstand capillary pressure when dried under ambient pressure drying condition, especially when the wet gels are dried from an alcoholic solvent. Therefore, in order to take advantages of the ambient pressure drying method to produce crack free aerogel-like monoliths with minimum dimensional shrinkage, we conducted polymer reinforcement approaches along with drying of wet gels from a low surface tension solvent.

In the previous chapter, we have studied the effect of different underlying silica on the physicochemical properties of tri-methacrylate cross-linked supercritical CO_2 ($scCO_2$) dried silica aerogels [201]. In that regard, the underlying silica structure was changed by altering the alkyl/aryl linker or bridge between secondary silica nanoparticles, according to the proposed molecular structures shown in Figure IV. 1. The alkyl and aryl bridges between secondary silica particles have been originated by introducing 1,6-Bis(trimethoxysilyl)hexane (BTMSH) and 1,4-Bis(triethoxysilyl)-benzene (BTESB) bis-silane precursors into the underlying silica structure prior to the cross-linking reaction.

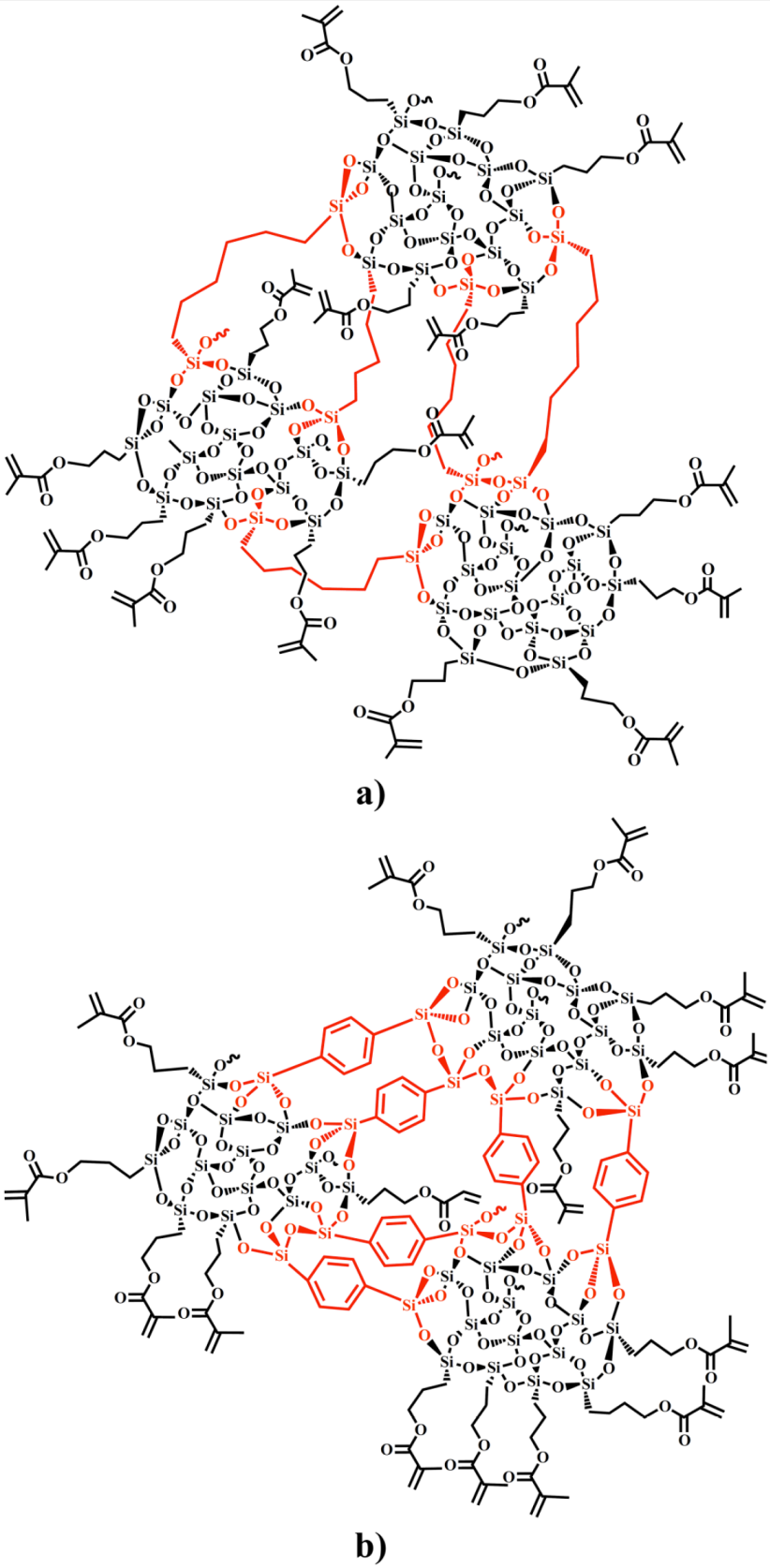

Figure IV. 1 Proposed molecular structures of silica gels having a) BTMSH and b) BTESB in the underlying structure.

In the aforementioned study, we were able to show fundamental properties differences between aerogels having akyl/aryl linking groups within the silica structure, along with drastic improvement in the mechanical strength and thermal insulation performance. The aerogels made by 10 mol% of silicon derived from BTESB, which have rigid aryl spacers, show less structural collapsing during SCD. Additionally, a drastic improvement in terms of extent of porosity/pore volume and surface area and an improvement in the thermal insulation performance for such aerogels have been achieved.

Motivated by the changing of the silica aerogels properties by altering the underlying silica structure, we have also investigated safe and cost efficient synthesis of ambient pressure dried tri-methacrylate reinforced silica aerogels. In order to be able to predict and control the density, mechanical strength and thermal conductivity of ambient pressure dried silica aerogels containing different underlying silica structures, optimization studies using central composite rotatable design (CCRD) of response surface methodology (RSM) were conducted.

Therefore, the aim of this study was to investigate the density, mechanical strength and thermal conductivity of ambient pressure dried tri-methacrylate cross-linked aerogels and determine the effect of the type of silica precursors as well as cross-linker concentration on these properties. For this, the linear, interaction and quadratic effects of [Si]% derived from BTMSH, and BTESB as well as cross-linker concentration were modeled leading to predictive models for the optimization of the test parameters. In this way, the levels of the variables using a response surface methodology (RSM) were determined.

The optimized ambient pressure dried (APD) aerogel-like properties were also compared with their $scCO_2$ dried counterparts for identical preparation conditions.

Our further attempt in this study was to explore the capability of optimized aerogel-like samples for being used in Space applications, by evaluating the materials specifications. For this purpose, thermal cycling and outgassing characteristics of the optimized APD aerogels

and $scCO_2$ dried aerogels were evaluated under the framework of several pre-defined standard tests.

IV. 2 Experimental

IV. 2.1 Materials

Tetramethylorthosilicate (≥99%; TMOS), 3-(trimethoxysilyl)propyl methacrylate (98%; TMSPM), ammonium hydroxide (NH_4OH; 28-30% V/V solution), methanol (MeOH; 99.8%), hexane (≥99%), ethanol (EtOH; ≥99.5%), tris[2-(acryloyloxy)ethyl]isocyanurate (99%), 2,2′-azobis(2- methylpropionitrile) (98%; AIBN), 1,4 - Bis(triethoxysilyl)-benzene (96%; BTESB) and acetone were purchased from Aldrich. 1,6 - Bis(trimethoxysilyl) hexane (98%; BTMSH) was purchased from Cymit. All reagents were used without further purification.

IV. 2.2 Methods

IV. 2.2.1 General

Variables used in this study include the bis-silane type (BTMSH, BTESB), the mole fraction of the total silicon derived from BTMSH and BTESB (note that these precursors contribute with two silicon atoms in every molecule, and the rest of the silicon is derived from TMOS and TMSPM). The amount of silicon derived from BTMSH varied from 0 to 40 mol%; in the aerogel derived from BTESB, the amount of silicon from BTESB had values of 5 to 10 mol% of the total silicon. The amount of cross-linker (tri-methacrylate) was given as mole fraction to TMSPM. The water/total silicon mole ratio (r) was kept at a value of 4 for all formulations, which is higher than the stoichiometric value for hydrolysis and condensation of TMOS (r = 2).

IV. 2.2.2 Preparation of polymer-reinforced ambient pressure dried (APD) silica aerogel-like monoliths

Apart from the drying step, the mechanically reinforced APD aerogels monoliths of this study followed the same synthesis procedure as their $scCO_2$ dried counterparts, which was explained in Chapter III. For reference, a typical procedure is outlined for a formulation with total silicon concentration of 1.3 mol/L in the sol, a BTMSH Si fraction of 40 mol% and the tri-methacrylate monomer in a 1.25 ratio to TMSPM (Run B_40_R_1.25 of Table IV. 3, in section IV. 3). A solution of 1.52 mL (10.56 mmol) of TMOS, 1.74 mL (10.56 mmol) of BTMSH, and 1.19 mL (5.2 mmol) of TMSPM was cooled to below 0°C in an ethanol mixed dried-ice bath (Solution 1). Solution 2 was prepared by adding 12.9 mL of the gelation solvent (methanol), 2.7 g of Tris[2-(acryloyloxy)ethyl] isocyanurate monomer, water (r = 4), 0.7 mL of NH_4OH solution and 0.27 g of AIBN (formulated to be 10 wt% of the organic monomer). The two solutions were mixed and poured into two propylene cylindrical molds, with 17.2 mm nominal diameter. The gels were formed within 5 min to 2 hours depending on the formulation. After 24 hours of aging, the wet gel was demolded and placed in a cylindrical reaction flask, containing enough ethanol solvent to cover the gel and the same concentration of initiator used in the gelation step. The sample was refluxed at 70°C, for 6 hours, to promote free radical polymerization of the organic monomers inside the pores of the wet gel with silica surface functionalities. After cross-linking, in order to remove the residual water and ethanol, the samples were washed three times with the gelation solvent, giving 8 hours interval between each washing step. Afterwards, methanol was slowly exchanged by hexane over a 24 hours period. Finally, the wet gels were carefully placed in the ventilated oven and dried several days in ambient pressure and temperature conditions.

The experimental procedure leading to the BTESB derived aerogel-like sample was exactly similar to the procedure described above. The only difference is in the preparation of Solution 1, in which the BTESB precursor with defined silicon mole percentages has been introduced to the solution instead of the BTMSH precursor.

IV. 2.3 Physicochemical analysis

Solid-state ^{29}Si and ^{13}C NMR spectra of the aerogels were obtained by an *Inova 500* spectrometer using a 4 mm solids probe with cross-polarization and magic angle spinning at 11 kHz. Infrared analysis was conducted with ATR-FTIR spectroscopy (*JASCO FTIR-4100*).

The bulk density (ρ_b) was determined by measuring the weight and volume of the sample. Dimensional shrinkage (%) was taken as the difference between the diameters of the aerogel monolith and of the 20 mL syringe mold (nominally 17.2 mm). He picnometry (*Accupyc 1330, Micromeritics*) was used to measure the real (skeleton) density of the samples. Combining the information of the skeleton and bulk densities, it was possible to evaluate the porosity and pore volume of the samples through equation (IV-1) and (IV-2), respectively:

$$Porosity\ (\%) = \frac{\frac{1}{\rho_b} - \frac{1}{\rho_s}}{\frac{1}{\rho_b}} \times 100 \qquad (IV-1)$$

$$Pore\ volume\ (cm^3\ g^{-1}) = \frac{1}{\rho_b} - \frac{1}{\rho_s} \qquad (IV-2)$$

In addition, we used the Nitrogen gas adsorption (*Accelerated Surface Area and Porosimetry ASAP 2000, Micromeritics*) for the determination of the specific surface area. Before the analysis, the sample was outgassed at 60ºC in vacuum (10^{-5} bar) during 24 h, to remove adsorbed species. In the analysis, volumes of the adsorbed nitrogen at five different

relative pressures (0.05 to 0.2) were taken at 77°K, to obtain the specific surface area by the BET theory. The average pore diameter of samples has been calculated from equation (IV-3):

$$Average\ pore\ diameter\ (nm) = \frac{4(pore\ volume)}{S_{BET}} \qquad (IV-3)$$

Scanning electron microscopy (SEM) (*JMS-5310, JOEL)* was used to observe the materials microstructure. Due to the low electrical conductivity of the highly porous silica-based samples, an Au film was deposited on their surfaces, using the Physical Vapor Deposition (PVD) technique during 20 s.

The thermal conductivity of the reinforced aerogels was measured using a transient method (*Thermal constants analyzer TPS 2500 S, Hot Disk*). The sensor is clamped between two identical disc shaped pieces of the sample, which have a diameter of 1 cm and thickness of 0.5 cm (conveniently cut from the cylindrical aerogel samples). This analysis was carried out at 20ºC and the equipment presents a reproducibility and accuracy over 1% and 5%, respectively.

For the mechanical test, samples were cut to meet a length:diameter ratio of 2:1, and were polished to make sure that top and bottom sides were smooth and parallel. The compression test was conducted following the *ASTM standard D695-02a*. All tests were done at nominal room conditions with a stroke speed of 1.3 mm/min.

IV. 2.4 Vacuum outgassing and thermal cycling screening tests

The thermal characteristics of developed aerogels have been evaluated by conducting two standard screening tests of vacuum outgassing (normative reference: *ECSS-Q-ST-70-02C*, European Space Agency for the members of ECSS, 2008) and thermal cycling (normative reference: *ECSS-Q-ST-70-04*, European Space Agency for the members of ECSS, 2008). The two standard tests of vacuum outgassing and thermal cycling have been conducted in a

vacuum drying oven (*Binder;* temperature range: 15ºC (59ºF) - 200ºC (392ºF); heating rate: 3ºC min^{-1}; pressure interval: 1 mbar - 1 atm).

Before conducting the standard tests, for each selected optimized aerogel and aerogel-like monoliths under study, three specimens (replicas) with minimum weight of 0.1 g were prepared by proper cutting from initial monoliths. For the outgassing test, after recording the initial weight of each sample (~0.3 g), the Total Mass Loss (TML) of the material outgassed during 24 hours, at constant temperature of 125ºC and minimum pressure of 1 mbar was evaluated. The Water Vapor Regained (WVR), which is defined as the mass of water vapor regained by the sample after a reconditioning step, is measured from the increase in the sample mass, after the test for TML, when exposed 2 hours to controlled conditions (relative humidity of 65% at room temperature of 22°C). The total mass of the specimen without adsorbed water, *i.e.* the Recovered Mass Loss (RML), is evaluated by the previous two quantities, according to the following expression:

$$RML = TML - WVR \quad \text{(IV-4)}$$

The outgassing requirement is RML < 1% in order to consider the material acceptable for use in Space applications.

After evaluating the values of TML, WVR and RML, the samples chemical properties were evaluated again by taking ATR FT-IR spectra.

For the thermal cycling test, for each selected sample, three replicas were prepared and precisely weighted, and then, samples were exposed to three successive thermal cycles from -78ºC to 125ºC. To do this, firstly the samples were immersed in liquid nitrogen (-78ºC) for about 1 min and, then, they were allowed to rest at ambient temperature for 30 min. After, the samples temperature was raised to 125ºC in an oven, for 30 min, under vacuum. This procedure was repeated for each sample after allowing the sample to rest in ambient

conditions for 2 hours. After each cycle, the information related to the sample outgassing and macroscopic changes in the samples was recorded.

IV. 2.5 Response Surface Methodology

Response Surface Methodology (RSM), developed by Box and Wilson in 1951 [202], is a collection of statistical and mathematical methods that are useful for designing experiments, building models, evaluating the effect of factors and searching for optimum conditions for desirable responses [203]. The RSM technique can improve product yields and provide better confirmation of the output response toward the target requirements. In recent years, RSM has played an important role in biotechnology and other fields [204]. The main advantage of RSM is the significant reduction of experimental runs required to provide sufficient information for statistically valid results. Moreover, RSM is faster and more informative than the classical full factorial design approach.

The RSM is a sequential process and its procedure can be summarized as follows [205]. First, a series of experiments is performed for adequate and reliable measurement of the response of interest. Second, a mathematical model of the response surface is developed, with the best fit, and, then, the optimal set of experimental parameters that produce a maximum or minimum value of the response is determined. Lastly, the direct and interactive effects of process parameters are represented through two- and three-dimensional (3D) plots, allowing the final verification.

In most RSM problems, the form of the relationship between the response and the independent variables is unknown. Thus, the first step in RSM is to find a suitable approximation for the true functional relationship between the response (Y) and the set of

independent variables [206]. If the response is well modeled by a linear function of the independent variables, then the approximation function is the first-order model below:

$$Y = \beta_0 + \beta_1 X_1 + \beta_2 X_2 + \cdots + \beta_k X_k + \varepsilon \quad \text{(IV-5)}$$

Where X_1, X_2, . . ., X_k are the independent variables, β_0 the constant coefficient, β_k the linear effect of the *k*th factor coefficients and ε is the error observed in the response *Y*.

If there is curvature in the system, then a polynomial of higher degree must be used, such as the second-order model that follows, written for the case of two variables:

$$Y = (\beta_0 + \varepsilon) + \sum_{i=1}^{2} \beta_i X_i + \sum_{i=1}^{2} \beta_{ii} X_i^2 + \sum_{\substack{i=1 \\ i<j}} \sum_{j=i+1} \beta_{ij} X_i X_j, \quad \text{(IV-6)}$$

Where β_{ii} represents the quadratic effect of the *i*th factor and β_{ij} represents the interaction effect, between the *i*th and *j*th factors. The goal of RSM is to find an approximation function for predicting future response and to determine factor values that optimize the response function. An important assumption is that the independent variables are continuous and controllable by experiments with negligible errors. The task then is to find a suitable approximation for the true functional relationship between independent variables and the response surface [205].

IV. 2.5.1 Central Composite Rotatable Design (CCRD)

Experimental design and analysis was conducted using *Design Expert 7.1.3* available from *State-Ease, Inc.* (Minneapolis).

Two 2-factor-5-level central composite rotatable designs (CCRD) with two replicas at the center were used to develop predictive models for some physical and mechanical property parameters of BTMSH and BTESB derived aerogels. It was deemed reasonable to set two CCRD for each type of APD-aerogel-like samples (with BTMSH or BTESB) to evaluate measured properties of cross-linked aerogels as a function of processing parameters. The two

factors' levels in terms of coded and uncoded (actual) values are shown in Table IV. 1 and Figure IV. 2 for BTMSH and BTESB derived aerogels.

Here in, the important variables under study as well as their levels have been previously defined by factor screening. Therefore, for each ambient pressure dried aerogel, two preparation conditions have been systematically varied: silicon concentration derived from BTMSH or BTESB (X_1) and values of R, which are defined as a molar ratio of tri-methacrylate to TMSPM (X_2). The variation of these two variables has previously demonstrated to have a strong effect on both mesoporous underlying structure and the extent of cross-linking [201].

This design includes a standard of 2*k* factorial points (coded as ±1 notation), 2*k* points fixed axially at a distance *a* from the center (±*a*), and N_0 replicate tests at the center (0) – Figure IV. 2. *k* is the number of operating variables. Center points, which are located in the midpoint of each factor range, give information about the existence of curvature.

Table IV. 1 Coded and actual levels of variables considered for design for APD BTMSH and BTESB derived aerogel-like monoliths.

Feed Factors	**Coded X_i**	**BTMSH derived silica xerogel**					**BTESB derived silica xerogel**				
		Variation levels					**Variation levels**				
		-1.41	-1	0	1	1.41	-1.41	-1	0	1	1.41
Si mol% of Bis-silane	X_1	0	6%	20%	34%	40%	5%	6%	7.5%	9%	10%
R	X_2	0.5	0.7	1.25	1.8	2	0.5	0.7	1.25	1.8	2

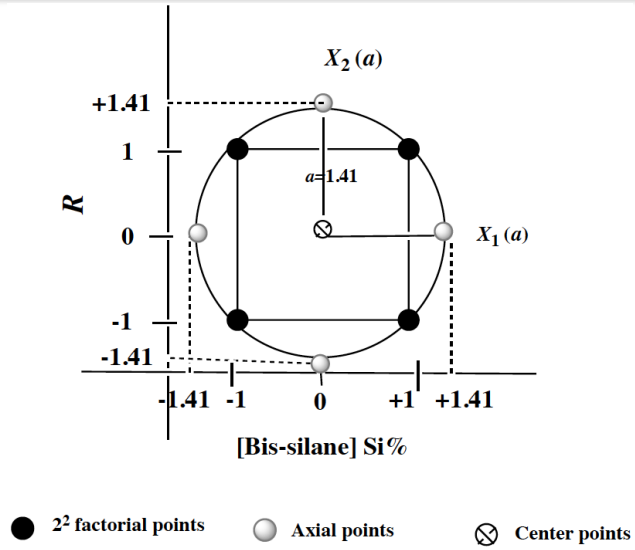

Figure IV. 2 Central composite rotatable design (CCRD) for two experimental factors, X_1 and X_2 variables, respectively Si mol% derived from BTMSH and BTESB, and *R* ratio.

The estimation of the pure quadratic properties of the model can be carried out by using the axial points. All these points were calculated as function of the range of interest for each factor [207]. The total number of design points in CCRD can be calculated from:

$$N=2k+2k+N_0 \quad \text{(IV-7)}$$

Where N is the total number of design points, k is the number of factors.

Rotatability was selected since these properties of the design are desirable. The design is rotatable if the variance of response is constant for all variables at a given distance from the design center [208]. The CCD is rotatable if:

$$\alpha = \sqrt[4]{2^k} \quad \text{(IV-8)}$$

Figure IV. 3 shows the CCRD in which two axes represent one of the two variables for APD- BTMSH aerogel-like samples. Designs with this property exhibit circular contours on the standard error plots.

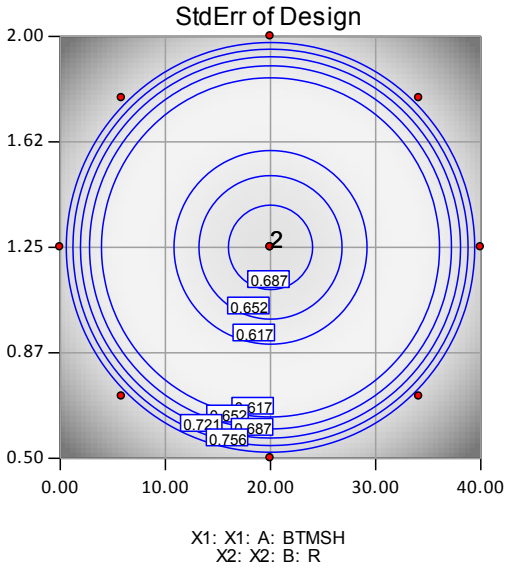

Figure IV. 3 Standard error of design plot for BTMSH derived aerogels.

The X_1 and X_2 variables were orthogonalized (transformed to -1 to 1 range) prior to the modeling, in order to minimize correlation between terms. The results were statistically evaluated by the analysis of variance (ANOVA) at the significance level of p=0.1 or 90% confidence. The software calculates F-test for significance of the model as well as the significance of each term. Apart from calculating p-values, the adequacy of the model was also evaluated by the coefficient of determination (R^2). The R-squared value of the final model indicates the amount of variation present around the mean that is explained by the model. The closer R-squared is to 1, the less variation exists around the model. The standard deviation of the model is also given. The standard deviation reported is the square root of the residual mean square, and is taken as an estimate of the standard deviation of the experiment. Multiple regression analysis was used and the second order polynomial equations as function of X_i were fitted for each variable assessed at each experimental point.

IV. 3 Results and discussion

As previously described [201] in Chapter III, the multifunctional methacrylate cross-linked silica aerogels were prepared firstly by reacting a mixture of tetramethylorthosilicate (TMOS), bis-silane precursors and 3-(trimethoxysilyl) propyl methacrylate (TMSPM), with base catalysis, to form a silica backbone, following by polymerization on the silica surface as shown in Figure IV. 4. TMSPM was incorporated as a site for tri-methacrylate cross-linking in these gels. In the aforementioned study, and because the tri-methacrylate cross-linker is soluble in methanol (gelation solvent), we added the organic monomer to the gelation solvent in the initial step of preparation of the sol. Then, polymerization occurs after the sol-gel process by applying post-gelation thermal treatment to the wet silica gels.

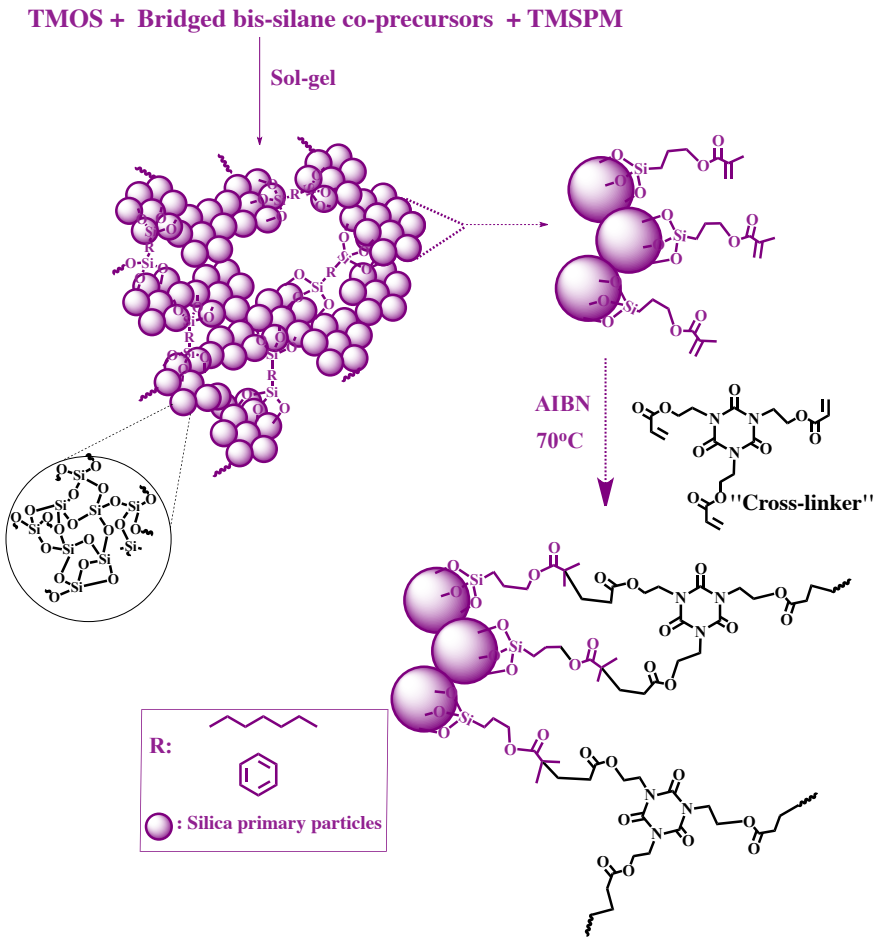

Figure IV. 4 Proposed cross-linking scheme with TMSPM and tri-methacrylate.

Such a one pot strategy leads to a significant simplification and time reduction in the preparation of silica gels. The chemical structures of the aerogels as well as the extent of cross-linking with various underlying silica structures were characterized by studying the obtained solid-state ^{13}CNMR [201], solid-state ^{29}SiNMR and ATR FT-IR spectra.

IV. 3.1 Chemical characterization

The solid ^{29}Si NMR spectra for the aerogel-like samples in which 40 mol% of total silicon was derived from BTMSH (Figure IV. 5a), and, 10 mol% of total silicon derived from BTESB (Figure IV. 5b) with the rest of silicon derived from TMOS and TMSPM precursors, are shown to study the reactivity of each silica precursor. The characteristic peaks that belong to TMOS are assigned as Q_n, being ‘’n’’ indicative of the degree of condensation of silica or extent of siloxane bond (‘’Si-O-Si’’) formation. The T_{nM}, T_{nB} and T_{nBz} are assigned to the characteristic peaks for TMSPM, BTMSH and BTESB precursors, respectively, with ‘’n’’ being the number of siloxane bonds in each precursor.

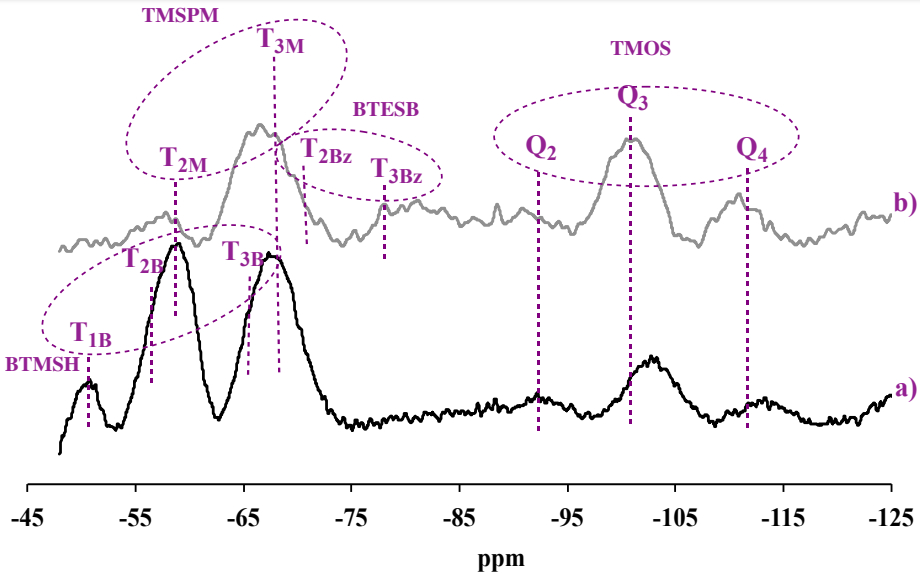

Figure IV. 5 Solid-state ^{29}Si NMR spectra of aerogel-like samples formulated by a) TMOS 40 mol% + BTMSH 40 mol% + TMSPMA 20 mol%, b) TMOS 70 mol% + BTESB 10 mol% + TMSPMA 20 mol%.

The ^{29}Si spectrum for both aerogel-like samples consists of three peaks Q_4, Q_3 and Q_2, being the largest population from Q_3 sites at -101 ppm, which is indicating that a large number of Si-OH sites in TMOS have undergone a condensation reaction. Also, the peak at T_{2M} (-61 ppm) integrates about half of the area of peak T_{3M} (-69 ppm), indicating that 2/3 of TMSPM silicon atoms had completely reacted. Referring to Figure IV. 5a and by subtracting T_{nM} peaks (by considering the equivalent peaks in Figure IV. 5b), the area of the T_{2B} peak at -58 ppm is to some extent larger than T_{3B} at -67 ppm. Therefore, it can be concluded that more than half of BTMSH silicon atoms are not fully reacted. In the spectrum of b, the T_{2Bz} peak at -71 ppm is strongly overlapped with the T_{3M} and has slightly larger peak area than T_{3Bz}, at -78 ppm, which indicates a non-complete reaction of BTESB during gelation.

ATR FT-IR spectra of the different monoliths show that at R = 2, almost all silica surface carbon double bonds, at 1628 cm^{-1}, are consumed during the cross-linking reaction – Figure IV. 6a-c. As expected, a peak due to the stretching vibration of C=O bonds of tri-methacrylate at 1690 cm^{-1} has appeared (*vd.* Figure IV. 6b, d). This is evidenced by the increasing area

under the characteristic peak of tri-methacrylate on the solid-state ^{13}CNMR spectrum and, in the thermo gravimetric analysis, by a drastic increase in the weight loss due to the cross-linker in the aerogel composites – Figure III. 13 of Chapter III [201]. The average number of monomer units (N_t), along with the mass percentage of the monomer contribution on the composites, for representative samples of this study containing different underlying silica and R = 2, were quantified and summarized in Table IV. 2. In the cross-linked aerogels without bis-silane precursors in the underlying silica, the extent of cross-linking is relatively higher than for those containing BTMSH and BTESB bis-silanes. The relative poor cross-linking reaction in the aerogel-like monoliths containing BTMSH may be due to the less accessibility of the silica surface methacrylate to the cross-linker, being sterically blocked by hexyl links from BTMSH [52].

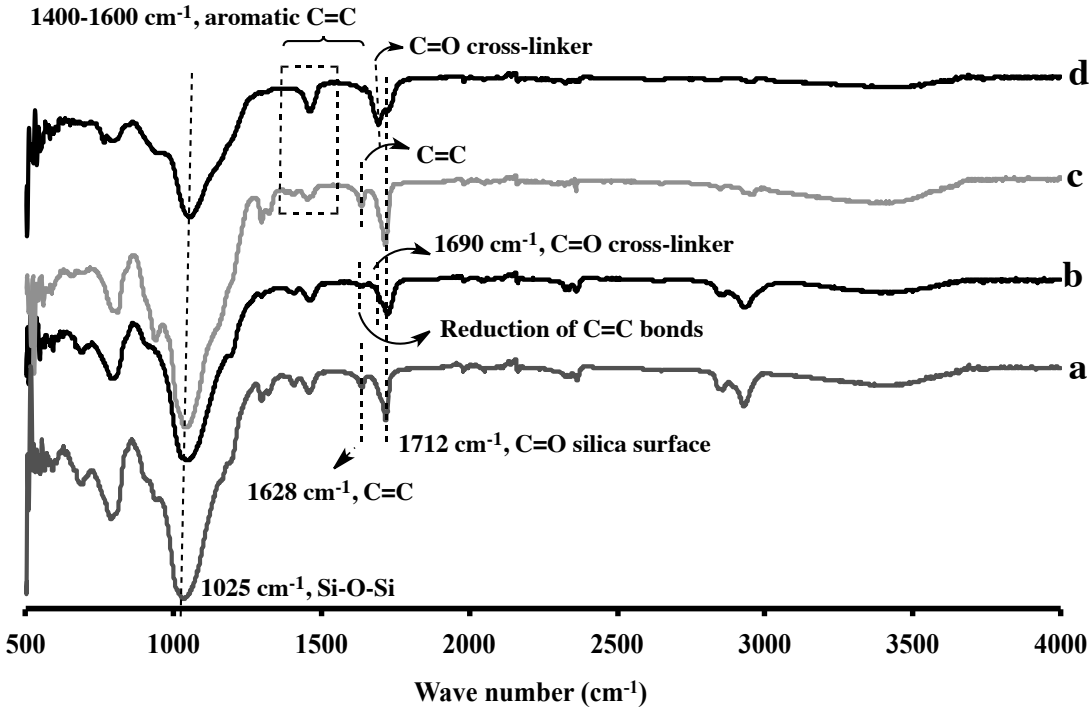

Figure IV. 6 ATR FT-IR spectra of a) Non-X-BTMSH 40 mol%, b) X-BTMSH 40 mol%, R=2, c) Non-X-BTESB 10 mol%, d) X-BTESB 10 mol%, R=2, (X: cross-linked).

Table IV. 2 Monomer contribution in the different aerogel-like composites.

	Cross-linked_BTMSH 40 mol%, *R*=2	**Cross-linked_BTESB 10 mol%, *R*=2**	**Cross-linked_without bis-silane, *R*=2**
Average number of monomer units (N_t)	1.7	2.5	3.2
Cross-linker (wt%) in the aerogel composites	23%	32%	41%

Hydrophobic behavior of some selected best samples was evaluated by studying their water contact angle values. As shown in Figure IV. 7, contact angles measured for representative samples in this study ranged from 100-151^o. The high contact angle (151^o) for BTMSH derived gels indicates that the hexyl groups from BTMSH are present in the silica surface and contributed to the superhydrophobic nature of the cross-linked aerogels. Additionally, the contact angle measured for this sample is higher than for its $scCO_2$ counterpart (θ = 102±2°), suggesting the importance of the drying condition on the hydrophobic properties of this material. The porous surface causes a complication on the accurate quantification of the contact angle, but here, due to the structural shrinkage of the aerogel by ambient pressure drying, the samples lose part of their porosity on the surface. The contact angle measured here is also higher than the contact angle for styrene reinforced aerogels containing BTMSH, which ranged from 112^o to 114^o depending on the BTMSH silicon mol% [52].

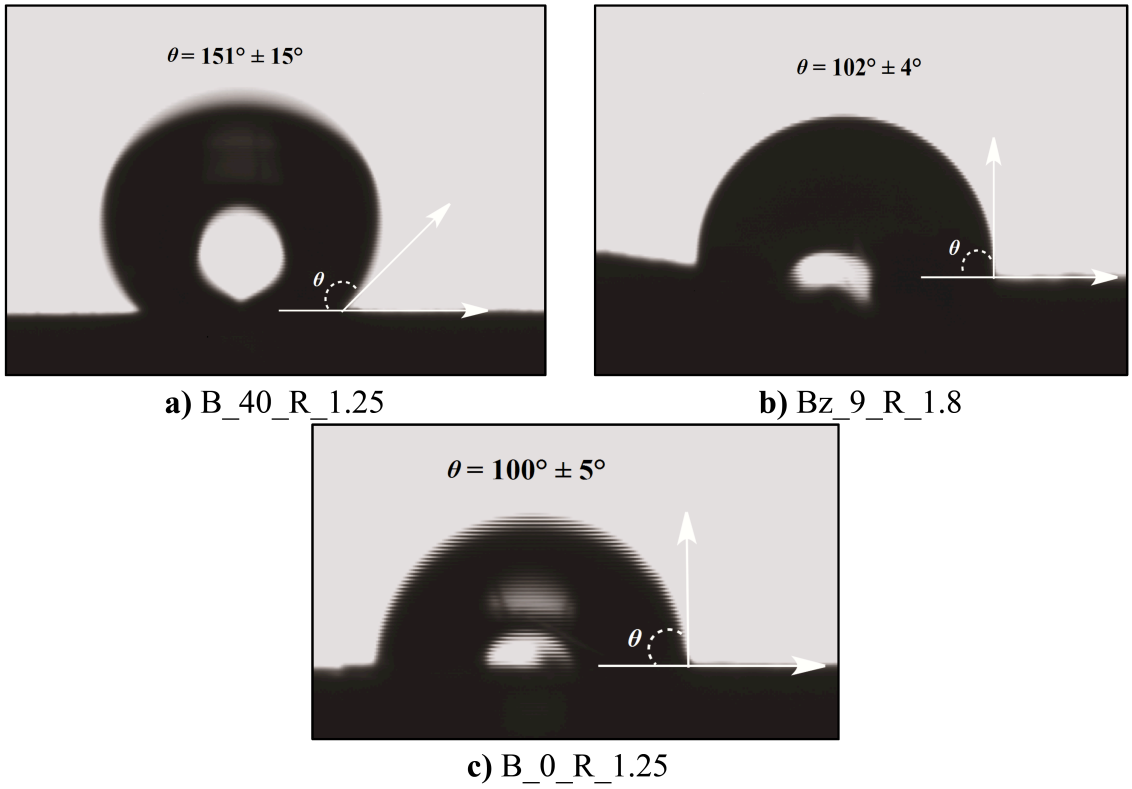

a) B_40_R_1.25 **b)** Bz_9_R_1.8

c) B_0_R_1.25

Figure IV. 7 Water contact angle measurements for the cross-linked aerogels with and without BTMSH and BTESB precursors.

IV. 3.2 Modeling the responses for BTMSH and BTESB derived aerogel-like materials

The experiments were carried out according to Central Composite Rotatable Design (CCRD), an optimal design that allows the calculation of linear and quadratic effects and interactions of factors with the best possible precision at a minimum number of experiments. In this work, 10 experimental runs were prepared, including four factorial points, four axial points and two replicas at the center for each aerogel type. All samples were characterized in terms of bulk density, thermal conductivity and maximum strength at break and the results are summarized in Table IV. 3. By using the multiple regression analysis, the second order polynomial equations as function of X_i were fitted for each variable assessed at each experimental point.

Table IV. 3 Coded operating variables with measured properties of BTMSH and BTESB derived aerogel-like monoliths.

Run no.	Coded level of variables		Experimental responses of BTMSH derived aerogel–like monoliths		
	X_1[a]	X_2[b]	Density (g cm^{-3})	Thermal conductivity (W/m^{-1} K^{-1})	Max. stress at break (MPa)
B[c]_20_R_1.25	0	0	0.50	0.079	2.80
B_20_R_1.25	0	0	0.54	0.081	3.20
B_6_R_0.7	-1	-1	0.48	0.071	0.31
B_34_R_0.7	1	-1	0.46	0.057	2.01
B_6_R_1.8	-1	1	0.66	0.101	1.12
B_34_R_1.8	1	1	0.34	0.065	0.59
B_0_R_1.25	-1.14	0	0.78	0.130	1.13
B_40_R_1.25	1.14	0	0.25	0.055	0.79
B_20_R_0.5	0	-1.14	0.52	0.088	1.03
B_20_R_2	0	1.14	0.56	0.073	4.00
Run no.	**Coded level of variables**		**Experimental responses of BTESB derived aerogel-like monoliths**		
	X_1[a]	X_2[b]	Density (g cm^{-3})	Thermal conductivity (W/m^{-1} K^{-1})	Max. stress at break (MPa)
Bz[d]_7.5_R_1.25	0	0	0.65	0.096	3.61
Bz_7.5_R_1.25	0	0	0.70	0.127	3.60
Bz_6_R_0.7	-1	-1	0.71	0.133	0.30
Bz_9_R_0.7	1	-1	0.64	0.105	0.20
Bz_6_R_1.8	-1	1	0.73	0.103	4.20
Bz_9_R_1.8	1	1	0.58	0.075	2.70
Bz_5_R_1.25	-1.14	0	0.79	0.138	0.34
Bz_10_R_1.25	1.14	0	0.68	0.096	3.30
Bz_7.5_R_0.5	0	-1.14	0.61	0.113	0.13
Bz_7.5_R_2	0	1.14	1.05	0.079	3.80

[a]X_1: Si mol % derived from BTMSH or BTESB
[b]X_2: R = [Tri-meth]/[TMSPM]
[c]B: BTMSH [d]Bz: BTESB

Summary statistics and significant terms in the models for both types of aerogel-like samples are shown in Table IV. 4.

Table IV. 4 Significant terms and statistics summary for response surface models for BTMSH derived aerogel-like material and BTESB derived aerogel-like material.

BTMSH derived aerogels	Significant terms	R^2	Standard error (RMS)
Density	X_1, X_1X_2	0.89	0.061
Maximum stress at break (power transformed)	X_1X_2	0.80	2.400
Thermal conductivity	X_1	0.82	0.009
BTESB derived aerogels	**Significant terms**	R^2	**Standard error (RMS)**
Density	X_2	0.81	0.040
Maximum stress at break (power transformed)	X_2, X_2^2	0.91	1.200
Thermal conductivity	X_1, X_2, X_1^2, X_2^2	0.99	0.001

Response surface plots were generated with the *Sigma Plot* software (*SigmaPlot 12.0*) and drawn by using the function of two factors. Note that the axes in the resulting surface response plots are sometimes rotated in order to best illustrate the particular surface. Therefore, with the derived empirical response surface models, significant effects of the variables on the measured properties were assessed. Multiple regression analysis was used and the second order polynomial equations as function of X_i were fitted for each variable assessed at each experimental point.

Graphs of the response surface models for bulk density, mechanical strength and thermal conductivity are shown in Figure IV. 8. These are plotted vs. mol% of Si derived from bis-silane and *R* ratio. As it is evident from Figure IV. 8a and Table IV. 4, and in agreement with previous studies, the most influential variable on the density of BTMSH derived aerogels is the percentage of BTMSH as well as the synergetic effect of the percentage of BTMSH and *R*. This is due to the insertion of additional mass of BTMSH and cross-linker on the aerogel-like samples. However, in terms of BTESB derived aerogels, due to the low incorporation of BTESB precursor, there is a less significant effect of bis-silane concentration on the measured density – Figure IV. 8d and Table IV. 4. The main influential factor in this case is *R*, and density increased positively by increasing the tri-methacrylate cross-linker concentration. In

addition, for the same preparation conditions, the bulk densities for these aerogel-like samples exceed the values for BTMSH derived counterparts. This is due to the substantial increase in the extent of cross-linking/number of repeating units incorporated per TMSPM unit as measured by solid ^{13}CNMR and TGA for BTESB derived aerogels - Table IV. 2. The actual effect of tri-methacryalate concentration on the density of these aerogels is a challenge, since these samples suffered a high level of shrinkage during the course of drying.

The BTMSH derived aerogels displayed a reduced structural collapse, with an average dimensional shrinkage of 20% upon ambient pressure drying, while BTESB derived aerogels showed an average shrinkage value as high as 30%. This effect is particularly visible at low cross-linker concentrations. Therefore, the increase in density for the BTESB derived aerogels is somehow related to the extent of dimensional shrinkage, as well. Due to the flexible nature of hexyl groups in the BTMSH derived monoliths, these samples recovered most part of their initial wet gel sizes after the ambient pressure drying process.

The graphs of the response surface models for mechanical strength for both aerogel-like samples is shown in Figure IV. 8b, e. As indicated, the most dominant factor in the mechanical strength of BTMSH based aerogel-like sample is the synergetic effect of BTMSH percentage with cross-linker concentration (Figure IV. 8b, Table IV. 4). In fact, the model indicates that with an increasing molar percentage of BTMSH, the compression strength increases when the cross-linker concentration is high, but the inverse occurs when the cross-liker concentration is low. In terms of BTESB derived aerogels, first and second order effects of cross-linker concentration have significant effects on the mechanical strength – Figure IV. 8e, Table IV. 4.

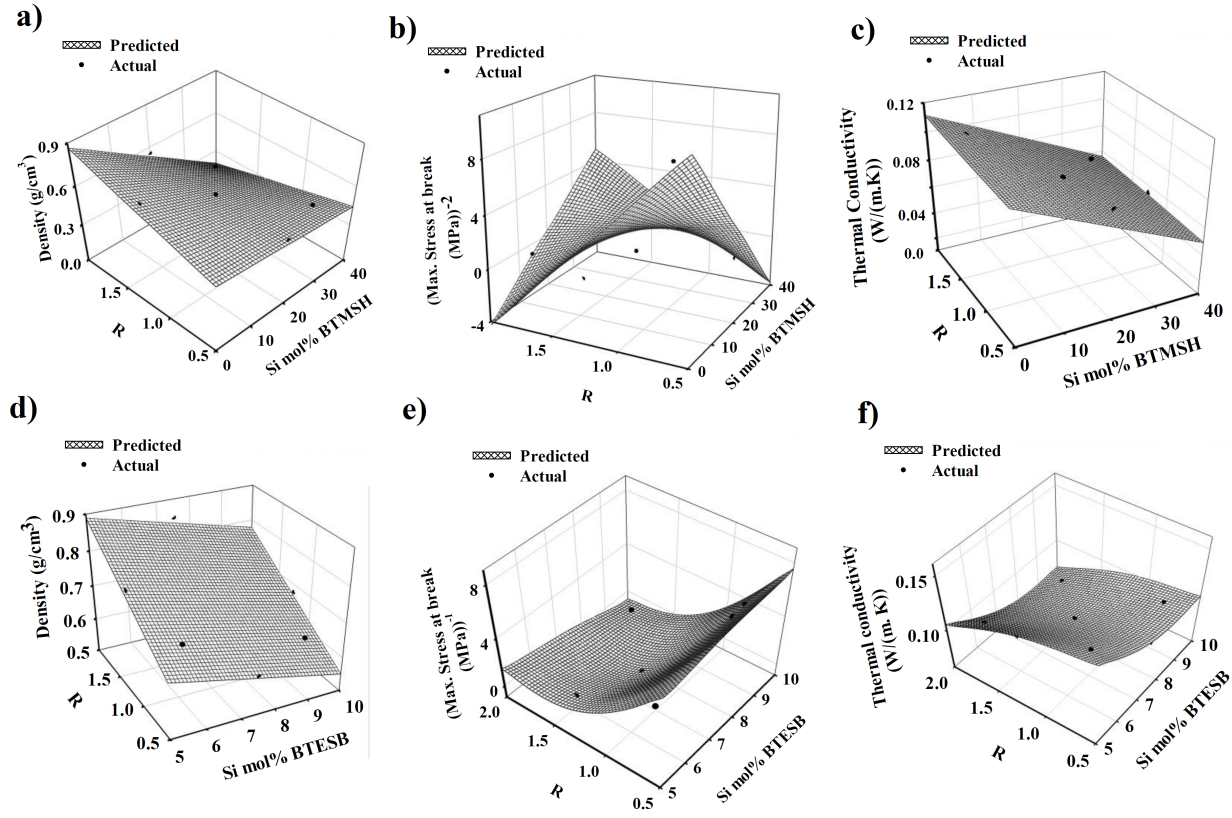

Figure IV. 8 Response surface models of a) density, b) mechanical strength and c) thermal conductivity of BTMSH derived APD-aerogel-like monoliths versus the mol% of silicon from BTMSH and *R;* response surface models of d) density, e) mechanical strength and f) thermal conductivity of BTESB derived APD-aerogel-like monoliths versus the mol% of silicon from BTESB and *R*.

The BTESB derived aerogels are stiffer (Young's modulus (*E)* ~ 0.05-1.8 MPa) when compared to the BTMSH derived aerogels (*E* ~ 0.01-0.43 MPa), due to the presence of rigid aryl spacer in their structures - Figure IV. 9a, b. Moreover, high extent of shrinkage in the APD process intensified this property (*vd.* Table III. 2 – Chapter III).

As expected, thermal conductivity is mostly influenced by the percentage of the BTMSH (Figure IV. 8c), in agreement with results from another reported work [201]. Upon increasing BTMSH molar percentage, the silica network has undergone less structural shrinkage, which led to create large spacing between silica secondary particles, and therefore thermal insulation performance of aerogels has subsequently improved. Response surface graph of thermal

conductivity for BTESB derived aerogels (Figure IV. 8f) indicates that, both the underlying silica structure and *R* have contribution to the thermal conductivity values of this type of aerogel-like samples. The effect of BTESB concentration can be better observed specially at R = 2, where the thermal conductivity decreases with the increasing of BTESB derived Si mol% from 5 to 10 mol%. This is probably due to the increase in the porosity values due to the rigid aryl spacer. Higher porosity favors low thermal conductivity, despite the drastic increase in the density upon drying for these aerogels.

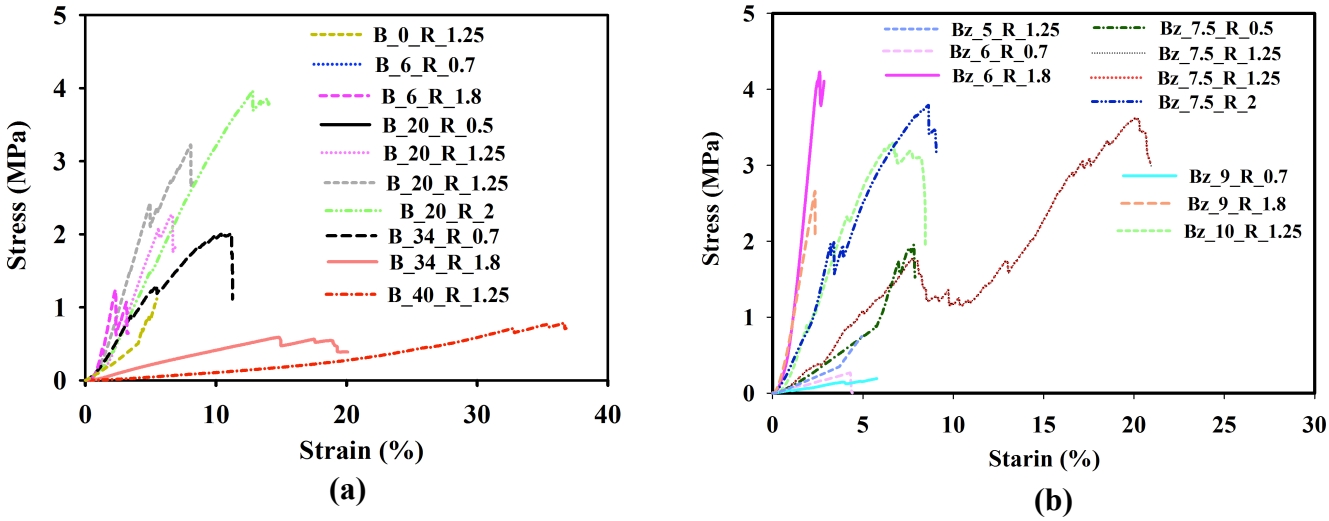

Figure IV. 9 Stress-strain curves of a) BTMSH and b) BTESB derived APD-aerogel-like monoliths.

The N_2 adsorption isotherms along with the pore volume, mean pore sizes and extent of porosity of some selected aerogel-like samples having the same cross-linker concentration but different underlying silica structures are shown in Figure IV. 10 and Table IV. 5, respectively. The N_2 adsorption volumes, the pore sizes and the porosity are extremely influenced by the degree of cross-linking as well as by the inorganic silica nanostructure. As indicated in Figure IV. 10, in the cross-linked aerogels, the N_2 adsorption volumes decreased due to the closing and collapsing of the network pores upon cross-linking by polymer. The reinforced BTESB aerogel-like samples, like their $scCO_2$ dried aerogels, despite the higher extent of polymerization on their surfaces (higher than the reinforced BTMSH aerogels), exhibited relatively high adsorption volumes and, consequently, high specific surface areas. Such

aerogels possess also relatively high extent of porosity (Table IV. 5**)** and, length scales of the pores (40 nm) are smaller than the mean free path of air molecules at standard temperature and pressure (≈ 80 nm). Therefore, improvement in the thermal insulation performance of this type of monoliths is expected, due to a decrease in the gaseous component of thermal conductivity.

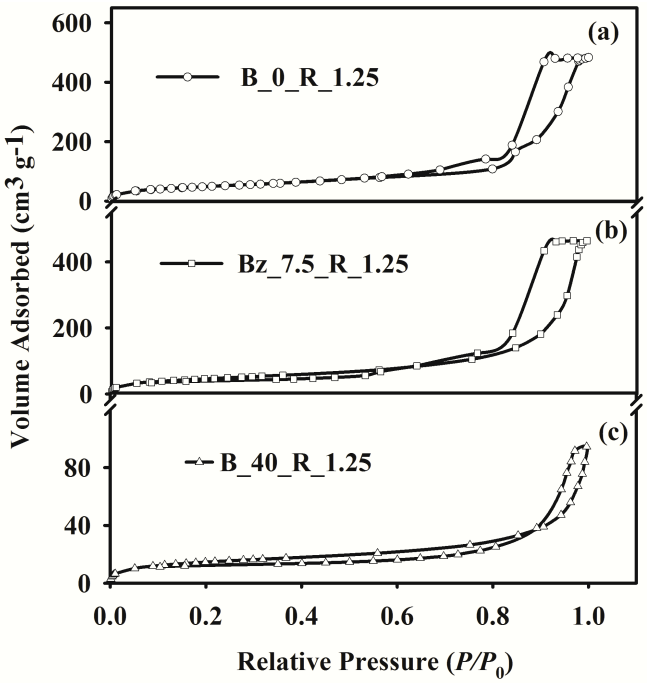

Figure IV. 10 a) Comparative N_2 sorption isotherms of selected cross-linked APD-aerogel-like monoliths.

Table IV. 5 Specific surface areas (BET), pore volumes, pore average sizes and porosity values of selected APD-aerogel-like monoliths.

Sample	BET (m^2 g^{-1})	Pore Volume (cm^3 g^{-1})	Average pore diameter (nm)	Porosity (%)
Bis-silane 0%, R=1.25	190.7	0.55	11.2	82%
BTMSH 40%, R=1.25	53.1	3.47	261	83%
BTESB 7.5%, R=1.25	166.1	2.01	40	90%

IV. 3.3 Optimization of the properties of ambient pressure dried BTMSH and BTESB derived aerogel-like samples

Optimization is an essential tool in the development of silica aerogels for the efficient adjustment of different important synthesis parameters to yield highly acceptable material properties. Optimization and adjustment of the mechanical properties of silica aerogels is a challenge due to the trade off between mechanical strength and bulk density and, therefore, thermal conductivity [29]. So, optimization of silica aerogels properties during mechanical reinforcement, preserving their initial important properties, must be carried out.

Here in, during the optimization of synthesis parameters of APD-aerogel-likes, several response properties describe the quality characteristics of the obtained samples. Some of these properties need to be maximized, while others need to be minimized. To optimize the process with two or more output responses, it is helpful to use the concept of desirability function [209]. The desirability function is one of the most widely used methods for optimization of multiple response processes in science and engineering [210]. Desirability varies from zero to one for specific responses. A value of one represents the ideal case, while zero indicates that one or more responses fall outside the desirable limits.

The main goal of this research was to find the best preparation conditions for the development of APD-aerogel-like samples with material properties near to their $scCO_2$ dried aerogel counterparts. In this context, the desirability allows to find the optimal bis-silanes type and their percentage along with optimal cross-linker concentration.

The desirability function for both aerogel-like types was adopted for the following criteria: maximum value for the compression strength and minimum values for density and thermal conductivity. In terms of density and thermal conductivity, the weight of responses are set at 5 which is determining the level of importance of these two responses in order to be close as

possible to the minimum. In terms of maximum strength, the weight of response is set at 3 in order to be close as possible to the maximum.

By applying the desirability function method, the optimum preparation conditions are demonstrated in Figure IV. 11a, b and Table IV. 6 and were found to be the following: for APD-BTMSH derived aerogels, the BTMSH Si mol% was 40 % and the *R* value was 1.56; for APD-BTESB derived aerogels, the BTESB Si mol% was 9.27 % and the *R* value was 1.8. From the response surface graph of desirability for BTMSH aerogel-like monoliths, the optimum density was determined as 0.26 g cm^{-3}, with maximum compression strength of 0.63 MPa and thermal conductivity of 0.054 W m^{-1} K^{-1}. On the other hand, optimum density value for APD-BTESB derived aerogels was determined as 0.70 g cm^{-3}, with higher maximum compression strength ranging of 2.4 MPa and thermal conductivity of 0.079 W m^{-1} K^{-1}.

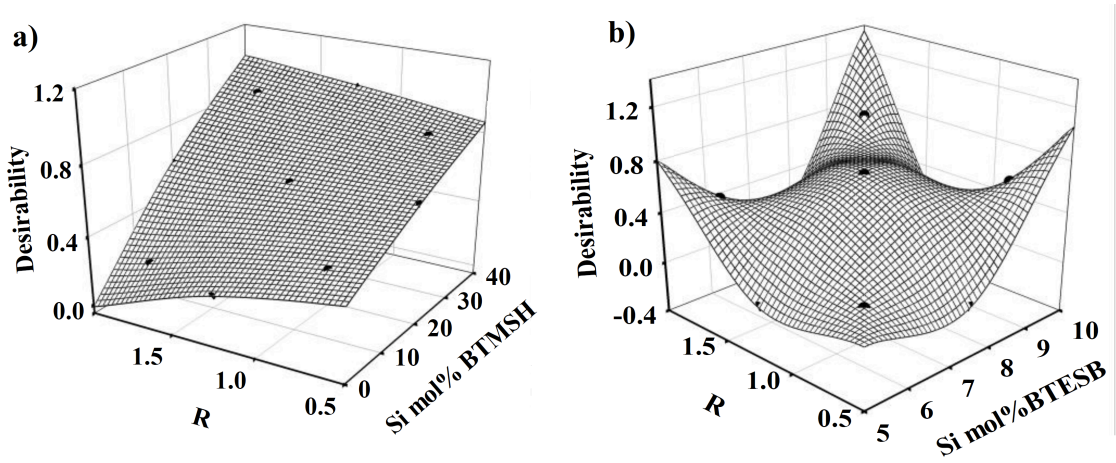

Figure IV. 11 a) Desirability versus Si mol% of BTMSH and *R* for BTMSH derived APD-aerogel-like monoliths, b) Desirability versus Si mol% of BTESB and *R* for BTESB derived APD-aerogel-like monoliths.

Table IV. 6 Optimal design points for BTMSH and BTESB derived aerogel-like monoliths with their predicted response values.

Bis-silane mol%	*R*	Density (g cm^{-3})	Thermal conductivity (W m^{-1} K^{-1})	Max. stress at break (MPa)	Desirability
BTMSH: 40 mol%	1.56	0.269	0.054	0.631	0.976
BTESB: 9.27 mol%	1.8	0.760	0.079	2.380	0.80

After the determination of APD-aerogel-like samples with optimized properties, our next attempt was to compare their important properties with the $scCO_2$ dried aerogel counterparts under the same preparation conditions. For both experimental approaches, we selected the design points that are near in terms of the preparation conditions to the defined optimized APD-aerogel-like monoliths, according to the formulations indicated in Table IV. 6. The selected optimized samples have been synthesized by subjecting the wet gels to extra post-gelation washing with hexane so that all methanol and residual water could be removed. Then, several important properties, including physical and mechanical properties, of both types of samples were compared with those from their $scCO_2$ dried counterparts - Table IV. 7. It is interesting to note that, by increasing the number of the post-gelation treatment cycles of monoliths with hexane, the material properties of the sample have been improved over their previous values at Table IV. 3.

Table IV. 7 Comparison of important physical and mechanical properties of optimized APD-aerogel-like monoliths and $scCO_2$ dried aerogels under the same synthesis conditions.

Sample	Density (g cm^{-3})	Shrinkage (Diam.%)	BET (m^2 g^{-1})	Pore volume (cm^3 g^{-1})	Average pore diameter (nm)	Thermal conductivity (W m^{-1} K^{-1})	Max. stress at break (MPa)
SCD-B_40_R_1.25	0.22	11	82.2	3.5	170	0.060	0.523
APD-B_40_ R_1.25	0.24	14	53.1	3.47	261	0.055	0.786
SCD-Bz_9_R_1.8	0.29	12	208.9	3.94	75	0.052	1.146
APD-Bz_9_R_1.8	0.52	26	155.1	1.81	47.4	0.075	2.658

As indicated, BTMSH derived aerogel-like samples are stronger than their SCD counterparts with only marginal differences between density and thermal conductivity of both samples. Sample photos shown in Figure IV. 12a reveal that there are no major structural or physical differences in both aerogel and aerogel-like samples derived from BTMSH, and, both are strong and have enough structural integrity. However, compared to the SCD aerogels, aerogel-like samples, due to the relatively higher shrinkage upon drying from hexane, have exhibited less spring back or recovery of the gel initial size after drying. The higher shrinkage caused to some extent the losing of porosity and surface area in the APD aerogels. Analyzing the stress strain curves (Figure IV. 12c), they revealed that the $scCO_2$ dried BTMSH aerogel possesses slightly high elastic properties, confirmed by its higher strain values, up to approximately 45% of the strain, when compared to the APD-aerogel-like monoliths that compressed up to 36% of the strain.

In terms of BTESB derived samples, <50% increase in the density and thermal conductivity along with significant increase in the mechanical strength is shown for the aerogel-like samples when compared to their $scCO_2$ dried counterparts. As mentioned before, BTESB derived APD-aerogel-like monoliths have suffered higher dimensional shrinkage when compared to the BTMSH derived samples. Therefore, a significant increase in density is noticed for the BTESB aerogel-like samples (Figure IV. 12b). It is worth noting that, despite

of higher *R* values for the optimized BTESB samples, their surface area is still high. This confirms their relatively high pore volume and extent of porosity even after large shrinkage with drying – Table IV. 7.

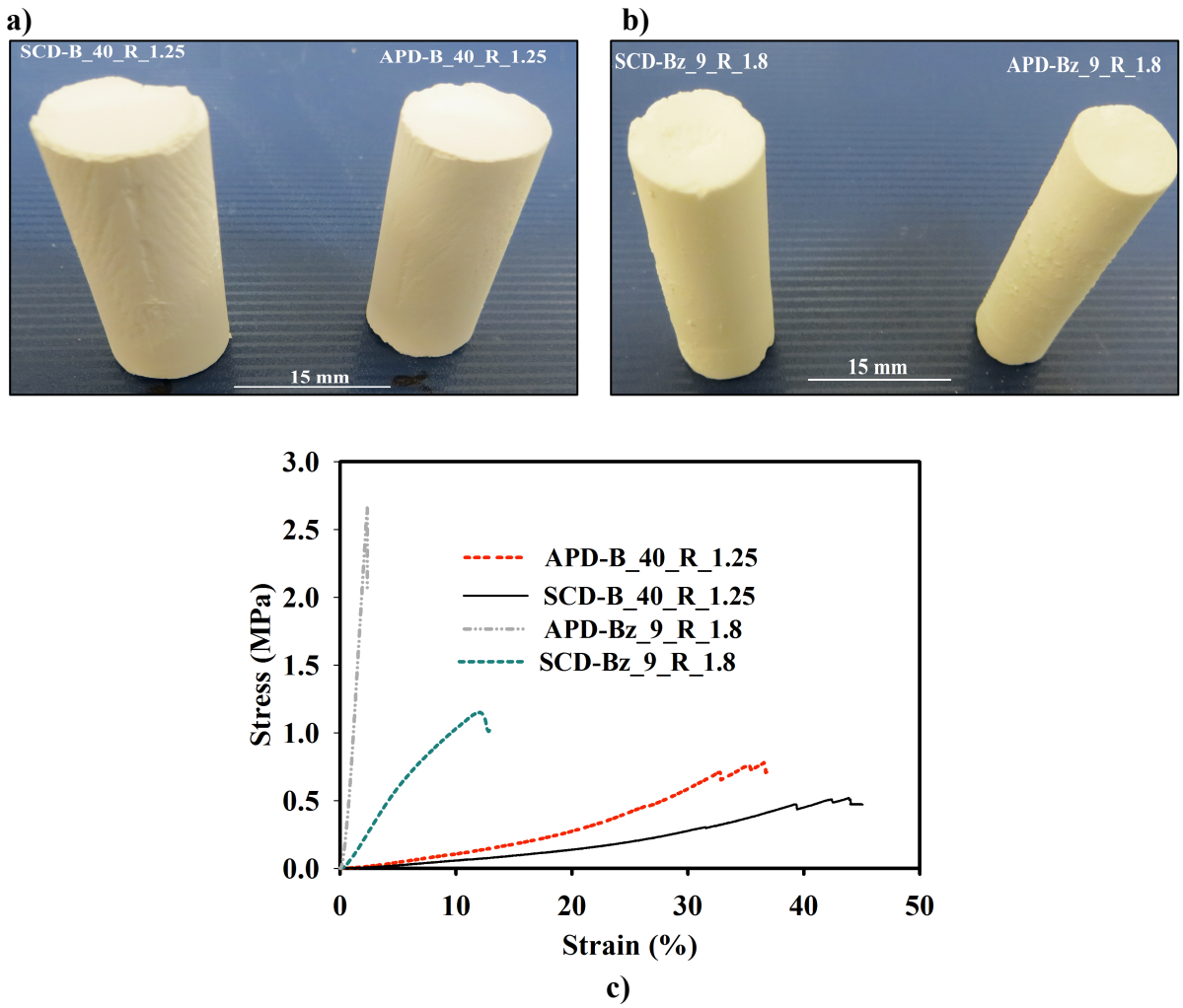

Figure IV. 12 a) Optimized APD-BTMSH derived aerogel-like samples and their $scCO_2$ dried counterparts and, b) optimized APD-BTESB derived aerogel-like samples versus their $scCO_2$ dried counterparts, c) stress-strain curves for monoliths in a) and b).

Scanning electron microscopy micrographs of both optimized APD samples and their $scCO_2$ dried aerogel counterparts are shown in Figure IV. 13, under the same preparation conditions. The SEM micrographs of both types of samples revealed a conformal polymer coating on the silica that forms the skeletal framework of the aerogel. The optimized APD cross-linked BTMSH derived aerogels retain a microstructure, which is practically identical to that of

aerogels dried under supercritical conditions. On the contrary, the optimized cross-linked APD-BTESB derived aerogel monolith shows clear signs of collapse (*i.e.* a virtual disappearance of mesoporosity and irregularities in the silica particle morphology). This result is in agreement with a high extent of shrinkage and relatively low surface area and porosity when compared to the $scCO_2$ dried aerogel, already discussed before.

These results suggest that the properties of cross-linked aerogels dried from hexane under ambient pressure are to some extent similar to those dried supercritically.

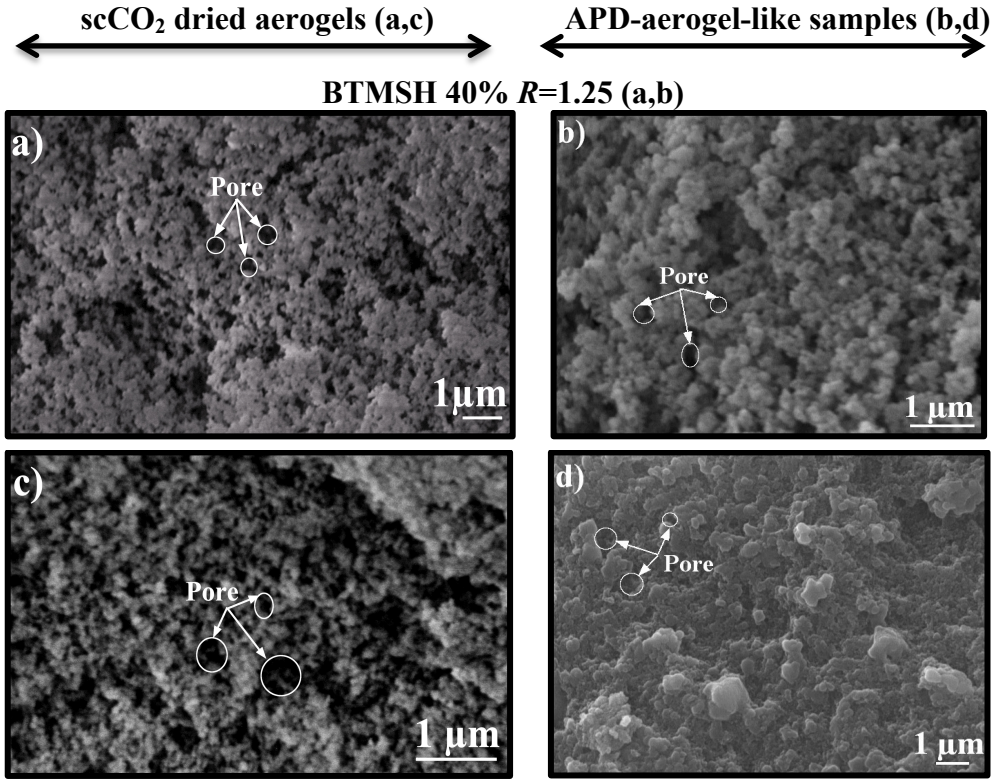

Figure IV. 13 SEM images of optimized APD and $scCO_2$ dried aerogels.

IV. 3.4 Evaluation of sample properties for Space applications

Aerogel and aerogel-like materials properties should fulfill the requirements for service in the environments to which they will be exposed. The aerogels in this study are being developed for Space applications; therefore, the material properties should comply with

thermal characteristics of the Space environment. There are several standard tests to evaluate the material specification with the purpose of Space use [211]. These standards apply to materials used for structural, semi-structural, electronic, electrical as well as both manned and unmanned Space craft applications. The standards should consider some constrains that are specific to Space, *i.e.* vacuum and radiation. These constrains are applied in order to ensure that the material satisfies the requirements during mission. Vacuum outgassing [212] and thermal cycling [213] are two important examples of those important standard tests to qualify materials for Space use. Vacuum outgassing test is applied to evaluate outgassing characteristics of the proposed materials under high vacuum, when they are developed for use in the fabrication of spacecraft and their associated equipment.

The summary of results for the samples subjected to outgassing is presented in Table IV. 8, revealing that, for optimized APD-aerogel-like samples and their $scCO_2$ dried aerogels, the RML values are far less than 1%, which indicates the compatibility of samples with simulated thermal and vacuum characteristics of Space environment. The chemical structure inspection by ATR FT-IR also confirms that there are no structural degradation/dissociation on the chemical bonds of the aerogels after 24 hours outgassing at $T = 125^{o}C$ – Figure IV. 14a, b.

The thermogravimetric analysis indicated that both BTMSH and BTESB derived aerogels are almost thermally stable, since there is no significant mass loss until $T = 125^{o}C$, except for the mass loss of water adsorbed on the aerogel network - Figure IV. 15.

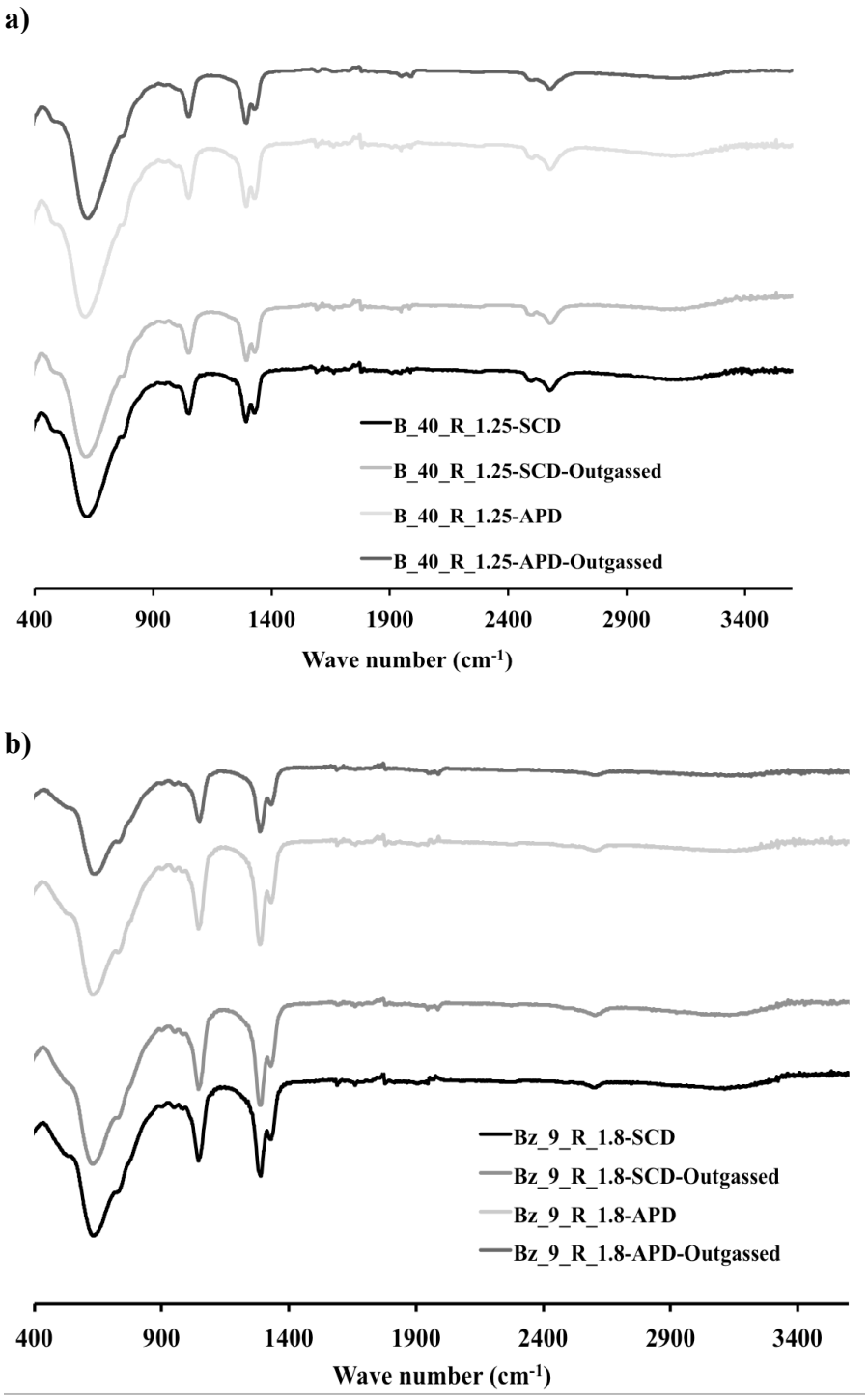

Figure IV. 14 ATR FT-IR spectra of a) BTMSH and b) BTESB derived APD-aerogel-likes and $scCO_2$ dried aerogels after vacuum outgassing test.

Table IV. 8 Vacuum outgassing data for optimized APD-aerogel-like samples and $scCO_2$ dried aerogel samples.

Sample	TML %	RML %	WVR %
SCD-B_40_R_1.25	0.92±0.08	0.29±0.002	0.64±0.002
APD_B_40_ R_1.25	1.28±0.006	0.46±0.006	0.82±0.0003
SCD-Bz_9_R_1.8	1.08±0.002	0.23±0.003	0.85±0.005
APD-Bz_9_R_1.8	1.5±0.001	0.46±0.002	1.04±0.0006

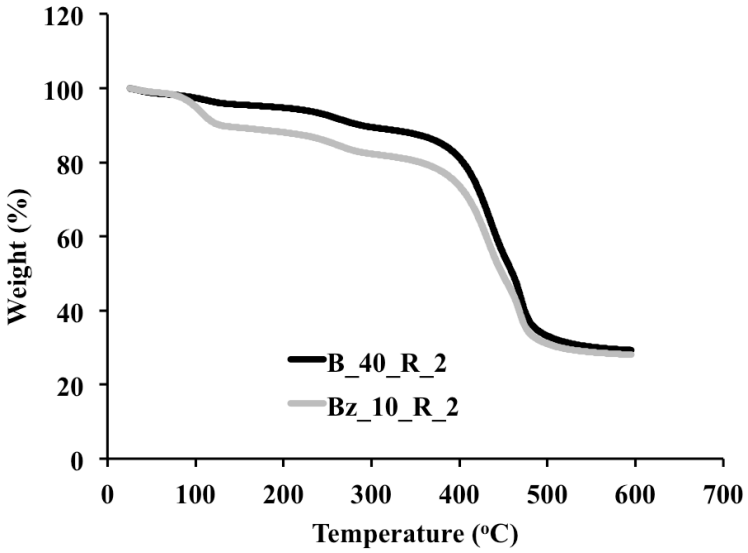

Figure IV. 15 Thermogravimetric analysis (TGA) data of BTMSH and BTESB derived APD-aerogel-like monoliths.

Thermal cycling is the other standard test, in which material is subjected to a certain number of thermal cycles under vacuum. The purpose of this test is to evaluate the capability of the material to withstand thermal stresses in the intended Space environment. For this, temperature oscillates within a defined temperature range in order to anticipate or evaluate the material resistance to some deleterious, namely outgassing, fracture or cracking due to sudden dimensional changes and so forth. Here in, the optimized APD and $scCO_2$ dried aerogel samples were subjected to three successive thermal cycles by applying temperature in the

range of -78 to 125°C in each cycle, under vacuum. Subsequently, the tested samples were inspected by visual examination, outgassing recording and mechanical properties evaluation. Summary of the outgassing behavior of the samples during three referred cycles is shown in Table IV. 9 These results reveal that samples are stable even after three thermal cycles.

Table IV. 9 Thermal cycling data for optimized APD and $scCO_2$ dried aerogels.

Sample	**1st thermal cycle**		
	TML_1 (%)	RML_1 (%)	WVR_1 (%)
SCF-B_40_R_1.25	1.090 ± 0.006	0.580 + 0.003	0.510 ± 0.004
APD_B_40_R_1.25	0.960 ± 0.005	0.620 ± 0.003	0.340 ± 0.002
SCF-Bz_9_R_1.8	1.130± 0.006	0.560 ± 0.002	0.580 ± 0.004
APD-Bz_9_R_1.8	0.910 ± 0.002	0.780 ± 0.002	0.130 ± 0.001
	2nd thermal cycle		
	TML_2 (%)	RML_2 (%)	WVR_2 (%)
SCF-B_40_R_1.25	0.86 ± 0.13	0.29 ± 0.01	0.53 + 0.02
APD_B_40_ R_1.25	0.88 ± 0.13	0.20 ± 0.05	0.66 ± 0.05
SCF-Bz_9_R_1.8	1.03 ± 0.30	0.47 ± 0.03	0.56 ± 0.12
APD-Bz_9_R_1.8	1.0 ± 0.13	0.41 ± 0.03	0.59 ± 0.20
	3rd thermal cycle		
	TML_3 (%)	RML_3 (%)	WVR_3 (%)
SCF-B_40_R_1.25	1.43 ± 0.27	0.030 ± 0.007	1.400 ± 0.007
APD_B_40_ R_1.25	0.95 ± 0.05	0.310 ± 0.041	0.640 ± 0.035
SCF-Bz_9_R_1.8	0.84 ± 0.10	0.040 ± 0.040	0.800 ± 0.140
APD-Bz_9_R_1.8	1.27 ± 0.20	0.540 ± 0.010	0.730 ± 0.210

IV. 4 Conclusion

In summary, ambient pressure dried silica aerogels with different underlying silica structures have been synthesized. The polymer cross-linked silica aerogel monoliths developed here can be dried under ambient pressure from hexane with no need for supercritical fluid extraction. The key properties of APD-aerogel-like materials, including

bulk density, thermal conductivity and mechanical properties, were studied and modeled by using a statistical design of experiments. The empirical models derived for each type of aerogel-like samples allowed us to define the optimized preparation conditions by means of a desirability function that included all the referred key properties. Comparing the optimized APD aerogels' properties with those of their $scCO_2$ dried counterparts, we proved the similarity in the some properties with ~2× increase in the mechanical strength, which confirmed the adequacy of the proposed synthesis and drying method. Also, the cross-linked aerogels of this study are more than 400× stronger than the underlying plain silica framework, and thus they have been able to withstand the surface tension forces during ambient pressure drying. Such drastic increase in mechanical strength was accompanied by less than two time increase in the bulk density for BTMSH based aerogel-like samples over their nonreinforced counterparts. Additionally, the optimized aerogel-like and aerogel samples of this study have been inspected in terms of their material characteristics for use at intended Space applications. It has been shown that the material characteristics of the developed aerogels are suitable for the simulated Space environment condition. This appears to be the first report on aerogels addressing successfully the aerogels' material specification for Space environments.

Finally, monolithic materials developed here have a broad practical impact. In fact, due to their hydrophobicity, higher mechanical strength and the need of simple ambient pressure drying, they can replace their supercritical counterparts in some applications, enabling large-scale production.

Chapter V. Develoment of mechanically reinforced silica aerogels *via* Surface-Initiated Reversible Addition-Fragmentation Chain Transfer (RAFT) Polymerization.

This chapter comprises the work published in Journal of Materials Chemistry A (2014), DOI: 10.1039/C4TA05618C, by: Hajar Maleki, Luísa Durães, António Portugal.

V. 1 Introduction

Reinforcement of the silica network with polymers synthesized by step growth polymerization from initiators attached to the surface has been demonstrated to produce strong aerogels [48]. Similarly, free radical polymerizations from attached initiators was only recently achieved with the synthesis of an azobisisobutyronitrile (AIBN) bridged silsesquioxane monomer (5 mol%) that upon co-polymerization with tetraethylorthosilicate (TEOS) was inserted into the silica matrix of the aerogel [177]. Heating the silica gel modified with the azo bridged silsesquioxane to 70°C led to the decomposition of the azo compound to form radicals attached to a silane. These radicals were used to initiate the polymerization of vinyl monomers (methyl methacrylate, styrene and divinylbenzene) grafted from the surface of the silica gel. However, a significant portion of the initiator remained buried in the silica matrix and was not useful to the polymerization of vinyl monomers. The polymer grafted was of high polydispersity, as the polymerization was uncontrolled, not allowing for structure property relationships to be established. Additionally, heating the gels resulted in decomposition of the azo bridged silsesquioxane which cause a weakening of the silica gel mechanical properties.

To ascertain the grafted polymer's molecular weight influence on the mechanical properties of silica aerogels, Boday *et al.* [24] utilized atom transfer radical polymerization (ATRP) from surface bound initiators. This approach led to the incorporation of well-defined poly (methyl methacrylate) with low polydispersity and, therefore, allowed to establish a tunable structure-property relationship between the molecular weight of grafted polymers and the toughening of the hybrid aerogel.

To date, controlled polymerization techniques are scarcely investigated as an approach to improve silica aerogels' mechanical properties. In this study, we extend the previous approaches to grow vinyl polymers from the colloidal particles of silica gels. Inspired on the previous work of Boday *et al.* [24] that seeks to establish a tunable correlation between polymer molecular weight and mechanical properties of aerogels, we also report the preparation of mechanically enhanced hybrid aerogels using surface initiated reversible addition-fragmentation chain transfer (SI-RAFT) [214, 215] polymerization to grow well-defined polystyrene and poly (butyl acrylate) from the silica surface.

This work included the synthesis of sol-gel processable RAFT initiators, sol-gel polymerization for RAFT initiator-modified gels, RAFT from the surface of gels, supercritical drying for aerogels formation and characterization of the mechanical properties of the resulting aerogel composites. Not only this approach will allow the incorporation of well defined polymers into aerogels, but its versatile methodology allows for the polymerization of a number of vinyl and cross-linkable monomers, without the initiator causing the weakening of the silica network [177].

V. 2 Background of controlled radical polymerization

In conventional free radical polymerizations, the radicals generated from the decomposition of free radical initiators, such as azobisisobutyronitrile (AIBN) or benzoyl peroxide (BPO),

follow rapid propagation and rapid termination [216]. In these polymerizations, high molecular weight polymers are obtained and the formed polymers are polydisperse.

Controlled radical polymerizations (CRP) differ from conventional free radical polymerizations since, in the former case, the propagating radical is present [217]. As mentioned, conventional free radical polymerizations undergo chain transfer or termination of the propagating radical within seconds of initiator decomposition. CRP is based on a dynamic equilibrium of dormant and active propagating sites, in which the conversion from a dormant site to a propagating radical and back to dormant is very rapid. To achieve this dynamic equilibrium, CRP utilizes deactivators or transfer agents that react with the propagating radical making it dormant. This process allows for the preparation of well-defined polymers.

In the past two decades, the field of CRP has been rapidly growing with a number of techniques developed to prepare well-controlled polymers. The most prevalent methods used to prepare well-defined polymers using CRP are stable free radical polymerizations (*i.e.* nitroxide mediated polymerization (NMP)) [218], metal catalyzed radical polymerizations (*i.e.* atom transfer radical polymerization (ATRP)) [219] and degenerative transfer radical polymerizations (*i.e.* reversible addition-fragmentation chain transfer (RAFT)) [220]. As we use RAFT in this study, a brief summary of this polymerization technique is included to provide an adequate background of this method.

V. 2.1 Reversible Addition-Fragmentation Chain Transfer (RAFT) polymerization technique

RAFT polymerization has now became one of the most powerful CRPs because of its good control over the polymer structures, its applicability to a wide range of monomers and the mild reaction conditions [221-223]. It is a degenerative chain transfer process and is free

radical in nature. Implementing a RAFT polymerization can be as simple as introducing a suitable chain transfer agent (also known as RAFT agent, normally thiocarbonylthio compounds) into a conventional free radical polymerization system. The RAFT agents have a significant effect on the controllability of the RAFT polymerization and thus should be carefully chosen for a specific polymerization system.

As shown in Figure V. 1, RAFT polymerization starts with a standard initiation step as in the conventional radical polymerization (with *e.g.* AIBN or BPO initiator), where the homolytic bond cleavage of a normal radical initiator I_2 leads to two reactive primary free radicals I^o. I^o then reacts with monomer molecules to form a propagating polymeric radical P^o_n, which further adds to the C=S bond of the initial RAFT agent 1 to yield a carbon-centered intermediate RAFT radical 2. Fragmentation of this intermediate gives rise to either the original reactants (1 and P^o_n) or a polymeric RAFT and a new radical R^o, which is able to reinitiate polymerization and can generate its own active center by reacting with monomer molecules, providing eventually a new polymeric radical P^o_m. Ultimately, a rapid equilibrium is established between the actively growing polymeric radicals (P^o_m and P^o_n) and the dormant polymeric RAFT compounds 3, which provides equal probability for all chains to grow and allows for the production of narrowly dispersed polymers with a thiocarbonylthio end group.

In comparison with other CRPs techniques, RAFT polymerization offers the benefit of being able to readily synthesize well-defined polymers for a wider range of monomers (almost all monomers suitable for the conventional free radical polymerization) under mild reaction conditions. Furthermore, it can also be used in all modes of free radical polymerization such as solution, emulsion, and suspension polymerizations. Therefore, since RAFT polymerization is probably the most versatile living radical polymerization process [223], it is deemed to have a bright future in both academic and industrial fields [224].

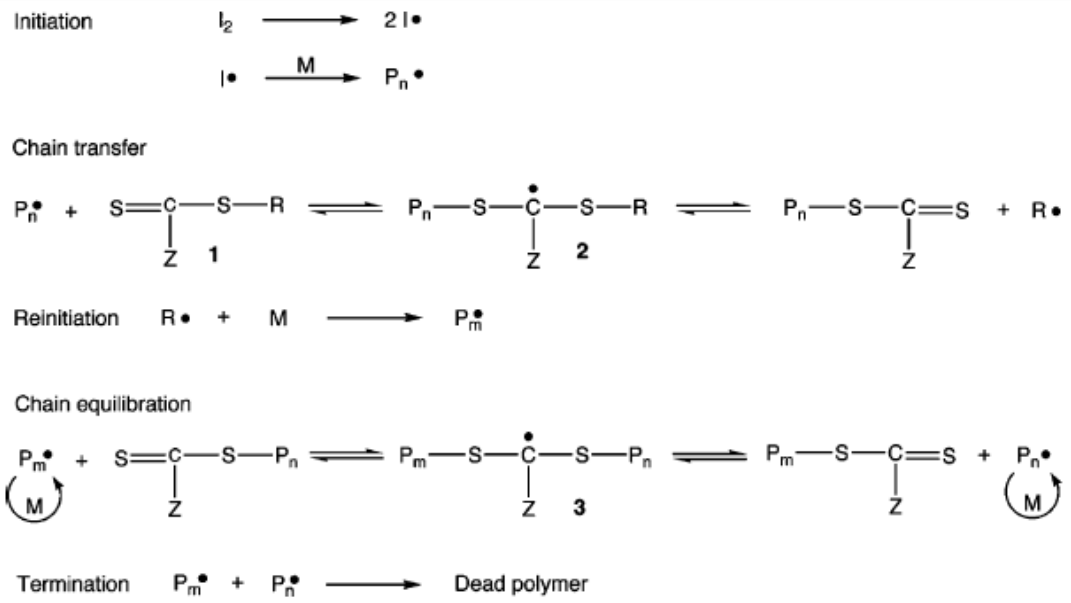

Figure V. 1 Mechanism of RAFT polymerization.

V. 2.2 RAFT polymerization on solid supports

A number of hybrid materials have been prepared by grafting organic polymers with low polydispersities to a number of inorganic substrates, using the above mentioned RAFT methods. Until now, RAFT polymerization has been successfully used to graft a wide range of polymeric chains onto various solid supports such as functionalized silica particles [225-228], silicon wafers [229-231], gold nanoparticles [232, 233], CdSe nanoparticles [234], carbon nanotubes [235, 236], cotton [237], cellulose [238, 239] and Merrifield resin [240, 241]. In general, RAFT polymerization based on solid supports can be performed using both (a) the R-group approach, where the chain transfer agent (CTA) is attached to the backbone via the leaving and reinitiating R group, and (b) the Z-group approach, where the CTA is attached to the backbone via the stabilizing Z group. Both methods have advantages and limitations [220, 222, 242]. In the R-group approach, where the solid support is part of the leaving R group, higher molecular weight of grafted polymers and grafting density can be achieved, but the molecular weight distribution may be broadened by the possible chain

coupling [225-227]. In the Z-group approach, where the backbone is part of Z group, the RAFT process involves the reaction of linear radical chains with the functional backbone, leading to a monomodal molecular weight distribution and a better-defined grafted polymer, but the grafting density is liable to decrease due to the shielding effect [243, 244].

In this study, the Z-supported RAFT polymerization of two vinyl monomers mediated by silica-supported S-Benzyl S′-trimethoxysilylpropyltrithiocarbonate (Si-BTPT) was investigated.

V. 3 Materials

Tetramethoxysilane (98%), anhydrous methanol (99.5%), toluene (99%), tetrahydrofuran (THF), 3-(mercaptopropyl)trimethoxysilane (95%), 1-propanethiol (98%), carbon disulfide anhydrous >99%, benzyl choloride (99%), sodium methoxide (25 wt% solution in methanol), butyl acrylate (BA, <99%), styrene (St, <99%), 2,2′-azobisisobutyronitrile (AIBN, 99%) and ammonium hydroxide (NH_4OH, 28-30 wt% solution) were purchased from Sigma-Aldrich. All reagents were used without further purification.

V. 4 Method

V. 4.1 Preparation of *S*-Benzyl *S′*-trimethoxysilylpropyltrithiocarbonate (BTPT) and *S*-benzyl *S′*-propyltrithiocarbonate (BPTT)

In a typical run, a solution of sodium methoxide in methanol (25 wt%, 6.48 g, 30 mmol) was added dropwise, under nitrogen, to a stirred solution of 3-(mercaptopropyl)trimethoxysilane (95%, 6.20 g, 30 mmol) in 50 mL of anhydrous methanol. After stirring for 30 min, CS_2 (3.05 g, 40 mmol) was added dropwise to the solution, and the mixture was then stirred at ambient

temperature for 5 h. Benzyl chloride (98%, 3.43 mL, 30 mmol) was added to the resultant yellow solution, and the mixture was stirred overnight under nitrogen. The mixture was concentrated, diluted with dichloromethane, filtered off, and concentrated under reduced pressure until constant weight. *S*-benzyl *S′*-trimethoxysilylpropyltrithiocarbonate (BTPT, 10.8 g, 30 mmol, 102%) was obtained as an orange oil and used without further purification – Figure V. 2. Other chain transfer agent (CTA) of BPTT was synthesized according to a similar procedure using 1-propanethiol as raw material and obtained in almost quantitative yield.

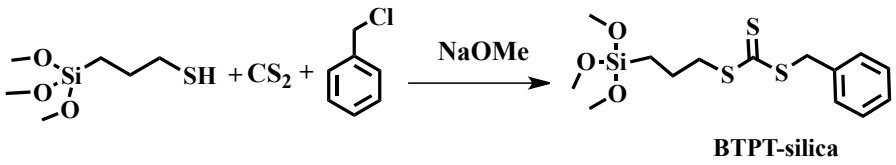

Figure V. 2 Preparation of *S*-Benzyl *S′*-trimethoxysilylpropyltrithiocarbonate (BTPT) to be used as a surface bond RAFT initiator.

BTPT: ^{1}H NMR ($CDCl_3$): δ 7.30 (m, 5H, PhH), 4.60 (s, 2H,CH_2), 3.56 (s, 9H, CH_3O), 3.39 (t, J7, 2H, CH_2S), 1.84 (m, 2H, CH_2), 0.77 (t, J8, 2H, CH_2Si) (*vd.* spectra a at Figure V. 3).

BPTT was obtained as a yellow liquid product in 98.5% isolated yield.

1H NMR ($CDCl_3$): δ 7.33 (m, 5H, PhH), 4.61 (s, 2H, CH_2), 3.35 (t, J7, 2H, CH_2S), 1.75 (m, 2H, CH_2), 1.02 (t, J7, 3H, CH_3) (*vd.* spectra of b at Figure V. 3).

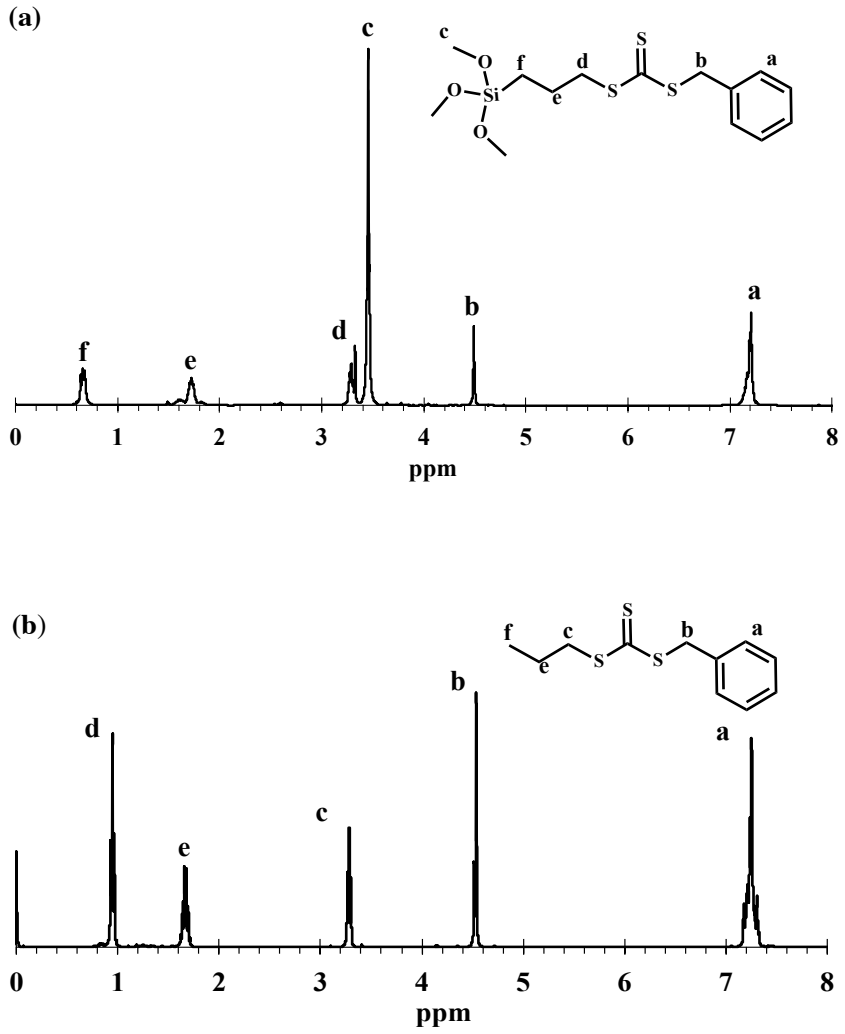

Figure V. 3 ^{1}HNMR spectra of a) *S*-Benzyl *S′*-trimethoxysilylpropyltrithiocarbonate (BTPT), and b) *S*-benzyl *S′*-propyltrithiocarbonate (BPTT).

V. 4.2 Synthesis of RAFT modified silica (RAFT-Silica) aerogels

A solution containing tetramethoxysilane (TMOS, 2.15 mL, 14.7 mmol) and *S*-benzyl *S′*-trimethoxysilylpropyltrithiocarbonate (BTPT) (0.1 mL, 0.3 mmol) was prepared. The second solution was prepared by adding 11.2 mL of the gelation solvent (methanol), H_2O (1.08 mL, r=[Si]/[water]=4) and 0.4 mL of NH_4OH (28-30 wt%). The two solutions were mixed for one minute, then poured in a poly(propylene) container, with 17.2 mm nominal diameter, at room temperature. The final volume was 15 mL. Gelation occurred within ~5 minutes. Gels were

aged at room temperature for 48 h followed by 48 h at 50°C. Once removed from the poly(propylene) container, the methanol was slowly exchanged with toluene over 48 h for the RAFT process - Figure V. 4. If processed for silica aerogel formation, gels were dried using the optimal procedure for supercritical carbon dioxide drying affording a RAFT -modified silica aerogel.

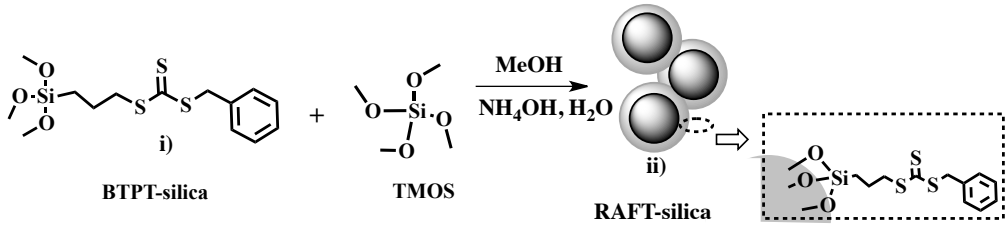

Figure V. 4 Copolymerization of TMOS and silica-BTPT for preparation of a wet gel with surface bound RAFT initiator

V. 4.3 RAFT Polymerizations

Initiator-modified gels were placed into a Schlenk flask along with toluene (50 mL). The Schlenk vial was sealed and purged with argon for 30 minutes. In a separate vial the monomer and radical initiator of AIBN was deoxygenated by bubbling azote for 30 minutes. Then the deoxygenated monomer (45 mmol) and radical initiator of AIBN (0.1 gr) was transferred into the schlenk flask under argon containing the gel in toluene via syringe.

Solutions were allowed to equilibrate for 3 h, after which the Schlenk flask was placed into a thermostated oil bath at 70°C. The time left in the oil bath depended upon the composite density desired - Figure V. 5. The density of the polymer composites can be controlled by varying the polymerization times. After a specific reaction time, the composite silica aerogels were removed from the vial and washed several times with toluene in order to purify the

composite gels from free polymers and other residues. Afterward, the toluene solution was slowly exchanged for methanol, which is needed for supercritical drying.

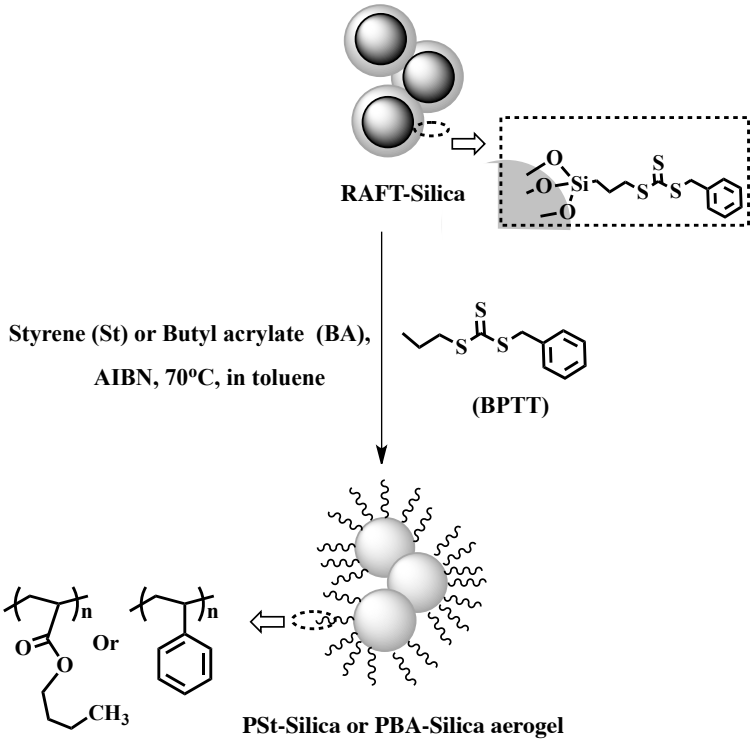

Figure V. 5 RAFT growth of PSt and PBA on silica surface.

V. 4.4 General procedure to cleave grafted chains from the silica surface by aminolysis

The grafted polymers were cleaved from the silica surface according to a method similar to the literature [214]. In a typical run, the following compounds were added to a glass tube: 100 mg of polymer-silicaaerogels, 5.0 mL of THF, and one drop of a dilute aqueous solution of $Na_2S_2O_4$. The solution was degassed with nitrogen for 5-10 min, and then 0.1 mL of degassed *n*-hexylamine was injected into the mixture. After stirring at ambient temperature overnight, the solution was subjected to centrifugation, and the recovered polymer was used for SEC analysis.

V. 5 Characterization techniques

V. 5.1 Size exclusion chromatography - determination of molecular weight and molecular weight distributions of grafted polymers

Molecular weights of the PBA and PSt grafted from the surface of silica aerogel were determined by size-exclusion chromatography (SEC) (HPSEC) (Viscotek (*ViscotekTDAmax*) with a differential viscometer (DV); right-angle laser-light scattering (RALLS, *Viscotek*); low-angle laser-light scattering (LALLS, *Viscotek*) and refractive index (RI) detectors). The column set consisted of a PL 10 mm guard column (50 ×7.5 mm^2) followed by one *Viscotek T200* column (6 mm), one *MIXED-EPL* gel column (3 mm) and one *MIXED-C PLgel* column (5 mm). A HPLC dual piston pump was set with a flow rate of 1 mL min^{-1}. The eluent (HPLC THF) was previously filtered through a 0.2 mm filter. The system was also equipped with an on-line degasser. The tests were conducted at 30°C using an *Elder CH-150* heater. Before injection (100 µL), the samples were filtered through a poly(tetrafluoroethylene) (PTFE) membrane with 0.2 µm pore. For PBA and PSt, $M_{n,GPC}$ and PDI values were determined by conventional calibration with PSt standards between 1820 and 96 000. 400 MHz 1H nuclear magnetic resonance (NMR) spectra of samples of the reaction mixture were recorded on a *Bruker Avance III 400 MHz* spectrometer, with a 5 mm TXI triple resonance detection probe, in $CDCl_3$ with tetramethylsilane (TMS) as an internal standard.

V. 5.2 Bulk and skeleton density and nitrogen gas adsorption

The bulk density (ρ_b) was determined by measuring the weight and volume of the samples. Dimensional shrinkage (%) was taken as the difference between the diameters of the aerogel monolith and of the 20 mL syringe mold (nominally 17.2 mm). He picnometry (*Accupyc*

1330, *Micromeritics*) was used to measure the real (skeleton) density of the samples. Combining the information of the skeleton and bulk densities, it was possible to evaluate the porosity of the samples. In addition, we used the Nitrogen gas adsorption (*Accelerated Surface Area and Porosimetry ASAP 2000, Micromeritics*) for determination of the specific surface area, pore size distribution, pore surface area and pore volume of the materials. Before the analysis, the sample was outgassed at 60^{o}C in vacuum (10^{-5} bar) during 24 h, to remove adsorbed species. In the analysis, volumes of the adsorbed nitrogen at five different relative pressures (0.05 to 0.2) were taken at 77 K, to obtain the specific surface area by the BET theory. The desorption isotherm and the BJH theory were used for the porosimetry evaluation.

V. 5.3 Thermo gravimetric analysis (TGA)

Thermal gravimetric analysis (TGA) was performed using a *TA* model *TGA-Q500* instrument with a heating rate of 10°C min^{-1}, from room temperature to 600°C, under nitrogen atmosphere.

V. 5.4 Scanning electron microscopy (SEM)

Scanning electron microscopy (SEM) (*JMS-5310, JOEL*) was used to observe the materials microstructure. Due to the low electrical conductivity of the highly porous silica-based samples, an Au film was deposited on their surface, using the PVD (Physical Vapor Deposition) technique during 20 s.

V. 5.5 Thermal conductivity and mechanical properties

The thermal conductivity of the reinforced aerogels was measured using a transient method

(*Thermal constants analyzer TPS 2500 S, Hot Disk*). The sensor is clamped between two identical disc shaped pieces of the sample, which have a diameter of 1 cm and thickness of 0.5 cm (properly cut from the cylindrical aerogel samples). This analysis was carried out at 20ºC and the equipment presents a reproducibility and accuracy over 1% and 5%, respectively.

For the mechanical test, samples were cut with length:diameter ratio of 2:1, and were polished to make sure that top and bottom side were smooth and parallel. The compression test was conducted following the *ASTM standard D695-02a*. All tests were done at nominal room conditions with a stroke speed of 1.3 mm/min.

V. 6 Results and discussion

Silica aerogels-polymer composites in this study have been synthesised through several steps. Firstly, trimethoxysilane-containing chain transfer agent (S-benzyl S´-trimethoxysilylpropyltrithiocarbonate (BTPT-silica) as a RAFT-silane coupling agents was synthesized [214]. Then, a modified silica wet gel (RAFT-silica) was synthesized by conducting sol-gel polymerization reaction between tetramethoxysilane (TMOS) and BTPT-silica. The lower reactivity of the trimethoxysilyl group compared to tetramethoxysilane during sol–gel reaction ensured that the majority of initiating groups would be inserted to the aerogel surface [245]. The RAFT polymerization process is initiated from the chain transfer agent (CTA) modified silica, and, finally the resulted aerogel composites are supercritically dried. The degree of polymerization $[M]_o/[I]_o$= 150 was chosen. Polymerization times were varied from 6 to 30 h, thus allowing for control over the grafted polymers molecular weight (Table V. 1)

SI-RAFT of vinyl monomers was conducted in solution using a AIBN and BPTT as a free CTA in the presence of a monolithic gel.

.Table V. 1 Properties of silica, PBA and PSt-silica aerogel composites.

Sample	M_W (g mol^{-1})	PDI	Density [b] (g cm^{-3})	Thermal Conductivity (W m^{-1} k^{-1})	Mechanical Strength (kPa)	Porosity [c] %	Surface Area [d] (m^2 g^{-1})	Av. pore Diameter (nm)	Pore Volume (cm^3 g^{-1})
0[a]	-	-	0.0910±0.004	0.032± 0.007	14	96	850	21	4.3
6h-PBA	10 315	1.60	0.140±0.006	0.036± 0.001	58	94	518	16	3.9
20h-PBA	13 529	2.27	0.160±0.009	0.039±0.007	77	92	487	15	2.9
30h-PBA	19 895	2.37	0.170±0.010	0.042± 0.002	98	91	352	11	2.1
6h-PSt	2 798	1.54	0.130±0.007	0.034± 0.008	32	94	779	13	4.2
20h-PSt	3 016	2.04	0.140±0.004	0.035± 0.006	55	93	676	14	3.8
30h-PSt	3 184	2.18	0.150±0.006	0.037± 0.001	124	93	501	14	2.7

[a] Silica aerogel prepared without PBA/PSt (Silica-RAFT). [b] Density values are an average from three prepared gels. [c] Porosity calculated from $\frac{\frac{1}{\rho_b}-\frac{1}{\rho_s}}{\frac{1}{\rho_s}} \times 100\%$, ρ_b = bulk density ρ_s = skeletal density. [d] Surface area calculated from the N_2 adsorption isotherm using the BET method.

The monolithic gels were subjected to the several solvent exchanges with the initiators and free CTA at room temperature before heating to start the polymerizations. For surface RAFT polymerization, the addition of free RAFT-CTA is a useful approach to help control the polymerization process when the concentration of surface-bound RAFT-CTA is insufficient [246].

Imaging the PBA and PSt silica aerogel composite using SEM (Figure V. 6b, c) revealed the composites aggregate structure had been thickened compared to the polymer free RAFT initiator silica aerogel (Figure V. 6a). Thickening of the aerogels aggregate structure would be expected from the grafted PSt and PBA leading to a reinforcement of the weak necks inside aerogels network structure.

TGA, FT-IR and elemental analysis (EA) confirmed that chain transfer agents were successfully immobilized on the silica surface. The elemental analysis revealed that loading of BTPT-silica (CTA agents) was 0.017 mmol of CTA per g of solid. In FT-IR spectra of plain BTPT-silica aerogel samples (spectrum a of Figure V. 7a strong and broad absorption band corresponding to the asymmetric stretching vibration of Si-O-Si was noted at 1020-1050

cm^{-1} and characteristic absorption bands of benzene ring were observed at 1464 and 1616 cm^{-1}.

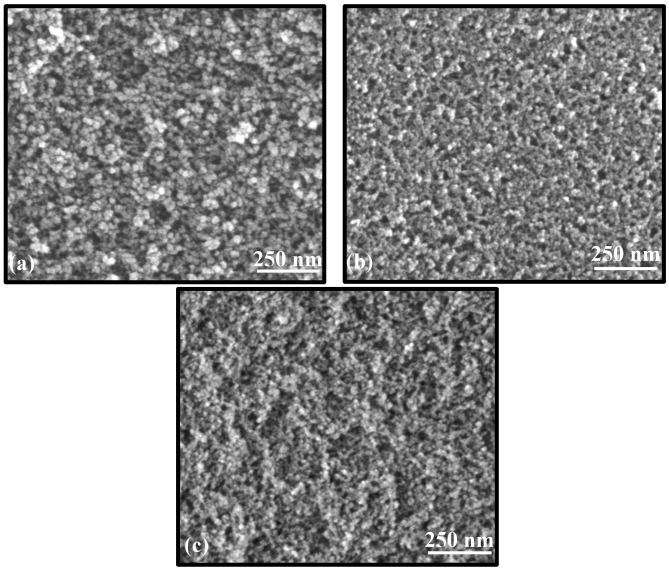

Figure V. 6 a) SEM image of surface functionalized silica aerogel with RAFT-silica, b) PBA-silica aerogel composite and c) PSt-silica aerogel composite after 30h polymerization.

The characteristic absorption bands of C=O stretching were observed at 1727 cm^{-1} (PBA-silica, spectrum b of Figure V. 7); and characteristic peaks of PSt-silica appeared at 1452, 1492 and 1601 cm^{-1} (Figure V. 7c).

Determination of tethered PSt and PBA molar mass was achieved by detaching the polymer from SiO_2 by aminolysis using n-hexylamine [214] and size exclusion chromatography (SEC) of recovered polymers.

Controlled SI-RAFT was achieved, as evidenced by SEC of cleaved PBA in the range of M_w=10-20 Kg mol^{-1} and PSt in the range of M_w=2-3 Kg mol^{-1} with polydispersities (M_w/M_n) of 1.5-2.1 and 1.6-2.4, respectively - Figure V. 8a, b. Clearly, the molecular weight of PSt and PBA increased with the polymerization time, thus providing strong evidence for controlled growth of the polymer.

The PDI, which was initially quite low, became moderate and then even quite high at higher polymer loadings.

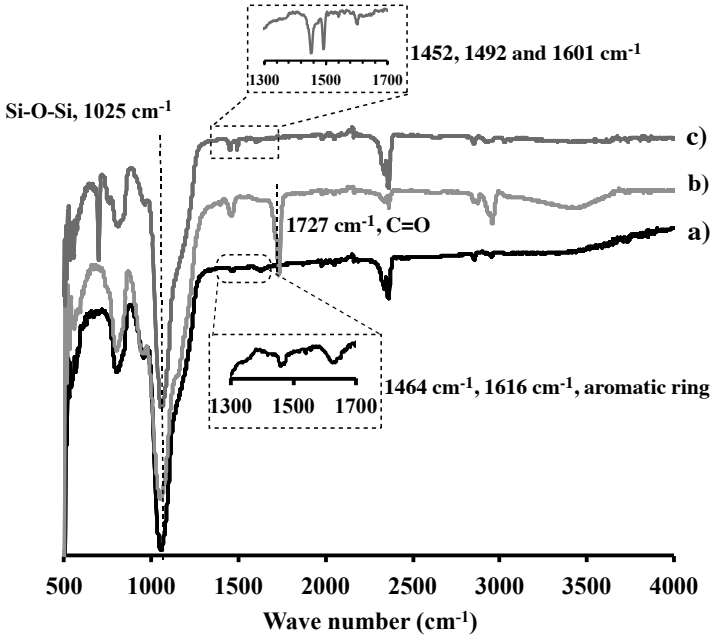

Figure V. 7 FT-IR spectra of RAFT-silica (a), PBA-silica (b) and PSt-silica aerogels.

These molecular weight distributions were broader than those observed for typical homogeneous free polymer in solution. It is very common that the polydispersity of grafted polymers from highly porous materials is higher than those prepared in the absence of a substrate. Typically it ranges from 1.14 to 2.59, which were found to be higher with increased molecular weight. Moreover, the complex environment of aerogel and the concave surface geometry lead to sterically inaccessible initiation sites that affected the overall control of the SI-RAFT [247]. The thermal stability and grafting ratio of polymer on the silica surface were studied by thermogravimetric analysis (TGA). The increase in the molecular weight of polymer was correlated with the content of the polymer in PSt or PBA-silica aerogel composites- Table V. 2. Figure V. 9 indicates that the onset temperature of non-reinforced silica aerogels increased by incorporation of polymer on the silica surface.

a)

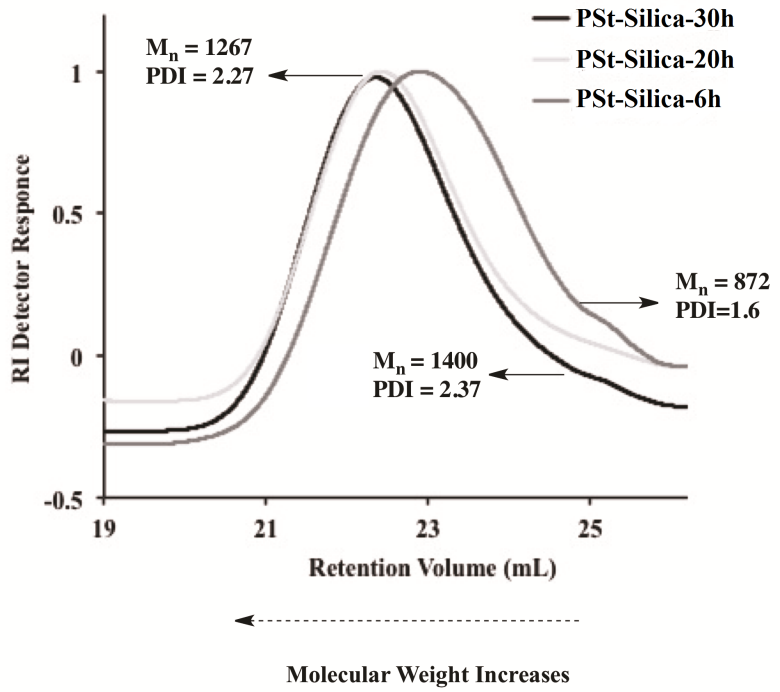

b)

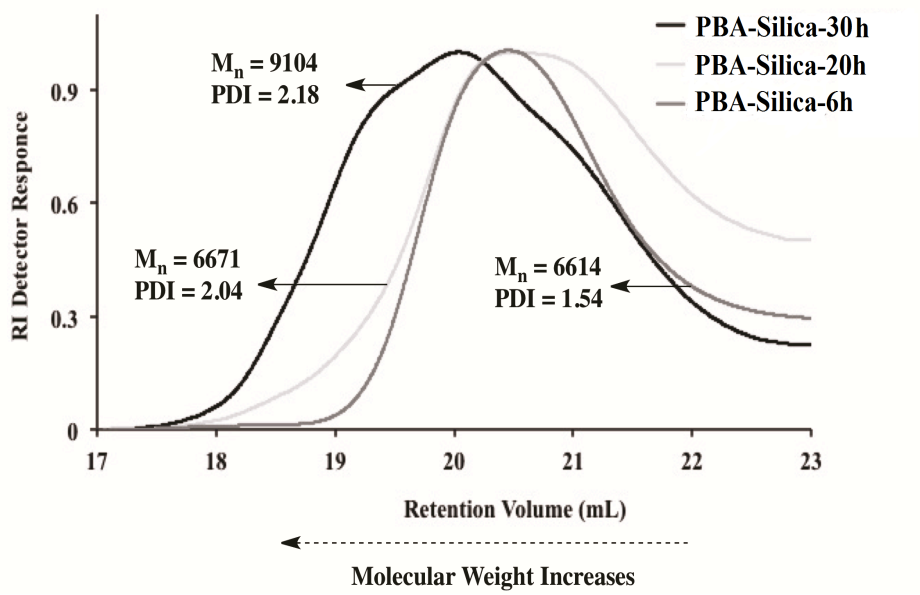

Figure V. 8 Size exclusion chromatography traces for a) PSt, and b) PBA polymers isolated from silica composites.

This result also suggests that thermal stability of silica composites increased by increasing the grafting ratio to the composites.

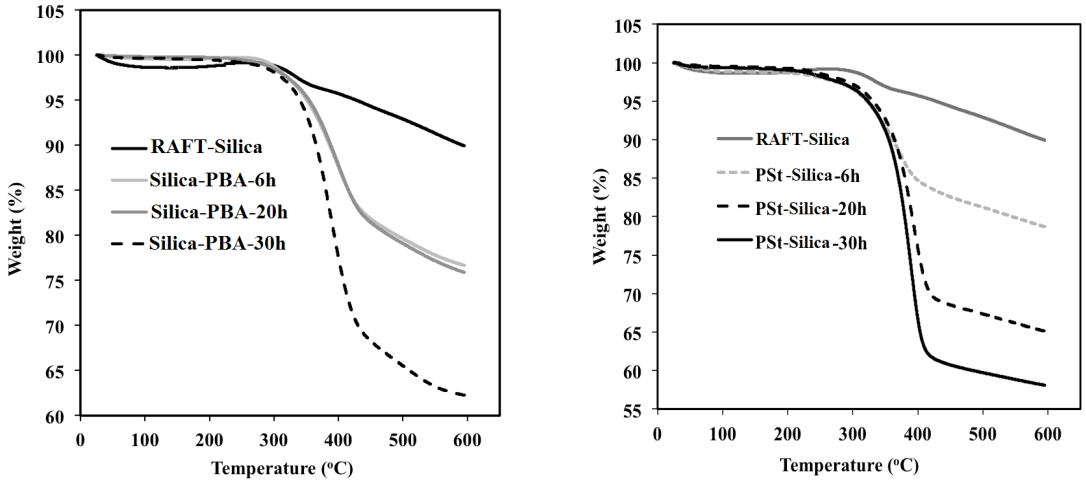

Figure V. 9 TGA curves of a) PBA-silica aerogels and b) PSt-silica aerogel composites.

On the basis of SEC, TGA and gas adsorption data, the initiator efficiency, that is, the ratio of the number of grafted polymer chains to the number of initiation sites, has been determined and ranged between 1.5-24% - Table V. 2. The apparent decrease in the grafting density and initiation efficiency for the PBA in composite may be related to the coupling of chains at later stages of the grafting process where the pores are nearly completely filled with the polymer and the monomer cannot readily diffuse to convert the propagating chains to the dormant species [247]. This observation is consistent with the more than two-fold increase in the molecular weight and the broadening of the molecular weight distribution at this stage. This broadening in the PDI' grafted polymers can also be explained by comparing the composition/organic content of outer and inner side of PBA-silica aerogels prepared in the 20h and 30h of polymerization (Figure V. 10). After thirty hours of RAFT, the difference in the organic content between center and exterior part has increased to 10%. While the growth of polymer chains inside the pores was hindered because of the scarcity of available space, the chains growing on the external surface had no such restriction. Therefore, as the polymerization proceeds, it would cause second molecular weight distribution and the increase in the PDI's grafted polymers.

Table V. 2 Results of TGA and SEC analysis for RAFT graft Polymerization.

Aerogel	T_{onset} (°C)	Wt% polymer[b]	G_r (%)[c]	G_p (μmol g^{-1})[d]	Initiator efficiency[e] (%)
0[a]	314	-	-	-	-
6h-PBA	336	21	0.16	0.24	1.4
20h-PBA	340	23	0.30	0.44	2.5
30h-PBA	350	36	0.46	0.50	2.9
6h-PSt	320	20	0.15	1.72	10.1
20h-PSt	357	34	0.41	3.20	19.0
30h-PSt	358	40	0.56	4.00	24.0

[a]Silica aerogel prepared without PBA/PSt (RAFT-Silica)
[b]Wt%: weight percent of PBA/PSt in PBA- and PSt-silica composites, estimated from TGA data ;
[c]Weight grafting ratio of polymeric chain on silica surface, $G_r = \frac{Wt_{\%\ \text{polymer-silica}}}{100 - Wt_{\%\ \text{polymer-silica}}} - \frac{Wt_{\%\ \text{CTA-silica}}}{100 - Wt_{\%\ \text{CTA-silica}}}$;
[d]Molar grafting ratio of polymeric chain on silica surface, $G_p = \frac{G_r}{M_n\,(g)}$;
[e]Initiator efficiency = no. grafted polymer chains/no. of initiation sites.

The porous nature of aerogel composites was evaluated by nitrogen physisorption (Figure V. 11a, b). The detailed results are summarized in Table V. 1.

It was found that the isotherms of almost whole samples were following the type IV according to the IUPAC classification, which is the characteristic of mesopore structures with cylindrical pores. The specific surface areas and the pore size distributions were evaluated from the adsorption and desorption branches of the isotherms applying the Brunauer-Emmett-Teller (BET) and Barrett-Joyner-Halenda (BJH) methods, respectively (Figure V. 11d, c). The nitrogen adsorption of silica composites decreases gradually as the polymerization time increases. Grafting of PSt (Figure V. 11a) and PBA (Figure V. 11b) resulted in a gradual decrease in the volume of nitrogen adsorbed as the density of the composites increase. Volume of adsorbed gas decreases due to the expected gradual filling of the mesopores within the RAFT-modified silica aerogels. As a consequence, the average pore size shifts to lower values as the composites (PSt-Silica and PBA-silica) density increases.

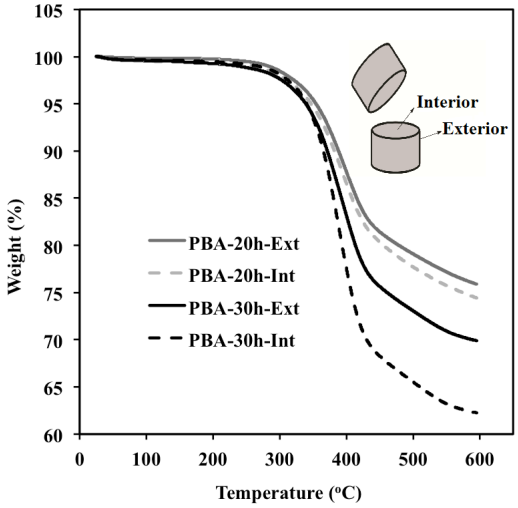

Figure V. 10 TGA analysis of samples from interior and exterior of silica aerogels RAFT modified with PBA for 20 and 30 hours.

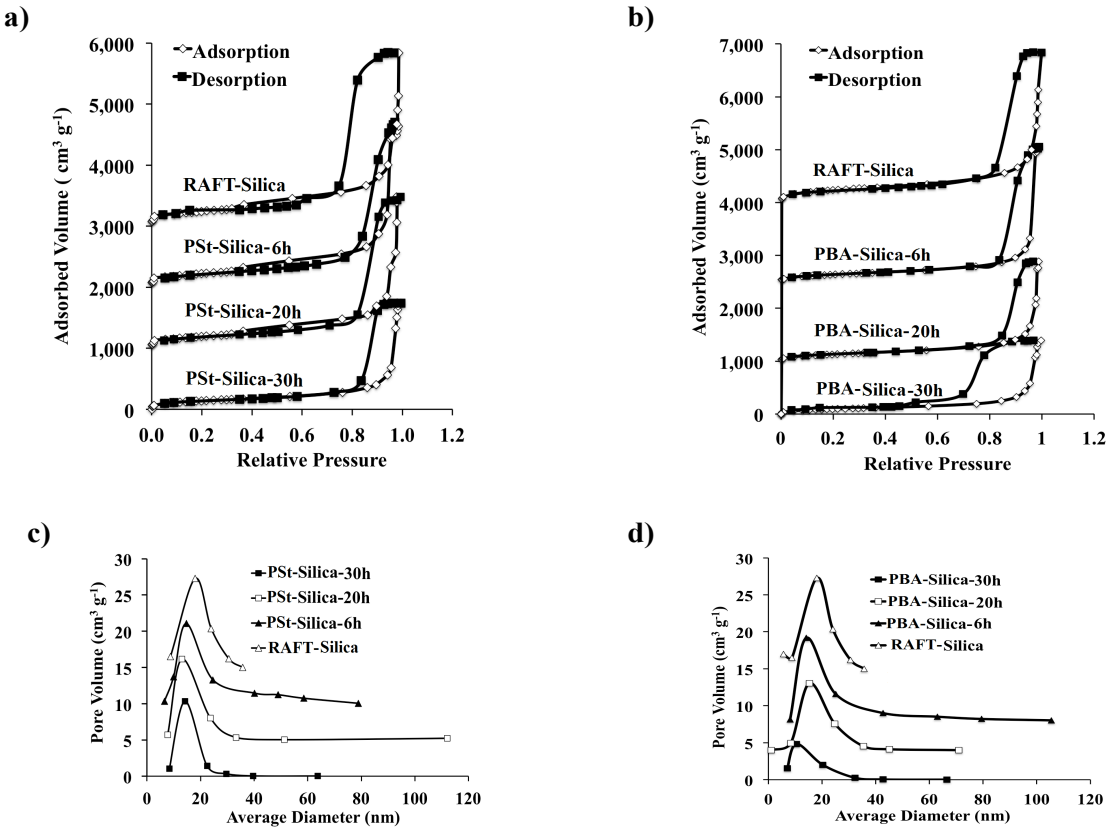

Figure V. 11 Nitrogen adsorption and desorption isotherms (a, b) and Barrett–Joyner–Halenda (BJH) pore-size distribution (c, d) of aerogels calculated from the desorption branch of the isotherm. Relative pressure=P/P_0.

The thermal conductivity of synthesized aerogels has been measured by non-steady state (transient) approach and the results for nonreinforced and reinforced aerogels are indicated at Table V. 1 and Figure V. 12.

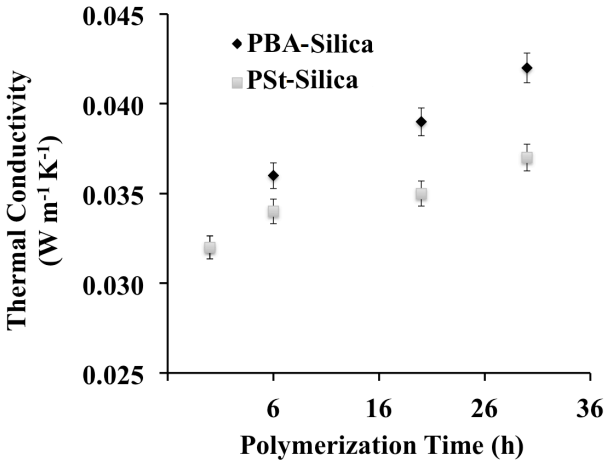

Figure V. 12 Thermal conductivity versus polymerization time.

The thermal conductivity of aerogels are strongly depend on the number of network connectivity and applied mass to reinforce them and ranging from 0.036 to 0.042 W m^{-1} K^{-1} for PBA-reinforced aerogels and from 0.034 to 0.037 W m^{-1} K^{-1} for PSt-reinforced aerogels. The thermal conductivity of reinforced aerogels slightly increases by increasing the molecular weight of the grafted polymer and density of aerogel composites. However for PSt reinforced aerogels, due to the low molecular weight of grafted polymer compared to the grafted PBA, the increasing in the thermal conductivity is less pronounced.

The effects of grafting PSt and PBA to strengthen aerogels are evaluated from sample stress-strain curves shown in Figure V. 13a. The values of the compression strength (maximum) obtained from these curves are summarized in Table V. 1. The RAFT-silica aerogel, which is that of the initiator modified with (no PSt and PBA), with average density of 0.091 g cm^{-3}, is slightly weaker than pure silica aerogels (max. strength ~ 30 kPa) with the same density.

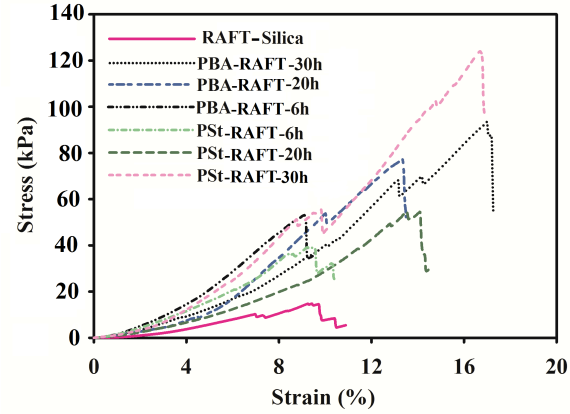

a)

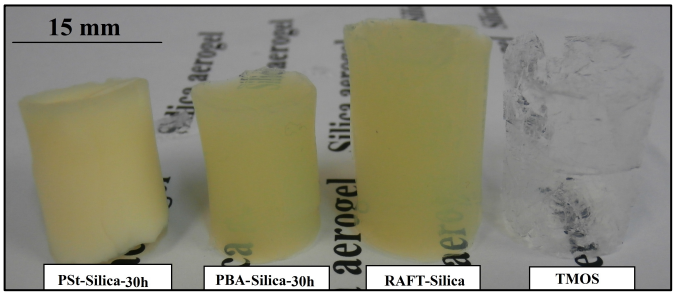

b)

Figure V. 13 a) stress strain curves of different developed reinforced and nonreinforced aerogels b) photograph of plain TMOS-derived aerogel and initiator-modified aerogel (RAFT-silica) along with reiforced PBA-silica and PSt-silica aerogels with 30 hours polymerization time.

The reduction in strength is observed in other silica aerogels synthesized by other co-monomers of trialkoxysilane [24]. The strength of the PBA and PSt–silica aerogel composites increases with the density of the composite aerogel and the molecular weight of the polymer. The sample photos at Figure V. 13b show that reinforced aerogels have enough structural integrity and high mechanical strength compared to the native TMOS based and RAFT modified aerogels.

The brittle behavior of the silica aerogel remains after the introduction of RAFT initiator. However, even a low polymer content promotes a clear improvement of the mechanical properties of the material. The Young's modulus increases, and the maximum compression strength become 5-9 times higher. Furthermore, the mechanical behavior improvement is

noticeable from the much higher energy that the hybrid aerogel is able to absorb up to the maximum compression strength (roughly the area under the stress-strain curve).

The initiator-modified aerogels are transparent and less dense; the transparency somehow is retained in case of the PBA reinforced aerogels. The PSt aerogel looks opaque and stronger than RAFT-silica and PBA-silica aerogels.

PBA–silica aerogel composite prepared from a polymerization time of 30 h with a grafted molecular weight of ~20 kg mol^{-1} increased the compression strength to 98 kPa. This is approximately 7× stronger than the initiator modified aerogels with less than 2× increases in the density (ρ=0.17 g cm^{-3}). The strongest PSt–silica aerogel composite had a density of 0.15 g cm^{-3}, a molecular weight (M_w) of 3 kg mol^{-1} and compression strength of 124 kPa. This is 9× stronger than the initiator modified silica aerogel. As indicated at Figure V. 13a, despite of the low molecular weight of PSt compared to PBA, the PSt reinforced aerogels were at the same time stronger, tougher and stiffer than PBA reinforced aerogels for all polymerization time. For the same polymerization time and same density, these aerogels even were stronger than PMMA reinforced aerogels (48 kPa) with higher M_w of 63 kg mol^{-1} [24]. Therefore, from these results, it can be concluded that the molecular weight of the grafted polymer plays an important role in the composites mechanical properties and depending on the type and nature of growing polymers, different results can be achieved for mechanical strength of aerogels.

V. 7 Conclusion

In summary, we have demonstrated the controlled growth of grafted polymers from the surface of a silica gel, by implementing *RAFT* polymerization technique for the first time. The polydispersities were in the range 1.5-2.4. We established relationship of silica aerogel composites main properties (density, bulk mechanical properties and thermal insulation) and

the molecular weight of polymers used to reinforce the composite. It was found that, as the molecular weight increases, so do the composites mechanical properties, but many of the aerogel's physical properties are retained.

Although we only have briefly explored this methodology to prepare silica aerogel composites, this method should provide a versatile approach to prepare silica aerogel composites with tailored properties. The approach described herein for the synthesis of polymer-composite aerogels promises to be applicable to a wide variety of polymers that can be polymerized in a controlled way via RAFT.

Chapter VI. Conclusions and brief perspective on future directions

The main focus of this work was to develop silica aerogel composites with improved mechanical properties while retaining the characteristic physical properties of the native aerogels. In this regard, we successfully established a one pot streamline synthesis procedure for the development of supercriticaly dried tri-methacrylate reinforced silica aerogels with different silica nanostructures (Chapter III). The same synthesis procedure but with safer drying conditions has been implemented to prepare different APD silica aerogels with different silica nanostructures and optimized properties. (Chapter IV). The property optimization of APD aerogels was accomplished by means of the statistical CCRD methodology, in order to develop monoliths with material properties near to their $scCO_2$ dried aerogels counterparts. All aerogel and aerogel-like composites exhibited increases in compression strength. The strengths of the monoliths synthesized in this project compared to other previous reinforced aerogels, namely silica reinforced by addition of silica, cross-linked with polymer networks and reinforced by chemical vapor deposition of methyl cyanoacrylate (MCA-CVD) on amine modified silica aerogels at Figure VI. 1. This figure indicates that the composite aerogels and aerogels-like prepared here along with MCA-CVD aerogels are stronger at lower densities compared to the previous aerogels of the literature.

Aerogel and optimized aerogel-like composite monoliths prepared in the present work along with aerogels prepared by methyl cyanoacrylate CVD on phenylene-bridged polysilsesquioxanes were stronger than any low density silica or silica-polymer aerogel composites ever prepared.

The red box in the plot indicates materials that are stronger than the traditional native aerogels

and have lower density than other polymer reinforced silica aerogels. This result shows that our strategy to develop aerogels and their optimized APD counterparts was a successful in generating high strength aerogels with little change in the density. Excluding MCA-CVD approach, none of the other materials prepared by other researchers in this field come close to reaching the mechanical strength at the low densities defined by the red box in Figure VI. 1.

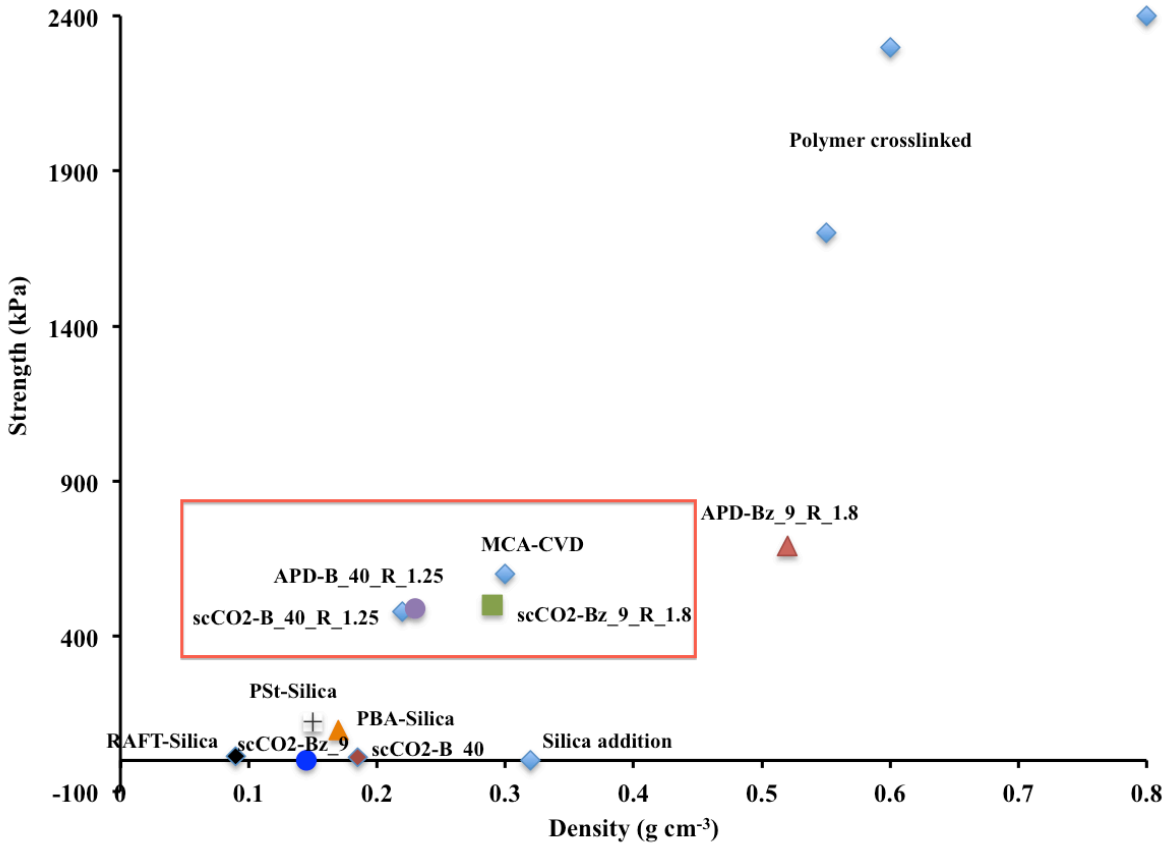

Figure VI. 1 Mechanical strength of silica aerogel composites plotted against their density. Different polymer crosslinked silica aerogels are listed at Table II. 2 in Chapter II.

Not only the aerogel composites and their aerogel-like counterparts prepared by one pot synthesis strategy are stronger, they were made faster than other polymer-modified aerogels (Figure VI. 2). Generally, the total processing time (gel formation, polymer reinforcement and

supercritical drying) for the preparation of silica aerogels and aerogel-like composites is under 75 hours, which is even lower than preparation time of aerogels prepared by CVD of methyl cyanoacrylate which normally takes 200 hours. Preparation of the CVD-modified aminated silica aerogel (MCA-CVD) composites took approximately 380 hours because of the time spent exchanging solvents required for surface silylation to produce a relatively water free surface. Also, polymer-reinforced aerogels in multistep procedures, due to the time spent for exchanging solvents and post gelation washing and drying, often take ~ 450 hours.

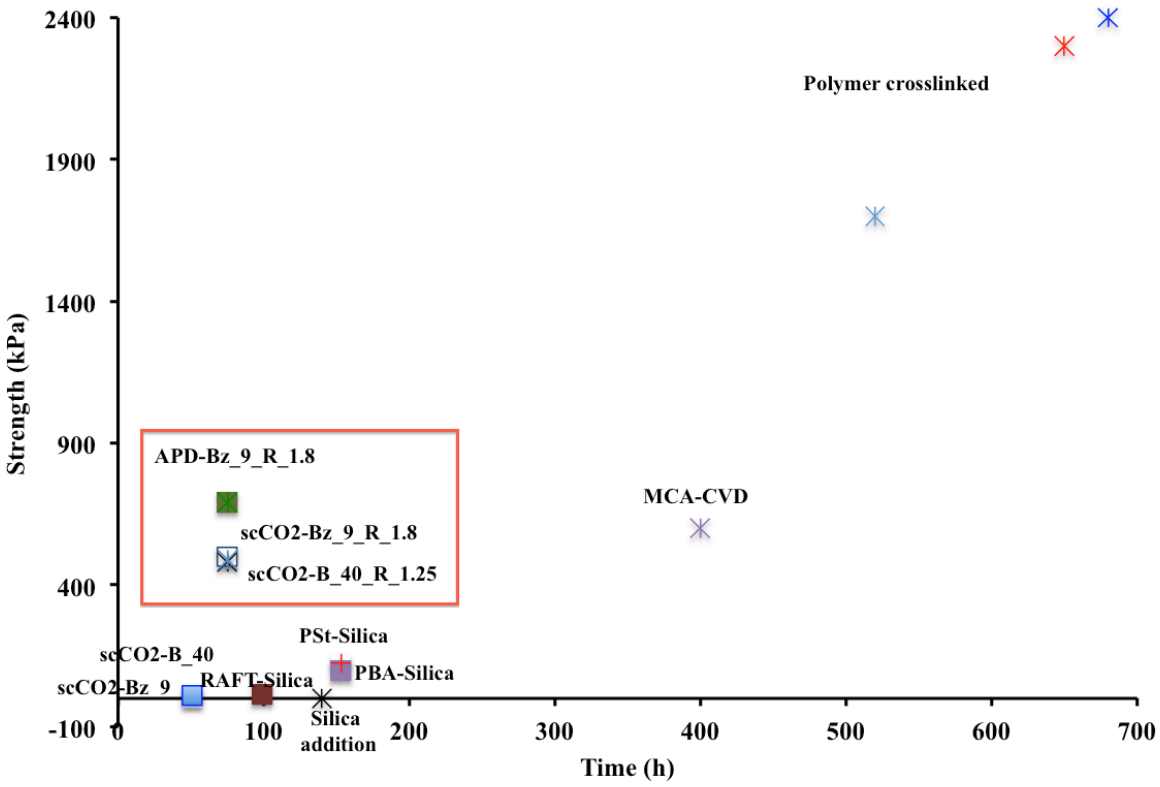

Figure VI. 2 Strength of silica aerogel composites plotted against the processing time required to prepare them.

Normalizing for density, our composites have mechanical strengths higher than previous aerogel composites reinforced by polymer and with the rapid processing time achieved in their preparation.

The red box in Figure V. 2 maps out the strength versus processing time domain. It shows that

stronger aerogels prepared in minimum time, have preparation time approximately less than twice of their native counterparts'. Only the optimized APD and SCD aerogel and aerogel-like monoliths with properties listed in Table IV. 7 have the processing time and mechanical strength to lie within the red box. The $scCO_2$-BTESB derived aerogel-like composites are the strongest of the low density aerogels and are the most quickly prepared.

Additionally, we developed the first approach to graft low polydispersity poly butyl acrylate and polystyrene (Chapter V) from the surface of initiator-functionalized silica gels, with control over the grafted polymers molecular weight, using Surface-Initiated Reversible Addition-Fragmentation Chain Transfer polymerization (SI-RAFT). Controlling the grafted polymers molecular weight allowed us to draw a correlation of the molecular weight of polymers used to reinforce the silica aerogel to the bulk composite mechanical properties. As expected, the strength increased as the molecular weight of the polymers attached to the surface increased. The PBA and PSt reinforcement of silica aerogels moderately improved the mechanical properties and to some extent, retained other characteristic physical properties of native aerogels.

Evaluating our approaches and other approaches used to improve the mechanical properties of silica aerogels, it is concluded that the main key in further strength improvements of aerogels must start from a strong as possible aerogel aggregate structure. Additionally, our work has shown that the processing time required to prepare silica aerogel composites through a one pot single step is fast, thus, other systems must be explored using this methodology. Specifically, those in which the polymerization is conducted through free radical polymerization techniques. Lastly, for silica aerogels to become a viable material to be used in a number of applications, the supercritical dying step must be removed. Our work has shown a significant improvement in the field of reinforcing silica aerogels and drying approach, and contained meaningful results that will allow for future research to prosper.

Chapter VII. References

VII. 1 References

[1] Jr. C.E.Carraher, General topics: silica aerogels-properties and uses, Polym. News 30 (2005) 386–388.

[2] J.M. Schultz, K.I. Jensen, F.H. Kristiansen, Super insulating aerogel glazing, Sol. Energ. Mat. Sol. C 89 (2005) 275-285.

[3] J.P. Da Cunha, F. Neves, M.I. Lopes, On the reconstruction of Cherenkov rings from aerogel radiators, Nucl. Instrum. Meth. A, 452 (2000) 401-421.

[4] V. Wittwer, Development of aerogel windows, J. Non-Cryst. Solids 145 (1992) 233-236.

[5] V. Gibiat, O. Lefeuvre, T. Woignier, J. Pelous, J. Phalippou, Acoustic properties and potential applications of silica aerogels, J. Non-Cryst. Solids 186 (1995) 244–255.

[6] J.W. Long, K.E. Swider Lyons, R.M. Stroud, D.R. Rolison, Design of pore and matter architectures in manganese oxide charge-storage materials, Electrochem. Solid-State Lett. , 3 (2000) 453–456.

[7] D.A. Ward, E.I. Ko, Preparing catalytic materials by the sol-gel method, J. Ind. Eng. Chem. Res., 34 (1995) 421–433.

[8] C.T. Wang, C.L. Wu, I.C. Chen, Y.H. Huang, Humidity sensors based on silica nanoparticle aerogel thin films, Sens. Actuators B 107 (2005) 402–410.

[9] M.L.N. Perdigoto, R.C. Martins, N. Rocha, M.J. Quina, L. Gando-Ferreira, R. Patrício, L. Durães, Application of hydrophobic silica based aerogels and xerogels for removal of toxic organic compounds from aqueous solutions, J. Colloid Interface Sci. , 380 (2012) 134–140.

[10] S.M. Jones, Aerogel: space exploration applications, J. Sol-Gel Sci. Technol., 40 (2006) 351–357.

[11] H.H. Tang, E.S. Orndoff, L.A. Trevino, 36th International Conference on Environment Systems, Norfolk, American Institute of Aeronautics and Astronautics, Reston, 2006, pp. 2235.

[12] H.L. Paul, K.R. Diller, Pressure wave propagation in fluid-filled co-axial elastic tubes. Part 2: Mechanisms for the pathogenesis of syringomyelia, J. Biomech. Eng., 125 (2003) 639–647.

[13] J.A. Del Corso, W.E. Bruce, K.A. Liles, S.J. Hughes, 20th AIAA Aerodynamic Decelerator Systems Technology Conference and Seminar, Seattle, American Institute of Aeronautics and Astronautics, Reston, 2009, pp. 2009-2925.

[14] M.T. Guise, B. Hosticka, B.C. Earp, P.M. Norris An experimental investigation of aerosol collection utilizing packed beds of silica aerogel microspheres, J. Non-Cryst. Solids, 285 (1995) 317–322.

[15] L.W. Hrubesh, Aerogel applications, J. Non-Cryst. Solids 225 (1998) 335–342.

[16] M. Schmidt, F. Schwertfeger, Applications for silica aerogel products, J. Non-Cryst. Solids 225 (1998) 364–368.

[17] M.M. Moner-Girona, E.A. Roig, J. Esteve, E. Molins, Sol-gel processing parameters and carbon addition, J. Non-Cryst. Solids 285 (2001) 1-3.

[18] A.V. Rao, D. Haranath, Effect of methyltrimethoxysilane as a synthesis component on the hydrophobicity and some physical properties of silica aerogels, Micropor. Mesopor. Mater. , 30 (1999) 267-273.

[19] A.V. Rao, S.D. Bhagat, H. Hirashima, G.M. Pajonk, Synthesis of flexible silica aerogels using methyltrimethoxysilane (MTMS) precursor, J. Colloid Interface Sci., 300 (2006) 279–285.

[20] D.Y. Nadargi, S.S. Latthe, H. Hirashima, A.V. Rao, Studies on rheological properties of methyltriethoxysilane (MTES) based flexible superhydrophobic silica aerogels, Micropor. Mesopor. Mater., 117 (2009) 617-626.

[21] H. Guo, B.N. Nguyen, L.S. Mccorkle, B. Shonkwilerb, M.A.B. Meador, Elastic low density aerogels derived from bis[3- (triethoxysilyl)propyl]disulfide, tetramethylorthosilicate and vinyltrimethoxysilane via a two-step process, J. Mater. Chem. , 19 (2009) 9054–9062.

[22] N. Leventis, A. Sadekar, N. Chandrasekaran, C. Sotiriou-Leventis, Click Synthesis of Monolithic Silicon Carbide Aerogels from Polyacrylonitrile-Coated 3D Silica Networks, Chem. Mater. , 22 (2010) 2790–2803.

[23] M.A.B. Meador, L.A. Capadona, L. Mccorkle, D.S. Papadopoulos, N. Leventis, Structure-Property Relationships in Porous 3D Nanostructures as a Function of Preparation Conditions: Isocyanate Cross-Linked Silica Aerogels, Chem. Mater. , 19 (2007) 2247-2260.

[24] D.J. Boday, P.Y. Keng, B. Muriithi, J. Pyun, D.A. Loy, Mechanically reinforced silica aerogel nanocomposites via surface initiated atom transfer radical polymerizations, J. Mater. Chem., 20 (2010) 6863–6865.

[25] D.J. Boday, R.J. Stover, B. Muriithi, M.W. Keller, J.T. Wertz, K.A.D. Obrey, D.A. Loy, Strong, Low-Density Nanocomposites by Chemical Vapor Deposition and Polymerization of Cyanoacrylates on Aminated Silica Aerogels, ACS Appl. Mater. Interfaces 1 (2009) 1364-1369.

[26] N. Leventis, Three Dimensional Core-Shell Superstructures: Mechanically Strong Aerogels, Acc. Chem. Res., 40 (2007) 874-884.

[27] M.A.B. Meador, S.L. Vivod, L. Mccorkle, D. Quade, R.M. Sullivan, L.N. Ghson, Clark, L.A. Capaclona, , Reinforcing polymer cross-linked aerogels with carbon nanofibers, J. Mater. Chem., 18 (2008) 1843-1852.

[28] N. Leventis, C. Sotiriou-Leventis, G. Zhang, A.-M.M. Rawashdeh, Nanoengineering Strong Silica Aerogels, Nano. Lett. , 2 (2002) 957-960.

[29] J.P. Randall, M.A.B. Meador, S.C. Jana, Tailoring Mechanical Properties of Aerogels for Aerospace Applications, ACS Appl. Mater. Interfaces 3 (2011) 613-626.

[30] N.C. Holmes, H.B. Radousky, M.J. Moss, W.J. Nellis, S. Henning Silica at ultrahigh temperature and expanded volume, Appl. Phys. Lett., 45 (1984) 626–628.

[31] P. Tsou, Silica aerogel captures cosmic dust intact, J. Non-Cryst. Solids, 186 (1995) 415–427.

[32] N. Leventis, H. Lu, M.M. Koebel (Ed.), Aerogel Handbook, Springer, 2010, pp. 315-334.

[33] S.L. Vivod, M. A. B. Meador, B. N. Nguyen, R. Perry, Flexible di-isocyanate cross-linked silica aerogels with 1,6-bis(trimethoxysilyl)hexane incorporated in the underlying silica backbone, Polym. Prepr., 50 (2009) 119–120.

[34] S.J. Kramer, F. Rubio-Alonso, J.D. Mackenzie, Organically modified silicate aerogels, "Aeromosils", Mater. Res. Soc. Symp. Proc., 435 (1996) 295-300.

[35] D.A. Loy, K.J. Shea, Bridged polysilsesquioxanes: highly porous hybrid organic-inorganic materials, Chem. Rev. , 95 (1995) 1431-1442.

[36] J. Fricke, Aerogels - highly tenuous solids with fascinating properties, J. Non-Cryst. Solids, 100 (1988) 169-173.

[37] R.W. Pekala, L.W. Hrubesh, T.M. Tillotson, C.T. Alviso, J.F. Poco, J.D. Lemay, MRS Symposium W: Scaling in Disordered Materials, Boston, November (1990) Materials Research Society: Warrendale, PA, 1990.

[38] J. Fricke, A. Emmerling, Aerogels—Recent Progress in Production Techniques and Novel Applications, J. Sol-Gel Sci.Technol., 13 (1998) 299–303.

[39] J. Gross, J. Fricke, Scaling of elastic properties in highly porous nanostructured aerogels, J. NanoStruct. Mater., 6 (1995) 905.

[40] T. Woignier, J. Reynes, A. Hafidialaoui, I. Beurroies, J. Phalippou, Different kinds of structure in aerogels: relationships with the mechanical properties, J. Non-Cryst. Solids 241 (1998) 45–52.

[41] A.C. Pierre, Kluwer Academic Publishers, Boston, 1998.

[42] C.J. Brinker, G.W. Scherer, Sol-Gel Science: The Physics and Chemistry of Sol-Gel Processing, Academic Press, 1990.

[43] A.C. Pierre, G.M. Pajonk, Aerogels and their applications, Chem. Rev., 102 (2002) 4243-4265.

[44] A.P. Ambekar, P. Bagade, A review on: "aerogel - world's lightest solid" Popular Plastics & Packaging 51 (2006) 96-102.

[45] L. Kocon, J. Phalippou, Aerogels. Material aspect Techniques de l'Ingenieur, Sciences Fondamentales, AF196 (2005) AF3610/3611-AF3610/3621.

[46] G.M. Pajonk, Some applications of silica aerogels, Colloid Polym. Sci. , 281 (2003) 637-651.

[47] Soleimani Dorcheh, A.; Abbasi, M. H.;, Silica aerogel; synthesis, properties and characterization, J. Mater. Proc. Technol. , 199 (2008) 10-26.

[48] M.A.B. Meador, E.F. Fabrizzio, F. Ilhan, A. Dass, G. Zhang, P. Vassilaras, J.C. Johnston, N. Leventis, Crosslinking amine modified silica aerogels with epoxies: Mechanically strong lightweight porous materials, Chem. Mater., 17 (2005) 1085-1098.

[49] M.A.B. Meador, B.N. Nguyen, D. Quade, S.L. Vivod, Epoxy Reinforced Aerogels Made Using a Streamlined Process, ACS Appl. Mater. Interfaces, 2 (2010) 2162-2168.

[50] J. K. Lee, G. L. Gould, W. Rhine, Polyurea based aerogel for a high performance thermal insulation material, J. Sol-Gel Sci.Technol., 49 (2009) 209–220.

[51] L.A. Capadona, M.A.B. Meador, A. Alunni, E.F. Fabrizio, P. Vassilaras, N. Leventis, Effect of Processing Conditions on Chemical make-up of di-isocyanate crosslinked silica aerogels, Polymer, 47 (2006) 5754–5761.

[52] B.N. Nguyen, M.A.B. Meador, M.E. Tousley, B. Shonkwiler, L. Mccorkle, D.A. Scheiman, A. Palczer, Tailoring elastic properties of silica aerogels cross-linked with polystyrene, ACS Appl. Mater. Interfaces 1 (2009) 621-630.

[53] U.F. Ilhan, E.F. Fabrizio, L. Mccorkle, D.A. Scheiman, A. Dass, A. Palczer , M.A.B. Meador, J.C. Johnston, N. Leventis, Hydrophobic monolithic aerogels by nanocasting polystyrene on amine-modified silica, J. Mater. Chem. , 16 (2006) 3046-3054.

[54] N. Leventis, H. Lu, M.M. Koebel (Ed.), Aerogel Handbook, Springer, 2010, pp. 252-285.

[55] H. Maleki, L. Durães, A. Portugal, An overview on silica aerogels synthesis and different mechanical reinforcing strategies, J. Non- Cryst. Solids, 385 (2014) 55–74.

[56] R. A. Bideaux, K. W. Bladh, M. C. Nichols, J. A. Anthony Handbook of Mineralogy. Volume II; Silica and Silicates, Part 1: Mineral Data Publishing, (1995).

[57] R. W. Douglas, The History Glass Making, G.T. Foulis & Co. LtD. Henley on Thames, Oxforshire, (1972).

[58] J. Hecht, The Laser Guidebook: McGraw-Hill, (1999).

[59] J. Berzelius, J. Examen, De Quelques Composés Qui Dépendent D'affinités Très-Faibles, Ann. Chem. Phys. , 14 (1820) 363-369.

[60] J. Ebelmen, J. Ann., 57 (1846) 331.

[61] A. M. Buckley, M. Greenblatt, The Sol-Gel Preparation of Silica Gels, J. Chem. Educ., 71 (1994) 599-602.

[62] H. Schroeder, Phys. Thin Films, 5 (1969) 87.

[63] W. A. Patrick, Silica gel and process making same, U.S. patent 1,297,724. , (1919).

[64] S.S. Kistler, Coherent expanded aerogels, J. Phys. Chem., 36 (1932) 52–64.

[65] S. Mclean, Anit-relection coatings using colloidal silica, U.S. Patent 2,639,999., (1953).

[66] R. K. Iler, P.S. Pinkney, Ind. Eng. Chem. Res., 39 (1947) 1379.

[67] B. E. Yoldas, Alumina gels that form porous transparent Al2O3, J. Mater. Sci. , 10 (1975) 1856-1860.

[68] J. L. Kelly, A. T. Kleinsteuber, S. D. Clinton, O. C. Dean, Sol-Gel Process for Preparing Spheroidal Particles of Dicarbides of Thorium and Thorium-Uranium Mixtures, Ind. Eng. Chem. Process Des. Dev., 4 (1965) 212–216.

[69] E. Wainer, German Patent 1,249,832. , (1968).

[70] H. Dislich, New Routes to Multicomponent Oxide Glasses, Angew. Chem. Int. Ed. Engl., 10 (1971) 363-370.

[71] S. Saka, J. Sol-Gel Sci. Tech. , 37 (2006) 135.

[72] S.Sakka (Ed.), Handbook of Sol-Gel Science and Technology: Processing, Characterization and Applications, The kluwer International Series in Engineering & Computer Science, (Springer, 2005).

[73] N. Leventis, H.Lu, M.M. Koebel (Ed.), Aerogel handbook, Springer, 2010, pp. 21-45.

[74] S.S. Kistler, Coherent Expanded Aerogels and Jellies, Nature, 127 (1931) 741-741.

[75] C.J. Lee, G.S. Kim, S.H. Hyun, Synthesis of silica aerogels from waterglass via new modified ambient drying, J. Mater. Sci., 37 (2002) 2237–2241.

[76] G. Nicolaon, S. Teichner, New preparation process for silica xerogels and aerogels, and their textural properties, Bulletin de la Société Chimique de France, 5 (1968) 1900-1906.

[77] G. Wu, J. Wang, J. Shen, T. Yang, Q. Zhang, B. Zhou, Z. Deng, F. Bin, D. Zhou, F. Zhang, Properties of sol-gel derived scratch-resistant nano-porous silica films by a mixed atmosphere treatment, J. Non-Cryst. Solids, 275 (2000) 169-174.

[78] C . Alie´, F. Ferauche, R. Pirard, A.-J. Lecloux, J.-P. Pirard, Preparation of low-density xerogels by incorporation of additives during synthesis, J. Non-Cryst. Solids 289 (2001) 88-96.

[79] F. Kirkbir, H. Murata, D. Meyers, S. Ray Chaudhuri, A. Sarkar, Drying and sintering of sol-gel derived large SiO_2 monoliths, J. Sol-Gel Sci. Technol. , 6 (1996) 203-217.

[80] X. Zhang, S. Huang, Single step on-column frit making for capillary high-performance liquid chromatography using sol-gel technology, J. Chrom. , 910 (2001) 13-18.

[81] A.P. Rao, A.V. Rao, J.L. Gurav, Effect of protic solvents on the physical properties of the ambient pressure dried hydrophobic silica aerogels using sodium silicate precursor, J. Porous Mater., 15 (2008) 507–512.

[82] B. Karmakar, G. D, D. Ganguli Dense silica microspheres from organic and inorganic acid hydrolysis of TEOS, J. Non-Cryst. Solids 272 (2000) 119-126.

[83] L. Durães, M. Ochoa, A. Portugal, N. Duarte, J.P. Dias, N. Rocha, J. Hernandez, Tailored Silica Based Xerogels and Aerogels for Insulation in Space Environments, Adv. Sci.Tech., 63 (2010) 41-46.

[84] A.-M. Siouffi, Silica gel-based monoliths prepared by the sol–gel method: facts and figures, J. Chromatogr. A 1000 (2003) 801–818.

[85] P.B. Wagh, A. V. Rao, D. Haranath, Influence of molar ratios of precursor, solvent and water on physical properties of citric acid catalyzed TEOS silica aerogels, Mat. Chem. Phys., 5 (1998) 41–47.

[86] S.D. Bhagat, A.V. Rao, Surface chemical modification of TEOS based silica aerogels synthesized by two step (acid–base) sol–gel process, Appl. Surf. Sci. , 252 (2006) 4289–4297.

[87] A.V. Rao, G.M. Pajonk, S.D. Bhagat, Comparative studies on the surface chemical modification of silica aerogels based on various organosilane compounds of the type RnSiX4−n J. Non-Cryst. Solids, 350 (2004) 216-223.

[88] A. Jitianu, A. Britchi, C. Deleanu, V. Badescu, M. Zaharescu, Comparative study of the sol–gel processes starting with different substituted Si-alkoxides J. Non-Cryst. Solids 319 (2003) 263-227.

[89] N. Leventis, H. Lu, M.M. Koebel (Ed.), Aerogel Handbook, Springer, 2010, pp. 79-100.

[90] L. Durães, S. Nogueira, A. Santos, C. Preciso, J. Hernandez, A. Portugal, Flexible silica based xerogels and aerogels for spatial applications, in: E. Ferreira (Ed.) Proc. of the 10th International Chemical and Biological Engineering Conference—CHEMPOR, Department of Biological Engineering of University of Minho, Braga, 2008, pp. 563.

[91] M. Ochoa, L. Duraes, A.M. Beja, A. Portugal, Study of the suitability of silica based xerogels synthesized using ethyltrimethoxysilane and/or methyltrimethoxysilane precursors for aerospace applications, J. Sol-Gel Sci. Technol., 61 (2012) 151–160.

[92] G. Schottner, Hybrid Sol-Gel-Derived Polymers: Applications of Multifunctional Materials, Chem. Mater. , 13 (2001) 3422-3435.

[93] A.V. Rao, N.D. Hegde, H. Hirashima, Absorption and desorption of organic liquids in elastic superhydrophobic silica aerogels, J. Colloid. Interf. Sci. , 305 (2007) 124–132.

[94] K.J. Shea, D.A. Loy, Bridged Polysilsesquioxanes. Molecular-Engineered Hybrid Organic−Inorganic Materials, Chem. Mater. , 13 (2001) 3306- 3319.

[95] G. Zhang, A. Dass, A.-M.M. Rawashdeha, J. Thomas, J.A. Counsil, C. Sotiriou-Leventis, E.F. Fabrizio, F. Ilhan, P. Vassilaras, D. Scheiman, L. Mccorkle, A. Palczer, J.C. Johnston, M.A.B. Meador, N. Leventis, Isocyanate-crosslinked silica aerogel monoliths: preparation and characterization, J. Non-Cryst. Solids 350 (2004) 152-164.

[96] E.J.A. Pope, J.D. Mackenzie, Structural Studies of Silica-Aerogel – A Mass–Fraktal Model System. , J. Non-Cryst. Solids, 87 (1986) 185.

[97] C.J. Brinker, K.D. Keefer, D.W. Schaefer, R.A. Assink, B.D. Kay, C.S. Ashley, , Sol-gel transition in simple silicates, J. Non-Cryst. Solids 63 (1984) 45-59.

[98] A. Bisson, A. Rigacci, D. Lecomte, E. Rodier, P. Achard, Drying of Silica Gels to Obtain Aerogels: Phenomenology and Basic Techniques, Dry. Technol. , 21 (2003) 593–628.

[99] M. Einasrud, M. Dahle, S. Lima, S. Hæreid, Preparation and properties of monolithic silica xerogels from TEOS-based alcogels aged in silane solutions, J. Non-Cryst. Solids 186 (1995) 96-103.

[100] J. Estella, J.C. Echeverria, M. Laguna, J. Garrido, Effects of aging and drying conditions on the structural and textural properties of silica gels, Micropor. Mesopor. Mater., 102 (2007) 274-282.

[101] R.A. Strom, Y. Masmoudi, A. Rigacci, G. Petermann, L. Gullberg, B. Chevalier, M.-A. Einarsrud, Strengthening and aging of wet silica gels for up-scaling of aerogel preparation, J. Sol-Gel Sci. Technol., 41 (2007) 291-298.

[102] M.-A. Einarsrud, E. Nilsena, A Rigaccib, G.M. Pajonk, S Buathier, D. Valette, M. Durant, B. Chevalier, P. Nitz, F. Ehrburger-Dolle, Strengthening of silica gels and aerogels by washing and aging processes, J. Non-Cryst. Solids, 285 (2001) 1–7.

[103] H. Hdach, T. Woignier, J. Phalippou, G.W. Scherer,, Effect of Aging and pH on the Modulus of Aerogels, J. Non-Cryst. Solids 121 (1990) 202-205.

[104] D. Y. Nadargi, S. S. Latthe, A. V. Rao, Effect of post-treatment (gel aging) on the properties of methyltrimethoxysilane based silica aerogels prepared by two-step sol-gel process, J. Sol-Gel Sci.Technol., 49 (2009) 53–59.

[105] Y.D. Tretyakov, O.A. Shlyakhtin, Recent progress in cryochemical synthesis of oxide materials, J. Mater. Chem., 9 (1999) 19–24.

[106] G.M. Pajonk, M. Repellin-Lacroix, S. Abouarnadasse, J. Chaouki, D. Klvana From sol-gel to aerogels and cryogels, J. Non-Cryst. Solids, 121 (1990) 66–67.

[107] F. Schwertfeger, D. Frank, M. Schmidt, Hydrophobic waterglass based aerogels without solvent exchange or supercritical drying, J. Non-Cryst. Solids 225 (1998) 24-29.

[108] M.A. Einarsrud, M.B. Kirkedelen, E. Nilsen, K. Mortensen, J. Samseth, Structural development of silica gels aged in TEOS, J. Non-Cryst. Solids 231 (1998) 10-16.

[109] C. Allie, N. Tcherkassova, F. Ferrauche, S. Lambert, B. Heinrich, R. Pirard, J.P. Pirard, Multigram scale synthesis and characterization of low-density silica xerogels, J. Non-Cryst. Solids, 352 (2006) 2763-2771.

[110] L. Durães, M. Ochoa, N. Rocha, R. Patrício, N. Duarte, V. Redondo, A. Portugal, Effect of the Drying Conditions on the Microstructure of Silica Based Xerogels and Aerogels, J. Nanosci. Nanothnol. , 12 (2012) 6828-6834.

[111] L. Duffours, T. Woignier, J. Phalippou, Plastic behavior of aerogels under isostatic pressure, J. Non-Cryst. Solids 186 (1995) 321-327.

[112] D.L. Meixner, P.N. Dyer, Influence of Sol-Gel Synthesis Parameters on the Microstructure of Particulate Silica Xerogels, J. Sol-Gel Sci. Techn., 14 (1999) 223-232.

[113] M. Park, V.C. Menon, S. Komarneni, Ethanol Washing Effect on Textural Properties of the Sodium-Silicate Derived Silica Xerogel, J. Sol-Gel Sci. Techn., 12 (1998) 15-20.

[114] X. Wang, W. Li, G. Zhu, S. Qiu, D. Zhao, B. Zhong, Effects of ammonia/silica molar ratio on the synthesis and structure of bimodal mesopore silica xerogel, Micropor. Mesopor. Mat., 71 (2004) 87-97.

[115] A. Karout, A.C. Pierre, Silica xerogels and aerogels synthesized with ionic liquids, J. Non-Cryst. Solids., 353 (2007) 2900-2909.

[116] G.W. Scherer, D.M. Smith, X. Qiu, J.M. Anderson, Compression of aerogels, J. Non-Cryst. Solids 186 (1995) 316-320.

[117] S.S. Prakash, C.J. Brinker, A.J. Hurd, S.M. Rao Silica aerogel films prepared at ambient pressure by using surface derivatization to induce reversible drying shrinkage, Nature, 374 (1995) 439–443.

[118] N.D. Hegde, A.V. Rao, Physical properties of methyltrimethoxysilane based elastic silica aerogels prepared by the two-stage sol–gel process, J. Mater. Sci. Lett., 42 (2007) 6965-6971.

[119] D.M. Smith, R. Deshpande, C.J. Brinker, Preparation of low-density aerogels at ambient pressure, Mat. Res. Soc. Symp. Proc., 271 (1992) 567–572.

[120] S.-W. Hwang, H.-H. Jung, S.-H. Hyun, Y.-S. Ahn, Effective preparation of crack-free silica aerogels via ambient drying, J. Sol-Gel Sci. Techn., 41 (2007) 139-146.

[121] C.E. Kim, J.S. Yoon, H.J. Hwang, Synthesis of nanoporous silica aerogel by ambient pressure drying, J. Sol-Gel Sci. Techn., 49 (2009) 47-52.

[122] S.D. Bhagat, Y.-H. Kim, M.-J. Moon, Y.-S. Ahn, J.-G. Yeo, A cost-effective and fast synthesis of nanoporous SiO_2 aerogel powders using water-glass via ambient pressure drying route, Solid State Sci., 9 (2007) 628-635.

[123] A. M. Kartal, C. Erkey, Surface modification of silica aerogels by hexamethyldisilazane–carbon dioxide mixtures and their phase behavior, J. Supercrits. Fluids, 53 (2010) 115–120.

[124] A.P. Rao, A.V. Rao, G.M. Pajonk Hydrophobic and physical properties of the ambient pressure dried silica aerogels with sodium silicate precursor using various surface modification agents. , Applied Surface Science 253 (2007) 6032–6040.

[125] T. Adachi, S. Sakka, Effect of formamide additive on the chemistry of silica sol- gels: Part I: NMR of silica hydrolysis, J. Non-Cryst. Solids, 79 (1986) 177-194.

[126] F.A.L. Dullien, Porous Media: Fluid Transport and Pore Structure, Academic Press, San Diego, 1992.

[127] J. B. Peri, Infrared Study of OH and NH2 Groups on the Surface of a Dry Silica Aerogel, J. Phys. Chem., 70 (1966) 2937–2945.

[128] A. Hunt, M. Ayers, "History of Silica Aerogels", http://eande.lbl.gov/ECS/aerogels/sa-home.html. .

[129] P.H. Tewari, A. J. Hunt, K.D. Lofftus, , Ambient temperature supercritical drying of transparent silica aerogels, Materials Letters, 3 (1985) 363.

[130] P.H. Tewari, A.J. Hunt, K.D. Lofftus, Ambient-temperature supercritical drying of transparent silica aerogels, Mater. Lett., 63 (1985) 363–367.

[131] M.J. Bommel, A.B. De Haan, Drying of silica aerogel with supercritical carbon dioxide, J. Non-Cryst. Solids, 186 (1995) 78-82.

[132] F. Kirkbir, H. Murata, D. Meyers, S.R. Chaudhuri, Drying of aerogels in different solvents between atmospheric and supercritical pressures, J. Non- Cryst. Solids, 225 (1998) 14-18.

[133] N. Leventis, H. Lu, M.M. Koebel (Ed.), Aerogel Handbook, Springer, 2010, pp. 56-57.

[134] F. Mammeri, E.L. Bourhis, L. Rozesa, C. Sanchez, Mechanical properties of hybrid organic–inorganic materials, J. Mater. Chem. , 15 (2005) 3787-3811.

[135] J.H. She, T. Ohji, Porous mullite ceramics with high strength, J. Mater. Sci. Lett. , 31 (2002) 1833-1834.

[136] H.-S. Ma, A.P. Roberts, J.-H. Prevost, R. Jullien, G.W. Scherer, Mechanical structure-property relationship of aerogels, J. Non-Cryst. Solids 277 (2000) 127-141.

[137] S. Hæreid, J. Anderson, M.A. Einarsrud, D.W. Hua, D.M. Smith, Thermal and temporal aging of TMOS based aerogel precursors in water, J. Non-Cryst. Solids, 185 (1995) 221-226.

[138] E.M. Lucas, M.S. Doescher, D.M. Ebenstein, K.J. Wald, D.R. Rolison, Silica aerogels with enhanced durability, 30-nm mean pore-size, and improved immersibility in liquids, J. Non-Cryst. Solids 350 (2004) 244-252.

[139] H.H. Huang, B. Orler, G.L. Wilkes Structure-property behavior of new hybrid materials incorporating oligomeric species into sol-gel glasses. 3. Effect of acid content, tetraethoxysilane content, and molecular weight of poly(dimethylsiloxane), Macromolecules, 20 (1987) 1322–1330.

[140] T-J. Yim, S.Y. Kim, K-P. Yoo, Fabrication and thermophysical characterization of nano-porous silicapolyurethane
hybrid aerogels by sol-gel processing and supercritical solvent drying technique, Korean. J. Chem. Eng., 19 (2002) 159–166.

[141] Z. Zhang, J. Shen, X. Ni, G. Wu, B. Zhou, M. Yang, X. Gu, M. Qian, Y. Wu, Hydrophobic Silica Aerogels Strengthened with Nonwoven Fibers, Macromol. Sci. Part A, 43 (2006) 1663-1670.

[142] L. Li, B. Yalcin, B.N. Nguyen, M.A.B. Meador, M. Cakmak, Flexible Nanofiber reinforced aerogel (xerogel): synthesis, manufacture and characterization, ACS Appl. Mater. Interfaces, 1 (2009) 2491-2501.

[143] B.Yuan, S. Ding, D. Wang, G. Wang, H. Li, Heat insulation properties of silica aerogel/glass fiber composites fabricated by press forming, Mater. Lett., 75 (2012) 204–206.

[144] X. Lu, R. Caps, J. Fricke, C.T. Alviso, R.W. Pekala, Correlation between structure and thermal conductivity of organic aerogels, J. Non-Cryst. Solids, 188 (1995) 226-234.

[145] A.V. Rao, M.M. Kulkarni, G.M. Pajonk, D.P. Amalnerkar, T. Seth, Synthesis and Characterization of Hydrophobic Silica Aerogels Using Trimethylethoxysilane as a Co-Precursor, J. Sol-Gel Sci. Technol. , 27 (2003) 103-109.

[146] K. Kanamori, M. Aizawa, K. Nakanishi, T. Hanada, New transparent methylsilsesquioxane aerogels and xerogels with improved mechanical properties, Adv. Mater. , 19 (2007) 1589-1593.

[147] D. Y. Nadargi, A.V. Rao, Methyltriethoxysilane: New precursor for synthesizing silica aerogels, J. Alloy. Compd. , 467 (2009) 397–404.

[148] P. R. Aravind, G. D. Soraru, High surface area methyltriethoxysilane-derived aerogels by ambient pressure drying, J. Porous. Mater., 18 (2011) 159-165.

[149] H. Schmidt, New type of non-crystalline solids between inorganic and organic materials, J. Non-Cryst. Solids 73 (1985) 681-691.

[150] D.S. Ravaine, Y. Charbouillot, M. Vincens, A new family of organically modified silicates prepared from gels, J. Non-Cryst. Solids, 82 (1986) 210-219.

[151] L. Mascia, Developments in organic-inorganic polymeric hybrids: Ceramers, Trends. Polym. Sci. , 3 (1995) 61-66.

[152] R.A. Nass, W. Glaubitt, H. Schmidt, Modelling of ORMOCER coatings by processing, J. Non-Cryst. Solids 121 (1990) 370-374.

[153] D.A. Loy, G.M. Jamison, B. M. Baugher, A.S. Myers, R. A. Assink, K.J. Shea Sol-gel synthesis of hybrid organic-inorganic materials. hexylene- and phenylene-bridged polysiloxanes, Chem. Mater., 8 (1996) 656–663.

[154] M.A.B. Meador, A.S. Weber, A. Hindi, M. Naumenko, L. Mccorkle, D. Quade, S.L. Vivod, G.L. Gould, S. White, K. Deshpande, Structure−Property Relationships in Porous 3D Nanostructures: Epoxy-Cross-Linked Silica Aerogels Produced Using Ethanol as the Solvent, ACS Appl. Mater. Interfaces, 1 (2009) 894-906.

[155] K.J. Shea, D.A. Loy, A Mechanistic Investigation of Gelation. The Sol−Gel Polymerization of Precursors to Bridged Polysilsesquioxanes, Acc. Chem. Res. , 34 (2001) 707-716.

[156] S.L. Vivod, M.A.B. Meador, B.N. Nguyen, D.J. Quade, J.P. Randall, Di-isocyanate crosslinked aerogels with 1,6-bis(trimethoxysilyl)hexane incorporated in silica backbon, The 236th ACS National Meeting, Philadelphia, 2008.

[157] C. Sanchez, B. Julia, P. Belleville, M. Popall, Applications of hybrid organic–inorganic nanocomposites, J. Mater. Chem., 15 (2005) 3559–3592.

[158] C. Sanchez, F. Ribot, B. Lebeau, Molecular design of hybrid organic–inorganic nanocomposites synthesized via sol–gel chemistry, J. Mater. Chem., 9 (1999) 35–44.

[159] C. Sanchez, P. Bellevill, M. Popall, L. Nicolea, Applications of advanced hybrid organic–inorganic nanomaterials: from laboratory to market, Chem. Soc. Rev., 40 (2011) 696–753.

[160] B.M. Novak, D. Auerbach, C. Verrier, Low-density, mutually interpenetrating organic-inorganic composite materials via supercritically drying techniques, Chem. Mater. , 6 (1994) 282–286.

[161] G. Gould, D. Ou, R. Begag, W.E. Rhine Highly-transparent polymer modified silica aerogels, Polymer Preprints, 49 (2008) 534–535.

[162] R. Reisfeld, Spectroscopy and applications of molecules in glasses, J. Non-Cryst. Solids, 121 (1990) 254-266.

[163] J. Mckiernan, E. Simoni, B. Dunn, J.I. Zink, Proton diffusion in the pores of silicate sol-gel glasses, J. Phys. Chem., 98 (1994) 1006–1009.

[164] O.-H. Park, Y.-J. Eo, Y.-K. Choi, B.S. Bae, Preparation and Optical Properties of Silica–Poly(ethylene oxide) Hybrid Materials, J. Sol–Gel Sci. Technol., 16 (2000) 235–241.

[165] R. Takahashi, S. Sato, T. Sodesawa, M. Suzuki, K. Ogura, Preparation of Microporous Silica Gel by Sol–Gel Process in the Presence of Ethylene Glycol Oligomers, Bull. Chem. Soc. Jpn., 73 (2000) 765–774.

[166] K. Iwashita, K. Tadanaga, T. Minami, Water Permeation Properties of SiO2–$RSiO_{3/2}$ (R = Methyl, Vinyl, Phenyl) Thin Films Prepared by Sol–Gel Method on Nylon-6 Substrate, J. Appl. Polym. Sci., 61 (1996) 2173–2177.

[167] X. Tong, T. Tang, Z. Feng, B. Huang, Preparation of Polymer/Silica Hybrid through Sol–Gel Method Involving Emulsion Polymers: II. Poly(ethyl acrylate) / SiO_2, J. Appl. Poly. Sci., 86 (2002) 3532–3536.

[168] J.M. Lin, C.C.M. Ma, F.Y. Wang, H.D. Wu, S.C. Kuang, Thermal, Mechanical and Morphological Properties of Phenolic Resin/Silica Hybrid Ceramers, J. Polym. Sci., Part B: Polym. Phys., 38 (2000) 1699–1706.

[169] K. Nakane, T. Yamashita, K. Iwakura, F. Suzuki, Properties and Structure of Poly(vinyl alcohol)/Silica Composites, J. Appl. Polym. Sci., 74 (1999) 133–138.

[170] A. Bandyopadhyay, M.D. Sarkar, A.K. Bhowmick, Poly(vinyl alcohol)/silica hybrid nanocomposites by sol-gel technique: Synthesis and properties, J. Mater. Sci., 40 (2005) 5233-5241.

[171] D. Fragiadakis, P. Pissis, L. Bokobza, Modified chain dynamics in poly(dimethylsiloxane)/silica nanocomposites, J. Non-Cryst. Solids, 352 (2006) 4969-4972.

[172] D. Fragiadakis, P. Pissis, Glass transition and segmental dynamics in poly(dimethylsiloxane)/silica nanocomposites studied by various techniques. , J. Non-Cryst. Solids 353 (2007) 4344-4352.

[173] N. Leventis, A. Palcezer, L. Mccorkle, Nanoengineered Silica-Polymer Composite Aerogels with No Need for Supercritical Fluid Drying, J. Sol-Gel Sci.Tech., 35 (2005) 99–105.

[174] Y. Hu, J. Mackenzie, Rubber-like elasticity of organically modified silicates, J. Mater. Sci., 27 (1992) 4415–4420.

[175] H. Zou, S. Wu, J. Shen, Polymer/Silica Nanocomposites: Preparation, Characterization, Properties, and Applications, Chem. Rev. , 108 (2008) 3893–3957.

[176] A. Katti, N. Shimpi, S. Roy, H. Lu, E.F. Fabrizio, A. Dass, L.A. Capadona, N. Leventis, Chemical, Physical, and Mechanical Characterization of Isocyanate Cross-linked Amine-Modified Silica Aerogels, Chem. Mater., 18 (2006) 285-296.

[177] S. Mulik, C. Sotiriou-Leventis, G. Churu, H. Lu, N. Leventis, Cross-Linking 3D Assemblies of Nanoparticles into Mechanically Strong Aerogels by Surface-Initiated Free-Radical Polymerization, Chem. Mater. , 20 (2008) 5035–5046.

[178] H.Yang, X. Kong, Y. Zhang, C. Wu, E. Cao, Mechanical properties of polymer-modified silica aerogels dried under ambient pressure, J. Non-Cryst. Solids 357 (2011) 3447–3453.

[179] H. Guo, M.A.B. Meador, L. Mccorkle, D.J. Quade, J. Guo, B. Hamilton, M. Cakmak, G. Sprowl, Polyimide Aerogels Cross-Linked through Amine Functionalized Polyoligomeric Silsesquioxane, ACS Appl. Mater. Interfaces 3 (2011) 546–552.

[180] Y. Duan, S.C. Jana, B. Lama, M.P. Esp, Reinforcement of Silica Aerogels Using Silane-End-Capped Polyurethanes, Langmuir 29 (2013) 6156−6165.

[181] D.J. Boday, R.J. Stover, B. Muriithi, M.W. Keller, J.T. Wertz, K.A.D. Obrey, D.A. Loy, Formation of Polycyanoacrylate-Silica Nanocomposites by Chemical Vapor Deposition of Cyanoacrylates on Aerogels, Chem. Mater. , 20 (2008) 2845-2847.

[182] M. Knez, K. Nielsch, L. Niinistö, Synthesis and Surface Engineering of Complex Nanostructures by Atomic Layer Deposition, Adv. Mater. , 19 (2007) 3425–3438.

[183] Choy, K.L., Chemical vapour deposition of coatings, Prog. Mater. Sci. , 48 (2003) 57–170.

[184] B.N. Nguyen, M.A.B. Meador, A. Medoro, V. Arendt, J. Randall, L. Mccorkle, B. Shonkwiler, Elastic Behavior of Methyltrimethoxysilane Based Aerogels Reinforced with Tri-Isocyanate, ACS Appl. Mater. Interfaces 2 (2010) 1430–1443.

[185] Y.-S. Ye, Y.-N. Chen, J.-S. Wang, J. Rick, Y.-J. Huang, F.-C. Chang, B.-J. Hwang, Versatile Grafting Approaches to Functionalizing Individually Dispersed Graphene Nanosheets Using RAFT Polymerization and Click Chemistry, Chem. Mater. , 24 (2012) 2987−2997.

[186] K. Matyjaszewski, Atom Transfer Radical Polymerization (ATRP): Current Status and Future Perspectives, Macromolecules, 45 (2012) 4015–4039.

[187] Y. Duan, S.C. Jana, A.M. Reinsel, B. Lama, M.P. Espe, Surface Modification and Reinforcement of Silica Aerogels Using Polyhedral Oligomeric Silsesquioxanes, Langmuir, 28 (2012) 15362−15371.

[188] A. Fidalgo, J. P.S. Farinha, J.M.G. Martinho, M.E. Rosa, L.M. Ilharco, Hybrid Silica/Polymer Aerogels Dried at Ambient Pressure, Chem. Mater., 19 (2007) 2603-2609.

[189] Laura Martin, J. Oriol Osso, S. Ricart, A. Roig, O. Garciad, Roberto Sastre, Organo-modified silica aerogels and implications for material hydrophobicity and mechanical properties, J. Mater. Chem., 18 (2008) 207–213.

[190] M. A. B. Meador, L. A. Capadona, L. Mccorkle, D. S. Papadopoulos, N. Leventis, Structure-Property Relationships in Porous 3D Nanostructures as a Function of Preparation Conditions: Isocyanate Cross-Linked Silica Aerogels, Chem. Mater. , 19 (2007) 2247-2260.

[191] K. J. Shea, D. A. Loy, O. Webster, Arylsilsesquioxane Gels and Related Materials. New Hybrids of Organic and Inorganic Networks, J. Am. Chem. Soc., 114 (1992) 6701-6710.

[192] R.M. Stroud, J.W. Long, J.J. Pietron, D.R. Rolison, A practical guide to transmission electron microscopy of aerogels, J. Non-Cryst. Solids 350 (2004) 277–284.

[193] T. Xie, Y.-L. He, Z-X.Tong, W.-X. Yan, X.-Q. Xie Transient heat transfer characteristic of silica aerogel insulating material considering its endothermic reaction, Int. J. Heat Mass Transfer, 68 (2014) 633–640.

[194] R.W. Pekala, L.W. Hrubesh, T.M. Tillotson, C.T. Alviso, J.F. Poco, J.D. Lemay, Mechanical Properties of Porous and Cellular Materials, Mater. Res. Soc. Symp. Proc., 207 (1991) 197–200.

[195] T.-Y. Wei, S.-Y. Lu, Y.-C. Chang, Transparent, Hydrophobic Composite Aerogels with High Mechanical Strength and Low High-Temperature Thermal Conductivities, J. Phys. Chem. B, 112 (2008) 11881–11886.

[196] Wu, G., Yuxi Yu, X. Chenga, Y. Zhang, Preparation and surface modification mechanism of silica aerogels via ambient pressure drying, Mater. Chem. Phys., 129 (2011) 308–314.

[197] Rao, A. P., A. V. Rao, G. M. Pajonk, Hydrophobic and physical properties of the ambient pressure dried silica aerogels with sodium silicate precursor using various surface modification agents. , Appl. Surf. Sci., 253 (2007) 6032–6040.

[198] L. Martin, J. Oriol Osso, S. Ricart, A. Roig, O. Garci , R. Sastre, Organo-modified silica aerogels and implications for material hydrophobicity and mechanical properties, J. Mater. Chem., 18 (2008) 207–213.

[199] Maleki, H., L. Duraes, A. Portugal, An overview on silica aerogels synthesis and different mechanical reinforcing strategies, J. Non-Cryst. Solids, 385 (2014) 55-74.

[200] A. Maia, A. Portugal, L. Duraes Influence of sol-gel conditions on the key properties of silica based aerogels for thermal insulation in Space, Proceeding of International sol-gel conference, Madrid 2013. .

[201] Maleki, H., L. Duraes, A. Portugal, Synthesis of lightweight polymer-reinforced silica aerogels with improved mechanical and thermal insulation properties for space applications, Micropor. Mesopor. Mater. , 197 (2014) 116–129.

[202] G.E.P. Box, K.B. Wilson, On the experimental attainment of optimal conditions, J. Roy. Statist. Soc. B, 13 (1951) 1–45.

[203] P.S. Panesar, Application of response surface methodology in the permeabilization of yeast cells for lactose hydrolysis, Biochem. Eng. J. , 39 (2008) 91–96.

[204] N. Aslan, Application of response surface methodology and central composite rotatable design for modeling the influence of some operating variables of a multi-gravity separator for coal cleaning, Fuel, 86 (2007) 769–776.

[205] V. Gunaraj, N. Murugan, Application of response surface methodology for predicting weld bead quality in submerged arc welding of pipes, J. Mater. Process.Technol. , 88 (1999) 266–275.

[206] A. Idris, F. Kormin, M.Y. Noordin, , Application of response surface methodology in describing the performance of thin film composite membrane, Sep. Purif. Technol. , 49 (2006) 271–280.

[207] D.C. Montgomery, Design and Analysis of Experiments, John Wiley & Sons New York, USA, 2006.

[208] J. Goupy, L. Creighton, Introduction to Design of Experiments with JMP Examples, SAS Institute Inc. , Cary, NC, USA, 2007.

[209] G. Derringer, R. Suich Simultaneous Optimization of Several Response Variables, J. Qual. Technol., 12 (1980) 214-219.

[210] C. Cojocaru, M. Khayet, G. Zakrzewska-Trznadel, A. Jaworska,, Modeling and multi-response optimization of pervaporation of organic aqueous solutions using desirability function approach, J. Hazard. Mater., 167 (2009) 52–63.

[211] Data for selection of space materials and processes, European Cooperation for Space Standardization, ECSS-Q-70-71A rev. 1, (2004).

[212] Thermal vacuum outgassing test for the screening of space materials, European Cooperation for Space Standardization, ECSS-Q-ST-70-02C, (2008).

[213] Thermal testing for the evaluation of space materials, processes, mechanical parts and assemblies, European Cooperation for Space Standardization ECSS-Q-ST-70-04C, (2008).

[214] Y. Zhao, S. Perrier, Reversible Addition-Fragmentation Chain Transfer Graft Polymerization Mediated by Fumed Silica Supported Chain Transfer Agents, Macromolecules 40 (2007) 9116-9124.

[215] J. Moraes, K. Ohno, T. Maschmeyer, S. Perrier, Synthesis of silica–polymer core–shell nanoparticles by reversible addition–fragmentation chain transfer polymerization, Chem. Commun., 49 (2013) 9077-9088.

[216] G. Moad, D. H. Solomon The Chemistry Free Radical Polymerization, Pergamon: Oxford, England, , (1995).

[217] T.E. Patten, K. Matyjaszewski, Atom Transfer Radical Polymerization and the Synthesis of Polymeric Materials, Adv. Mater. , 10 (1998) 901-915.

[218] C. J. Hawker, A. W. Bosman, E. Harth, New polymer synthesis by nitroxide mediated living radical polymerizations, Chem. Rev. , 101 (2001) 3661-3688.

[219] K. Matyjaszewski, J. Xia, Atom Transfer Radical Polymerization, Chem. Rev., 101 (2001) 2921–2990.

[220] G. Moad, E. Rizzardo, S. H. Thang, , Living Radical Polymerization by the RAFT Process, Aust. J. Chem. , 58 (2005) 379–410.

[221] G. Moad, E. Rizzardo, Sh. Thang Radical addition-fragmentation chemistry in polymer synthesis, Polymer, 49 (2008) 1079–1131.

[222] S. Perrier, P. Takolpuckdee, Macromolecular design via reversible addition-fragmentation chain transfer (RAFT)/xanthates (MADIX) polymerization, J. Polym. Sci. Part A: Polym. Chem., 43 (2005) 5347–5393.

[223] J.B. Mcleary, B. Klumperman RAFT mediated polymerisation in heterogeneous media, Soft Matter 2(2006) 45–53.

[224] C. Barner-Kowollik, S. Perrier The future of reversible addition fragmentation chain transfer polymerization, J. Polym. Sci. Part A: Polym. Chem., 46 (2008) 5715–5723.

[225] Y. Tsujii, M. Ejaz, K. Sato, A. Goto, T. Fukuda, Mechanism and kinetics of RAFT-mediated graft polymerization of styrene on a solid surface. 1. experimental evidence of surface radical migration, Macromolecules 34 (2001) 8872–8878.

[226] C.Z. Li, B.C. Benicewicz Synthesis of Well-Defined Polymer Brushes Grafted onto Silica Nanoparticles via Surface Reversible Addition−Fragmentation Chain Transfer Polymerization, Macromolecules, 38 (2005) 5929–5936.

[227] C.Z. Li, J. Han, C.Y. Ryu, B. C. Benicewicz, A Versatile Method To Prepare RAFT Agent Anchored Substrates and the Preparation of PMMA Grafted Nanoparticles, Macromolecules, 39 (2006) 3175–3183.

[228] T.-Y. Guo, P. Liu, J.-W. Zhu, M.-D. Song, B.-H. Zhang, Well-Defined Lactose-Containing Polymer Grafted onto Silica Particles, Biomacromolecules, 7 (2006) 1196–1202.

[229] M. Baum, W.J. Brittain Synthesis of Polymer Brushes on Silicate Substrates via Reversible Addition Fragmentation Chain Transfer Technique, Macromolecules, 35 (2002) 610–615.

[230] M.H. Stenzel, L. Zhang, W. T. S. Huck, Temperature-Responsive Glycopolymer Brushes Synthesized via RAFT Polymerization Using the Z-group Approach, Macromolecular Rapid Communications, 27 (2006) 1121–1126.

[231] Q. Peng, D.M.Y. Lai, E.T. Kang, K. G. Neoh, Preparation of Polymer−Silicon(100) Hybrids via Interface-Initiated Reversible Addition-Fragmentation Chain-Transfer (RAFT) Polymerization, Macromolecules, 39 (2006) 5577–5582.

[232] J. Raula, J. Shan, M. Nuopponen, A. Niskanen, H. Jiang, E. I. Kauppinen, H. Tenhu Synthesis of Gold Nanoparticles Grafted with a Thermoresponsive Polymer by Surface-Induced Reversible-Addition-Fragmentation Chain-Transfer Polymerization, Langmuir, 19 (2003) 3499–3504.

[233] B.S. Sumerlin, A.B. Lowe, P. A. Stroud, P. Zhang, M.W. Urban, C.L. Mccormick, Modification of Gold Surfaces with Water-Soluble (Co)polymers Prepared via Aqueous Reversible Addition−Fragmentation Chain Transfer (RAFT) Polymerization, Langmuir, 19 (2003) 5559–5562.

[234] H. Skaff, T. Emrick, Reversible addition fragmentation chain transfer (RAFT) polymerization from unprotected cadmium selenide nanoparticles, Angew. Chem. Int. Ed. Engl. , 43 (2004) 5383-5386.

[235] C.-Y. Hong, Y.-Z. You, C.-Y. Pan, Synthesis of Water-Soluble Multiwalled Carbon Nanotubes with Grafted Temperature-Responsive Shells by Surface RAFT Polymerization, Chem. Mater., 17 (2005) 2247–2254.

[236] C.-Y. Hong, Y.-Z.You, C.-Y. Pan, Functionalized multi-walled carbon nanotubes with poly(N-(2-hydroxypropyl)methacrylamide) by RAFT polymerization, J. Polym. Sci. Part A: Polym. Chem., 44 (2006) 2419–2427.

[237] S. Perrier, P. Takolpuckdee, J. Westwood, D.M. Lewis, Versatile Chain Transfer Agents for Reversible Addition Fragmentation Chain Transfer (RAFT) Polymerization to Synthesize Functional Polymeric Architectures, Macromolecules, 37 (2004) 2709–2717.

[238] M. H.-Guerrero, T.P. Davis, C. Barner-Kowollik, M.H. Stenzel, Polystyrene comb polymers built on cellulose or poly(styrene-co-2-hydroxyethylmethacrylate) backbones as substrates for the preparation of structured honeycomb films, Eur. Polym. J. , 41 (2005) 2264-2277.

[239] D. Roy , J.T. Guthrie, S. Perrier Graft Polymerization: Grafting Poly(styrene) from Cellulose via Reversible Addition−Fragmentation Chain Transfer (RAFT) Polymerization, Macromolecules 38 (2005) 10363-10372.

[240] S. Perrier, P. Takolpuckdee, C.A. Mars, Reversible Addition−Fragmentation Chain Transfer Polymerization Mediated by a Solid Supported Chain Transfer Agent, Macromolecules, 38 (2005) 6770–6774.

[241] P. Takolpuckdee, C.A. Mars, S. Perrier, Merrifield Resin-Supported Chain Transfer Agents, Precursors for RAFT Polymerization, Org. Lett., 7 (2005) 3449–3452.

[242] A. Favier, M. T. Charreyre, Experimental Requirements for an Efficient Control of Free-Radical Polymerizations via the Reversible Addition-Fragmentation Chain Transfer (RAFT) Process, Macromol. Rapid Commun. , 27 (2006) 653-692.

[243] X. Hao, C. Nilsson, M. Jesberger, M.H. Stenzel, E. Malmström, T.P. Davis, E. Östmark, C. Barner-Kowollik, Dendrimers as scaffolds for multifunctional reversible addition–fragmentation chain transfer agents: Syntheses and polymerization, J. Polym. Sci. Part A: Polym. Chem., 42 (2004) 5877–5890.

[244] M.H. Stenzel, T.P. Davis, Star polymer synthesis using trithiocarbonate functional β-cyclodextrin cores (reversible addition–fragmentation chain-transfer polymerization), J. Polym. Sci. Part A: Polym. Chem., 40 (2002) 4498–4512.

[245] Radhakrishnan, B., A. N. Constable, W. J. Brittain, A Novel Route to Organic–Inorganic Hybrid Nanomaterials, Macromol. Rapid Commun., 29 (2008) 1828–1833.

[246] Qu, Z., F. Hu, K. Chen, Z. Duan, H. Gu, H. Xu, A facile route to the synthesis of spherical poly(acrylic acid) brushes via RAFT
polymerization for high-capacity protein immobilization, J. Colloid Interf. Sci., 398 (2013) 82–87.

[247] Kruk, M., B. Dufour, E. B. Celer, T. Kowalewski, M. Jaroniec, K. Matyjaszewski, Grafting Monodisperse Polymer Chains from Concave Surfaces of Ordered Mesoporous Silicas, Macromolecules 41 (2008) 8584-8591.